DOCTOR OF PHILOSOPHY

Mathematical Modelling of the Immune Response to Cancer

Tough, Iona Kirsten

Award date:
2017

Mathematical Modelling of the Immune Response to Cancer

By

Iona Kirsten Tough

A Thesis submitted for the degree
of Doctor of Philosophy

University of Dundee

January 2017

Contents

Acknowledgements

I would like to thank many people who have so kindly and generously contributed to this thesis.

A special mention goes to my supervisor, Professor Mark A. J. Chaplain for his expert guidance, not only during my PhD, but also during my extended academic career. I am grateful for the wonderful opportunities he has given me and I thank him wholeheartedly.

I would also like to thank Dr Maciej Swat who has provided invaluable support with CompuCell3D. Moreover, I would also like to thank the University of Dundee Mathematics Department, of which each and every member has made my experience as a PhD student a joy. I will miss all the lunch gossip, but especially the outings to the pub. I would especially like to thank Nick, who not only gives excellent technological support but also provides fantastic conversation on all sorts of subjects.

I would also like to thank my parents for their continued support throughout my life, especially for all their encouragement and their unbreakable belief in my abilities. Lastly, I would also like to thank my husband John for all he has had to endure over the last four years of my PhD. We have made it through late nights, panic stricken never-ending coding problems and the

emotional struggles that a PhD brings. I am so grateful to have you in my life and I am looking forward to many more happy years together.

Declaration

I declare that the following thesis is my own composition and that it has not been submitted before in application for a higher degree.

Iona Kirsten Tough

Certification

This is to certify that Iona Kirsten Tough has complied with all the requirements for the submission of this Doctor of Philosophy thesis to the University of Dundee.

Prof. Mark A. J. Chaplain

Abstract

The immune system's vitality and function is of the upmost importance in the human body. The ingenuity and performance of this defence mechanism also plays a role in the prevention of mutated, transformed cells becoming malignant tumours (cancers). More recently, the subject of cancer immunology has been concerned with examining the local effects the immune system has on a pre-angiogenic tumour site. A recent immunological review article - "The Three Es of Cancer Immunoediting" - discusses the way the immune system interacts with cancer cells: elimination, equilibrium, and escape. This biological explanation underpins the mathematical modelling in this PhD thesis where mathematical models of pre-angiogenic immune-tumour interactions are presented and analysed. Chapter two develops an individual-based model of immune-cancer cell interactions using the computational simulation platform, CompuCell3D, to extend an earlier spatio-temporal model of tumour dormancy (Matzavinos et al. [2004]). Chapter three investigates and analyses an ODE model of the interaction of two immune cells and two tumour cells. This model is extended to include spatial movement terms for the tumour and immune cells (in both one and two dimensions) and investigates the rich heterogeneous spatio-temporal dynamics of the system in the presence of a

limit cycle in the reaction kinetics. Finally, chapter four extends the models in the previous two chapters by examining an individual based model of two immune cell populations interacting with two tumour cell populations.

Chapter 1

Introduction

A tumour can be described as: an abnormal mass of tissue whose growth exceeds that of normal tissue, is uncoordinated with that of the normal tissue, and persists in the same excessive manner after cessation of the stimuli which evoke the change (MacSween and Whaley [1992]). Cancer growth has three stages: avascular, angiogenesis and metastasis and invasion. Each of these cancer growth stages have their own dynamics, however this thesis will be concerned with the avascular stage of growth. Here, the tumour mass is in its infancy, and has a maximum size of around 10^6 cells in volume. It does not have a blood network and therefore survives only on the nutrient that is available to it in the local tissue. The theory of immunoediting, developed to try and categorise tumour-immune interactions has become quite popular within the literature, and this thesis will aim to explore it. There are three stages, named the three Es of immunoediting, which are: elimination, equilibrium and escape. Equilibrium can persist for a number of years; a phenomenon deemed "cancer dormancy". The exploration of the immune system's abil-

ity to fight cancer is extremely important for the destruction of the disease, however the complex nature of cancer continues to elude researchers. To aid in the pursuit of a cure, mathematical modelling is an advantageous tool, which can be used to predict and examine the most important aspects of the disease. This thesis has therefore aimed to mathematically model important aspects of the immune-tumour environment.

This thesis investigates multiple models that explore the immune system's defence against malignant growth. Sections 1.1, 1.2 and 1.3 give relevant biological and mathematical backgrounds. Chapter 2 develops an individual based model of $CD8^+$ T-cells when in interaction with a tumour population. These cells, often called cytotoxic T-cells, are immune cells that have vast targets and are potent to tumour cells. The uptake of oxygen by the cancer cells and immune cells is also modelled. The aim is to try and model the Es of immunoediting to better understand the dynamics which govern each stage. Chapter 3 is concerned with exploring the interaction of tumour cells with both cytotoxic T-lymphocytes and T-helper cells. Although, traditionally, cytotoxic lymphocytes have been thought of as the "gold standard" cells in the tumour-immune microenvironment, more recently, the $CD4^+$ T-cell has been shown to provide better immunological defence against tumours in certain situations. Moreover, this chapter will also examine different phenotype of cancer cells, whereby one tumour cell is more potent than the other. Chapter 4, extends both of the previous chapter's models, by utilising a discrete model to investigate different tumour phenotypes and the Warburg effect. Finally, Chapter 5 explores the improvement and possible extensions of the mathematical models developed in this thesis.

1.1 Cancer Immunology

This section discusses the immune system's ability to destroy cancer cells. An overview of the immune system is examined in the first section, focusing on different types of immune cells and their functions within the body. The second section explores the hypothesis of "immunoediting", which describes the process by which tumour cells can be eliminated by the immune system, kept at an equilibrium state by the immune system, or evade immune destruction. Moreover, this chapter then examines the role different phenotypes of tumours and immune cells play in the microenvironment. The last section explores the "Warburg Effect" and how this fuels cancer cell growth and their ability to evade immune detection.

1.1.1 The Immune System

In a world teeming with hostile, subtle, and rapidly evolving pathogens, how does a fragile and slowly evolving human survive? Like all other multicellular organisms, we have evolved several different mechanisms to resist infection by pathogens (Alberts et al. [2008]). The immune system is the body's natural defence mechanism against any foreign attack. Through something called the immune response, the body is able to attack these foreign invaders and destroy them. In the case of humans, there are two different types of barriers, namely, the innate and adaptive immune systems. Each of these has its own individual methods and abilities to help our bodies stay healthy, interacting with one another to kill harmful invaders. It has also become evident that the immune system plays some sort of role in the protection of the body from

cancerous cells. However, both the functioning of the immune system and the growth of tumours involve highly complex processes, and coupled, the tumour-immune interactions form an elaborate system that is not yet fully understood by either experimentalists or theoreticians (Malet and de Pillis [2006]).

The innate immune system is present in all animals and is the first line of defence against pathogens. It has three levels of protection against pathogens. Firstly, there are physical barriers, such as the skin, and chemical barriers, such as the acid in the stomach. The second line of defence comprises cell-intrinsic response, by which an individual cell recognises that it has been infected and takes measures to kill or cripple the pathogen (Alberts et al. [2008]). Finally, the innate immune system can activate specific cells and proteins against invaders. This includes: professional phagocytes, natural killer cells (NK) and the complement system.

The complement system is composed of about 20 different proteins, made mainly by the liver, that interact with one another to kill any foreign invaders and signal to the other cells of the immune system. This type of immune defence is extremely old and can be observed in sea urchins, which evolved approximately 700 million years ago (Sompayrac [2012]). There are three different pathways by which the complement system can be activated: the classical pathway, the lectin pathway and the alternative pathway. Essentially, these three different pathways activate C3, which then in turn then signals to professional phagocytes and NK cells to kill the invader.

NK cells are part of a class of white blood cells called lymphocytes. They are generally found in the blood, where they can be called upon, and then

rapidly proliferate in the problem area. When NK cells receive signals from other immune system cells, they can give off cytokines, which in turn signals other immune cells to come and help defend an infected area. Also, natural killer cells can destroy tumour cells, virus infected cells, bacteria, parasites and fungi. NK cells kill these cells by forcing them to undergo apoptosis (Sompayrac [2012]).

The "professional phagocytes" consist of different types, for example neutrophils, dendritic cells and macrophages. Each of these types of cell start as monocytes, which are produced by stem cells in the bone marrow. The monocytes then enter the blood stream where they travel to the capillaries and try to penetrate any holes in the endothelial wall. After they enter the tissue they then mature into different types of white blood cells. Neutrophils, are cells which are short lived and like NK cells are "on call" when there is an attack. They exit the blood stream, navigating their way to the issue where they proliferate and kill the pathogen. Macrophages are the most famous of the professional phagocytes. Their name comes from the Greek word "phage", meaning "to eat", and "macro", meaning "big", therefore macrophages are "big eaters". Macrophages recognise invaders by using their receptors to search for anything unusual. When a bacterium, for example, is present in the body it will display foreign carbohydrates and fats on their cell wall. The macrophages' receptors can recognise these, move towards it and kill it by a process called "phagocytosis".

Phagocytosis is the method macrophages, and indeed other phagocytes, employ to kill an invader. Firstly it will produce a phagosome, a vesicle, which will encase the bacterium. It then binds the phagosome with a lyso-

some, a vesicle which contains very powerful enzymes and chemicals, to kill the bacterium. Whilst undergoing phagocytosis a macrophage will also secrete proteins called cytokines, which alert other cells of the immune system to traverse to the affected area. Neutrophils also secrete cytokines.

Macrophages have three different types of states. The first is when they lie dormant in the system, mainly cleaning up internal debris. Secondly, a macrophage can act as an antigen presenting cell. When the defences are put under pressure and a macrophage has engulfed an invader, it presents class II MHC proteins on its surface. Helper T-cells can read these "billboards" and activate to help. Finally, the third state of a macrophage is "hyperactivation". In this case, for example, a macrophage can be activated by molecules that are secreted by a bacterium called lipopolysaccharide, a component of the outer cell wall of Gram-negative bacteria, or by a carbohydrate, that is an ingredient of the cell walls in many pathogens, called mannose. When the macrophage receives these signals, it goes into a heightened state of alert. This in turn stops the macrophages proliferating in order to focus on killing. Moreover, in this state the macrophages do not only increase their size and their phagocytic abilities, but they can secrete something called a tumour necrosis factor (TNF). This is a cytokine, which can kill tumour cells and virus infected cells, as well as activate other immune cells (Sompayrac [2012]).

In summary, the innate immune system is the first line of defence against pathogens. Its tools consist of three different types: the complement system, professional phagocytes and natural killer cells. However, sometimes the innate system cannot neutralise the problem on its own, for example the innate system is not good at destroying viruses, and therefore, it must

activate the adaptive immune system. Before discussing how the innate system actives the adaptive, the different cells and responses that govern the adaptive immune system must first be addressed.

Whereas the innate immune responses are general defence reactions, the adaptive responses are highly specific to the particular pathogen that induced them, and they provide long-lasting protection (Alberts et al. [2008]). Any substance capable of eliciting an adaptive immune response is called an antigen. If one contracts something like the measles then, after the virus has been killed, the adaptive immune system will remember it and therefore, provide long lasting immunity against it. This is why vaccination works. The cells that make up the adaptive immune system retain some mature cells that have knowledge of this encounter, which are aptly named "memory cells". It is also necessary to point out that the adaptive immune system is very destructive and therefore this is why it lies dormant until activated. If this does not happen, and the immune system is in a hyperactive state, it will try to kill normal tissue cells and conditions like autoimmune disease arise.

White blood cells, called lymphocytes, are what the adaptive immune system uses to kill antigens. There are two classes of response: antibody response, in the form of B-cells from the bone marrow; and T-cell mediated responses from the thymus. B-cells and T-cells are extremely similar in appearance and cannot be differentiated under a microscope; it is only when activated their guise becomes apparent. They do, however, have some distinct differences, which will come to light later.

B-cells mature in the bone marrow and act as antibody factories. Antibodies are made up of two different proteins, the heavy chain (Hc) and the

light chain (Lc). Due to this structure each molecule has two identical Fab Regions that can bind to antigens. The Fab regions of each antibody are designed to bind to a specific type of antigen, even if the host has not been exposed to it. To generate all of these different types of antibodies, B-cells have been found to change their DNA structure to accommodate the millions of types of antibodies needed, which is called "modular design". In addition to this, the antibody also has a constant region "tail" (Fc) that can bind to Fc receptors on cells of the innate immune system (Sompayrac [2012]). The purpose of antibodies is to find an invader and bind to it. This does two things: it prevents the antigen from binding to the cells of normal tissue and it also allows cells like macrophages to bind to the tail of the antibody. This then elicits a phagocytic response from the phagocyte. When an antibody binds to a phagocyte, it essentially acts as a bridge between an immune cell and an antigen, tagging it for destruction. In the case, where the antibody binds to a macrophage, it increases the appetite of the macrophage making it more phagocytic and allows it to bind to a bigger pool of antigens, making the macrophage more potent. Unfortunately, once an antigen has entered a normal cell, the antibodies become obsolete and a different type of immune cell is needed.

T-cells, from the thymus, consist of three distinct groups: the helper T-cell, the cytotoxic T-cell (CTL) and the regulatory T-cells. The helper T-cell activates macrophages, dendritic cells, B-cells and CTLs by secreting a variety of cytokines, like interleukin 2 (IL-2) and interferon gamma (IFN-γ), and displaying a variety of co-stimulatory proteins on their surface. The CTL, or killer T-cell, directly kills a virus infected cell by programming it for

apoptosis. The third type of T-cell, the regulatory T-cell, suppresses other cells of the immune system, preventing them from attacking normal tissue.

There are also distinct differences between B-cells and T-cells other than where they mature. A B-cell can secrete its receptors, but a T-cell's remain on its surface. Moreover, antibodies can recognise any organic molecules, whereas T-cells specialise in recognising antigens. Also, B-cells can act over distance, whereas T-cells act locally. More importantly, B-cells can identify an antigen without any other form of communication, whereas a T-cell relies on other cells of the immune system. In order for a T-cell to direct a response at a target, there is a mechanism that must first active them.

Dendritic cells provide the link between the innate and adaptive immune system. Dendritic cells cleave the proteins of the pathogens into peptide fragments, which then bind with the MHC proteins, that then carry the fragments to the cell surface (Alberts et al. [2008]). They also display cell-surface co stimulatory proteins. This in turn activates the T-cells where cytokines, secreted by the dendritic cells, determine an effective response.

The way an antigen cell is presented to a T-cell is different depending on the type of T-cell. Proteins called major histocompatibility complex proteins (MHC), using peptides, present to T-cells. There are two classes of MHC molecules: class I and class II. Class I MHC molecules are "billboards" that display, on the surface of a cell, fragments of proteins manufactured by that cell called "endogenous proteins". They act as information ports for the CTLs, declaring if there is a problem and activating them. Class II MHC molecules are only found on specific cells namely, antigen presenting cells (APCs). APCs are cells that display foreign antigen complexed with an

MHC protein on the cell surface for presentation to lymphocytes. These APCs can be, for example, macrophages and dendritic cells, whose role is to internalise and destroy the invader. When, for example, a macrophage has internalised an antigen, it will load peptides onto class II MHC molecules for display on their surface. The class II MHC molecules are utilised by both helper T-cells and regulatory T-cells. They then "read" this information and alert other cells of the immune system. In summary, class I MHC molecules activate killer T-cells and class II MHC molecules, by way of an antigen presenting cell, activate helper T-cells which initiates a response from other immune cells. However, to activate the adaptive immune system there is one more mechanism that needs to be triggered.

As previously discussed, the adaptive immune system is very destructive; therefore a secondary safety tool has been employed. B-cells and T-cells require another signal to activate them. For a helper T-cell it must first recognise its cognitive antigen displayed by class II MHC molecules on the surface of a dendritic cell (acting as an APC). The second signal is the same for any antigen and it involves a protein, e.g. B7, on the surface of an APC, which plugs into its receptor, e.g. CD28, on the surface of a helper T-cell. After this has happened, the helper T-cell can then proliferate, whose receptors recognise the same antigen (Sompayrac [2012]). The activation of B-cells is slightly different. It activates by cross-linking its receptors and then receiving a co-stimulatory signal. It can do this on its own or by way of a helper T-cell. The activation of killer T-cells is not quite fully understood, but it appears that dendritic cells directly activate them. They recognise their cognitive antigen, displayed by MHC class I molecules on the dendritic

cell and then they also receive the co-stimulation they need from the same dendritic cell. Therefore, an activated dendritic cell is all that is necessary to activate a killer T-cell. In summary, the dendritic cell plays a key role in the activation of the adaptive immune system, but it also shows that extra precautions have been put in place to make sure the immune system does not attack the host.

In conclusion, the innate and the adaptive immune systems are powerful weapons against many pathogens that a human is exposed to. The innate immune system, through activation of phagocytes, the complementary system and the NK cell, provides the second line of defence against foreign invaders that get past the initial physical and chemical barrier the body provides. This system copes very well and provides a broad spectrum of protection, activating extremely quickly. However, if the innate system is overwhelmed it will activate the adaptive immune system through a series of mechanisms. The adaptive immune system, by way of the lymphocytes, provides further protection from more powerful pathogens, called antigens. However, the activation of this system, takes some time and therefore, the innate system must hold until then. As previously discussed, there are certain measures within the immune system that can deal with cancer cells, which is the focus of this thesis.

1.1.2 Immunoediting

A neoplasm (solid tumour) may be defined as an abnormal mass of tissue whose growth exceeds that of normal tissue, and is uncoordinated with that

of the normal tissue (Matzavinos et al. [2004]). Cancer has three key stages: avascular tumour growth, angiogenesis, and invasion and metastasis. The avascular stage of growth reaches a steady state at roughly 1-3mm in diameter (approximately 10^6 cells in total). There are over 100 types of cancer, whether being viral, blood based or solid. Many cancer studies, whether clinical or theoretical, have, in recent years, been greatly influenced by Hanahan and Weinberg [2000]. This paper proposes six hallmarks of cancer and discusses what their roles are in helping to promote tumour growth. These are: self-sufficiency in growth signals, insensitivity to antigrowth signals, tissue invasion and metastasis, limitless replicative potential, sustained angiogenesis and evading apoptosis. Recently, the original six hallmarks have been updated and several new ones have been added in a "next generation paper" (Hanahan and Weinberg [2011]). Most interestingly, one of the new hallmarks was identified to be when the tumour mass "evades immune destruction".

The long standing theory of immune surveillance proposes that cells and tissues are constantly monitored by an ever alert immune system, and that such immune surveillance is responsible for recognising and eliminating the vast majority of incipient cancer cells and thus nascent tumours (Hanahan and Weinberg [2011]). This was first proposed in 1909 (Ehrlich [1909]), where it was hypothesised that one of the functions of the immune system is to eliminate cancerous cells. However, this could not be tested experimentally at the time due to the lack of immunological knowledge and technology. Good review of the history behind immunosurveillence can be found in Dunn et al. [2002] and Dunn et al. [2004b]. It wasn't until the 1950s, when a better understanding of immune and transplantation theories were available, when

meaningful experiments were conducted in order to create the theory of immune surveillance. It was postulated that immune cells, attracted by tumour antigens, attacked and attempted to destroy nascent tumours (Burnet [1957, 1964, 1970]). However, the type of mice that were used in the experiments were only immunocompromised not immunodeficient, therefore the experiments did not produce enough evidence for the theory to be widely accepted.

In 1990s, the theory of immune surveillance was revisited and two important discoveries were made, due to advances in monoclonal antibody production and the use of "knock out" mice, a type of mouse whose genes can be altered, to deem them immunoincompetent. Firstly, endogenously produced interferon-γ (IFN-γ) was shown to protect the host against transplanted tumours and the formation of primary chemically induced and spontaneous tumours (Street et al. [2001a,b]; Kaplan et al. [1998]; Dighe et al. [1994]). IFN-γ is thought to induce cytokines, which help the host immune system target the tumour, by sending a signal to produce more immune cells. Secondly, mice lacking in perforin, a cytolytic protein found in the granules of Cytotoxic T-lymphocytes (CTLs) and NK cells, were found to be more susceptible to MCA-induced and spontaneous tumour formation (Street et al. [2001b,a]; van den Broek et al. [1996]; Smyth et al. [2000a,b]; Russell and Ley [2002]). Since then many studies have been conducted, producing data from experiments with mice, along with correlative clinical human data, strengthening the theory of immune surveillance, reviewed in Dunn et al. [2002, 2004a,b]; Swann and Smyth [2007]. Immunosurveillence has also been observed in viral cancers, such as cervical cancer related to HPV. Further proof can also be gained from AIDs victims who are more likely to contract certain

types of cancer (O'Byrne and Dalgleish [2001]). This would seem intuitive as the adaptive immune system is excellently equipped to deal with viruses. Therefore, if impaired the host system will not respond in the correct manner. Weighing up all of the new breakthroughs in immunology, the original theory of immunosurveillance does not fully encompass all of the biological processes that take place in the different stages a tumour goes through to evade immune destruction.

A new theory, which includes immunosurveillance, has been proposed namely, "Cancer Immunoediting" (Dunn et al. [2004b]). Immunoediting, essentially an extension to immunosurveillence, proposes three different stages of the immune response to cancer: elimination, equilibrium and escape. These stages have been named the "three Es of cancer immunoediting". Elimination refers to the inflammatory response of the immune system to cancer and subsequent destruction of a tumour mass; the original immune surveillance theory. If the tumour mass is able to evade immune destruction in the elimination stage, it enters the equilibrium stage. Here, the tumour is kept at roughly the same size and is prevented from inducing an angiogenic response.

"Cancer dormancy" has been widely proposed, whereby a tumour is thought to be at near steady state size, for an explanation to something that occurs in oncology. From experimental data, it has become apparent that defective immunological surveillance of tumours leads to a higher frequency of tumours arising in the host (Vajdic and van Leeuwen [2009]). In the past, dormancy has been indirectly evident in experiments in mice transplants (Teng et al. [2008]). A good overview of other equilibrium models

containing data on mice and humans can be found in Teng et al. [2008]. Tiny solid tumours have also been found in humans, who have died, leading clinicians to theorise that tumours can persist for long periods of time in a dormant state. Sometimes patients can also relapse after being in clinical remission for at least ten years. In fact, even after long periods of clinical remission greater than 10 years, patients are still found to have some circulating, disseminated tumour cells (Stewart et al. [1991]; Sagalowsky and Molberg [1999]; Herrlinger et al. [2005]; Demicheli et al. [1996]; Callaway and Briggs [1989]; Matsui et al. [2006]; Meng et al. [2004]). Also, in donor patients there is evidence that a defective immune system can result in transplanted tumour cells being grown in a new host even if the donor has never had the disease or has been in clinical remission for many years (Teng et al. [2008]; Ryungsa et al. [2007]). But what drives this dormant state?

The mechanisms that govern cancer dormancy are poorly understood. There are a few theories that have been proposed aside from the immune response: cellular intrinsic and angiogenic extrinsic dormancy. Cellular dormancy occurs when the tumour cells enter a quiescent stage and angiogenic dormancy is where apoptosis and proliferation of cancer cells are in balance, preventing vascularisation. It is unknown how these systems work or even if they work independently or together, however, it is known that good cancer prognosis is correlated with detection of circulating cancer CTLs (Montagna et al. [2006]; Pages et al. [2010]; Nelson [2008]). A recent mouse model has attempted to validate this clinical observation, detecting small, inert lesions, containing tumour cells in an equilibrium state (Koebel et al. [2007]). Here, it is suggested that highly specific adaptive T-cell immunity is the component

of the immune system that maintains equilibrium. Specifically, mice deficient in the production of $CD8^+$ cytotoxic T-lymphocytes, $CD4^+$ T_h1 helper T-cells and natural killer cells have been found to be much more susceptible to nascent tumours (Teng et al. [2008]; Ryungsa et al. [2007]).

The last "E" of immunoediting is escape. Whilst in the equilibrium stage, it is thought that the interactions of the tumour cells and immune cells produce two eventual outcomes: cancer elimination or cancer escape. In the first, the cancer is eliminated by the immune system, making this outcome equivalent to the immunosurveillence stage, albeit over a longer period of time. The second outcome is when the cancer cells have managed to, through different factors, supersede the immune system. It is thought that the interaction of the immune cells and tumour cells over a long period of time creates a "Darwinian" selective process, whereby the immune system kills more immunogenic tumour cells leaving the less immunogenic tumour cells to proliferate and grow, essentially changing the phenotype of the cancer cells and creating a less immunogenic tumour. Therefore, the immune system attack is neutralised and the tumour can secrete growth factors to gain a regulatory blood network.

The focus of these investigations has been on the ability of cytotoxic T-lymphocytes to kill tumour cells. However, CTLs may not be a viable killer on their own against solid tumours. CTLs are mainly found throughout the blood system, the lymph and secondary lymphoid organs. Therefore, if a tumour appears in the lung, for example, normally CTLs will not be in the area to react and provide the necessary surveillance of the tumour cells. Moreover, if a CTL does encounter a tumour cell in the tissue of the

lung, and is activated by a tumour antigen presenting cell, it requires co-stimulation from the cell that presents the antigen. The tumour cell will not provide this co-stimulation, therefore the CTL would most likely be killed or anergised. Unfortunately, there is a third problem. Naive T-cells are prevented from entering the tissues, unless there is an attack, to prevent them from attacking normal tissue cells. This makes it unlikely that the naive T-cells would ever encounter tumour antigens expressed in the lung (Sompayrac [2012]). However, there are other cells that, when introduced into the system, could help CTLs.

Macrophages and natural killer cells could provide some defence against tumour cells. As previously discussed, macrophages when in a hyper activated state, secrete a cytokine called "tumour necrosis factor" (TNF). Essentially this chemical attacks the blood vessels that support the nutrients to the tumour, causing the tumour to become necrotic. Macrophages are also found throughout the tissue, therefore can provide immediate surveillance against the tumour. There has been some success in activating macrophages with vaccinations. For example, in the treatment of bladder cancer, a cousin of tuberculosis is injected into the tumour causing the macrophages to become hyperactive and subsequently destroying the tumour. In the case of NK cells, they target cells that express low levels of class I MHC proteins and cells that indicate that they are stressed. Collectively, both macrophages and NK cells are part of the innate immune system, therefore they can be instantly activated, unlike CTLs that may take a week to activate. Both NK cells and macrophages collectively also recognise diverse targets, therefore the chances of them being fooled a single small mutation is minimal (Sompayrac

[2012]). This provides some motivation for using macrophages in mathematical models, along with other types of cells of the immune system, in future work.

1.1.3 Tumour cell heterogeneity

Historically, a cancer mass has been thought of as a homogeneous collection of mutated cells. This in fact could not be further from the truth as tumour cell variation within a neoplasm is vast. The mutations a cancer cell develops from, is handed down the generation by means of cellular division where further mutations are created as the tumour grows. It has also been argued that cancer cells are derived from different cancer stem cells, creating subpopulations, which through self-renewing, create vast differences in daughter cells (Hanahan and Weinberg [2011]). It is this heterogeneity that often protects it from destruction.

Not only do cancer cells form spontaneous mutations, but they are also very versatile. Tumour cells are extremely well suited to many situations that a healthy cell is not, such as a low pH environment, and expression of enzymes which deplete important amino acids, managing to overcome many biological fail safes in order to continue aggressive proliferation and survive to invade and metastasise. In fact, cancer, although a clever disease, is actually the bane of its own existence, killing the host and therefore killing itself. These adaptive subpopulations of cancer cells are called phenotypes.

This unique ability also allows the cancer cells to elude the immune system. As the immune system attacks a tumour, the hypothesis is that the

tumour cells become more immunogenic, evading immune destruction by disabling components of the immune system that have been dispatched to eliminate them (Hanahan and Weinberg [2011]; Mattes et al. [2003]). The way in which cancer cells do this is not fully understood but can be attributed to certain processes. The cancer cell can secrete chemicals, such as the tumour growth factor, TGF-β. This chemical has the ability to immobilise cytotoxic T-lymphocytes and NK cells. The recruitment of certain cells, called inflammatory immune cells, can also promote tumour growth by means of clearing the local environment of debris, allowing more space and nutrient for growth. Hanahan and Weinberg [2011] notes that, *"inflammation can contribute to multiple hallmark capabilities by supplying bioactive molecules to the tumor microenvironment, including growth factors that sustain proliferative signaling, survival factors that limit cell death, proangiogenic factors, extracellular matrix-modifying enzymes that facilitate angiogenesis, invasion, and metastasis, and inductive signals that lead to activation of epithelial-mesenchymal transition (EMT) and other hallmark-facilitating programs"*. It has also been noted that cells such as tumour infiltrating macrophages promote tumour growth and cancer cells can change the immune cell's phenotype (Wang et al. [2000]). Indeed, tumour-infiltrating macrophages are associated with a poor prognosis in melanoma and breast cancer (Mattes et al. [2003]).

In normal circumstances, healthy tissues express antigens on their surface that the immune cells can understand, allowing them to act on the healthy cell's needs and requirements. Tumour cells also express antigens that the cells of the adaptive immune system can recognise (Mattes et al. [2003]; Melief et al. [2000]). The activation of the immune system and subsequent clearing

of nascent tumours is still debated, however there is growing evidence that supports this theory (Haabeth et al. [2014]; Koebel et al. [2007]). It is even thought that the immune system can target more established tumour cells (Haabeth et al. [2014]; Dudley et al. [2002]; Quezada et al. [2010]). The main players of the immune system that play an important role in targeting cancer cells are $CD8^+$ and $CD4^+$ T-cells. As previously discussed, MHC protein pathways act as the guide to which the immune cells can recognise and eradicate tumour cells, through peptide antigens and the colonially distributed T-cell receptor (TCR). In experiments, it has been shown that cancer cells in MHC 1 positive mice are directly targeted by $CD8^+$ T-cells and can work even in the absence of $CD4^+$ T-cells. Moreover, there is a vast amount of evidence supporting the importance of $CD8^+$ T-cells, with support from $CD4^+$ T-cells, as overall patient survival is better when a high number of CD8 memory T-cells are present. Unfortunately tumour cells can downgrade their MHC protein pathways in order to evade the immune response (Mattes et al. [2003]; Marincola et al. [2000]). More specifically, the down regulation of MHC I tumours effectively makes $CD8^+$ T-cells impotent within the immune response, therefore, $CD4^+$ T-cells become the dominant cancer killer. However, most studies on the immune response to cancer have focused on the cytotoxic ability of $CD8^+$ T-cells and the $CD4^+$ T-cells role in improving their ability. However, as previously discussed, the immunoselection of tumour cells can help to promote tumour growth by evading these cells, therefore further investigation on how to boost the immune system is required.

$CD4^+$ T-cell's role within the body is to help other cells of the immune

system, for example when an antigen-presenting cell expresses an antigen on MHC class II, a $CD4^+$ T-cell will aid those cells through a combination of cell to cell interactions. It has also been noted that $CD4^+$ T-cell activation is essential in the initiation of the immune reaction even in the presence of $CD8^+$ T-cells (Ossendorp et al. [1998]). $CD4^+$ T-cells can be subcategorised into two different cell types: Th1 and Th2. Th1 cells mainly partner with macrophages and $CD8^+$ T-cells and produce the cytokines: interferon-γ, the tumour necrosis factor-β and interleukin 2 (IL-2). Conversely, Th2 cells manage recruit B-cells and eosinophils and produce IL-4, IL-5 and IL-10. The study of $CD4^+$ T-cells, in association with cancer has mainly focused on a supporting role, providing a boost to $CD8^+$ T-cells (Kern et al. [1986]; Ossendorp et al. [1998]; Mattes et al. [2003]). It has always been thought that Th1 cells only provided this supporting role to $CD8^+$ T-cells, although this has been challenged of late. It has been suggested that both types of $CD4^+$ T-cells act independently of $CD8^+$ T-cells and that they may in fact play a much more direct role in eradicating neoplasms than first thought (Mattes et al. [2003]; Hung et al. [1998]; Nishimura et al. [1999]; Mumberg et al. [1999]; Quezada et al. [2010]).

There are two ways in which it is thought that $CD4^+$ T-cells can actively eliminate a tumour. Firstly, as previously mentioned, the secretion of cytokines by immune cells are very important to tumour clearance as certain types are cytotoxic to cancer cells. In this case, the $CD4^+$ T-cells would secrete a cytokine in the presence of a tumour cell, rendering it immobile. The second way would be through the active recruitment of different immune cells to target the tumour cells. The down regulation of the MHC I protein path-

way by cancer cells does not seem to effect the cytotoxic ability of the $CD4^+$ T-cells (Mattes et al. [2003]; Haabeth et al. [2014]; Quezada et al. [2010]; Ossendorp et al. [1998]; Wang et al. [2000]; Hanahan and Weinberg [2011]; Perez-Diez et al. [2007]). However, many report that the cells still utilise the MHC II protein pathway, and recruit immune cells such as eosinophils (Mattes et al. [2003]) and NK cells (Perez-Diez et al. [2007]). However, there is some research that suggests even without the MHC II protein pathway, the $CD4^+$ T-cell can still mount an effective immune attack (Ossendorp et al. [1998]).

In this thesis, the interplay between $CD4^+$ T-cells and $CD8^+$ T-cells will investigated, through mathematical models. This is to try and understand the underlying eccentricities of the system.

1.1.4 The Warburg Effect

Energy supply for cells is intrinsic to all life. In a newly formed earth, oxygen was not as abundant as it is today and cells gained energy by the process known as "glycolysis". Evolution and rising oxygen levels shifted the way energy was gained for certain organisms. In multicellular organisms, but more importantly mammals, cells primarily rely on mitochondrial oxidative phosphorylation (OXPHOS) in order to generate energy (Zheng [2012]). This metabolic pathway uses enzymes to oxidise cells in order to release energy. The process takes place in the mitochondria; an area deemed "the power house" of the cell. The main ingredient in the process of OXPHOS is glucose, which is harnessed to produce adenosine 5' triphosphate (ATP). This

acts as a chemical carrier for metabolic processes such as cell motility and proliferation. In fact, glycolysis is used in conjunction with OXPHOS in order to gain the optimal amount of energy for a specific cell. In the presence of oxygen, most cells will primarily metabolise glucose in this way. The process begins by oxidation of the glycolytic pyruvate, which is produced by glycolysis in the cytoplasm, in the mitochondrial tricarboxylic acid cycle (TCA). This produces nicotinamide adenine dinucleotide (NADH), which then produces ATP through oxidative phosphorylation (Van der Heiden et al. [2009]). It should also be noted that this process produces minimal lactate. If there is no oxygen available the cell will be under anaerobic conditions and the pyruvate is reduced to lactate, which is then excreted into the extracellular space (Van der Heiden et al. [2009]; Zheng [2012]; Bartrons and Caro [2007]; Lu et al. [2015]; Liberti and Locasale [2016]; Wu and Zhao [2013]; Upadhyay et al. [2013]). OXPHOS is also much more efficient at producing energy than glycolysis as it produces 36 ATPs whereas, glycolysis only produces 2. However, glycolysis is still used in certain areas of the body such as the liver, brain and muscles(Zheng [2012]; Brooks [2009]; Vaishnavi et al. [2010]).

Tumour cells have the unique ability to adapt to their surroundings. By changing their phenotype they can survive even in the most hostile of environments, and indeed, are therefore, very hard to destroy. In normal cells many fail-safes are put into place to ensure that no mutations form during the cell cycle. If one of the processes goes wrong the cell will go into arrest and subsequently undergo apoptosis. Moreover, there are control systems that are put into place to prevent uncontrollable cell growth, as nutrient is available in constant supply to most cells in the body. Healthy cells are only

triggered to grow when indicated to by growth factors. However, in contrast, cancer cells do not have these mechanisms in place and are allowed to mutate and grow at an exponentially high rate and uptake glucose indefinitely.

The metabolic phenotype has been well known now for over a century and is considered a "hallmark of cancer". In the 1920s, Otto Warburg observed that cancer cells seem to take up unusually large amounts of glucose and exhibit anaerobic glycolysis to produce energy (Warburg et al. [1924]; Warburg [1925]; Warburg et al. [1927]). Additionally, it was also observed that this continued even if the cells had enough oxygen to sustain OXPHOS (Warburg et al. [1956]; Liberti and Locasale [2016]), deemed aerobic glycolysis i.e. glycolysis in the presence of oxygen. This phenomenon, in the 1970s, was dubbed "The Warburg Effect" (Racker [1972]). Although there is no clear answer as to why this happens, it is thought that it is the combined result of many different reasons such as tumour hypoxia, mutated mtDNA, tumour suppressors and oncogenes, among others. Warburg attributed this to an anomaly in the mitochondria; however, this was disproved as many cancer cell's mitochondria function normally. Furthermore, Warburg's discovery was over looked for a long period of time and has only recently, over the last 15 years, come into light again through the discovery of proton emission tomography (PET), whereby the Warburg Effect formed the basis of the research. Here, 18-fluorode-oxyglucose (FDG) accumulates in tumour cells due to the rapid uptake of glucose, which can then be imaged using a PET scan (Lu et al. [2015]). Interestingly, as previously mentioned, aerobic glycolysis is an inefficient way of producing ATP, however glucose is produced at a much higher rate than by OXPHOS.

Cancer spreads often in a finger like fashion, and is well known not to have just one specific cell type, but is heterogeneous by nature. Just as in the human body, a multitude of cells are required for many biological processes. Each tumour mass, depending upon where it is located within the body, will have its own set of nutritional needs. Even if the cancer is of the same type, each neoplasm will be completely different to the next, subsequently making the tumour hard to kill. If OXPHOS is available why would cancer use glycolysis if it is an inefficient way of producing ATP?

Cancer has many different attributes such as fast cellular motility, poorly formed tumour boundaries, different cellular shapes, but, most importantly, for the sake of this section, uncontrollable growth. The changing of receptor-initiated signalling pathways in tumour cells seem to activate the uptake and metabolism of nutrients that both promote cell survival and fuel cell growth (Van der Heiden et al. [2009]). For cells to divide, it is necessary to uptake enough energy for the parent cell to pass onto the daughter cells i.e. the passing of enough metabolic intermediaries to form a new cell. Therefore, by switching to glycolysis, the promotion of cell proliferation and cell survival is more maintainable even if it an inefficient way to produce ATP. It is important to note however, that glycolysis is also used by lymphocytes when rapid growth is required, boosting evidence of the Warburg hypothesis. Moreover, It is well known that cancer cells exhibit hypoxia when there is little oxygen available in the microenvironment. In this situation, it seems prudent for cancer cells to switch on anaerobic glycolysis as a way to survive in this very arid environment. As a direct result of this, lactate is excreted into the microenvironment. Lactate is very acidic, and the drop in pH allows the cancer

cells to thrive. Normal cells cannot survive in an acidic environment. The host immune system is evaded and healthy tissue degrades, promoting cancer invasion and metastasis (Pederson [2007]). Van der Heiden et al. [2009] also attributes the excretion of lactate by the cancer cells to allow a faster uptake of nutrients into the biomass, which facilitates rapid proliferation. Lastly, glycolysis produces less reactive oxygen species (ROS). ROS, are chemically reactive molecules which contain oxygen and have substantial roles in both homeostasis and cell signalling. The damage these molecules can inflict on tumour cells, if at a high enough concentration, is divisive and cell death will occur.

However, there is an argument that glycolysis is used in co-ordination with OXPHOS. Zheng [2012], attributes some reasoning as to why cancer cells may use both. Firstly, the authors hypothesises that as the need for nutrients for cancer growth is paramount, the cells can gain energy from both glycolysis and the TCA cycle, in order to have enough metabolic intermediaries to divide. Secondly, the rapid production of ATP can have a knock on effect. ADP can be converted to ATP, which, through the inhibition of phosphofructokinase 1 (PFK1) and pyruvate kinase 1 (PK1), will inhibit glycolysis. As previously discussed, anaerobic glycolysis also causes the production of an acidic environment by way of lactate. In this hypoxic situation, lactic acidosis inhibits glycolysis and favours OXPHOS as a means of energy generation.

The biological processes and dynamics behind the Warburg effect is not yet clear. To elucidate this, more scientific research is needed in order to discover more compatible therapies, which can target and destroy cancer. In

this thesis, the hypoxic generation of anaerobic glycolysis will be investigated.

As one can see, the biology of immunoediting is extremely complex and full of uncertainties. One tool to aid in the understanding of these intricate processes is mathematical modelling.

1.2 Mathematical Modelling of Cancer and Immunotherapy

This section will discuss the literature on mathematical models produced in relation to cancer immunology. It will examine different types of models including homogeneous and spatial models, as well as individual based models. The first section is a general overview of cancer modelling and the second section focuses on the literature that explores the interaction between the immune system and cancer.

1.2.1 Mathematical Cancer Modelling

The use of mathematical models for cancer research has become increasingly popular and is used as a tool to aid in the understanding of cancer environments. Biological processes within the body, in relation to cancer, have mostly been modelled using the classical techniques: Ordinary (ODE) and Partial (PDE) Differential Equation systems.

A system of homogeneous ordinary differential equations is used to show a change in reaction kinetics between different variables, utilising an investigation of parameter values in order to understand the dynamics of the system. The earliest use of modelling, within an ODE setting, in terms of mathematical biology was in genetics and evolution, but has recently exploded into all aspects of the biological world. This type of equation system often allows the modeller to investigate the importance of certain underlying dynamics, for example cell-cell interactions. Although a simplified process, it allows the

user to mathematically investigate, through analytical or numerical means, a system to elucidate only the most important factors in that environment; a good aid if the cancer system is very complex. The technique assumes the cancer environment is a "well mixed vat", covering different spatial and temporal scales. The law of mass action, whereby different reaction rates between individual elements may be modelled, then governs the dynamics of the system.

ODE systems are of great use when modelling tumour growth, as they may be able to tell if there are any interesting phenomena within the system, such as Hopf bifurcations or chaotic behaviour. For the purpose of this thesis, the Hopf bifurcation is of significant importance. These tools can lead to a greater understanding of the intricate interactions between species or indeed other activities within the cancer environment. Matzavinos et al. [2004] utilises a homogeneous system of differential equations in order to investigate the presence of a traveling wave solution. It was found that a Hopf bifurcation was present within the system, which was driving the oscillatory behaviour. However, the need to understand the spatial habits of cells and chemicals calls for a different technique.

Partial differential equation systems allow for the inclusion of more biologically relevant features and can portray additional variables such as chemical diffusion. The equations are concerned with the rates of change with respect to continuous variables and can model cellular and chemical concentration at given times. Some of the earliest influential PDE cancer models were produced in the 1970s. In Greenspan 1972, the growth of a tumour spheroid in the avascular stage of development was modelled by the diffusion of a

nutrient and an internal pressure. A tumour spheroid is thought to consist of many different internal layers and Greenspan's model, after a certain period of time, developed three different layers: a necrotic core, where cells are starved of nutrient; a quiescent zone, which surrounds the internal necrotic core; and a proliferating zone, where there is a thin layer of cells around the edge. The internal pressure was used to try and represent cell-cell adhesion. This paper shows that if the nutrient concentration goes below a certain critical threshold, then proliferating cells will become quiescent, then necrotic if the nutrient level continues to fall. Cells in the quiescent zone are unable to divide and are said to be in a "resting state". Proliferating cells, at the rim of the tumour mass have access to all the available nutrient within the system and therefore can divide, increasing the tumour size. The internal pressure was added to try and maintain the different tumour zones and the results show an inward motion of cells, which constituted a possible hypothesis as to why an avascular tumour mass has a maximum size.

Greenspan (1976) then extended this work in order to investigate the perturbations of the tumour spherical shape under steady state conditions. As before, the tumour mass consists of a proliferating ring, quiescent zone and necrotic core, each governed by nutrient concentration and an internal pressure, representing the surface tension of the tumour and cell-cell adhesion. The results showed, as the tumour size increased, the tumour shape became less stable. This was an important result as perturbations in the tumour shape may allow an investigation as to why a tumour can become invasive. Over the years, these models have been explored and extended into many different systems, such as Byrne and Chaplain [1996], and have been utilised

in many different fields associated with mathematical cancer systems, such as immune-cancer cell modelling.

1.2.2 Mathematical Immune Cancer Modelling

There have been many attempts over the years to model the interaction of the immune system and cancer to try and help clinicians and experimentalists drive their studies. These include deterministic models, in the form of spatial and non spatial studies, and stochastic models. Most of the scientific research conducted on studies of the immune system and cancer has been based on white blood cells, and hence most of the modelling is based on the interaction of white blood cells with tumour cells. Specifically, many studies focus on $CD8^+$ killer cells, natural killer cells and macrophages, as they have been shown to successfully lyse tumour cells (Quesnel [2008]), such as Boon and van der Bruggen [1996], Khar [1997], Kuznetsov et al. [1994] and Lejeune and El Akili [2008].

In terms of deterministic non spatial models, these have incorporated many different aspects of the immune-tumour environment such as: cytokines/chemokines (Kirschner and Panetta [1998], Arciero et al. [2004], Byrne et al. [2004]); multiple immune cell co-operation (de Pillis et al. [2003], Owen and Sherratt [1998], de Pillis et al. [2005], Eftimie et al. [2010]); tumour antigens (Joshi et al. [2009], Fishman and Perelson [1993]); and interactions with normal tissue (Owen and Sherratt [1998], Radunskaya and de Pillis [2003], de Pillis and Radunskaya [2001], Byrne et al. [2004]). There has also been a growing number of models based on the effect of immunotherapy

drugs by direct injection of T-cells or cytokines, and also the investigation of T-cell tumour regression and chemotherapy (Kuznetsov and Knott [2001], Kirschner and Panetta [1998], Kogan et al. [2010], d'Onofrio [2008]). Moreover, Gu et al. [2006] have modelled the effects of combining immunotherapy and chemotherapy. The tumour-immune mathematical models tend to have up to four differential equations that govern the system. Models with larger numbers of elements will require more estimation in terms of parameter values as well as the obligatory time element in solving the system numerically. It is also more difficult to find certain mathematical aspects of the system, for example hopf bifurcations, which provide vital clues as to the nature of the system. However, there are a few papers that have successfully studied larger ODE models of immune-cancer interaction such as Deboer et al. [1985], Cappuccio et al. [2006], Kronik et al. [2008] and Kronik et al. [2010]. A good review of non spatial models that study interactions between immune and cancer cells can be found in Eftimie et al. [2011]. While ODE models are a good basis for modelling research, it is also prudent to model spatial movement. This can be accomplished at cellular and sub cellular level. A good example of the need for a spatial model would be when trying to study a tumour mass which consists of different tumoral cellular zones. It would also possibly need to incorporate the movement of fields associated with the growing tumour mass.

Deterministic spatial models using partial differential equations to mimic the biological processes in immunoediting have also been undertaken. Here, spatial aspects of the immune tumour environment can be examined and studied, for example, through the investigation of travelling waves and the

utilisation of differing tumour geometries. This includes the modelling of, cytotoxic T-cells with chemoattractants (Kuznetsov and Stepnova [1992] Matzavinos et al. [2004], Matzavinos and Chaplain [2004]); the effects of the immune system on the tumour phenotype (Al-Tameemi et al. [2012]); interactions between cancer promoting chemicals, tumour cells and immune cells (Wang et al. [2009]); tumour cells, Th1 cells and IL-27 (Laio et al. [2014]); tumour cells and macrophages (Owen and Sherratt [1997], Owen and Sherratt [1999], Webb et al. [2007]); and macrophage targeted gene therapy with chemotherapy (Owen et al. [2011]). Numerical and bifurcation analysis of these models have demonstrated diverse patterns of spatio temporal dynamics of the immune and tumour cells within tumour tissue, even in dormant tumours, which are being controlled by cyctotoxic lymphocytes (Matzavinos et al. [2004]). The "gold standard" of immune modelling has utilised the effects of $CD8^+$ T-lymphocytes on the tumour bulk, however there is ample evidence, as discussed in section 1.1.3, that $CD4^+$ T-cells may also play a bigger role than first thought in immune-cancer interactions.

The modelling of $CD4^+$ T-cells in mathematics is somewhat in its infancy, however there are models which encompass the idea that $CD4^+$ T-cells can recruit other cells to inflict damage on the tumour mass. One such model is that of Nwabugwu et al. [2013], extended from Nwabugwu et al. [2012], where the inactivation of the MYC oncogene is modelled using ODEs. It shows that the cellular senescence of tumour cells is dependent on $CD4^+$ T-cells, leading to relapse of tumours in immunocompromised hosts. The introduction of macrophages, recruited by the T-helper cells was shown to achieve sustained tumour regression if in the presence of an immunocompetent individual. An-

other model is that of Eftimie et al. [2010], where the modelling of Th1 and Th2 cells are investigated in relation to the rejection of melanoma by way of an ODE model. It was found that neither the Th1 nor Th2 cells could clear the cancer alone, however cancer clearance was observed when the Th2 cells recruited eosinophils. It is also noted in Eftimie et al. [2011], that the development of these models would allow a better understanding of this type of biological system, providing evidence to support experimental studies in order to elucidate the underlying dynamics that exist between $CD4^+$ T-cells and the tumour environment.

Among other types of techniques there are stochastic and discrete (individual) based models. Stochasticity may arise from genetic mutations that occur during the evolution of cancer cells or from variations in the environment (Eftimie et al. [2011]). This includes: models of a deterministic origin, which have had stochastic elements added (Bose and Trimper [2009]); and individual agent based models (Lollini et al. [2006]; Pappalardo et al. [2006]). Moreover, discrete based modelling arises from two separate modelling techniques: cellular automata and agent based models, which normally focus on the interactions of cancer cells and the local tumour environment (Malet and de Pillis [2006]; Mansury et al. [2006]). These attempt to describe how cells behave by either specifying rules to each individual cell (agent based), or by defining specific rules associated with a grid system, in which each grid may contain one or more cells (cellular automata). Agent based models can also be subdivided into two different categories based on their geometry: on lattice and off lattice. When utilising an off lattice model, cells are not confined by grid restriction allowing a more biologically relevant geometrical repre-

sentation. On lattice models can be thought of as an extension of cellular automata models because cells are represented by a grid system.

An extension to the cellular automata model has been created in the form of a cellular potts model. Here, the model is comprised of pixels with each cell, or cellular compartment, made up of several connecting pixels. Therefore, the cells are no longer modelled as single points, but as spatial objects whose size and shape can be altered. The simulation progresses through a series of monte carlo steps (MCS), which attempt to minimise the overall effective energy within the system. At each MCS, attempts are made to transform neighbouring pixels at the boundary of each cell to increase its volume. If the transformation, known as a "flip", reduces the overall effective energy then the pixel in question will be changed. The use of this type of model allows for much more biologically relevant models, in that each individual element of the system can be modelled actively using numerous different rules. This type of model has been successfully transformed into user friendly software. CompuCell3D is one of these programmes.

CompuCell3D is a very useful tool when modelling tumour immune interactions. It allows the user to easily model an idealistic tumour environment where individual cells interact with one another. Numerous different additions to the software can be implemented using python coding, allowing the modelling, for example, of: chemical fields, cell structure, cell size, cell shape and cell-cell adhesion. It is also relatively easy to formulate, for a simple system, not only a two dimensional model but a three dimensional model. One very complex model, in CompuCell3D, is Hester et al. [2011]. In this paper, a model of somitogeneis is undertaken, which is observed in the

development of all vertebrate embryos and results in segmentation, requiring a enormous amount of co-ordination between different biological process on multiple scales. Tumour growth has also been modelled and includes the modelling of: avascular tumour growth in gliomas in 2-D and 3-D (Poplawski et al. [2009] Poplawski et al. [2010]); vascular tumour growth (Merks and Glazier [2006], Merks et al. [2008], Bauer et al. [2007], Bauer et al. [2009], Shirinifard et al. [2009]); and tumour invasion (Andasari et al. [2012]). CompuCell3D has also been used to model cell cycle heterogeneity among cells and how this can affect how a tumour responds to chemotherapeutic drugs (Powathil et al. [2014]). It has also been used to model selection pressures in somatic evolution leading to the development of tumour cell aggression in solid tumours in Swat et al. [2015].

1.3 Mathematical Methods

Understanding mathematical numerical methods, including their advantages and limitations, is essential knowledge for anyone using computer software environments. Therefore, this section aims to 'tease away' the underlying mathematical methods that are utilised for the inbuilt tools in numerical software packages relevant to this thesis. The first section describes the methods used to solve ODE and PDE models and the second section focuses on the tools used to solve individual based models.

1.3.1 Numerical methods of ODEs and PDEs

It is prudent to point out that there are many excellent inbuilt numerical tools in different computing environments of which many academics have spent years working on. For the everyday user, these tools will be sufficient for most of their needs however, choosing the right inbuilt tool depends on their ability to mathematically determine the right package for their problem. It is only when one of these tools does not 'fit the bill' that writing a new method is necessary and should be undertaken. In this thesis Matlab will be the main programme used for 1-D systems and Comsol for 2-D.

Matlab, based on C, has the ability to numerically solve mathematical models using different inbuilt tools. For all of the ODE models in this report, ODE45, has been used which is Runge-Kutta method. The Runge-Kutta method is a one step approximation scheme, whereby each step is determined by the previous step i.e. it is an explicit method. The order of the method that should be used depends on the problem, but in general the higher the

order of the method the more accurate the system. Issues arise when the problem is too stiff for the method and explicit methods simply do not work, e.g. there maybe large differences in time scales in the problem, and therefore the ability of the method is damaged by the amount of time the solver takes to solve the system. Matlab, therefore, has different solvers for this e.g. ODE15s, which is essentially a linear multistep backward difference method. However, for the purposes of the models in this report a 4th order Runge-Kutta method, in the form of ODE45, is used and the general method is formulated by:

$$u' = f(t, \mathbf{u}), \quad u(0) = u_0 \tag{1.3.1}$$

$$\begin{aligned}
&\mathbf{k}^1 = \Delta t \mathbf{f}(t^n, \mathbf{u}^n) \\
&\mathbf{k}^2 = \Delta t \mathbf{f}\left(t^n + c_2 \Delta t, \mathbf{u}^n + a_{2,1}\mathbf{k}^1\right), \\
&\mathbf{k}^3 = \Delta t \mathbf{f}\left(t^n + c_3 \Delta t, \mathbf{u}^n + a_{3,1}\mathbf{k}^1 + a_{3,2}\mathbf{k}^2\right), \\
&... \\
&\mathbf{k}^s = \Delta t \mathbf{f}\left(t^n + c_s \Delta t, \mathbf{u}^n + a_{s,1}\mathbf{k}^1 + ... + a_{s,s-1}\mathbf{k}^{s-1}\right), \\
&\mathbf{u}^{n+1} = \mathbf{u}^n + \sum_{i=1}^{s} b_i \mathbf{k}^i.
\end{aligned} \tag{1.3.2}$$

This can be also written as part of a Butcher tableau (Griffiths and Higham [2011]).

The RK method uses intermediate steps namely k_i to determine the value

of the system at the next time step. To compute the approximate answer, $\mathbf{u}^{u+1} \approx \mathbf{u}(t^n)$, one simply needs to compute the values of the intermediate values, k_i, to get the next time step. This is an explicit method as the method uses the initial condition u_0, along with the time step Δt, to compute the first point $\mathbf{k}_1$. Then, $\mathbf{k}_1$ is used, again with Δt and $\mathbf{u}^1$, to compute $\mathbf{k}^2$ and so on until the next time step is achieved depending on the order of the method (Griffiths and Higham [2011]). The classical fourth order Runge Kutta Method is shown in system (1.3.3) (Griffiths and Higham [2011]) :

$$\begin{aligned}
\mathbf{k^1} &= \Delta t \mathbf{f}\left(t^n, \mathbf{u}^n\right) \\
\mathbf{k^2} &= \Delta t \mathbf{f}\left(t^n + \frac{1}{2}\Delta t, \mathbf{u}^n + \frac{1}{2}\mathbf{k}^1\right), \\
\mathbf{k^3} &= \Delta t \mathbf{f}\left(t^n + \frac{1}{2}\Delta t, \mathbf{u}^n + \frac{1}{2}\mathbf{k}^2\right), \\
\mathbf{k^4} &= \Delta t \mathbf{f}\left(t^n + \Delta t, \mathbf{u}^n + \mathbf{k}^3\right), \\
\mathbf{u}^{u+1} &= \mathbf{u}^n + \left(\frac{1}{6}\mathbf{k}^1 + \frac{1}{3}\mathbf{k}^2 + \frac{1}{3}\mathbf{k}^3 + \frac{1}{6}\mathbf{k}^4\right).
\end{aligned} \tag{1.3.3}$$

After solving a non-dimensionalised ODE system, spatial elements will be added to give a PDE system. This requires a different tool in Matlab, namely PDEPE. PDEPE solves initial-boundary value problems for parabolic-elliptic PDEs in 1-D. The ODEs resulting from discretisation in space are integrated to obtain approximate solutions within a given time range. What is produced, in models in this report, are cells densities over the domain. One would have to integrate over the domain to get the concentrations of cells at a point.

For 2-D PDE time independent simulations, the computer programming

package"Comsol" will be used. Comsol, formerly "Femlab", has many different uses within engineering, physics and mathematics. For the purposes of this report, the computer environment is utilised to implement the finite element method in time independent PDE systems, over given domains, to approximate the solutions over a set time. The PDEs may be entered directly or in their 'weak form'. Again, it is best to understand the inner workings of such a method before proceeding with a computer package.

Fundamentally, the finite element method is a way to solve boundary value problems. Unlike the finite difference method, a collection of small triangular domains is used to approximate the given domain and minimise the error. This would be used when working with shapes like circles that are difficult to approximate at their boundary due to their curved nature. A generalisation of the process one has to carry out to solve a BVP with the FEM is:

1. Reformulate the PDE to give a weak form.

2. "Triangulate" the domain i.e. divided the domain into triangles and/or quadrilaterals.

3. Define a general continuous piecewise polynomial on the triangulation.

4. Use the weak form to generate a system of linear algebraic equations in the coefficients in the piecewise polynomial representation of the approximate solution. It is at this stage that the Dirichlet boundary conditions are enforced.

5. Solve the algebraic system to generate a finite element approximation.

6. Post-process the solution to extract the required information.

This process can become exceptionally difficult, especially in large problems at step five above, and therefore, specialised linear algebra packages like Comsol are required.

1.3.2 CompuCell3D

In order to numerically solve individual based models, within this thesis, CompuCell3D has been utilised. CompuCell3D, as previously discussed in Chapter 1.2, is an open source solver, which uses the Cellular Potts Method or Glazier-Graner-Hogeweg (GGH) model (Glazier et al. [2007] and reviewed in Rejniak and Anderson [2011]). It was developed to allow the modelling of a large number of cells and their interactions. The system was created in the programming language C++, but allows models to be created in a user-friendly manner in the XML and Python languages. The CPM also makes use of PDEs to represent non-discrete fields. CompuCell3D models have a range of different uses within mathematical biology, whereby each simulation can model varying biological processes and objects such as cells and chemicals.

Firstly, spatially operative generalised cells are created, which can represent clusters of cells, single cells, sub compartments of cells or indeed small subdomains of non-cellular materials (Izaguirre et al. [2004]). Each model is made up of objects, a description of their interactions and appropriate initial conditions. The power of CompuCell3D is its ability to create models in two or three dimensions. The objects in each model are comprised of lattice sites,

called pixels in 2D and voxels in 3D. Each cell is assigned a type and each lattice site is represented by a vector of integers, i. The cell index, occupying pixel i, is $\sigma(i)$ (generalised cell) and the cell type is referred to as $\tau(\sigma(i))$. Either increasing or decreasing the number of pixels it contains can change the size of the cell. Alternatively, groups of cells may be clustered together to simulate, for example, a tumour. Cell shape, polarity, intracellular membranes and cell-shape changes can also be modelled. A cell type may have many attributes associated with it such as surface area, volume, adhesion and motility.

The solver uses the "effective energy" to describe the interactions between cells. This determines many characteristics such as cell size, shape, motility, adhesion strength and the reaction to gradients of chemotactic fields. It is these interaction descriptions and dynamics that define how the objects behave both biologically and physically. The user defines the parameters for the effective energy for each cell type and these determine the characteristics of each cell. During a simulation, cells will attempt to extend their boundaries to minimise the effective energy. This happens through a series of index-copy attempts, whereby a lattice site will "flip" to belong to a different cell if it is favourable to do so. The success of an index-copy attempt is governed by the Boltzmann acceptance function, and if it is successful the cell will increase in volume by a lattice site and the neighbouring cell will decrease in volume. Once all of the boundary pixels in the simulation have performed an index-copy attempt, a Monte Carlo Step has been completed.

As previously discussed, CompuCell3D can also adequately model nutrients, chemical gradients or the extra cellular matrix by using a field compo-

nent. Partial differential equations are used to describe the fields and most simulations require secretion, absorption, diffusion and decay components. For these, simple ODE forward Euler methods can be employed to solve the discretised PDEs. This type of method means that the parameter values must be chosen carefully, in order to ensure the stability of the solution. Auxiliary equations describe cells' absorption and secretion of chemical diffusants and extracellular materials, e.g. their interactions with fields, state changes within the cells, mitosis and cell death. These can be simple, using Euler methods, or complex, utilising RK solvers.

1.3.3 Compucell3D model makeup

Effective energy

Cellular Potts Models, as mentioned above, employ the effective energy to describe cell behaviour and interactions. All equations in the section can be found in more detail in (Izaguirre et al. [2004]). There are two different ways to portray the energy in the model: boundary energy or constraints. It is first prudent to look at the mechanism that describes cell adhesion. This is one of the most important descriptions in the model, as if cells did not bind together then complex structures and indeed intelligent life as we know it would not exist. Adhesion is defined by the boundary energy $J(\tau(\sigma), \tau(\sigma'))$, which is the boundary energy per unit area between two cells, (σ, σ'), of given types $(\tau(\sigma), \tau(\sigma'))$, at the boundary between two neighbouring pixels. This is then calculated by summing over all neighbouring pairs of lattice sites, i and j:

$$H_{\text{boundary}} = \sum_{\substack{i,\,j \\ \text{neighbours}}} J(\tau(\sigma(\vec{i})), \tau(\sigma(\vec{j})))(1 - \delta(\sigma(\vec{i}), \sigma(\vec{j}))). \tag{1.3.4}$$

The second method of energy use in the model is by way of constraints on cell behaviour. Constraints are written in a general elastic form and are represented by:

$$H_{\text{constraints}} = \lambda(\text{value} - \text{target}_{\text{value}})^2. \tag{1.3.5}$$

As one can see, if the $value = target_{value}$ then the energy is zero and the constraint, known as the equilibrium condition, has been satisfied. The exponent, 2, establishes the elasticity of the constraint. This creates an ideal spring, which pushes on the cells' effective energy. By minimising the effective energy and utilising this idealised spring, CompuCell3D will drive the constraint to equilibrium. However, due to the stochastic nature of the simulations, the condition does not always have to be met, creating two or more possible constraint conflicts where the constraints are partially met, resulting in random fluctuations. The spring constraint (a positive real number), represented by λ, determines how far the value can deviate from the target. Large values of λ will result in a larger effective energy change, essentially preventing a flip, whereas small values allow for much more deviation from the equilibrium condition.

Constraint energy has also been implemented to restrict the size of a

cell to a specified target volume. CompuCell3D models cells' volume at any given time, as well as their surface area. A volume constraint is employed to restrict volume variations of generalised cells from their target volumes, modelled by:

$$H_{\text{vol}} = \sum_{\sigma} \lambda_{\text{vol}}(\sigma)(v(\sigma) - V_t(\sigma))^2, \tag{1.3.6}$$

where $\lambda_{\text{vol}}(\sigma)$ is the inverse compressibility of the cell, $v(\sigma)$ is the number of pixels in the cell and $V_t(\sigma)$ is the cell's target volume in pixels. The internal pressure inside the cell is $P \equiv -2\lambda(v(\sigma) - v_t(\sigma))$. A positive internal pressure in a cell is produced when $v < V_t$ whereas, when $v > V_t$ there is a negative internal pressure.

The surface area constraint is given by:

$$H_{\text{surf}} = \sum_{\sigma} \lambda_{surf}(\sigma)(s(\sigma) - S_t(\sigma))^2, \tag{1.3.7}$$

where; $s(\sigma)$ is the surface area of the cell, σ; D_t is the cell's target surface area; and $\lambda_{\text{surf}}(\sigma)$ is its inverse membrane compressibility.

By adding together the boundary and volume constraints, from equations (1.3.4) and (1.3.6), the basic GGH effective energy is obtained:

$$H_{\mathrm{GGH}} = \sum_{\substack{i,\,j \\ \text{neighbours}}} J(\tau(\sigma(\vec{i})), \tau(\sigma(\vec{j})))(1 - \delta(\sigma(\vec{i}), \sigma(\vec{j}))) + \sum_{\sigma} \lambda_{\mathrm{vol}}(\sigma)(v(\sigma) - V_t(\sigma))^2. \tag{1.3.8}$$

A Monte-Carlo step

CompuCell3D measures time in a simulation by Monte-Carlo Steps, which indicate when every pixel on the lattice has made an index-copy attempt. Each index-copy attempt begins by the software randomly selecting a lattice site, which is chosen as the target pixel, $\vec{i}$. A neighbouring lattice site is then chosen to be a source pixel, namely $\vec{i'}$. An attempt is then made to flip the target pixel, governed by the effective energy, to the same generalised cell as the source pixel, increasing the volume of the source cell and decreasing the volume of the target cell. Cells that belong to the same cell, i.e. $\sigma(\vec{i}) = \sigma(\vec{i'})$, do not need to attempt a flip and the effective energy will not be calculated. Index copies are governed by a probability where:

$$P(\sigma(\vec{i}) \to \sigma(\vec{i'}) = \begin{cases} exp(-\Delta H/T_m), & \Delta H > 0, \\ 1, & \Delta H \leq 0, \end{cases} \tag{1.3.9}$$

where ΔH is the change in effective energy and T_m is the effective cell motility (or the amplitude of cell membrane fluctuations). The classical GGH implements a modified version of a classical stochastic Monte-Carlo pattern-evolution dynamics, called Metropolis dynamics with Boltzmann acceptance

function, displayed in equation 1.3.9. If the change in the effective energy is less than or equal to zero, then the index copy attempt will be successful. Moreover, if it is greater than zero the attempt may still be successful with the probability $exp(-\Delta H/T_m)$. Time can be converted here from the MCS by the average of parameters, ΔH and T_m.

Chapter 2

A Mathematical Model of Immune and Tumour Cell Interactions

2.1 Introduction

In this chapter, an individual-based mathematical model of a simplified biological process, whereby a nascent tumour, attacked by a host immune system, will be examined. Specifically, the potency of tumour infiltrating cytotoxic lymphocytes (TICLS) will be investigated when in interaction with a tumour population. This work will be based on Kuznetsov and Stepnova [1992]; Matzavinos et al. [2004]; Matzavinos and Chaplain [2004]; Al-Tameemi et al. [2012].

Having studied the models by Matzavinos et al. [2004]; Matzavinos and Chaplain [2004]; and Al-Tameemi et al. [2012], what can be seen is that the

use of ODE and PDE models, give an overall assessment of the underlying kinetics in a given system. However, both of these have weaknesses. In an ODE model there are no spatial components therefore everything is assumed to be well mixed, causing a lack of cell structure. Although PDE models include a spatial awareness, they do not incorporate important biological features such as cell-cell interactions, intracellular behaviour and individual cell properties. When numerically solving a PDE model, the results give an overall approximation of cell density throughout the whole domain, however they do not indicate key tumour-immune cell interactions. However, ODE and PDE models are a viable approach for mathematicians and biologists to replicate long term effects in a biological system, if armed with the correct mathematical structure.

An example of this is in Matzavinos et al. [2004], where the presence of a limit cycle gives the appearance of a dormant steady state and drives the results. However, this is a quite well known phenomenon within reaction-diffusion equations, therefore is this of biological relevance or is it a result of the mathematics? To answer this question, and to try and include more of the tumour-immune micro-environment, a good approach would be to create an individual-cell based model.

Individual based models enable the tracking of individual cells and key aspects of cellular behaviour. They allow the inclusion of: adhesion; motility; mitosis; growth; competition for space; shape; size; interactions between cells; intracellular signalling; secretion of chemoattractants and chemorepellents; and the effects of oxygen concentrations e.g. hypoxia and epithelial mesenchymal transition. The individual based model will be analysed using

"CompuCell3D", a modelling software environment and PDE solver. The software was developed to help researchers model materials without having to create their own code. CompuCell3d competently models key aspects of tumour-immune interactions. Therefore, in this chapter, an individual based model will be undertaken, giving a better understanding of the biological properties in cancer dormancy.

2.2 Mathematical model

This section will discuss the original findings from Matzavinos et al. [2004] and the formulation of the individual based model. It is hoped that the CompuCell3D model will be able to mimic the results of the PDE model found in Matzavinos et al. [2004], showing the three Es of immunoediting: elimination, equilibrium and escape.

Matzavinos et al. [2004] investigated the use of tumour infiltrating cytotoxic T-lymphocytes (TICLs) to eliminate a nascent tumour, using both homogeneous and heterogeneous equation systems. The original model involved a chemokine, which elicited a chemotactic response by the immune cells towards the tumour cells. The model was based on the schematic in Figure (2.1).

Figure (2.1) shows the original model kinetics where, a TICL (E) binds with a tumour cell (T) to form a TICL-tumour cell complex (C) at rate k_1, with the reverse reaction at rate k_{-1}. The complex (C) then breaks down to leave either a tumour cell and an inactivated TICL (E^*), at rate $k_2(1-p)$, or a TICL and a 'programmed for lysis' tumour cell (T^*), at rate $k_2 p$. Using

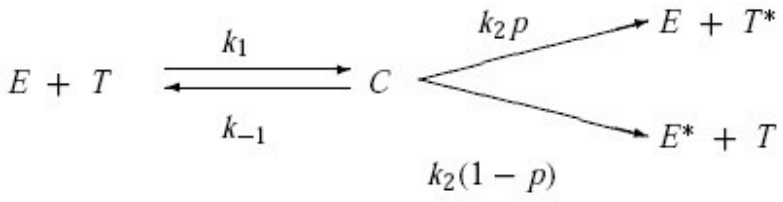

Figure 2.1: *Schematic of local interactions between the TICLs and tumour cells* in vivo. *Taken from Matzavinos et al. [2004] whereby full details can be found in Kuznetsov [1991]; Kuznetsov et al. [1994].*

the law of mass action on the scheme in Figure (2.1), adding spatial elements and non-dimensionalising, the heterogeneous PDE system was derived in Matzavinos et al. [2004] as:

$$\frac{\partial E}{\partial t} = \overbrace{\nabla^2 E}^{\text{random motility}} - \overbrace{\gamma\nabla(E\nabla\alpha)}^{\text{chemotaxis}} + \overbrace{\sigma h(x)}^{\text{supply}} + \overbrace{\frac{\rho C}{\eta + T}}^{\text{proliferation}} - \overbrace{\sigma E}^{\text{decay}} - \overbrace{\mu ET + \epsilon C}^{\text{local kinetics}}, \tag{2.2.1}$$

$$\frac{\partial \alpha}{\partial t} = \overbrace{\delta\nabla^2\alpha}^{\text{diffusion}} + \overbrace{\kappa C}^{\text{production}} - \overbrace{\epsilon\alpha}^{\text{decay}}, \tag{2.2.2}$$

$$\frac{\partial T}{\partial t} = \overbrace{\omega\nabla^2 T}^{\text{random motility}} + \overbrace{\beta_1(1-\beta_2 T)T}^{\text{logistic growth}} - \overbrace{\phi ET + \lambda C}^{\text{local kinetics}}, \tag{2.2.3}$$

$$\frac{\partial C}{\partial t} = \overbrace{\mu ET - \psi C}^{\text{local kinetics}}. \tag{2.2.4}$$

Zero flux boundary conditions were imposed and further details of the initial conditions can be found in Matzavinos et al. [2004].

When solving the PDE system numerically, using the computer solver "PDEPE" in "Matlab", a train of solitary like waves of tumour cells, was seen to be invading the tissue. This occurred when the probability of a TICL killing a tumour cell, p, was in a certain range. Moreover, a linear stability

analysis of the homogeneous system (from system (2.2.1)-(2.2.4)) was undertaken and a limit cycle was found. A bifurcation analysis was performed to investigate the appearance of the limit cycle. By solving numerically the ODE system, it was found that for p less than a critical value (approximately 0.9906), the limit cycle will disappear and all the orbits that correspond to non-heterogeneous solutions converge to a tumour invasive steady state. If p is above the critical value, the limit cycle becomes apparent through a subcritical Hopf birfurcation, common to dynamical systems (Sherratt et al. [1997]). In a follow up paper, Matzavinos and Chaplain [2004], a travelling wave analysis of system (2.2.1)-(2.2.4) was undertaken and a 1-D heteroclinic connection was found using the transversality theorem of Guckenheimer and Holmes (Guckenheimer and Holmes [1983]).

2.2.1 Individual-based model

This chapter will focus on an individual mathematical model, implemented to investigate the individual interactions of TICLs and tumour cells, to try and get similar qualitative results as the findings of the PDE model in Matzavinos et al. [2004]. It will have similar basic kinetics as the one shown in Figure (2.1). The extension of this work into an individual-based model allows the introduction of more biologically relevant information with a hope to enrich the validation of the results.

The technique that will be implemented to analyse the model will be the Cellular Potts Model (CPM) (or Glazier-Graner-Hogeweg (GGH) Model). It is important to realise that there is a force (F) and cell velocity (v) relation-

ship in the cell environment due to its highly viscous nature. The cellular potts model embeds a linear $F - \nu$ relation into a stochastic computational algorithm by minimising energy through the use of the Modified Metropolis Algorithm, and allows the use of experimental data to be used as parameter values (Powathil et al. [2013]). Further details of the workings of CompuCell3D can be found in Chapter 1.3.

The CPM was implemented in the computer software system CompuCell3D, an open source computer system (Swat et al. [2012]). In the simulation a 200x200 pixel 2D grid lattice has been utilised. The model represents each cell by a user defined set of pixels which contain the same index attributed to the specific cell type.

In order to mimic the dynamics of the system in Matzavinos et al. [2004], the CPM model utilises different aspects of CompuCell3D. Cells that are involved in this model are immune cells and tumour cells. Within the model, healthy tissue, represented by a block of cells, which are called "medium cells", is considered to be homogeneous. It is known that a cell is roughly between $10\mu m$-$20\mu m$ in diameter (Alberts et al. [2008]). A newly divided cell is determined to be $10\mu m$ and will not be allowed to divide until it has reached $20\mu m$. Each pixel in CompuCell3D can belong to any cell type. The size of each cell in CompuCell3D is modelled by first assuming that each newly divided cell is made up of 5x5 pixels, and that each pixel represents a square element of a cell that is $2\mu m$ x $2\mu m$, giving a total area of $4\mu m^2$. The model begins with a central 5x5 cell tumour mass and 4 randomly placed single immune cells in the domain. It also has a nutrient that would be available within the biological domain, such as oxygen, for the cells to feed

from. It is important to note that there are no chemotactic effects in this model, and therefore, cellular motility is random.

Mitosis occurs when a proliferating tumour cell grows to a critical size and then divides along a randomly orientated axis. Tumour cells try to reach maximum size of 50 pixels, before they divide into two daughter cells. This, however, is determined by how much available oxygen there is for the tumour cell. The tumour cell grows every Monte Carlo Step, by a different amount each time, determined by how much oxygen is available within the tumour cell. The oxygen concentration is calculated and the result is then added to the size of the tumour cell $\times$ 0.1. The tumour growth rate (TGR) is, therefore:

$$TGR = 0.1 \times \text{concentration of oxygen at proliferating tumour cell core.} \tag{2.2.5}$$

This allows tumour cells at the edge of the proliferating rim to grow much faster than those in the middle. If the oxygen goes below a critical level, the proliferating tumour cells turn quiescent. In this state, they have the ability to turn back into a proliferating cell if they can gain enough oxygen but they do not divide. If the quiescent cell's oxygen level falls below a level to which the cell cannot sustain its functions, the cell becomes necrotic and is allowed to disintegrate. Dead cells only disintegrate when in exposure with the medium. Initially, when the model was first written, the tumour cells were allowed to grow by one pixel every MCS, as long as the oxygen

at their core was enough to be a tumour cell. It provided no relationship between the oxygen level and cell growth and created exponential tumour cell proliferation, leading to the oxygen level being implemented as described above.

Immune cells do not divide and are supplied to the domain at a constant rate of 1 per 25 MCS, provided there is enough space in the medium. This is meant to mimic the process, in the body, where cytokines are sent by immune cells to signal and recruit more immune cells, in order to target the foreign object.

The migration rate in CompuCell3D determines how far a cell can move in each MCS, corresponding with the parameter μ. Each cell has a random orientation for each individual cell type, with immune cells having a faster capability than tumour cells. Quiescent and necrotic cells do not move unless pushed by a different cell type or by adhesion.

The nutrient in the model is represented by a partial differential equation, which is solved using the DiffusionSolverFE steppable in CompuCell3D. Nutrient in this model has been identified as oxygen and is supplied to the domain at a constant rate, secreted by the medium cells. Oxygen diffusion in the domain is "zero flux" at the boundary and is modelled by the PDE:

$$\frac{\partial c}{\partial t} = D\nabla^2 c - kc + secrection,$$

where D is the diffusion rate and k is the decay rate. k represents the uptake

of oxygen in a given cell with rates:

$$k = \begin{cases} 0.5, & \text{in the tumour cells} \\ 0.25, & \text{in the quiescent cells} \\ 0.5, & \text{in the immune cells} \\ 0, & \text{in the necrotic cells} \\ 0, & \text{in the dead immune and dead tumour cells.} \end{cases} \tag{2.2.6}$$

Within proliferating tumour and immune cells, the uptake of oxygen is much higher than quiescent tumour cells. The tissue, in this model, does not uptake oxygen but instead secretes it. Necrotic cells do not uptake oxygen. Hypoxic and necrotic effects of cells are not taken into consideration.

CompuCell3D allows the user to specify adhesion properties of cells. In this model, immune cells do not adhere to one another, whereas medium cells adhere strongly. Proliferating tumour cells adhere to each other, but not as strongly as immune cells adhere to proliferating tumour cells, allowing tumour cells to break free and form new tumour masses, locally. Immune cells do not adhere to necrotic and quiescent cells, however, tumour cells do, but much less than they do to themselves. Cells lysed by either tumour or immune cells adhere weakly to tumour cells. This can sometimes create a small wall of debris for the immune cell to have to work its way through before getting to a proliferating tumour cell, enhancing tumour cell growth.

When an immune cell comes into contact with a proliferating tumour cell there are two different outcomes: the immune cell kills the proliferating

tumour cell or the proliferating tumour cell kills the immune cell. This is the same basic killing method that is utilised in Matzavinos et al. [2004]. The dead cell is then allowed to disintegrate, again only when in contact with the medium. The control parameter p from Matzavinos et al. [2004] has been implemented into this model and is used to determine the probability of an immune cell killing a tumour cell. The age of the tumour cells does not come into consideration, as one of the main trademarks of cancer is that tumour cells evade apoptosis. This mechanism in cells is very important. When "healthy" cells go through the cell cycle, if there are issues at any of the stages, the cell will undergo programmed death, preventing any mutations that may arise. However, because cancer cells are able to avoid apoptosis the tumour cells will be able to divide, despite damage to DNA, into mutated daughter cells. In this model, therefore, the only way a tumour cell can be killed is by an immune cell or by cellular degradation, known as "necrosis". Necrosis occurs when there is a lack of oxygen for the cancer cell to survive. Immune cell death by lysis has been omitted in order to understand the underlying dynamics, however this would be a good extension to the model.

The simulations will run for a maximum of 50,000 MCS. The simulations, however, will stop if the immune cell kills all of the tumour cells and there are no quiescent cells left. It will also stop when the tumour cells kill all of the immune cells. Moreover, time can be implemented in a number of different ways. The most appropriate way for this model would be to take into consideration the average mitotic rate of a cancer cell. This is in the region of around 18-34 hours. For the purpose of this model, time is generic.

2.3 Results

The inidividual-based model, will aim to investigate the potency of T-lymphocytes, without chemotactic effects, on a latent tumour mass. As discussed in the previous section, oxygen will be made available in the tumour environment by tissue. When the oxygen levels in the tumour mass fall lower than certain threshold values, the tumour mass will form different "tumoural zones": the proliferating tumour rim, quiescent zone and necrotic zone.

Matzavinos et al. [2004] investigated a model, which described a pre-angiogenic tumour without a central necrotic core. The findings of this PDE model indicate that a dormant state can be found when the immune cells ($CD8^+$ T-lymphocytes) are suitably efficient at killing tumour cells. In using CompuCell3D, the hope is to get similar results qualitatively as the PDE model in Matzavinos et al. [2004], whereby a tumour mass is to be kept dormant by immune cells. However, by using an individual-based approach it allows the model to include more biological features of the tumour immune environment. The following results will again use $CD8^+$ T-lymphocytes as the effector cell. This section will focus on the results when implementing the model using CompuCell3D. The three elements of immunoediting will be investigated. This will be done by varying the success rate of the immune cells lysing tumour cells.

As one can see, from the previous section, there are slight differences in the basic model set up. Matzavinos et al. [2004] does not include different states of tumour cells and omits a central necrotic core. A tumour cell, in the individual-based model, also grows in relation to the amount of oxygen

concentration found at its core. The term in the model for the growth rate is multiplied by the oxygen concentration to determine how much the cell will expand by, at each growth step. This means that the cells on the outer rim of the proliferating tumour zone will grow much faster than the proliferating tumour cells on the border of the quiescent zone. In doing this, it adds a little more to the model, as rather than having a tumour cell constantly grow, no matter how much oxygen is available to it, it will have an added constraint. Also, this could be important if the model were to include the effects of hypoxia, however this has been omitted. For the figures in the results section, the colours of the cells are indicated next to their description in the following synopsis of the model in the next paragraph.

Initially, the model starts out with a central tumour mass (red) with four randomly placed immune cells (blue). The tumour mass is allowed to grow in relation to the oxygen level at its core and immune cells are constantly added to the system every 25MCS. Oxygen is secreted, at a constant rate, from the medium cells (grey) that represent the host tissue. As the model progresses, oxygen is used by the immune and tumour cells. Once the oxygen concentration goes below a threshold, the tumour cells turn quiescent (purple). Then, the quiescent cells either turn back to being proliferative, if the local tumour environment improves, or necrotic (black) if the oxygen levels are no longer sufficient to support it. It should also be noted, that the quiescent cells take up oxygen at half the rate of tumour cells. When an immune cell and tumour cell come into contact, their random motility is switched off, as is their ability to bind to another cell, meaning that the immune cells can only interact with one tumour cell at a time. Depending

on the outcome of this interaction, there will either be a dead immune cell (green) or a dead tumour cell (yellow). All dead cells disintegrate when they come into contact with the medium. It should also be pointed out that since this modelling technique is stochastic, results will vary every time a new simulation is undertaken, however a range of values will be given, showing a guide for each of the three sections of immunoediting.

2.3.1 Elimination-Immune destruction

In solving the model, cancer destruction by the immune system is possible in this idealised environment. As previously discussed, this is known as the elimination stage within the immunoediting description of immune-cancer interactions. In order for this to happen, the immune system needs to be very efficient at killing tumour cells. The results suggest that the immune cells must have a success rate of roughly 80% or more. This can be seen in Figures 2.2, 2.3 and 2.4.

At 80% immune success rate the immune cells seem to have the advantage over the tumour cells and usually kill off the tumour mass. Figure 2.2 represents the concentration of immune (blue) and tumour cells (red), Figure 2.3 shows the tumour and immune interactions, and Figure 2.4 represents the oxygen evolution over time. In Figure 2.2, the immune cells almost increase linearly, whereas the tumour cells have an oscillatory nature. Figure 2.3(a) depicts the tumour and immune cells at 200MCS, where a central cancer mass is present with surrounding immune cells. The tumour cells then grow and interact with the immune cells. This can be seen in Figures 2.3(b)-2.3(e).

Looking at Figures 2.3(b) and 2.3(c), the oscillatory nature of the tumour cell concentration can be seen, which is due to the tumour cells managing to regrow after waves of immune attack. By 10000MCS, in Figure 2.3(f), the immune cells have nearly successfully killed all the tumour cells and Figure 2.2 shows that the tumour cells' number are reduced to zero just after this Montecarlo Step. Figure 2.4 portrays the role oxygen concentration plays in this model. Initially, the tumour mass has enough oxygen to grow (Figure 2.4(a)), but as it gets larger, the tumour cells progress into a quiescent and then necrotic state, as the tumour environment can no longer support them (Figures 2.4(b)-2.4(e)). However, as the necrotic cells come into contact with the medium, they disintegrate and allow oxygen to flow into that area again.

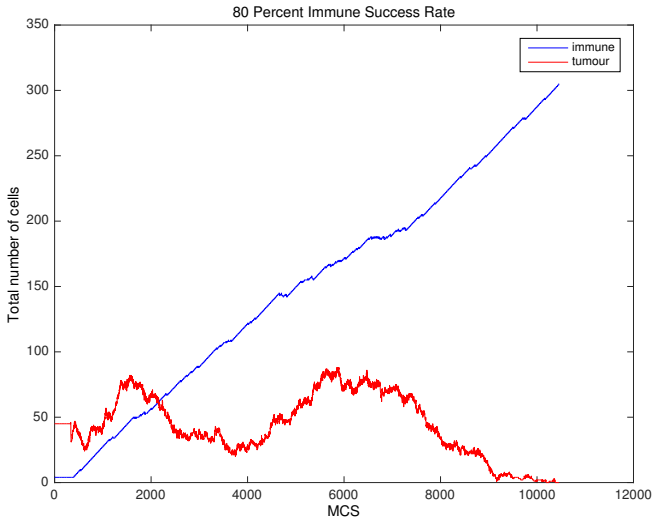

Figure 2.2: *Graph showing the total number of tumour and immune cells for 80% immune kill rate.*

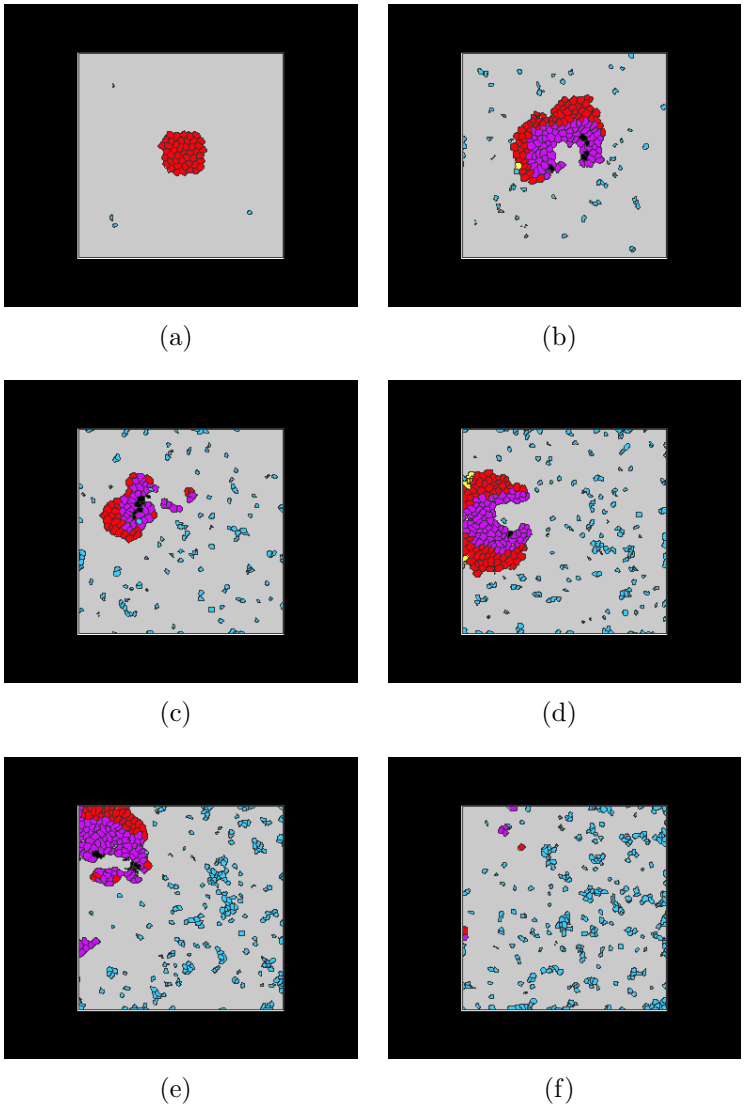

Figure 2.3: *Plots showing the growth of a tumour mass interacting with a host immune system. The types of cells and their corresponding colours in Figures 2.3(a)-2.3(f) are as follows: proliferative tumour cells in red, quiescent tumour cells in purple, necrotic cells in black, medium cells in grey, immune cells in blue, dead immune cells in green and lysed tumour cells in yellow, with the immune rate at 80%. Figures 2.3(a)-2.3(f) represent the model at 200MCS, 2000MCS, 4000MCS, 6000MCS, 8000MCS and 10000MCS respectively. The growth and oscillatory nature of the tumour mass is evident in Figures 2.3(b)-2.3(e). By 10000MCS the tumour mass is under control and will eventually be killed by the immune cells.*

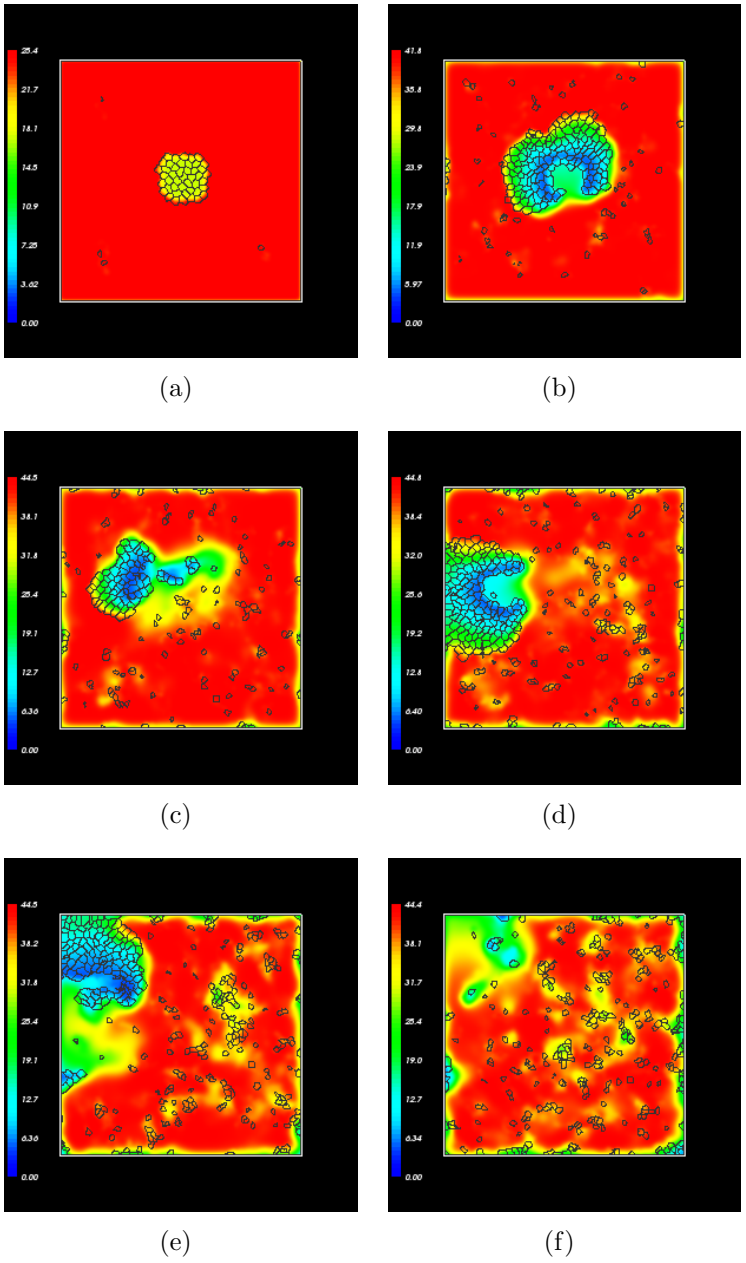

Figure 2.4: *Plots showing the oxygen concentration at times 200MCS, 2000MCS, 4000MCS, 6000MCS, 8000MCS and 10000MCS respectively with the immune rate at 80%. The oxygen concentration is high when it is red and low when it is blue. A bar on the left hand side of each picture represents the oxygen concentration. Oxygen is used up by the immune, tumour and quiescent cells, leaving areas where tumour cells can longer be supported, leading to necrosis. Once the necrotic cells have disintegrated, oxygen can flow into the area again via the medium cells.*

When building this model, the tumour cells, although adhering to each other, have been allowed to have random motility, in order for them to branch out and create new tumour mass sites. This is important as cancer does not follow a strict growth pattern nor does it stay uniform in nature, making resections and patient care plans very difficult. Looking at 2.5, it can be seen that for 80% to 83% immune success rate, elimination is possible. However, even at this high percentage, it isn't unusual for tumour cells to overcome the immune cells producing a cancerous state. As the results are stochastic in nature, there will be a new simulation with a new outcome every time, however the hope was to find a spectrum of results for each area of immunoediting. This unfortunately will not always bring about the correct results, as errors will always be found.

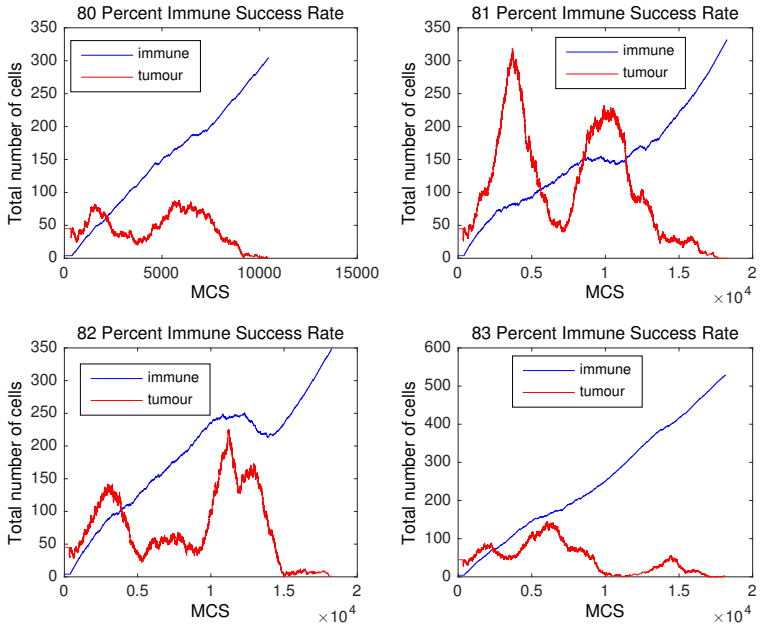

Figure 2.5: *Plots showing the total number of tumour and immune cells for 80-83% immune kill rate.*

2.3.2 Oscillatory Dynamics

The second type of dynamic, which the model is able to mimic, is tumour-immune equilibrium. Here, the tumour and immune cells have oscillatory dynamics. This is meant to represent the period of malignant dormancy within a patient. In order to obtain these dynamics, the success rate of the immune cells has been increased. What is evident from the results, is that there is a switching effect going on for certain values. At 72%, the tumour cells are still evading immune destruction, but then the dynamics change. At 73%, there is a slight tendency towards oscillatory dynamics, seen in Figure 2.6. The same can be said in Figure 2.7, for 77-80% immune kill success rate. Here, the dynamics are displaying similar results to Matzavinos et al. [2004].

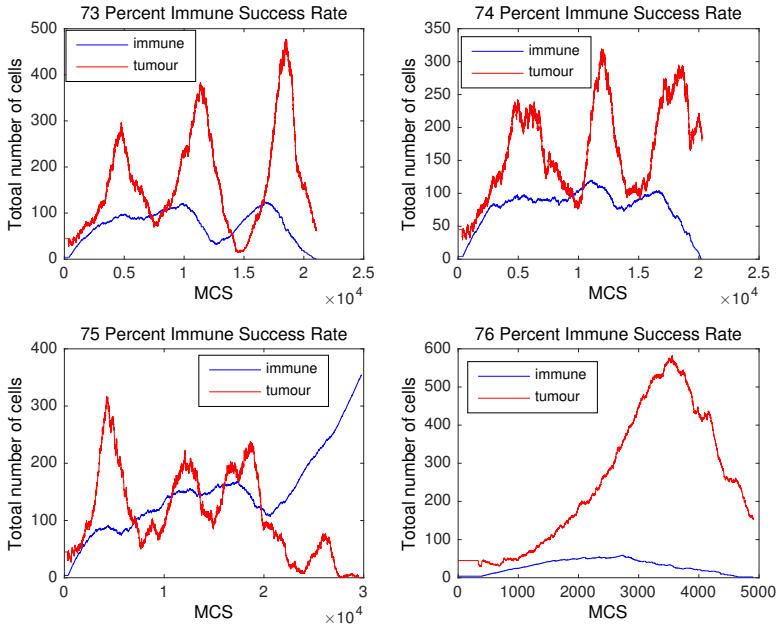

Figure 2.6: *Plots showing the total number of tumour and immune cells for 74-76% immune kill rate.*

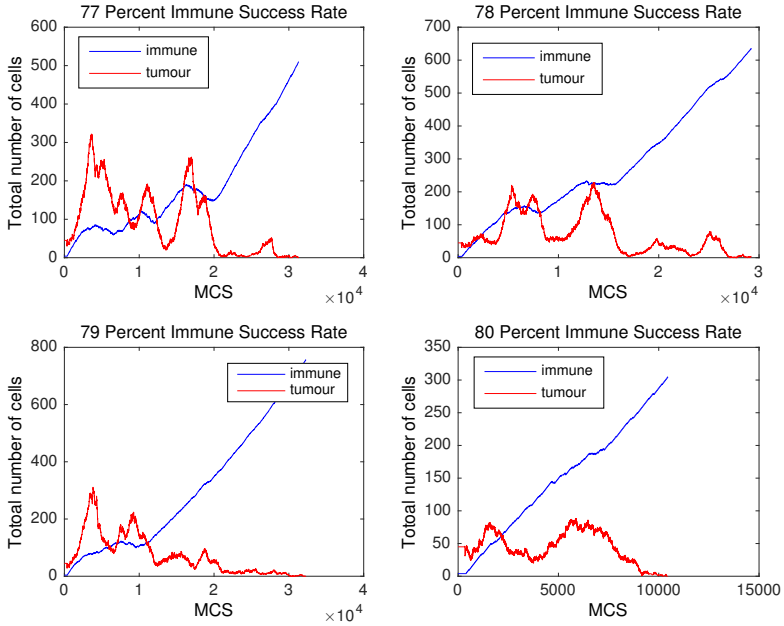

Figure 2.7: *Plots showing the total number of tumour and immune cells for 78-81% immune kill rate.*

It seemed prudent to look closer at the 75-78% immune success rate, in Figures (2.8)-(2.15), to see if a dynamic equilibrium can be found. These values were chosen as the system oscillates for a longer amount of MCS. What can be seen, is that the oscillatory dynamics last over a wide range of percentages. Looking at Figures 2.8-2.15, however, this does not always happen, as the tumour mass can often win, creating no oscillations. The 75-78 percentage range does yield the most abundant amount of equilibrium like dynamics however, even at 80 % immune success rate, this type of result can be seen. Looking at 75.9 % immune success rate in Figure 2.10, the simulation actually stops, however the immune and tumour cells are still battling each other. This could be seen as a possible steady state like dynamic. Another observation is that the oscillatory dynamics give a much better outlook for

the immune system, where the immune cells often win the battle. However, it is much nicer to look at some pictures of tumour cell growth to illustrate these points, captured in the next section.

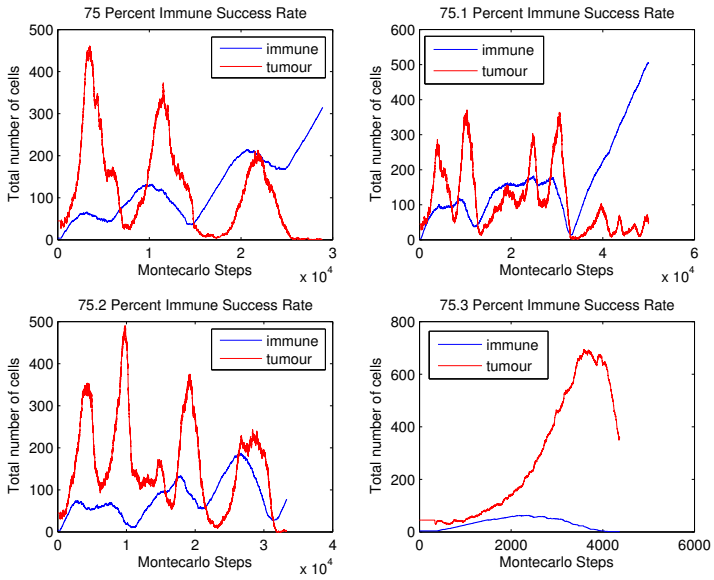

Figure 2.8: *Plots showing the total number of tumour and immune cells for 75-75.3% immune kill rate.*

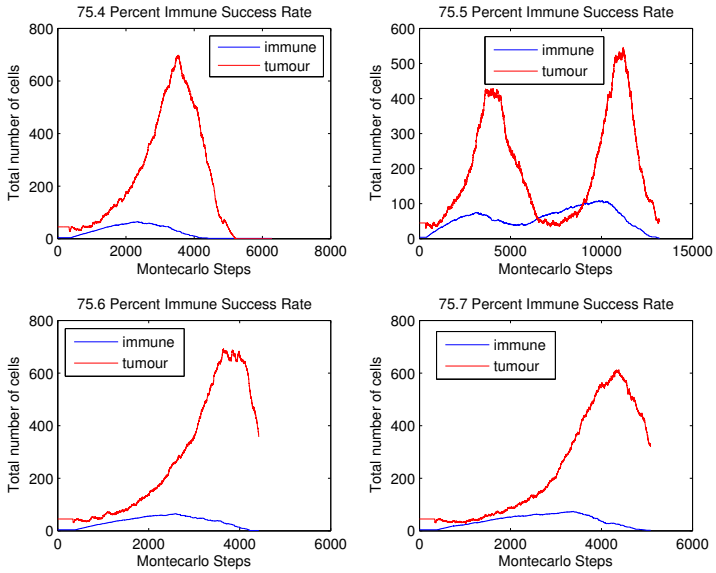

Figure 2.9: *Plots showing the total number of tumour and immune cells for 75.4-75.7% immune kill rate.*

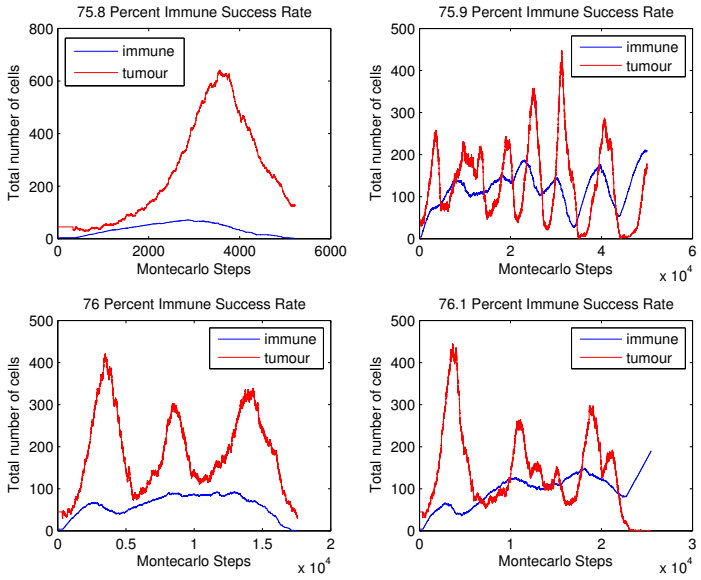

Figure 2.10: *Plots showing the total number of tumour and immune cells for 75.8-76.1% immune kill rate.*

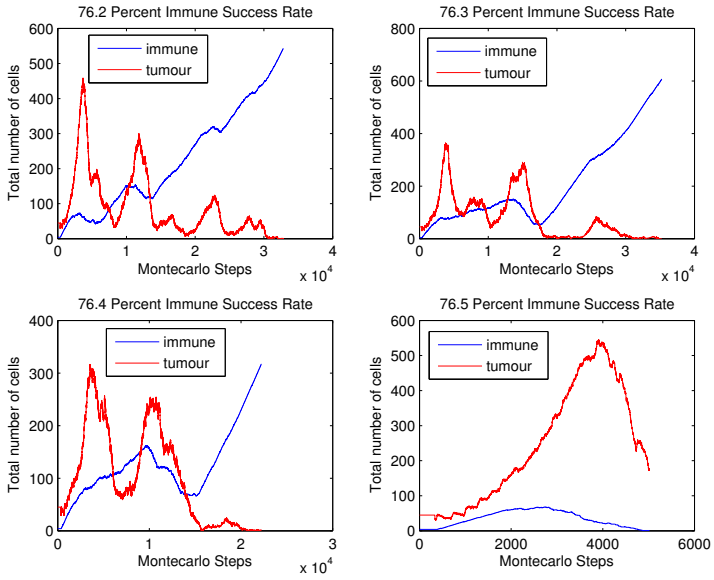

Figure 2.11: *Plots showing the total number of tumour and immune cells for 76.2-76.5% immune kill rate.*

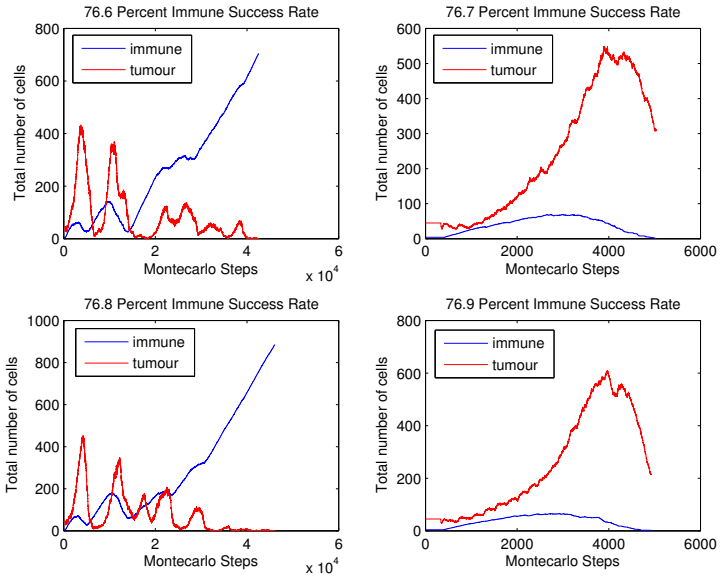

Figure 2.12: *Plots showing the total number of tumour and immune cells for 76.6-76.9% immune kill rate.*

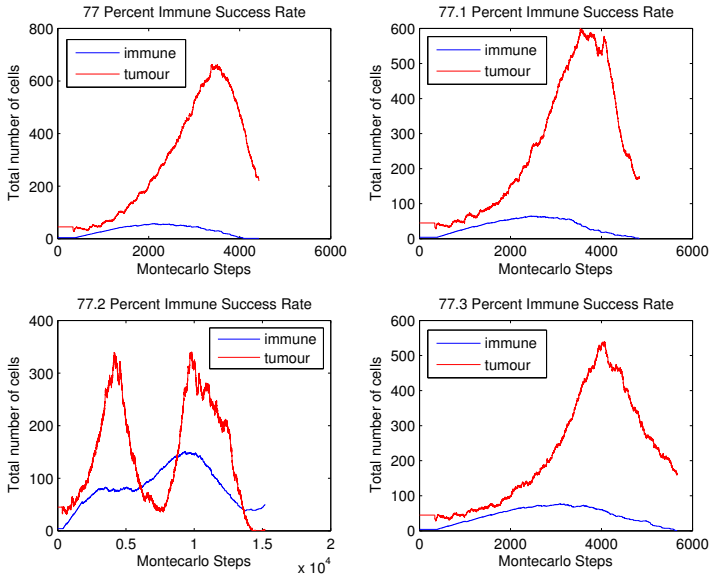

Figure 2.13: *Plots showing the total number of tumour and immune cells for 77-77.3% immune kill rate.*

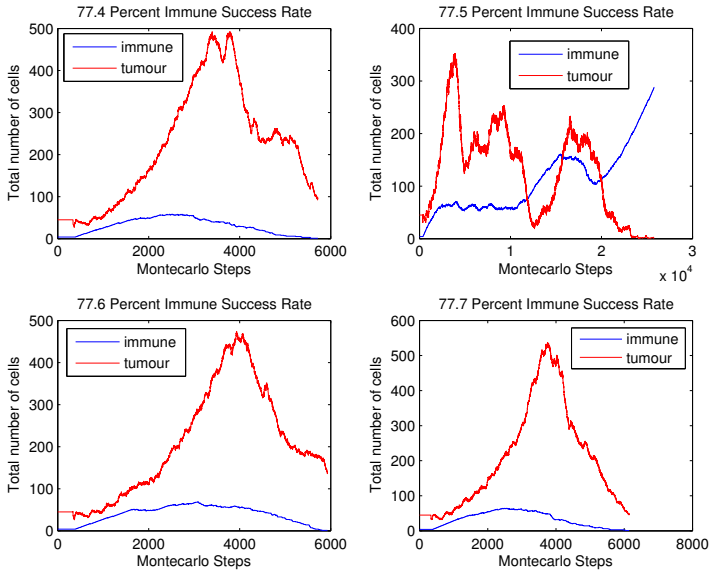

Figure 2.14: *Plots showing the total number of tumour and immune cells for 77.4-77.7% immune kill rate.*

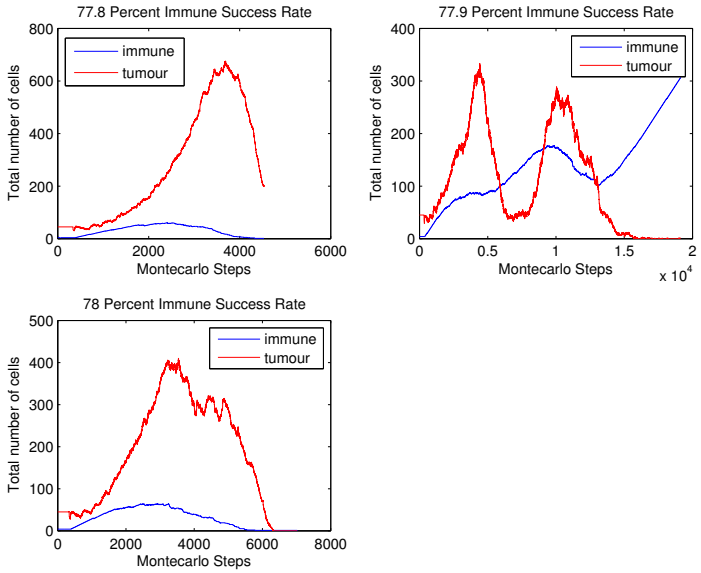

Figure 2.15: *Plots showing the total number of tumour and immune cells for 77.8-78% immune kill rate.*

Dormancy investigation

To look more closely at the dynamics needed for a equilibrium state to emerge, this section will focus on the values that show the change from tumour success to immune success. At 74% immune success rate, the immune cells and tumour cells are oscillatory in nature. The immune cells are mounting an attack, but unfortunately here the tumour growth is just too quick. This can be seen in Figures 2.16 and 2.17. At 77 % immune success rate however, the immune cells manage to overcome the tumour mass, seen in Figures 2.19 and 2.20.

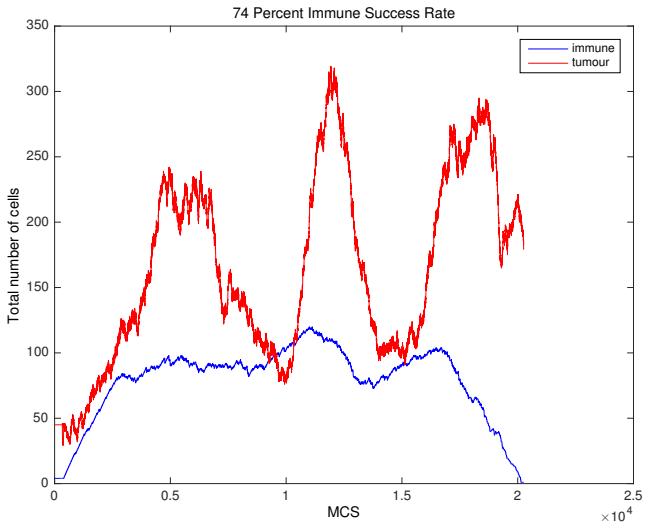

Figure 2.16: *Plots showing the total number of tumour and immune cells for 74% immune kill rate.*

While conducting these simulations, some observations were found regarding oxygen use and spatial restriction. Figures 2.18 and 2.21 represent oxygen concentration over time. In terms of space, the tumour can only use the oxygen available to it within the given domain. This has repercussions for

the tumour cells, as without a blood supply it will become necrotic, however, it also has negative effects for the immune assault.

What can be seen is that often the proliferating tumour cells are killed or nearly killed by the immune cells, however there is still a large residual quiescent and necrotic population, depicted in Figure 2.17(c) and 2.17(d), but more solidly in Figure 2.20(e). As oxygen is constantly supplied through the medium cells, the quiescent mass will be able to gain enough oxygen in order for them to become viable tumour cells again. This gives the tumour another lifeline, as the immune cells do not recognise, in this model, a quiescent cell as a threat. This quiescent mass can also prevent immune cells travelling to a more remote area of the domain, where tumour cells are proliferating, as they create a wall that the immune cell would find difficult to penetrate. Figure 2.20(c) is a good example of this. It is only when either the quiescent cells give way, by either creating a space due to their random motility or by becoming proliferative tumour cells again, that the immune cells can gain access to the tumour cells and attack. Therefore, the tumour has the ability to grow in a different region, which is slightly protected by either quiescent or necrotic cells, creating a new local tumour mass. If hypoxia were included in this model, the oxygen starved tumour would send signals in order to gain a blood supply. It also shows that it only takes either one quiescent cell or tumour cell to escape from the immune system, in a patient's body, for the tumour to re-grow and gain a hold. Even after resection, chemotherapy, radiotherapy or therapeutic drug therapy this may also be the case. In understanding this, patients who have been in remission for years, may not know their cancer is spreading and that the immune system is trying to

combat it, as small avascular tumours are undetectable. There is also the possibility that the tumour cells who have survived the first attack by the immune system, may undergo some phenotypic changes in order to avoid immune detection, leading to an advanced sub population of tumour cells.

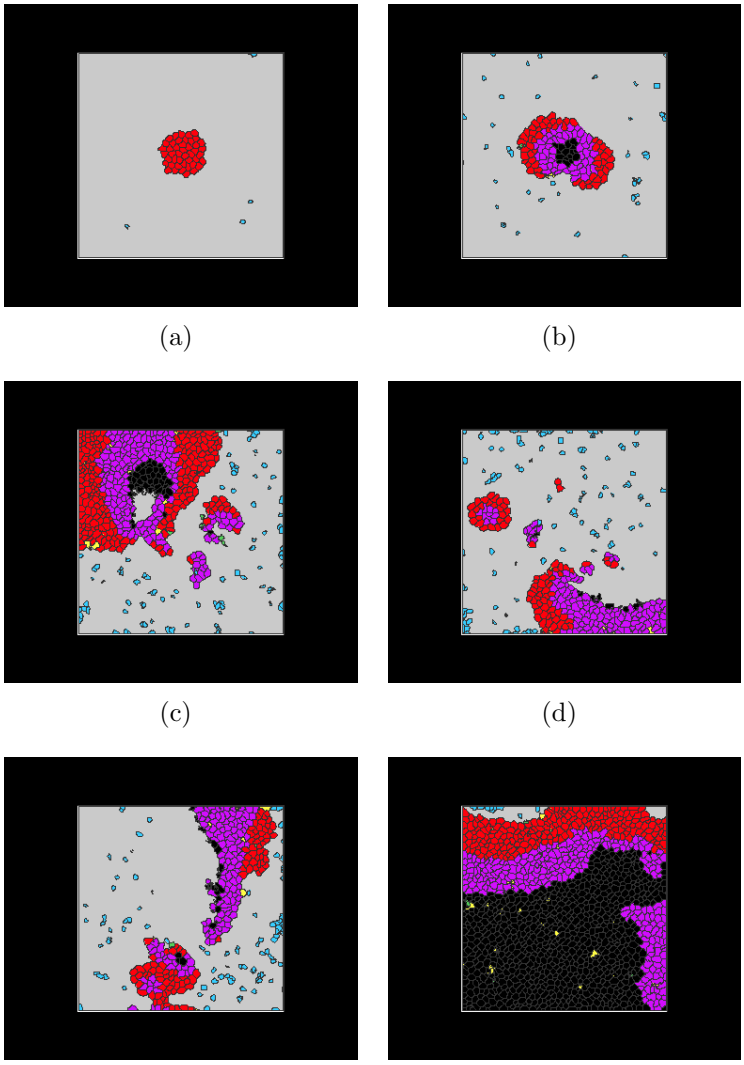

Figure 2.17: *Plots showing the growth of a tumour mass interacting with a host immune system. The types of cells and their corresponding colours in Figures 2.17(a)-2.17(f) are as follows: proliferative tumour cells in red, quiescent tumour cells in purple, necrotic cells in black, medium cells in grey, immune cells in blue, dead immune cells in green and lysed tumour cells in yellow, with the immune rate at 74%. Refer to Figure 2.16 for the overall cell concentrations. Figures 2.17(a)-2.17(f) represent the model at 200MCS, 1500MCS, 5000MCS, 10000MCS, 15000MCS and 20000MCS, respectively. Oscillatory dynamics are depicted here, whereby the tumour and immune cells try to battle for control. Here, the tumour completely floods the domain and evades the immune system.*

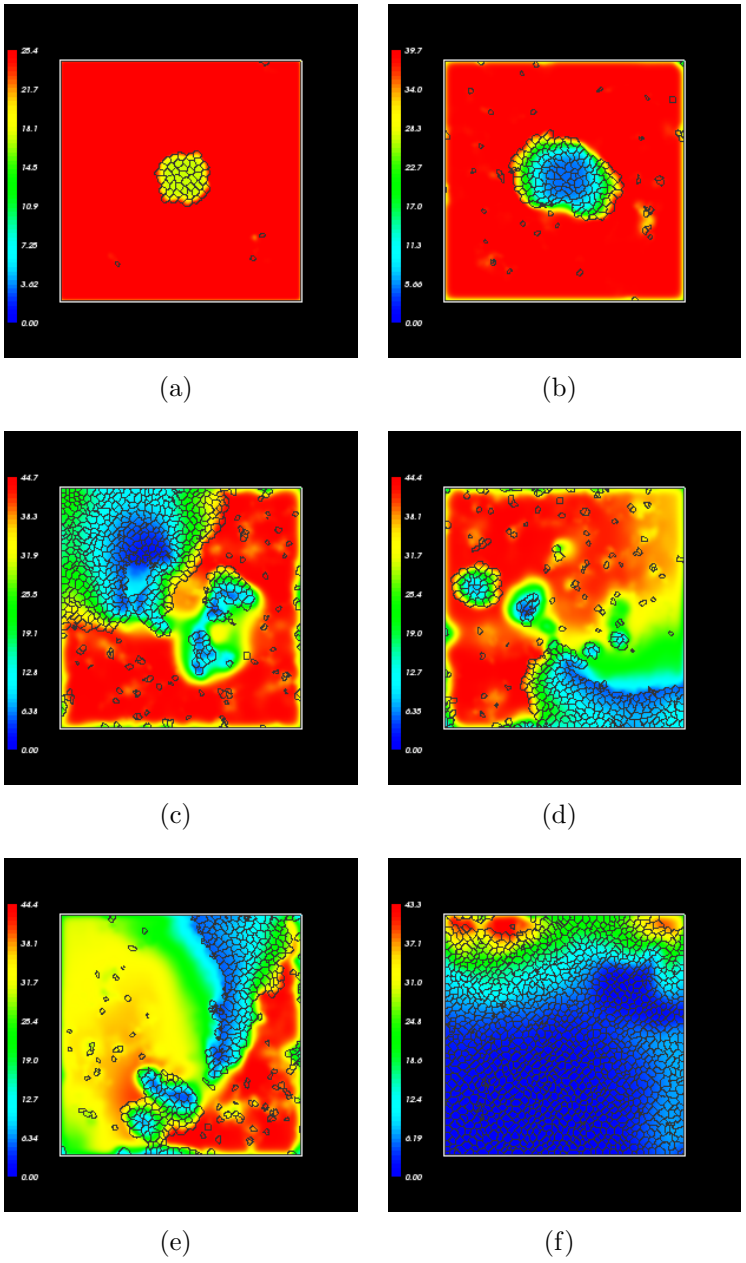

Figure 2.18: *Plots showing the oxygen concentration at times 200MCS, 1500MCS, 5000MCS, 10000MCS, 15000 MCS and 20000 MCS, respectively. Refer to Figure 2.16 for the overall cell concentrations where the immune cell success rate is 74%. The oxygen concentration is high when it is red and low when it is blue. A bar on the left hand side of each picture represents the oxygen concentration. Here, the tumour completely floods the domain and evades the immune system.*

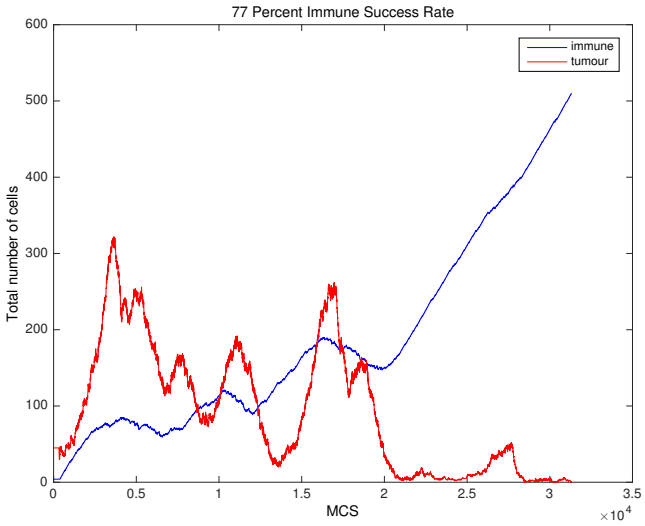

Figure 2.19: *Plots showing the total number of tumour and immune cells for 77% immune kill rate.*

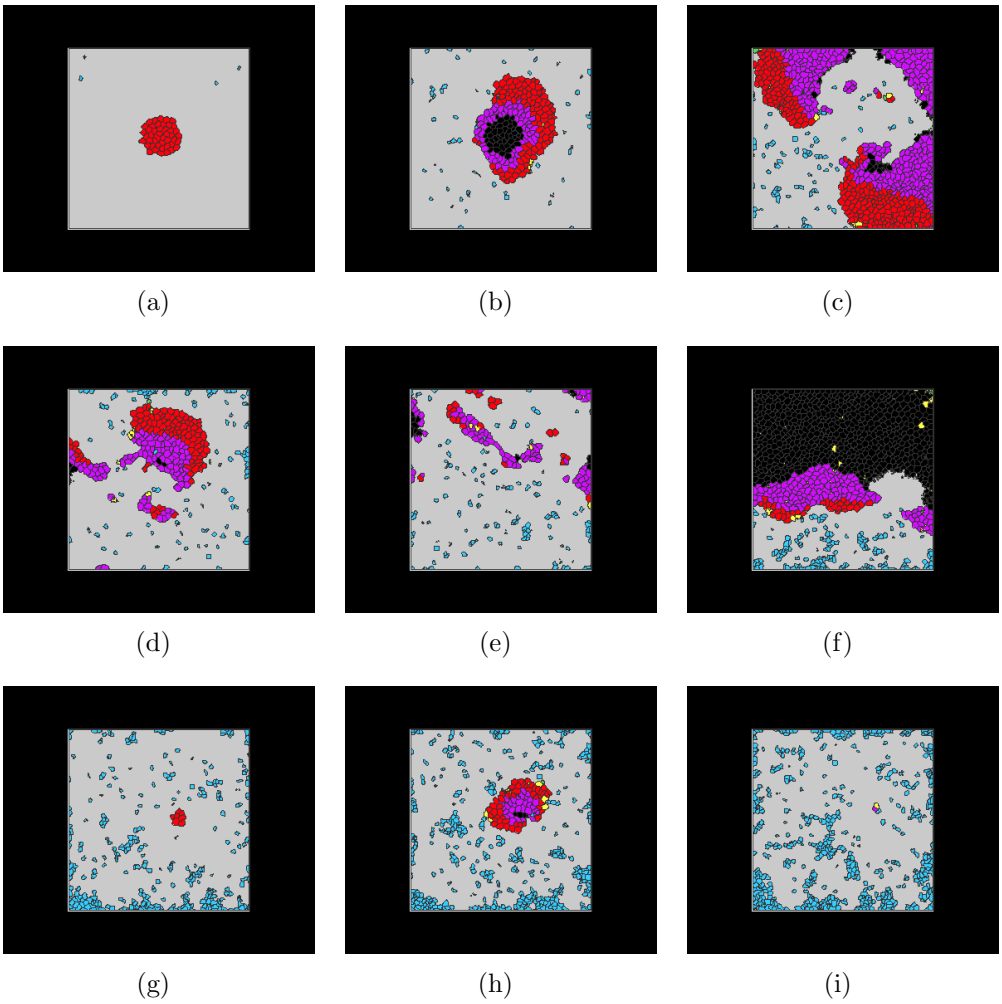

Figure 2.20: *Plots showing the growth of a tumour mass interacting with a host immune system. The types of cells and their corresponding colours in Figures 2.20(a)-2.20(i) are as follows: proliferative tumour cells in red, quiescent tumour cells in purple, necrotic cells in black, medium cells in grey, immune cells in blue, dead immune cells in green and lysed tumour cells in yellow. Figures 2.20(a)-2.20(i) represent the model at 200MCS, 1000MCS, 5000MCS, 10000MCS, 13700MCS, 20000MCS, 25000MCS, 27700MCS and 313000MCS, respectively. Refer to Figure 2.19 for the overall cell concentrations when the immune success rate is at 77%. Oscillatory dynamics are depicted here, whereby the tumour and immune cells try to battle for control. However, this time the tumour cells are destroyed by the host immune system.*

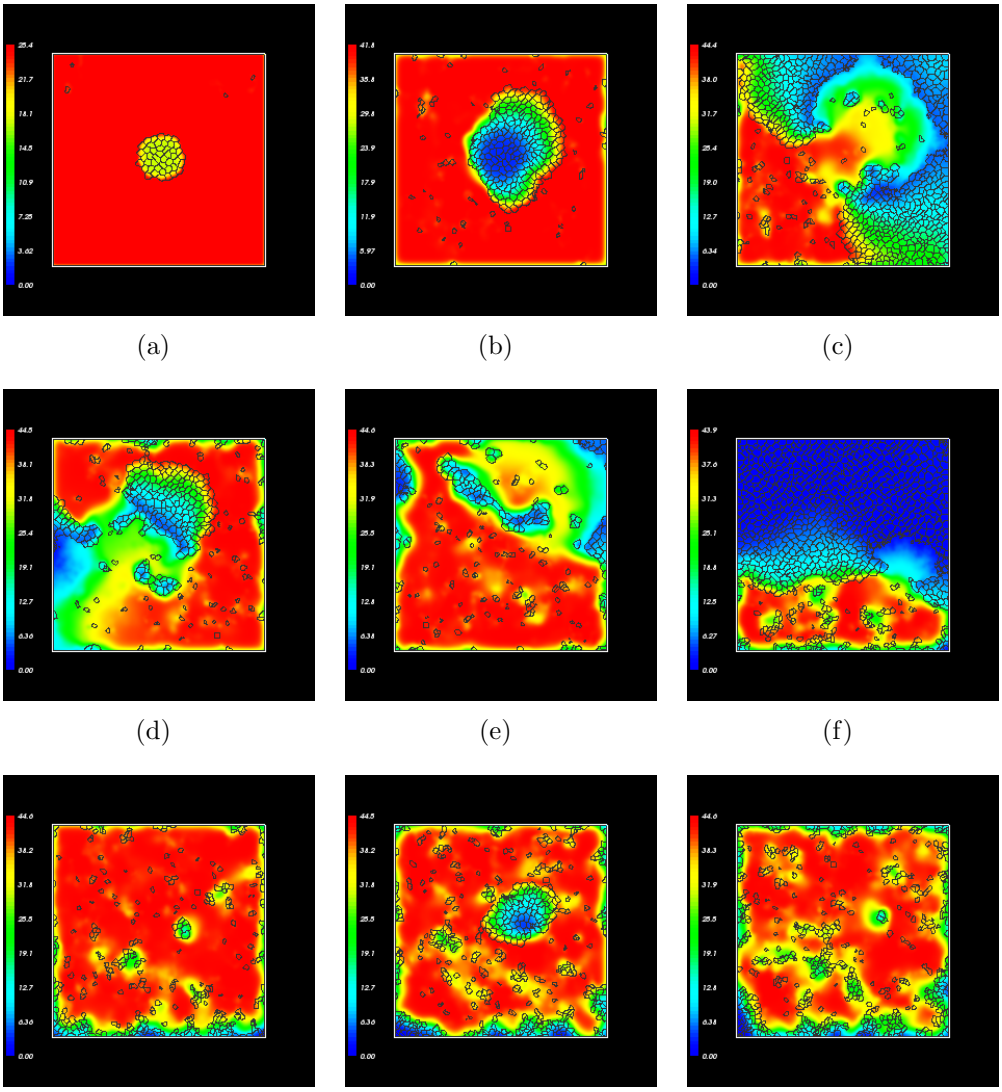

(a) (b) (c)

(d) (e) (f)

(g) (h) (i)

Figure 2.21: *Plots showing the oxygen concentration at times 200MCS, 2000MCS, 5000MCS, 10000MCS, 13700MCS, 20000MCS, 27700MCS AND 31300MCS, respectively. The oxygen concentration is high when red and low when blue. A bar on the left hand side of each picture represents the oxygen concentration. Refer to Figure 2.19 for the overall cell concentrations when the immune success rate is at 77%. Oscillatory dynamics are depicted here, whereby the tumour and immune cells try to battle for control. However, this time the tumour cells are destroyed by the host immune system.*

2.3.3 Immune evasion

The last "E" in immunoediting is "Immune Evasion". Here, the tumour cells successfully evade immune destruction when the success rate of the immune cells is roughly less than 73%, shown in Figure 2.22. Figures 2.23, 2.24 and 2.25 represent the model at 70% immune success rate. It is important to note that, looking at Figure 2.23, the tumour cells (red) peak to a certain level and then start to decrease. This is due to the domain being filled by tumour cells, which then turn quiescent, due to the lack of oxygen within the system. If no tumour cells, quiescent cells or immune cells remain in the domain the simulation stops. If the immune cells go to zero, the tumour has gained control. If a blood supply was added it would continue to grow, enter the blood stream and possibly begin to metastasise within the body.

Figure 2.24 shows the growth of a tumour mass over time while under attack from a host immune system. Here, the immune system does not have sufficient enough power to overcome the tumour and it floods the domain. In this figure, one can see the different zones of the tumour very well. As the tumour growth progresses, a quiescent zone forms, followed by a necrotic core. Once all the oxygen has been used up in the system, all the cells will become necrotic. In reality this wouldn't happen, as the tumour mass would try and gain a blood supply to fuel its growth. Oxygen evolution can also be seen in Figure 2.25.

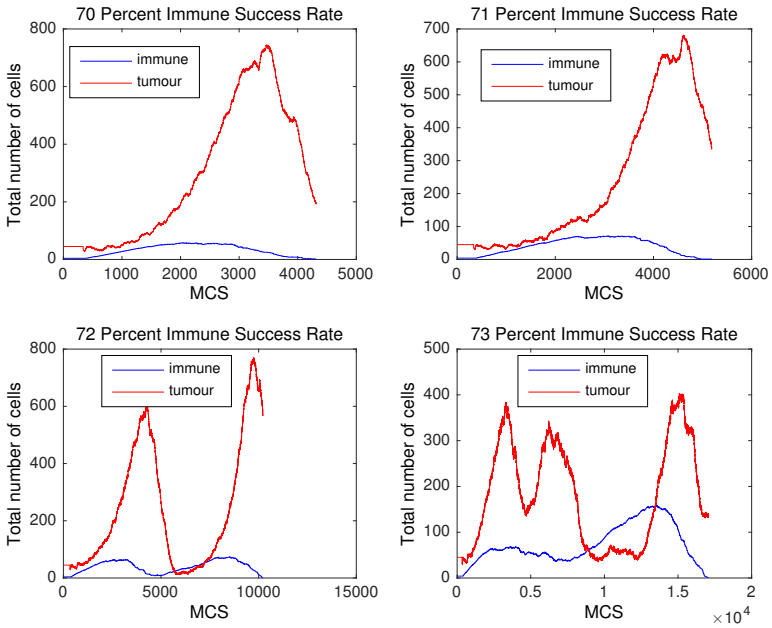

Figure 2.22: *Plots showing the total number of tumour and immune cells for 70-73% immune kill rate.*

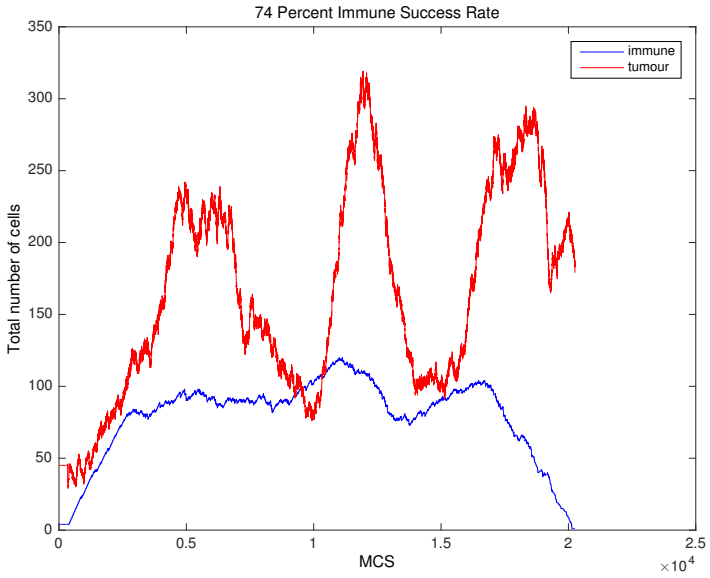

Figure 2.23: *Plots showing the total number of tumour and immune cells for 74% immune kill rate.*

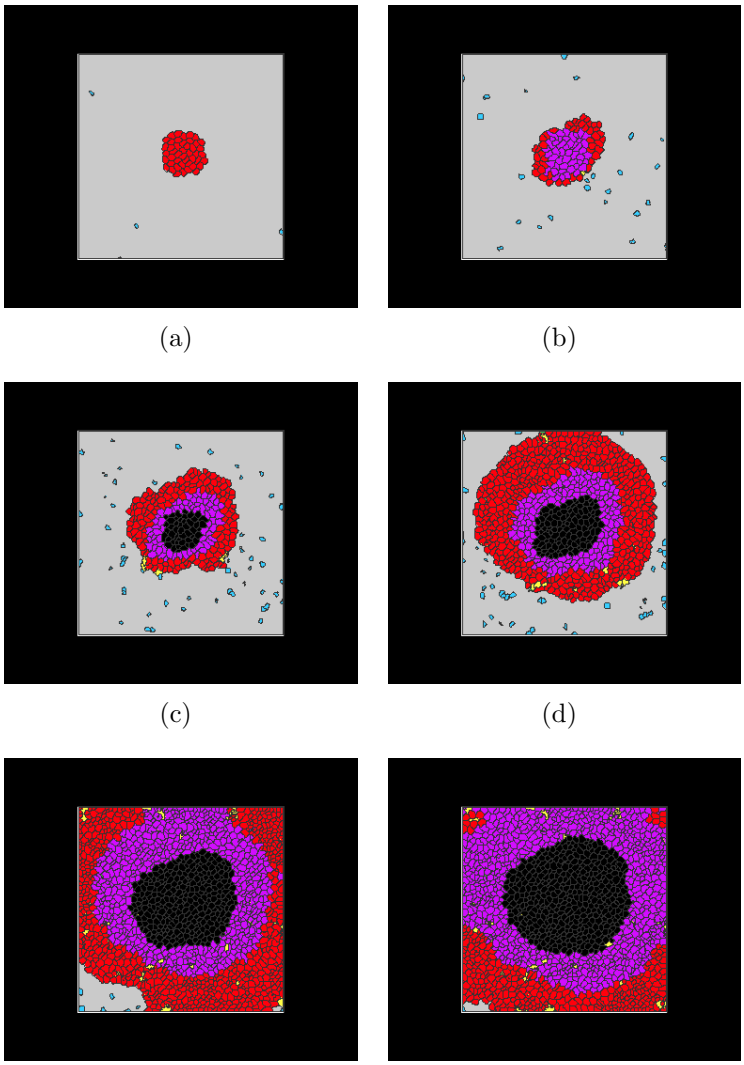

Figure 2.24: *Plots showing the growth of a tumour mass interacting with a host immune system. The types of cells and their corresponding colours in Figures 2.24(a)-2.24(f) are as follows: proliferative tumour cells in red, quiescent tumour cells in purple, necrotic cells in black, medium cells in grey, immune cells in blue, dead immune cells in green and lysed tumour cells in yellow. Figures 2.24(a)-2.24(f) represent the model at 200MCS, 1000MCS, 2000MCS, 3000MCS, 4000MCS and 4400MCS, respectively at 70% immune success rate. The growth of the tumour mass is evident in Figures 2.24(a) and 2.24(f). By 4400MCS the tumour mass has completely taken control.*

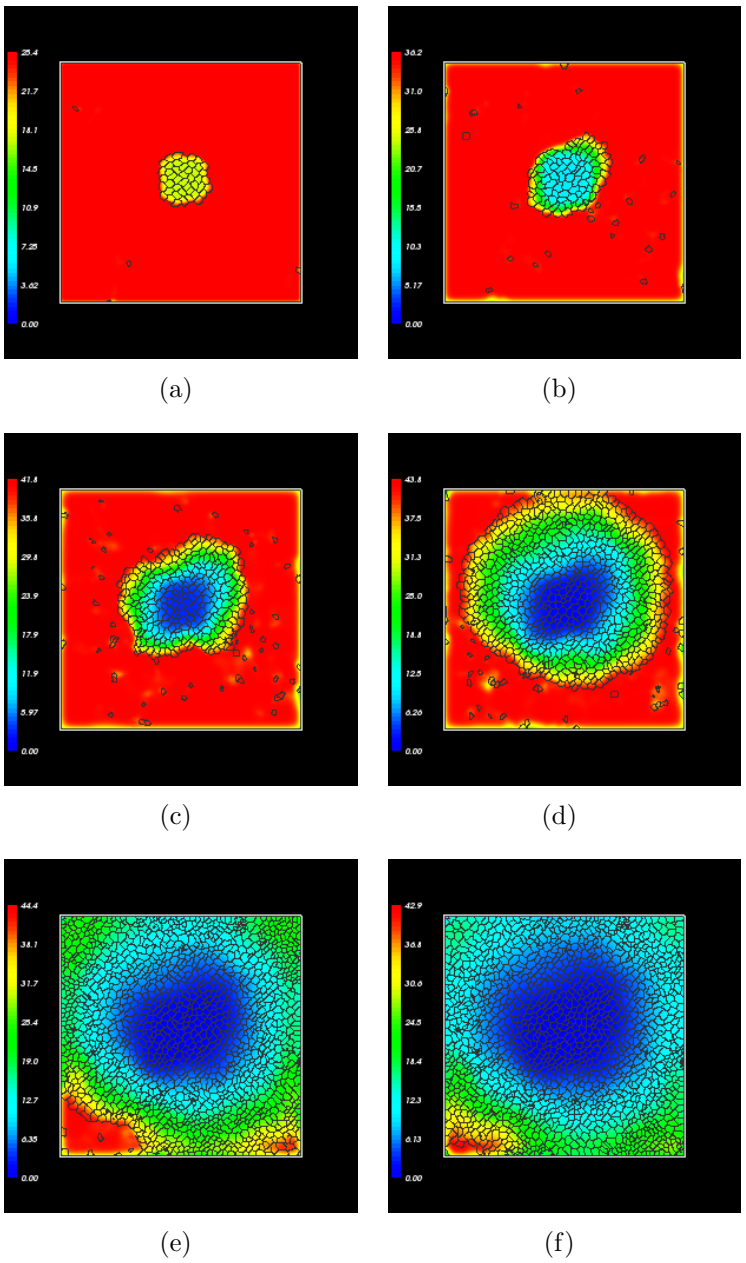

Figure 2.25: *Plots showing the oxygen concentration at times 200MCS, 1000MCS, 2000MCS, 3000MCS, 4000MCS, and 4400 MCS, respectively at 70% immune success rate. By 4400MCS the tumour mass has completely taken control.*

2.4 Conclusion

The model in this chapter has investigated, in a novel way, the impact $CD8^+$ T-cells have on a tumour mass before angiogenesis. It was based on the spatial model in Matzavinos et al. [2004], whereby the results showed the exhibition of a dormant cancer state, by way of a Hopf bifurcation identified in the homogenous model. Using CompuCell3d, the spatial system has been extended into an individual based model and the resulting simulations have tried to portray the three Es of immunoediting: elimination, equilibrium and escape. This model is stochastic in nature and, therefore, produces different results each time a new simulation is started. The model begins with a central tumour mass, which is attacked by immune cells. The tumour cells are allowed to divide when they reach a certain size, determined by how much oxygen is available to them. This creates different tumoural zones, whereby the tumour mass forms a proliferating rim, quiescent zone and necrotic core. The immune cells are constantly supplied to the domain at a rate of one every twenty-five MCS. For the killing mechanism, the immune cells are given a percentage of success rate against the tumour cells, mimicking the Hopf bifurcation control parameter from Matzavinos et al. [2004]. As this success rate is varied the three Es of immunoediting are realised.

Firstly, the elimination stage, where the immune cells are able to overcome the cancer cells, is simulated. Provided the success rate is over roughly 80% this state can be exhibited. However, as the model is stochastic in nature, the system can produce the opposite result. This is also due to other dynamics in the way in which the simulation progresses. The tumour cells are allowed

to break off from the main mass, and grow in a location where there maybe a larger abundance of oxygen, creating a new local tumour mass. This may also be twinned with the fact that often when the tumour cells go quiescent they can change back into a tumour cell when their oxygen is at a sufficient enough level. As the immune cells do not recognise quiescent cells as a threat, the tumour mass is often left undetected, sometimes hidden behind a wall of quiescent cells and necrotic material, promoting cancer growth. The second E of immunoediting, equilibrium, is exhibited when the immune success rate is roughly between $75 - 77\%$. This period is recognised when oscillatory dynamics are present over a significant number of time steps. Again as this system is stochastic in nature, one cell type will eventually win out, but the equilibrium dynamics are present here. Lastly, the escape stage is realised when the immune success rate is below 73%. This means that the cancer cells have sufficient enough leverage over the immune cells to gain a hold and possibly promote tumour growth factors to gain a regulatory blood network.

In conclusion, this system has provided a good snap shot of immunoediting and has attempted to mimic the dynamics produced in Matzavinos et al. [2004]. Further discussions and future work on the model can be found in Chapter 5.

Chapter 3

Modelling Multiple Cancer and Immune Cell Phenotypes

3.1 Introduction

The previous chapter modelled the interaction between a host immune system and a tumour population in an individual based model using the computer platform CompuCell3D. The model consisted of only one tumour and immune cell type, supplied by oxygen. The tumour mass was allowed to grow and the immune cells were introduced at a constant rate into the domain. The tumour and immune cells killed one another using a probability, inputed by the user, to favour one or the other. However, one of the hallmarks of cancer is that a tumour mass contains many different cells and phenotypes, as well as a host immune system that consists of different immune cells. This heterogeneity is discussed in section 1.1.3. It therefore seemed prudent to extend the model in order to capture more of the tumour microenvironment.

The previous model was based on the paper Matzavinos et al. [2004], whereby a partial differential equation system was introduced to try and describe the interactions between immune and tumour cells. This included an investigation on an ordinary differential equation system, whereby the authors removed the spatial elements in the PDE system, to better understand the underlying oscillatory dynamics. This paper was then extended, in Matzavinos and Chaplain [2004], to show that the oscillations, driven by a Hopf bifurcation, exhibited travelling wave solutions by way of a 1-D heteroclinic connection. Utilising these techniques, the model in this chapter has extended the model in chapter 2.

The biological focus of the previous model was on cytotoxic T lymphocytes, more specifically, $CD8^+$ cells, as it was thought that they produced the most effective means of clearance of nascent tumours. More recently however, it is thought that the T-helper cell or $CD4^+$ T-cell has the ability to target tumours, which have down graded their MHC I protein pathways. This down-regulation allows the tumour cells to elude the $CD8^+$ T-cells. As previously discussed, in section 1.1.3, the MHC protein pathways allow immune cells to recognise tumours by way of antigen presenting cells (APCs). $CD4^+$ T-cells indirectly kill tumour cells by either recruiting other immune cells, such as macrophages or eosinophils, to kill the tumour cells or will release cytokines, in the presence of a tumour cell, which are toxic.

There are two models in this chapter. One was developed to try and extend de Pillis et al. [2005], which ultimately failed. Tactics were changed and the model evolved into one that investigates the underlying dynamics of a tumour-immune system. This uses an ODE model, which will then be

extended to include more biological features and spatial interactions, in 1-D and 2-D. Although the individual based model can portray more biological features, it is also an advantage to work with PDE and ODE systems. More mathematical analysis can be done and the parameters that ultimately control the dynamics of the system can be more easily accessed. Modelling more and more interactions and dynamics is not always a benefit and can often prevent any findings due to the increasing complex nature of the model.

The next model has utilised some modelling techniques from de Pillis et al. [2005]. In this paper, a model of $CD8^+$ T-cells, NK cells and an immune population has been developed. The model uses experimental mice (Diefenbach et al. [2001]) and human data (Dudley et al. [2002]) and, therefore, has good quantitative results. The model is used to try and find "best fit" functional forms for the interaction terms between tumour and immune cells and to try and establish the underlying dynamics for tumour clearance. It is hoped that the model could aid in the development of therapeutic vaccines. The model is as follows:

$$\frac{dT}{dt} = \overbrace{aT(1-bT)}^{\text{logistic growth}} - \overbrace{cNT}^{\text{death by NK}} - \overbrace{D,}^{\text{death by CD8}^+} \tag{3.1.1}$$

$$\frac{dN}{dt} = \overbrace{\sigma}^{\text{supply}} - \overbrace{fN}^{\text{death rate}} + \overbrace{\frac{gT^2}{h+T^2}}^{\text{recruitment tumour}} - \overbrace{pNT,}^{\text{death by tumour}} \tag{3.1.2}$$

$$\frac{dL}{dt} = - \overbrace{mL}^{\text{death rate}} + \overbrace{\frac{jD^2}{k+D^2}}^{\text{recruitment tumour}} - \overbrace{qLT}^{\text{death by tumour}} + \overbrace{rNT,}^{\text{boost by NK}} \tag{3.1.3}$$

$$\text{where, } D = d\frac{(L/T)^\lambda}{s+(L/T)^\lambda}T. \tag{3.1.4}$$

Here, the tumour population is represented by the variable T, and the dynamics are described in equation (3.1.1); the NK cells' population is represented by the variable N, and described by equation (3.1.2); and the CD8$^+$ cells are represented by the variable L, and the dynamics are shown in equation (3.1.3). The model employs basic, but well used, mathematical modelling techniques for cell growth, supply and death, however, it uses more complex methods for recruitment and killing. The recruitment of immune cells are also represented by Michaelis Menten dynamics, utilised due to the term's saturation effects (Kirschner and Panetta [1998]). The CD8$^+$ T-cell equation, in (3.1.3), also contains the term rNT, that boosts the recruitment of the CD8$^+$ T-cells. As NK cells interact with the tumour cells, this initiates the activation of the CD8$^+$ T-cells. As the CD8$^+$ T-cells are activated

in this way, this prevents the activation of the $CD8^+$ T-cells prior to innate immunity.

The results of the investigation into finding a curve of "best fit", deduce that there is a distinct difference in the way an NK cell and $CD8^+$ T-cell interact with a tumour cell. While the dynamics of an NK cell killing a tumour can be described by a simple mathematical product interaction term, it was surmised that a $CD8^+$ T-cell's behaviour should be mathematically represented by a fractional response term. D denotes this fractional response term in equation (3.2.7). Here, λ represents how the lysis rate depends on the effector/target ratio, s allows a change in the steepness of the curve, and d is the maximum lysis rate/effectiveness of the immune cells.

In practice, saturation of the NK cells is not reached. Conversely, it is argued that the T-cells may require this type of saturation curve, represented by the fractional term, as they are targeting a specific tumour type and are, therefore, more effective in terms of cell-cell interactions. The results show that the experimental data can be replicated in the mathematical model. In light of this model, this thesis has tried to build on the dynamics and extend them.

3.2 Mathematical Model

This section will focus on the interactions between a host immune population, tumour cells and antigen presenting cells (APCs). As previously discussed, in section 1.1, the activation of immune cells is fulfilled by loaded APCs. These antigens are deemed loaded, as they have come into contact with a tumour

cell, and will display foreign antigen complexed with an MHC protein on the cell surface, for presentation to lymphocytes. APCs can be, for example, macrophages and dendritic cells. These cells can then be "read" by T-helper cells, by way of an epitope, which can elicit an immune response to the cancer cells.

The model has five variables: T, the tumour cell population; E_h, the T-helper or CD4$^+$ T-cell population; E_l, the CD8$^+$ T-cell population; A_u the inactivated/unloaded APCs; and A_a, the activated/loaded APCs. The dynamics are represented by system (3.2.1)-(3.2.6):

$$\frac{dT}{dt} = \overbrace{a_1(1-a_2T)T}^{\text{logistic growth}} - \overbrace{cE_hT}^{\text{death by CD4}^+} - \overbrace{D,}^{\text{death by CD8}^+} \tag{3.2.1}$$

$$\frac{dE_h}{dt} = \overbrace{u1}^{\text{supply}} - \overbrace{fE_h}^{\text{decay}} + \overbrace{\frac{gA_a^2}{h+A_a^2}E_h}^{\text{Activation by APC}} - \overbrace{cE_hT,}^{\text{death by tumour}} \tag{3.2.2}$$

$$\frac{dE_l}{dt} = \overbrace{u2}^{\text{supply}} - \overbrace{mE_l}^{\text{decay}} + \overbrace{\frac{jD^2}{k+D^2}E_l}^{\text{activation by tumour}} + \overbrace{rE_hE_l}^{\text{activation by CD4}^+} \tag{3.2.3}$$

$$- \overbrace{nE_lT,}^{\text{death by tumour}} \tag{3.2.4}$$

$$\frac{dA_u}{dt} = \overbrace{\alpha}^{\text{production inactivated}} - \overbrace{vA_u}^{\text{decay}} - \overbrace{qA_uT,}^{\text{removed class}} \tag{3.2.5}$$

$$\frac{dA_a}{dt} = \overbrace{qA_uT}^{\text{activated by tumour}} - \overbrace{\sigma A_a,}^{\text{decay}} \tag{3.2.6}$$

$$\text{where,} \quad D = d\frac{(E_l/T)^\lambda}{s+(E_l/T)^\lambda}T, \tag{3.2.7}$$

The idea behind the above system was to incorporate certain methods, used in de Pillis et al. [2005], to model different biological features. The

terms are described by the over-brace brackets above each term. Again, growth, supply and decay are all modelled by well known practices, however recruitment and immune cell kill rate are modelled differently. The inactivated APCs are activated, at rate q, this then activates the $CD4^+$ T-cells, at rate g, shown in equation (3.2.2), using a saturation type term. The $CD4^+$ T-cells can then go onto kill the tumour cells, at rate c. In turn, the tumour cells can also mount an attack on the $CD4^+$ T-cells. Both of these killing mechanisms, however, are simplified. It is thought, as discussed in section 1.1.3, that $CD4^+$ T-cells indirectly kill tumour cells by way of either released cytokines or by activating different cells of the immune system. The tumour cells also release enzymes, which are toxic to immune cells. The other immune cell in this model is the $CD8^+$ T-cell. Looking at equation (3.2.4), the $CD8^+$ T-cells are activated by the presence of the tumour cells, at rate j, utilising similar Michaelis Menten dynamics as de Pillis et al. [2005]. Moreover, the $CD8^+$ cells are enhanced by the presence of $CD4^+$ T-cells, at rate r. The $CD8^+$ T-cells kill the tumour cells, represented by the term D, in equation (3.2.1), using the same fractional response term developed in de Pillis et al. [2005]. The model was then non-dimensionalised, by setting:

$$T^* = \frac{T}{T_0}, \quad t^* = \frac{t}{\tau}, \quad E_h^* = \frac{E_h}{E_{h0}}, \quad E_l^* = \frac{E_l}{E_{l0}},$$
$$A_u^* = \frac{A_u}{A_{u0}}, \quad A_a^* = \frac{A_a}{A_{a_0}}$$

The new dimensionless system is:

$$\frac{dT}{dt} = \delta(1-\epsilon T)T - \eta E_h T - D_1, \tag{3.2.8}$$
$$\frac{dA_u}{dt} = \alpha_1 - \alpha_2 A_u T - v_1 A_u, \tag{3.2.9}$$
$$\frac{dA_a}{dt} = \alpha_2\alpha_3 A_u T - \sigma_1 A_a \tag{3.2.10}$$
$$\frac{dE_h}{dt} = u_1 - f_1 E_h + g_1\frac{A_a^2}{h_1 + A_a^2} - \omega E_h T, \tag{3.2.11}$$
$$\frac{dE_l}{dt} = -m_1 E_l + j_1\frac{D_1^2}{k_1 + D_1^2} + r_1 E_h E_l - n_1 E_h T. \tag{3.2.12}$$

where

$$\begin{aligned}
&a_1 t_0 = \delta, \quad a_2 T_0 = \epsilon, \quad t_0 c E_{h0} = \eta, \quad \frac{s}{\theta^\lambda} = s_1,\\
&dt_0 = d_1, \quad \frac{E_{l0}}{T_0} = \theta, \quad \frac{\alpha t_0}{A_{u0}} = \alpha_1, \quad t_0 v = v_1\\
&qT_0 t_0 = \alpha_2, \frac{A_{u0}}{A_{a0}} = \alpha_3, \quad \sigma t_0 = \sigma_1,\\
&t_0 f = f_1, \quad g t_0 = g_1, \quad \frac{h}{A_{a0}^2} = h_1, \quad pT_0 t_0 = \omega,\\
&mt_0 = m_1, \quad jt_0 = j_1, \quad rE_{h0} t_0 = r_1, \quad nT_0 t_0 = n_1, \frac{ut_0}{E_{h0}} = u_1\\
&\frac{k}{T_0^2} = k_1.
\end{aligned} \tag{3.2.13}$$

After finding and linearising around the steady states, bifurcation dynamics have remained elusive for this model. Discussions on possible ways to remedy this issue will be conveyed in the future work chapter.

3.3 The Basic Mathematical Model

Previously, a system that focused on $CD8^+$ T-cells and $CD4^+$ T-cells, in section 3.2, was developed, which ultimately proved too difficult to find any bifurcations. To try and investigate some sort of multiple immune/tumour cell modelling, the system in this section will be more general, and qualitative rather than quantitative. System (3.3.1)-(3.3.4), describes a host immune system in interaction with a tumour mass. The role of the APCs has been removed and it was decided it would be interesting to investigate two tumour populations, where one is deemed to have evolved into a more potent tumour phenotype. The evolution of tumour phenotypes has been discussed in this thesis in the immunoediting section, 1.1.2, whereby it is thought that the tumour cells evade immune destruction by the selective process of the immune system's killing; the immune system kills the more immunogenic cells, leaving a more powerful cancer mass. Moreover in section 1.1.3, it is argued that the tumour cells downgrade their MHC protein pathways in order to prevent immune cells recognising them. Both of these postulations are well known within theoretical biology, providing further reasoning behind the development of this system.

The model contains four variables: T_1, the tumour type one population; T_2, the tumour type two population; E_1, the immune type one population; and E_2 the immune type two population. The model is described by equations (3.3.1)-(3.3.4):

$$\overbrace{\frac{dT_1}{dt}}^{\text{Tumour 1}} = r_1 T_1 \left(1 - \frac{T_1}{K_1}\right) - \frac{a_1 E_1 T_1}{1 + T_1} - \frac{a_4 E_2 T_1}{1 + T_1}, \tag{3.3.1}$$

$$\overbrace{\frac{dT_2}{dt}}^{\text{Tumour 2}} = r_2 T_2 \left(1 - \frac{T_2}{K_2}\right) - \frac{a_2 E_1 T_2}{1 + T_2} - \frac{a_3 E_2 T_2}{1 + T_2}, \tag{3.3.2}$$

$$\overbrace{\frac{dE_1}{dt}}^{\text{Immune 1}} = b_1 + \frac{e_1 a_1 E_1 T_1}{1 + T_1} + \frac{e_2 a_2 E_1 T_2}{1 + T_2} - d_1 E_1, \tag{3.3.3}$$

$$\overbrace{\frac{dE_2}{dt}}^{\text{Immune 2}} = b_2 + \frac{e_3 a_3 E_2 T_2}{1 + T_2} + \frac{e_4 a_4 E_2 T_1}{1 + T_1} - d_2 E_2, \tag{3.3.4}$$

where, K_1, K_2, a_1, a_2, a_3 a_4, e_1, e_2, e_3, e_4, b_1, b_2, d_1 and d_2 are all positive parameters. Equation (3.3.1) represents the dynamics of the T_1 population. The growth and decay is represented by logistic growth, where K_1 is the carrying capacity, and the T_1 population is attacked by both E_1 and E_2 cells at rate a_1 and a_4 respectively. Equation (3.3.2) describes the evolution of the T_2 tumour cells. Logistic growth is again used to model growth and decay, with carrying capacity K_2 and the population is attacked by the E_1 and E_2 cells at rate a_2 and a_3. As in de Pillis et al. [2005], the use of a Hill function has been employed here to elucidate the killing mechanism of the immune cells. Further discussions on the derivation of Michaelis Menten techniques, in relation to the recruitment of immune cells, can be found in Kuznetsov

et al. [1994].

Moreover, equation (3.3.3) represents the E_1 population. The supply rate is constant and is represented by parameter b_1. The immune cells are enhanced by the presence of the tumour cells and their recruitment is represented by the terms $\frac{e_1 a_1 E_1 T_1}{1+T_1}$ and $\frac{e_2 a_2 E_1 T_2}{1+T_2}$. The E_1 population also decays at rate d_1 due to lysis. Similarly, equation (3.3.4) elucidates the E_2 population's dynamics where, b_2 is the constant supply rate and d_2 is the decay rate due to lysis. As in the E_1 equation, the immune cells interact with the tumour cells in terms $\frac{e_3 a_3 E_1 T_1}{1+T_1}$ and $\frac{e_4 a_4 E_1 T_2}{1+T_2}$. The aim of this model is to try and understand the dynamics which will allow the model to move into different cancerous states. The hope is to be able to capture dormancy steady states and try and explain the situations where these states disappear. In order to investigate this system the model has been deconstructed into three separate models.

Section 3.4 will concern a shortened version of system (3.3.1)-(3.3.4), whereby only the E_1 cells will attack the T_1 cells and the supply terms will be omitted. After non-dimensionalising, steady states and their stability will be examined in section 3.4.1. The results of this model, using ODE45 in matlab, will be discussed in section 3.4.4, along with bifurcation analysis. This is then extended into spatial models in 1-D, in section 3.5, and 2-D, in section 3.6, with their corresponding results in sections 3.5.2 and 3.6.1.

System (3.3.1)-(3.3.4), is then further investigated by removing only the E_2 immune cells ability to attack the T_1 cells in section 3.7. Again, steady states and their stability will be deduced, in section 3.7.1, and the results, along with bifurcation analysis, will be investigated in section 3.7.2. The

model is then extended into a spatial system in section 3.8, with the results in section 3.8.1.

The full system, displayed in (3.3.1)-(3.3.4), is explored in section 3.9 and, as before, any steady states, along with their stability, are examined, with results and bifurcation analysis displayed in section 3.9.2. Furthermore, the model is extended into a 1-D spatial model, in section 3.10, and the results are investigated in section 3.10.1.

3.3.1 Non-dimensionalisation

System (3.3.1)-(3.3.4) can be non-dimesionalised by letting:

$$t^* = \frac{t}{\tau}, \quad T_1^* = \frac{T_1}{T_{1_0}}, \quad T_2^* = \frac{T_2}{T_{2_0}}, \quad E_1^* = \frac{E_1}{E_{1_0}},$$
$$E_2^* = \frac{E_2}{E_{2_0}},$$

where:

$$\tau = \frac{1}{r_1}, \quad T_{1_0} = K_1, \quad T_{2_0} = K_2, \quad E_{1_0} = K_1 \quad \text{and} \quad E_{2_0} = K_2.$$

The non-dimensional system is therefore:

$$\frac{dT_1}{dt} = T_1(1 - T_1) - \gamma_1 \frac{E_1 T_1}{s_1 + T_1} - \gamma_4 \frac{E_2 T_1}{s_4 + T_1}, \tag{3.3.5}$$

$$\frac{dT_2}{dt} = \alpha_2 T_2(1 - T_2) - \gamma_2 \frac{E_1 T_2}{s_2 + T_2} - \gamma_3 \frac{E_2 T_2}{s_3 + T_2}, \tag{3.3.6}$$

$$\frac{dE_1}{dt} = z_1 + \frac{\psi_1 E_1 T_1}{s_1 + T_1} + \frac{\psi_2 E_1 T_2}{s_2 + T_2} - \omega_1 E_1, \tag{3.3.7}$$

$$\frac{dE_2}{dt} = z_2 + \frac{\psi_3 E_2 T_2}{s_3 + T_2} + \psi_4 \frac{E_2 T_1}{s_4 + T_1} - \omega_2 E_2, \tag{3.3.8}$$

where:

$$\frac{a_1}{r_1} = \gamma_1, \quad \frac{1}{K_1} = s_1, \quad \frac{r_2}{r_1} = \alpha_2, \quad \frac{a_2 K_1}{r_1 K_2} = \gamma_2,$$
$$\frac{a_3}{r_1} = \gamma_3 \quad \frac{1}{K_2} = s_2, \quad \tau e_1 a_1 = \psi_1, \quad \tau e_2 a_2 = \psi_2,$$
$$d_1 \tau = \omega_1, \quad \tau e_3 a_3 = \psi_3, \quad d_2 \tau = \omega_2, \quad z_1 = \frac{b_1}{r_1 K_1},$$
$$z_2 = \frac{b_2}{r_1 K_2}, \quad \gamma_4 = \frac{a_4 K_2}{r_1 K_1}, \quad \psi_4 = \tau e_4 a_4, \quad s_3 = \frac{1}{K_2},$$
$$s_4 = \frac{1}{K_1}.$$

3.4 Shortened model of cancer and immune cells

This shortened model of system (3.3.5)-(3.3.8) has omitted the supply terms, z_1 and z_2, for both immune types. Moreover, the E_2 cells attack on the T_1 tumour population has also been removed. It can be argued that the supply terms can be removed as the cells could already be present in the tumour microenvironment, although not practical. However, by scaling back on the model, it will allow more investigation into what dynamics change if the model is extended. It will show the most important influences within the model and how they effect any of the cell types. Setting γ_4=z_1=z_2=0 in system (3.3.5)-(3.3.8), the system now becomes:

$$\frac{dT_1}{dt} = T_1(1 - T_1) - \gamma_1 \frac{E_1 T_1}{s_1 + T_1}, \tag{3.4.1}$$

$$\frac{dT_2}{dt} = \alpha_2 T_2(1 - T_2) - \gamma_2 \frac{E_1 T_2}{s_2 + T_2} - \gamma_3 \frac{E_2 T_2}{s_3 + T_2}, \tag{3.4.2}$$

$$\frac{dE_1}{dt} = \frac{\psi_1 E_1 T_1}{s_1 + T_1} + \frac{\psi_2 E_1 T_2}{s_2 + T_2} - \omega_1 E_1, \tag{3.4.3}$$

$$\frac{dE_2}{dt} = \frac{\psi_3 E_2 T_2}{s_3 + T_2} - \omega_2 E_2. \tag{3.4.4}$$

Looking at the non-dimensional parameters, it can be seen that the E_1 immune cells kill the T_1 cancer cells at a faster rate than the E_2 cells. The

E_2 cells however kill the T_2 cells at a much faster rate than the T_1 cells do, but do not attack the T_1 population. The T_1 cells can be seen as mutated cancer cells, in the sense that they are phenotypically different to the T_2 cells. While the T_1 cells are being attacked by the E_1 cells, they have managed to evade detection by the E_2 cells and therefore can be classed as a more potent phenotype. It may become apparent in a clinical situation that the immune system would manage to thwart the T_2 cell population while allowing the T_1 cell population to grow "unchecked" by all but one type of immune cell, whose best efforts may not be enough to clear the tumour bulk, leading to metastasis and invasion. The two different types of immune cells could be, for example, a $CD8^+$ T-cell for the E_2 population and an NK cell for the E_1 population. This is a reasonable choice as the NK cells are part of the innate immune system and have vast targets. Similarly, the two immune cells could be a $CD8^+$ T-cell for the E_2 population and a $CD4^+$ T-cell for the E_1 population. In this scenario, the T_1 population may have down-regulated their MHC I protein pathway, evading immune detection by the $CD8^+$ T-cells, however the $CD4^+$ T-cells can still recognise them, as discussed in section 1.1.3. Moreover, Eftimie et al. [2010] recognises the difference between the action of Th1 and Th2 immune cells in relation to cancer rejection. Here, it was necessary for both immune cells to work together in order to kill the tumour.

The values of γ_1, γ_2 and γ_3 are important as they determine the saturation point of the cells i.e. if one were to plot the function where the E_1 cells are attacking the T_1 cells the curve would tend toward s_1. The gradient of the curve is influenced by the parameters s_1, s_2 and s_3. If these parameters are

decreased, the curve will become steeper, leading the immune cells to reach saturation point at a much faster rate, however increasing the parameters will have the opposite effect. It is now necessary to look at the number of steady states within the system and determine their stability.

3.4.1 Steady states and stability

Steady states are found by setting:

$$\frac{dT_1}{dt} = T_1(1 - T_1) - \gamma_1 \frac{E_1 T_1}{s_1 + T_1} = 0, \tag{3.4.5}$$

$$\frac{dT_2}{dt} = \alpha_2 T_2(1 - T_2) - \gamma_2 \frac{E_1 T_2}{s_2 + T_2} - \gamma_3 \frac{E_2 T_2}{s_2 + T_2} = 0, \tag{3.4.6}$$

$$\frac{dE_1}{dt} = \frac{\psi_1 E_1 T_1}{s_1 + T_1} + \frac{\psi_2 E_1 T_2}{s_2 + T_2} - \omega_1 E_1 = 0, \tag{3.4.7}$$

$$\frac{dE_2}{dt} = \frac{\psi_3 E_2 T_2}{s_2 + T_2} - \omega_2 E_2 = 0. \tag{3.4.8}$$

It is easy to see that the trivial steady state $(0, 0, 0, 0)$ exists. The other steady states are equated by setting:

$$T_1(1-T_1)(s_1+T_1)-\gamma_1 E_1 T_1=0, \tag{3.4.9}$$

$$\alpha_2 T_2(1-T_2)(s_2+T2)(s_3+T2)-\gamma_2 E_1 T_2(s_3+T_2)$$
$$-\gamma_3 E_2 T_2(s_2+T_2)=0, \tag{3.4.10}$$

$$\psi_1 E_1 T_1(s_2+T_2)+\psi_2 E_1 T_2(s_1+T_1)-\omega_1 E_1(s_2+T_2)(s_1+T_1)=0, \tag{3.4.11}$$

$$\psi_3 E_2 T_2-\omega_2 E_2(s3+T2)=0. \tag{3.4.12}$$

There are nine steady states: the trivial steady state, discussed previously; seven semi trivial steady states; and one coexistence steady state.

3.4.2 Numerical values of steady states

The numerical values of steady states are found using the parameter values as below:

$$\gamma_1=0.7778 \quad s_1=0.65, \quad \alpha_2=0.7778, \quad s_4=0.5,$$
$$\gamma_2=0.2222, \quad \gamma_3=0.7778, \quad s_2=0.5, \quad s_3=0.65,$$
$$\psi_1=0.3111, \quad \psi_2=0.0044, \quad \omega_1=0.1778, \quad \psi_3=0.2333$$
$$\omega_2=0.1333, \quad z_1=0.1778, \quad z_2=0.1333, \quad \gamma_4=0.1111$$
$$\psi_4=0.0022.$$

These parameter values are generic. It is prudent to point out that gaining experimental data for these types of systems is difficult. One could use

a number of different values from numerous academic materials, but this chapter is concerned with achieving a qualitative picture of the system and to examine the dynamics that can be achieved here. Time has been scaled in reference to the mitotic rate of the T_1 cells. Again different cancer cell types have different proliferation rates, however a cancer cell normally has a mitotic rate of somewhere between 18-34 hours.

$$s1 = (0, 0, 0, 0), \quad s2 = (1, 0, 0, 0)\,, \tag{3.4.13}$$

$$s3 = (0, 1, 0, 0)\,, \quad s4 = (1, 1, 0, 0), \tag{3.4.14}$$

$$s5 = (0.867, 0, 0.259, 0), \tag{3.4.15}$$

$$s6 = (0, 0.866, 0, 0.203), \tag{3.4.16}$$

$$s7 = (1, 0.866, 0, 0.203), \tag{3.4.17}$$

$$s8 = (0.835, 0.937, 0.315, 0), \tag{3.4.18}$$

$$s9 = (0.836, 0.866, 0.314, 0.103). \tag{3.4.19}$$

3.4.3 Linear stability analysis

To further investigate the dynamics of the system it is prudent to examine the stability of the steady states by carrying out a linear stability analysis.

After finding the steady states one now needs to work out the determinant of the Jacobian Matrix equal to zero, in order to investigate the eigenvalues. The Jacobian is worked out as follows:

$$J = \begin{bmatrix} \frac{\partial f_1}{\partial T_1} & \frac{\partial f_1}{\partial T_2} & \frac{\partial f_1}{\partial E_1} & \frac{\partial f_1}{\partial E_2} \\ \frac{\partial f_2}{\partial T_1} & \frac{\partial f_2}{\partial T_2} & \frac{\partial f_2}{\partial E_1} & \frac{\partial f_2}{\partial E_2} \\ \frac{\partial f_3}{\partial T_1} & \frac{\partial f_3}{\partial T_2} & \frac{\partial f_3}{\partial E_1} & \frac{\partial f_3}{\partial E_2} \\ \frac{\partial f_4}{\partial T_1} & \frac{\partial f_4}{\partial T_2} & \frac{\partial f_4}{\partial E_1} & \frac{\partial f_4}{\partial E_2} \end{bmatrix}$$

where

$$f_1 = \frac{dT_1}{dt} = T_1(1 - T_1) - \gamma_1 \frac{E_1 T_1}{s_1 + T_1}, \tag{3.4.20}$$

$$f_2 = \frac{dT_2}{dt} = \alpha_2 T_2(1 - T_2) - \gamma_2 \frac{E_1 T_2}{s_2 + T_2} - \gamma_3 \frac{E_2 T_2}{s_2 + T_2}, \tag{3.4.21}$$

$$f_3 = \frac{dE_1}{dt} = z_1 + \frac{\psi_1 E_1 T_1}{s_1 + T_1} + \frac{\psi_2 E_1 T_2}{s_2 + T_2} - \omega_1 E_1, \tag{3.4.22}$$

$$f_4 = \frac{dE_2}{dt} = z_2 + \frac{\psi_3 E_2 T_2}{s_2 + T_2} - \omega_2 E_2. \tag{3.4.23}$$

Now it is necessary to work out:

$$det J_{(T_1^*, T_2^*, E_1^*, E_2^*)} - \lambda I = 0, \tag{3.4.24}$$

where stability is determined by examining the eigenvalues (λ) of the steady state. The steady state is asymptotically stable if and only if all the real parts of the eigenvalues are less than zero i.e. $Re(\lambda) < 0$ as $t \to \infty$. If any of the eigenvalues have $Re(\lambda) > 0$ the steady state is unstable, provided each

eigenvalue exists.

The trivial steady state, $(0, 0, 0, 0)$, is unstable determined by

$$detJ_{(0,0,0,0)} - \lambda I = 0 \text{ and } \lambda = 0.7778, 1, -0.1333, -0.1778. \tag{3.4.25}$$

There are seven semi-trivial steady states. The stability of each is determined by the sign of the real part of their eigenvalues. Each is listed below:

- $(1, 0, 0, 0)$ and $\lambda = 0.0107, 0.7778, -0.1333, -1.000000000$
- $(0, 1, 0, 0)$ and $\lambda = 0.0081, 1, -0.1747, -0.7778$
- $(1, 1, 0, 0)$ and $\lambda = 0.0081, 0.0137, -0.7778, -1$
- $(0.867, 0, 0.259, 0)$, and $\lambda = 0.6625, -0.0130, -0.1333, -0.7779$
- $(0, 0.866, 0, 0.203)$, and $\lambda = 1, -0.0098, -0.1750, -0.6048$
- $(1, 0.866, 0, 0.203)$ and $\lambda = -1, 0.0135, -0.0098, -0.6048$
- $(0.835, 0.937, 0.315, 0)$ and $\lambda = 0.0045, -0.0175, -0.6972, -0.7249$

By looking at each of the steady states with their corresponding Eigenvalues, it is easy to see that all of the semi-trivial steady states are unstable.

For this system there is one "coexistence steady state" whereby each of the steady state values are greater than zero. The stability of the steady state is stable as each of the eigenvalues are negative.

$$detJ_{(0.836,0.866,0.314,0.103)} - \lambda I = 0 \text{ and } \lambda = -0.0049, -0.0174, -0.6063, -0.7262. \tag{3.4.26}$$

In order to change the stability of the trivial and semi-trivial steady states, the parameter values would have to be modified to achieve stability. This however was not of interest in this PhD as the most interesting and important dynamics are realised by examining the co-existence steady state.

3.4.4 Results

The results in this section will be worked out using ODE45 in Matlab, a black box solver, which utilises a 4th/5th order Runge Kutta method. Further details can be found in Chapter 1.3. It should also be noted that the initial conditions for this system are $(T_1, T_2, E_1, E_2) = (1, 1, 1, 1)$.

3.4.5 Oscillations/bifurcations

Limit cycles, derived from Hopf bifurcations, are extremely interesting to have in a model. By varying a parameter, a Hopf bifurcation may become apparent, showing that the variable will have some degree of control on the dynamics of the system. The steady state moves from a steady state of stable coexistence to an unstable steady state, which gives rise to oscillatory dynamics. A stable limit cycle will display oscillations, which have the same amplitude or damped oscillations, which get progressively smaller, gravitating towards the attractor. An unstable limit cycle will lead to oscillations whose amplitude get progressively bigger. Biologically, stable limit cycles, in the context of this model, mean that the immune system has managed to keep the tumour population under check, and a dormancy situation has become apparent. Parameter values for the results are shown in section 3.4.2.

There is a Hopf bifurcation when $s_1 = 0.279$. The bifurcation diagrams for T_1 and T_2 are shown in Figures 3.1-3.2 and similar diagrams can be obtained for the other two variables. A Hopf bifurcation is a critical point where the stability of the system switches and this gives rise to a periodic solution. The bifurcation diagrams have been generated using the computer programme, XPP AUTO. The red line indicates that the solution is stable, while the black line indicates the solution is unstable. The blue circles represent an unstable limit cycle and the green a stable limit cycle. Stable limit cycles are essentially attractors, where any small perturbation will cause the system to return to the attractor. Looking at the bifurcation diagrams, it can be seen that the limit cycles are stable in this case. Any value of parameter s_1, which is within the arc of the periodic, will give stable limit cycles. The amplitude of the Hopf bifurcation, within the arc, can be determined by looking at the difference between the maximum and minimum values for that given parameter value. For example, when looking at Figure 3.1 when $s_1 = 0.21$, this will give much larger amplitudes than if $s_1 = 0.24$.

Moreover, Figures 3.3-3.6 show the stable oscillatory dynamics for $s_1 = 0.225$. In these figures, the differences in the amplitude can be seen more clearly. Looking at the bifurcation diagram for the T_1 population, it can be seen that there is a much larger amplitude than in the figure for the T_2 population. Referring back to system 3.4.1-3.4.4, the T_1 population is attacked only by the E_1 cells, whereas the E_2 population is killed by both immune cell types. As previously discussed, reducing the parameter s_1 will cause the immune cells to reach saturation at a much faster rate. This could possibly be thought as the E_1 cells being more adept in cell-cell interactions.

However, if one looks at Figures 3.3-3.6, the T_2 tumour cell bulk is higher than the T_1 tumour cell bulk. This is due to the extra recruitment terms for the E_1 population. As the E_1 cells' recruitment term is much higher, they are better able to deal with the T_1 tumour bulk than the E_2 cells are with the T_2 tumour bulk. Although there is a Hopf bifurcation in E_2, the oscillations are too small to see. In Figure 3.6, it can be seen that there is a very low level of E_2 population, supporting the evidence that the recruitment of the E_2 cells is not high enough to provide T_2 clearance. Moreover, the value of the parameter γ_2 is much smaller than that of γ_1, therefore the E_1 population is also unable to lower the T_2 tumour bulk significantly from the steady state size. It should also be noted that the amplitude of the oscillations for T_1 and E_1 is much higher than for the other two. This is because the curve for the recruitment of the E_1 population and T_1 population is steeper due to the decrease in parameter s_1.

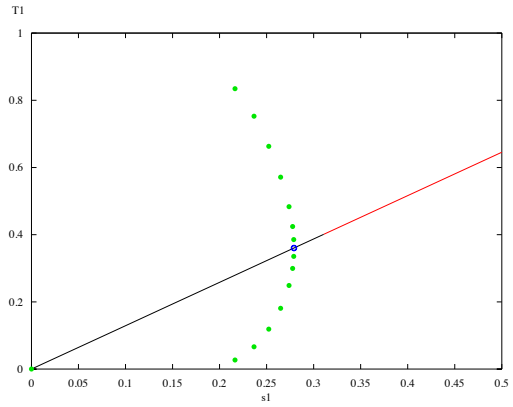

Figure 3.1: *Bifurcation diagram showing a hopf bifurcation in* T_1 *at* $s_1 = 0.279$*. The line in the diagram represents how the steady state changes as* s_1 *changes. The black part of the line indicates instability of the equilibria and the red, stability. Moreover, green dots indicate that the hopf bifurcation is stable and blue dots represent instability.*

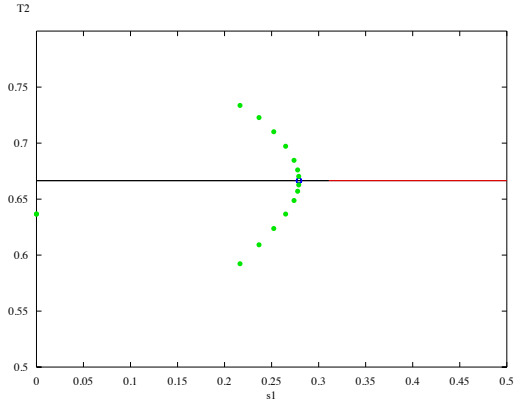

Figure 3.2: *Bifurcation diagram showing a hopf bifurcation in* T_2 *at* $s_1 = 0.279$*. The line in the diagram represents how the steady state changes as* s_1 *changes. The black part of the line indicates instability of the equilibria and the red, stability. Moreover, green dots indicate that the hopf bifurcation is stable and blue dots represent instability.*

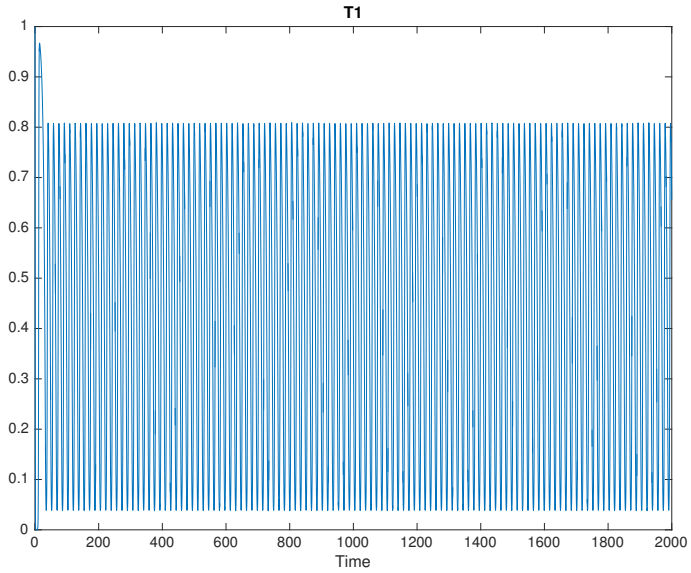

Figure 3.3: *Plot showing T_1 where oscillations are derived from the parameter space when the hopf bifurcation is present at $s_1 = 0.225$ at times 0 to 2000 seconds.*

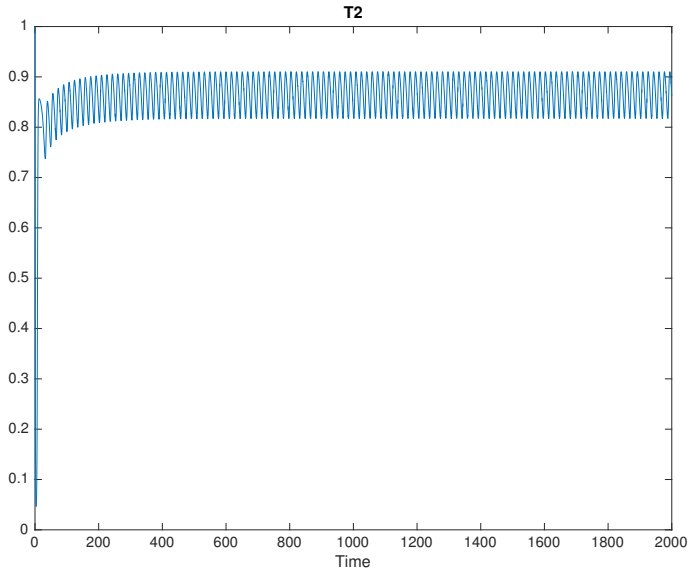

Figure 3.4: *Plot showing T_2 where oscillations are derived from the parameter space when the Hopf bifurcation is present at $s_1 = 0.225$ at times 0 to 2000 seconds.*

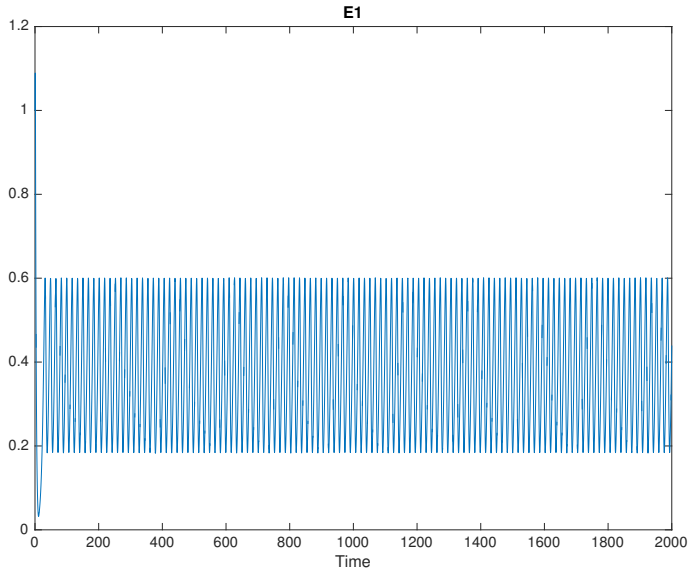

Figure 3.5: *Plot showing E_1 where oscillations are derived from the parameter space when the Hopf bifurcation is present at $s_1 = 0.225$ at times 0 to 2000 seconds.*

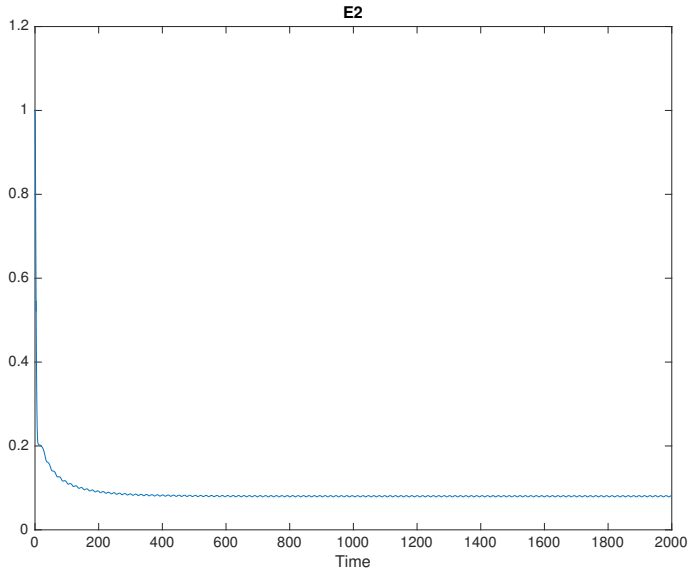

Figure 3.6: *Plot showing E_2 where very small oscillations are derived from the parameter space when the Hopf bifurcation is present at $s_1 = 0.225$ at times 0 to 2000 seconds.*

Moreover, there is a Hopf bifurcation when $\psi_1 = 0.8287$, which gives rise to a stable periodic solution. The bifurcation diagrams for T_1 and E_1 are shown in Figures 3.7-3.8 and similar figures can be plotted for the other variables. The parameter ψ_1 controls the saturation level of the term for E_1. As the parameter has been increased, the E_1 population has been allowed to grow to a higher level and therefore, the T_1 tumour bulk will be reduced. This is depicted in Figures 3.9 and 3.11. The E_1 cells now fluctuate between roughly 0.25 and 2.25, whereas the T_1 cells vary between 0 and 0.4. The E_2 cells, although beginning high, are reduced to a very low level as their recruitment is not high enough to overcome the effects of the decay term, leading to a high T_2 tumour bulk. This is depicted in Figures 3.10 and 3.12.

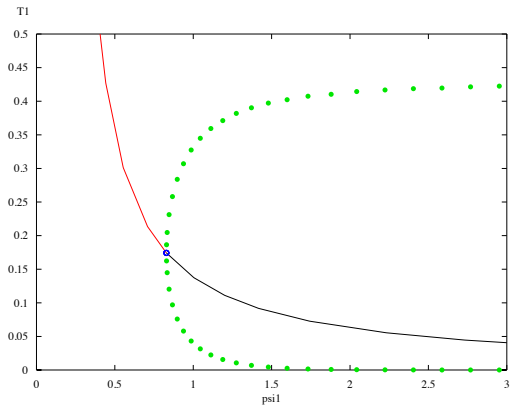

Figure 3.7: *Bifurcation diagram showing a hopf bifurcation in T_1 at $\psi_1 = 0.8287$. The line in the diagram represents how the steady state changes as ψ_1 changes. The black part of the line indicates instability of the equilibria and the red, stability. Moreover, green dots indicate that the hopf bifurcation is stable and blue dots represent instability.*

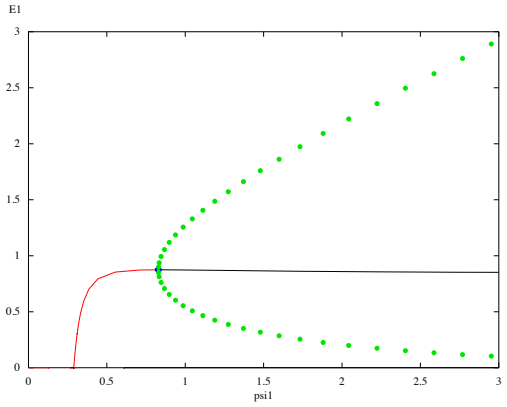

Figure 3.8: *Bifurcation diagram showing a hopf bifurcation in E_1 at $\psi_1 = 0.8287$. The line in the diagram represents how the steady state changes as ψ_1 changes. The black part of the line indicates instability of the equilibria and the red, stability. Moreover, green dots indicate that the hopf bifurcation is stable and blue dots represent instability.*

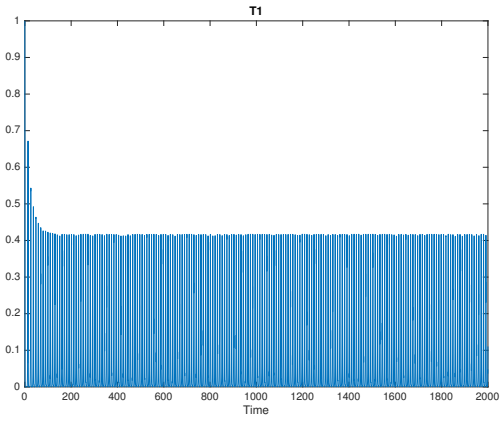

Figure 3.9: *Plot showing T_1 where oscillations are derived from the parameter space when the Hopf bifurcation is present at $\psi_1 = 2$ at times 0 to 2000 seconds.*

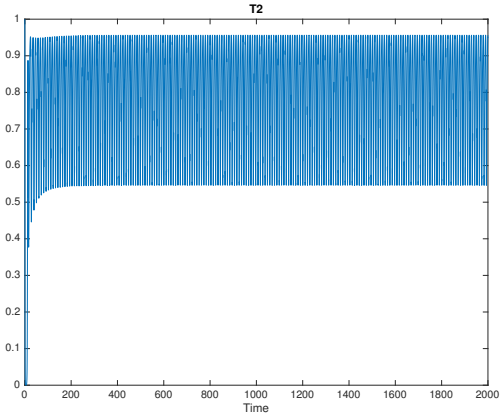

Figure 3.10: *Plot showing T_2 where oscillations are derived from the parameter space when the Hopf bifurcation is present at $\psi_1 = 2$ at times 0 to 2000 seconds.*

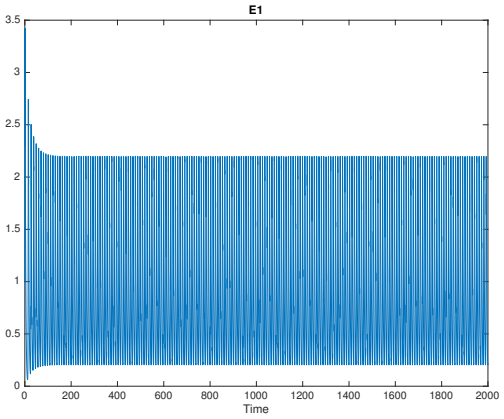

Figure 3.11: *Plot showing E_1 where oscillations are derived from the parameter space when the Hopf bifurcation is present at $\psi_1 = 2$ at times 0 to 2000 seconds.*

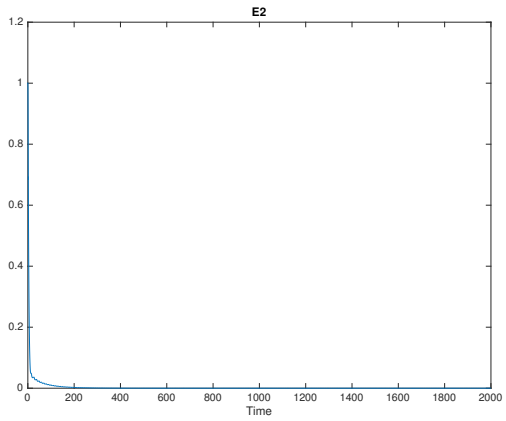

Figure 3.12: *Plot showing E_2 where $E_2 \to 0$ derived from the parameter space when the Hopf bifurcation is present at $\psi_1 = 2$ at times 0 to 2000 seconds.*

Another Hopf bifurcation is present when $\psi_3 = 0.4883$. The bifurcation diagram for E_2 is shown in Figure 3.13 and similar diagrams can be depicted for the other variables. Figures showing the oscillatory dynamics can be seen in Figures 3.14-3.17 when $\psi_3 = 1$. In this case, the ψ_3 term, which governs the saturation level for the E_2 cells, has been increased. This leads to a higher amount of E_2 cells and a reduced T_2 tumour bulk. The T_1 and E_1 cells are largely unaffected by this and moreover, the oscillations are too small to show.

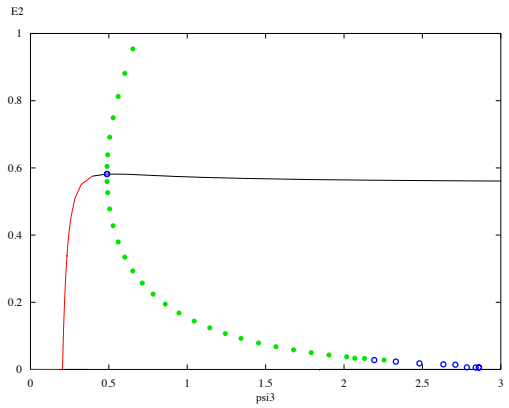

Figure 3.13: *Bifurcation diagram showing a hopf bifurcation in T_1 at $\psi_3 = 0.4883$. The line in the diagram represents how the steady state changes as ψ_1 changes.The black part of the line indicates instability of the equilibria and the red, stability. Moreover, green dots indicate that the hopf bifurcation is stable and blue dots represent instability.*

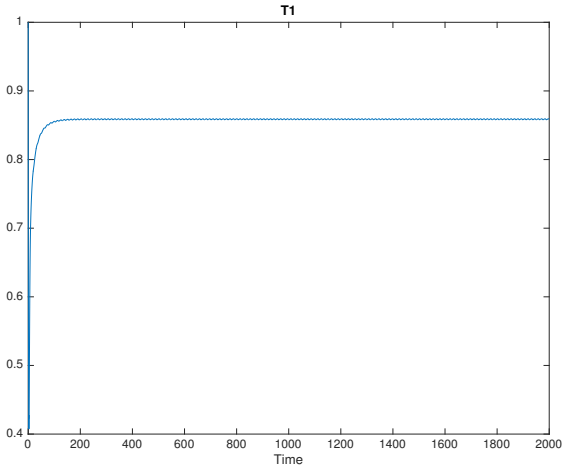

Figure 3.14: *Plot showing T_1 where oscillations are derived from the parameter space when the Hopf bifurcation is present at $\psi_3 = 1$ at times 0 to 2000 seconds.*

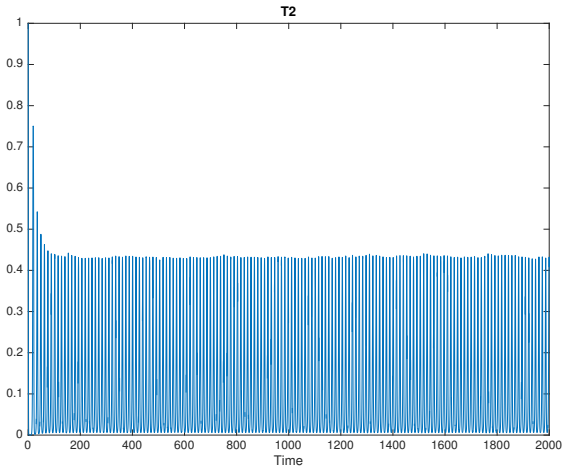

Figure 3.15: *Plot showing T_2 where oscillations are derived from the parameter space when the Hopf bifurcation is present at $\psi_3 = 1$ at times 0 to 2000 seconds.*

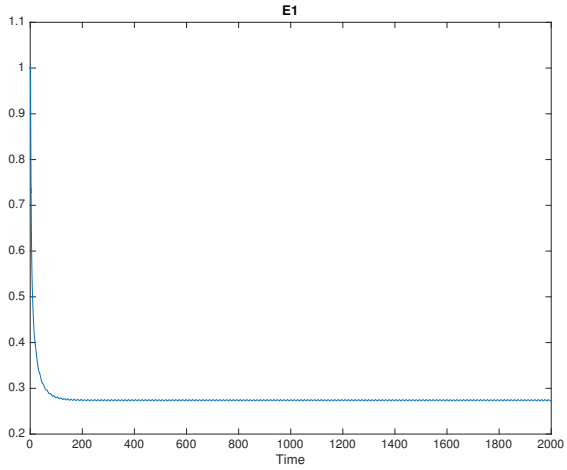

Figure 3.16: *Plot showing E_1 where oscillations are derived from the parameter space when the Hopf bifurcation is present at $\psi_3 = 1$ at times 0 to 2000 seconds.*

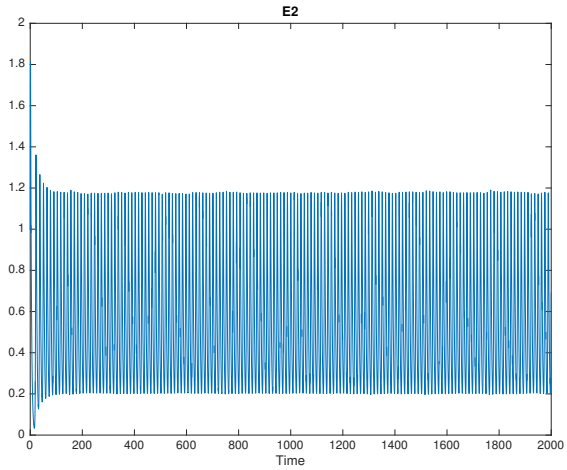

Figure 3.17: *Plot showing E_2 where oscillations are derived from the parameter space when the Hopf bifurcation is present at $\psi_3 = 1$ at times 0 to 2000 seconds.*

3.4.6 Discussion

This section has examined an ODE model of two types of immune cells and two tumour cells. The dynamics of the system has been explored using bifurcation analysis. By finding the terms that create periodic solutions, the control parameters and subsequent underlying dynamics of the system can be elucidated. Here, the parameters s_1, ψ_1 and ψ_3 are varied and periodic solutions are found by way of Hopf bifurcations. The model allows more analytical techniques to be used and gives a good understanding of the type of dynamics, which can become apparent when varying the control parameters. Although this ODE model has provided a good basis, it is now necessary to develop a spatial model to study the effects space may have.

3.5 Spatial Model

The model in section 3.4 has been extended in this section into a spatial system. This allows the exploration of cell-cell dynamics in a 1-D domain. The spatial system is as follows:

$$\frac{dT_1}{dt} = D_1\nabla^2 T_1 + T_1(1-T_1) - \gamma_1\frac{E_1T_1}{s_1+T_1}, \tag{3.5.1}$$

$$\frac{dT_2}{dt} = D_2\nabla^2 T_2 + \alpha_2 T_2(1-T_2) - \gamma_2\frac{E_1T_2}{s_2+T_2} - \gamma_3\frac{E_2T_2}{s_2+T_2}, \tag{3.5.2}$$

$$\frac{dE_1}{dt} = D_3\nabla^2 E_1 + \frac{\psi_1E_1T_1}{s_1+T_1} + \frac{\psi_2E_1T_2}{s_2+T_2} - \omega_1E_1, \tag{3.5.3}$$

$$\frac{dE_2}{dt} = D_4\nabla^2 E_2 + \frac{\psi_3E_2T_2}{s_2+T_2} - \omega_2E_2, \tag{3.5.4}$$

where the values of the spatial parameters are:

$$D_1 = D_2 = 0.000008 \text{ and } D_3 = D_4 = 0.0000075. \tag{3.5.5}$$

Moreover, these values are generic as the results in this section are concerned with studying the underlying mathematical dynamics of the system.

System (3.5.1)-(3.5.4) extends the previous ODE model by including diffusion terms for each of the cell types. These describe the random motility of the cells in the domain, with parameters $D_1 - D_4$ defining their velocity. The results utilise the same parameter values as found in section 3.4.2.

3.5.1 Initial and boundary conditions

Zero flux boundary conditions were imposed and the initial conditions used are similar to the ones used in Matzavinos et al. [2004] and are defined as:

$$T_1(x,0) = \begin{cases} T_{1_0}(1 - exp(-1000(x-l)^2)), & \text{if } 0 \leq x \leq l, \\ 0, \qquad \text{if } l < x \leq x_0, \end{cases} \tag{3.5.6}$$

$$T_2(x,0) = \begin{cases} T_{2_0}(1 - exp(-1000(x-l)^2)), & \text{if } 0 \leq x \leq l, \\ 0, \qquad \text{if } l < x \leq x_0, \end{cases} \tag{3.5.7}$$

$$E_1(x,0) = \begin{cases} 0, \qquad \text{if } 0 \leq x \leq l, \\ E_{1_0}(1 - exp(-1000(x-l)^2)), & \text{if } l < x \leq x_0. \end{cases} \tag{3.5.8}$$

$$E_2(x,0) = \begin{cases} 0, \qquad \text{if } 0 \leq x \leq l, \\ E_{1_0}(1 - exp(-1000(x-l)^2)), & \text{if } l < x \leq x_0. \end{cases} \tag{3.5.9}$$

The initial conditions are displayed in Figure 3.18, depicting a tumour wave front in T_1 and T_2, which encounter an immune cell front, E_1 and E_2. A one-dimensional domain has been created where $x \in [0,1]$ and l represents the point at which the two fronts interact. It should be noted that the heterogeneity of the results in this chapter does not result from any changes in initial conditions. The dynamics here are a well studied feature of reaction-diffusion equations (Sherratt et al. [1997]; Matzavinos and Chaplain [2004]) and are driven by the presence of a limit cycle.

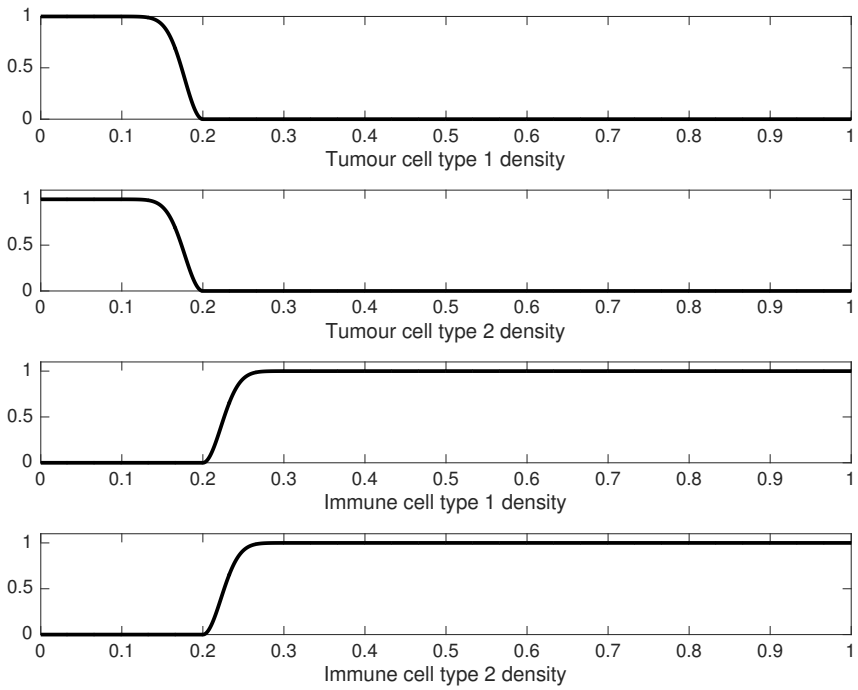

Figure 3.18: *Plots showing the Initial conditions for each cell type.*

3.5.2 Results

The results in this section have been numerically investigated by using the Matlab tool, PDEPE. The description of the results will focus on the similarities between that of the ODE model and the findings of the spatial model. In the ODE model it was found that s_1, ψ_1 and ψ_3 bifurcated and therefore this section will discuss the impact that the addition of a spatial element has on the system, with a focus on these specific parameter values.

As previously discussed, s_1 determines the steepness of the recruitment curve for the E_1 population while interacting with the tumour cells. The parameter has been set at the same value as in the ODE case to show a direct comparison. Figures 3.19-3.26 show the spatial density of the cells at times 0-2000 seconds and, as previously discussed, the time here is generic. What can be surmised from these figures is that there is a heterogeneous distribution of tumour cell density, which is invading the tissue. This is very similar to the PDE dynamics that were found in Matzavinos et al. [2004]. These type of dynamics are driven by the presence of a Hopf bifurcation in ODE systems and are deemed heterogeneous type travelling wave solutions. It can be argued that the immune system is keeping the tumour cells in check and a co-existence situation has arisen. As a result of higher rate of recruitment of the E_1 population in the ODE model, the amplitude of the oscillations in T_1 and E_1 was much higher than that of T_2 and E_2, and the spatial results portray similar dynamics. Moreover, the depletion of the E_2 cell population is also seen here, where very small oscillations are present, resulting in a higher T_2 tumour density.

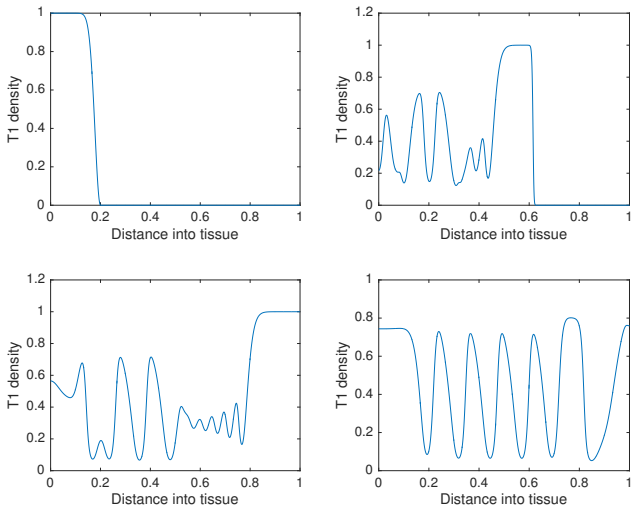

Figure 3.19: *Plots showing the spatial density of T_1 at times 0, 100, 200 and 400 seconds. The figures show heterogeneous travelling waves at $s_1 = 0.225$. This is derived from the same parameter space as the homogeneous system when the Hopf bifurcation is present.*

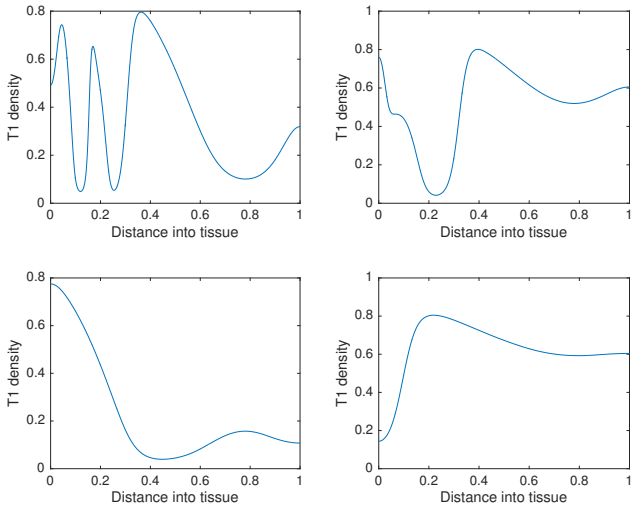

Figure 3.20: *Plots showing the spatial density of T_1 at times 800, 1000, 1500 and 2000 seconds. The figures show heterogeneous travelling waves at $s_1 = 0.225$. This is derived from the same parameter space as the homogeneous system when the Hopf bifurcation is present.*

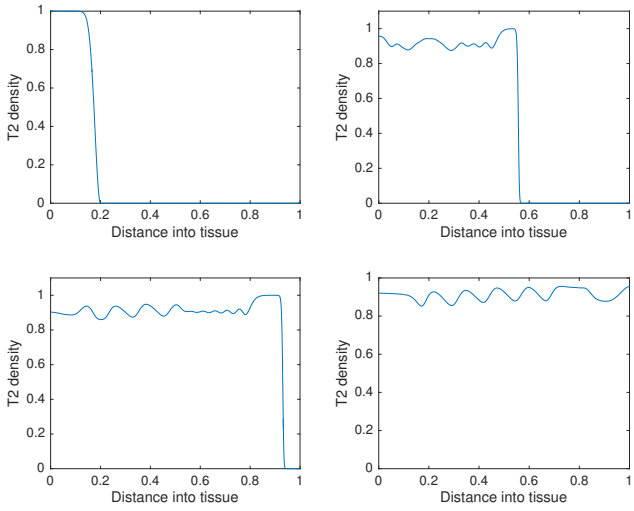

Figure 3.21: *Plots showing the spatial density of T_2 at times 0, 100, 200 and 400 seconds. The figures show heterogeneous travelling waves at $s_1 = 0.225$. This is derived from the same parameter space as the homogeneous system when the Hopf bifurcation is present.*

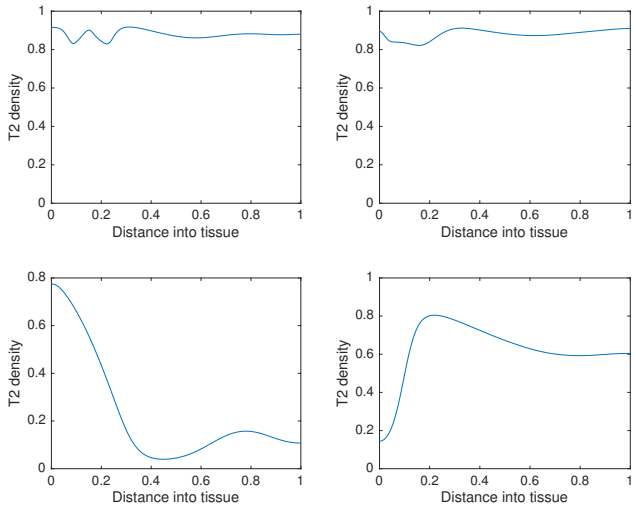

Figure 3.22: *Plots showing the spatial density of T_2 at times 800, 1000, 1500 and 2000 seconds. The figures show heterogeneous travelling waves at $s_1 = 0.225$. This is derived from the same parameter space as the homogeneous system when the Hopf bifurcation is present.*

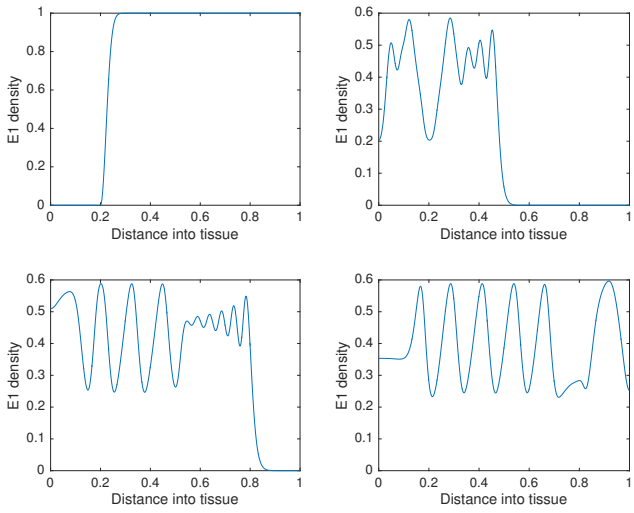

Figure 3.23: *Plots showing the spatial density of E_1 at times 0, 100, 200 and 400 seconds. The figures show heterogeneous travelling waves at $s_1 = 0.225$. This is derived from the same parameter space as the homogeneous system when the Hopf bifurcation is present.*

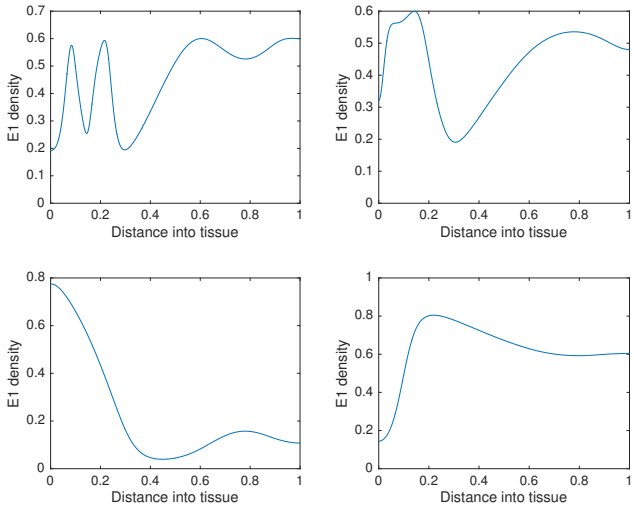

Figure 3.24: *Plots showing the spatial density of E_1 at times 800, 1000, 1500 and 2000 seconds. The figures show heterogeneous travelling waves at $s_1 = 0.225$. This is derived from the same parameter space as the homogeneous system when the Hopf bifurcation is present.*

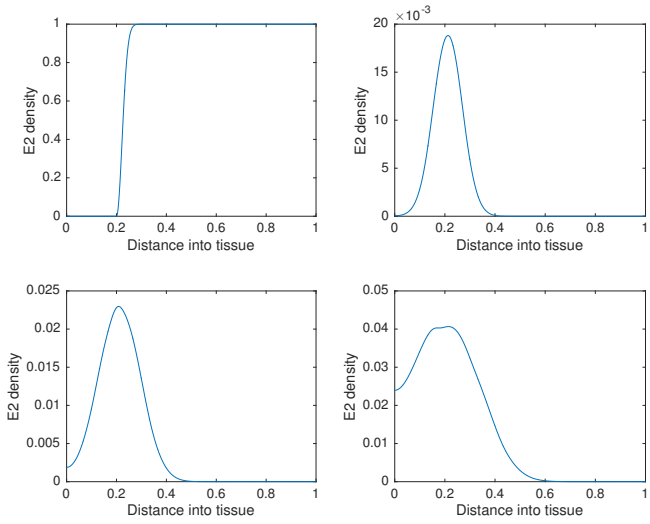

Figure 3.25: *Plots showing the spatial density of E_2 at times 0, 100, 200 and 400 seconds. The figures show heterogeneous travelling waves at $s_1 = 0.225$. This is derived from the same parameter space as the homogeneous system when the Hopf bifurcation is present.*

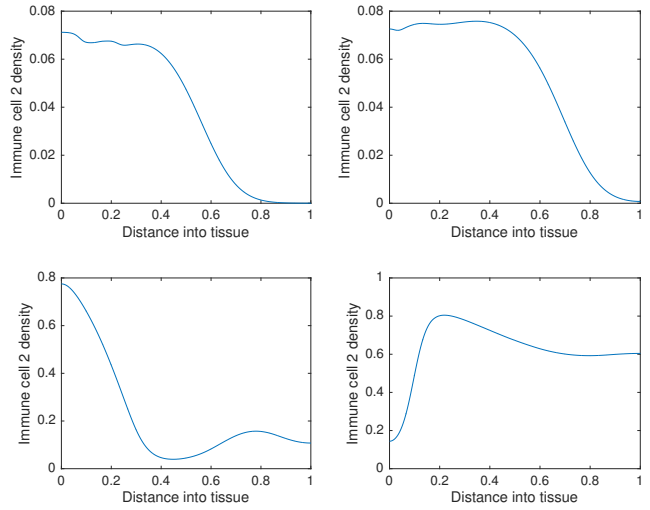

Figure 3.26: *Plots showing the spatial density of E_2 at times 800, 1000, 1500 and 2000 seconds. The figures show heterogeneous travelling waves at $s_1 = 0.225$. This is derived from the same parameter space as the homogeneous system when the Hopf bifurcation is present.*

The next parameter that was varied in the homogeneous model was ψ_1, which determines the saturation level of the E_1 cells when in interaction with T_1. The spatial density of the cells in the domain can be seen in figures 3.27-3.34 and $\psi_1 = 2$, which has been chosen as it was determined that there was periodic solutions here in the homogeneous model. As ψ_1 has been increased, more E_1 cells are in the domain, which subsequently lowers the T_1 tumour density. The figures also show that there is, again, the presence of heterogeneous type waves in the system, whereby the T_1 cells are seen to invade the tissue whilst in attack by the host immune system. Moreover, the E_2 cells again here do not have a sufficient recruitment rate to make any significant effect on the T_2 tumour density and the T_2 cells must be kept under check by the presence of the E_1 cells.

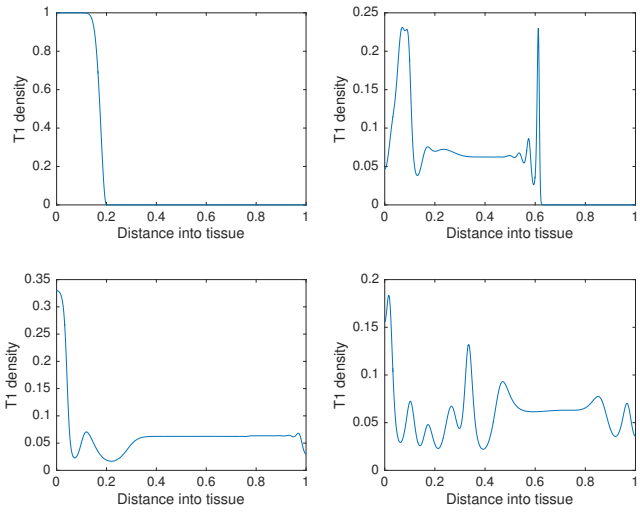

Figure 3.27: *Plots showing the spatial density of T_1 at times 0, 100, 200 and 400 seconds. The figures show heterogeneous travelling waves at $\psi_1 = 2$. This is derived from the same parameter space as the homogeneous system when the Hopf bifurcation is present.*

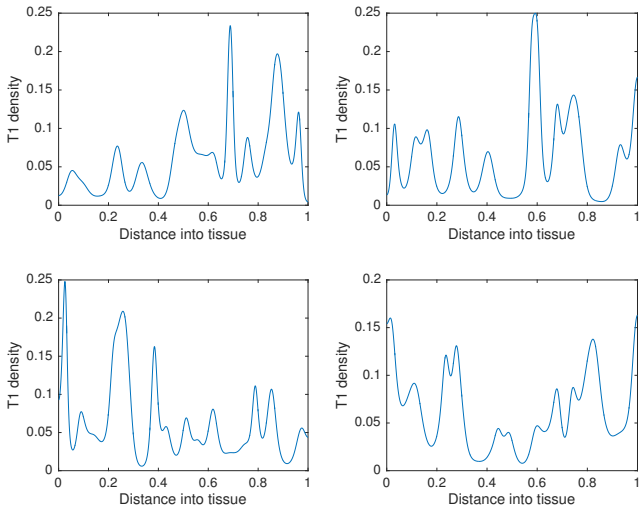

Figure 3.28: *Plots showing the spatial density of T_1 at times 800, 1000, 1500 and 2000 seconds. The figures show heterogeneous travelling waves at $\psi_1 = 2$. This is derived from the same parameter space as the homogeneous system when the Hopf bifurcation is present.*

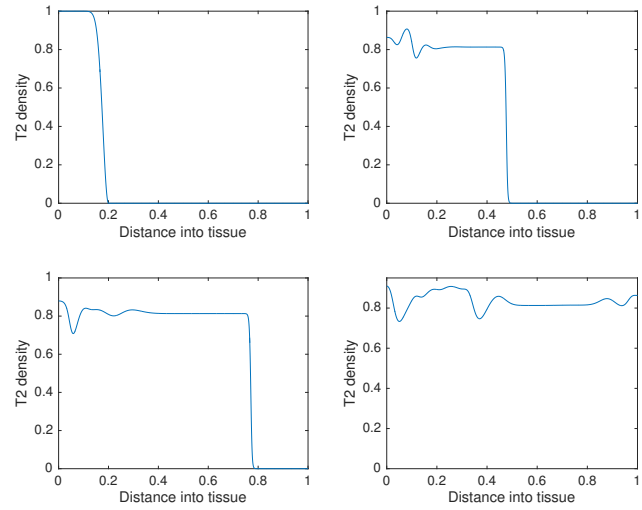

Figure 3.29: *Plots showing the spatial density of T_2 at times 0, 100, 200 and 400 seconds. The figures show heterogeneous travelling waves at $\psi_1 = 2$. This is derived from the same parameter space as the homogeneous system when the Hopf bifurcation is present.*

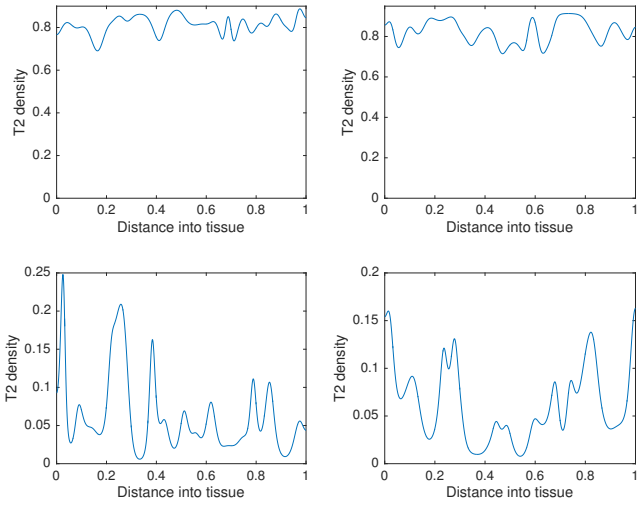

Figure 3.30: *Plots showing the spatial density of T_2 at times 800, 1000, 1500 and 2000 seconds. The figures show heterogeneous travelling waves at $\psi_1 = 2$. This is derived from the same parameter space as the homogeneous system when the Hopf bifurcation is present.*

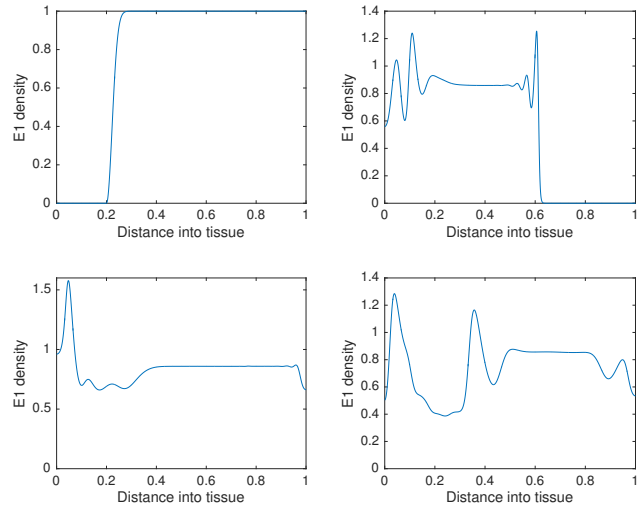

Figure 3.31: *Plots showing the spatial density of E_1 at times 0, 100, 200 and 400 seconds. The figures show heterogeneous travelling waves at $\psi_1 = 2$. This is derived from the same parameter space as the homogeneous system when the Hopf bifurcation is present.*

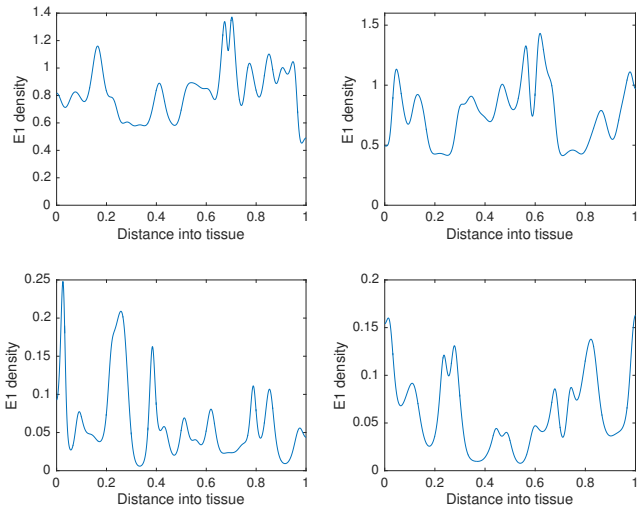

Figure 3.32: *Plots showing the spatial density of E_1 at times 800, 1000, 1500 and 2000 seconds. The figures show heterogeneous travelling waves at $\psi_1 = 2$. This is derived from the same parameter space as the homogeneous system when the Hopf bifurcation is present.*

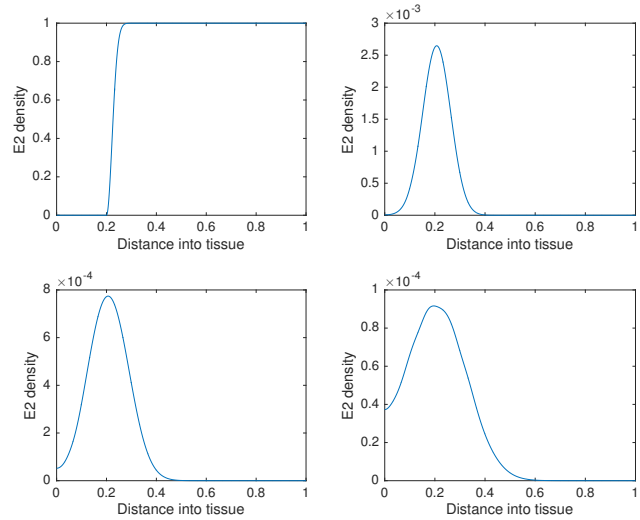

Figure 3.33: *Plots showing the spatial density of E_2 at times 0, 100, 200 and 400 seconds. The figures show heterogeneous travelling waves at $\psi_1 = 2$. This is derived from the same parameter space as the homogeneous system when the Hopf bifurcation is present.*

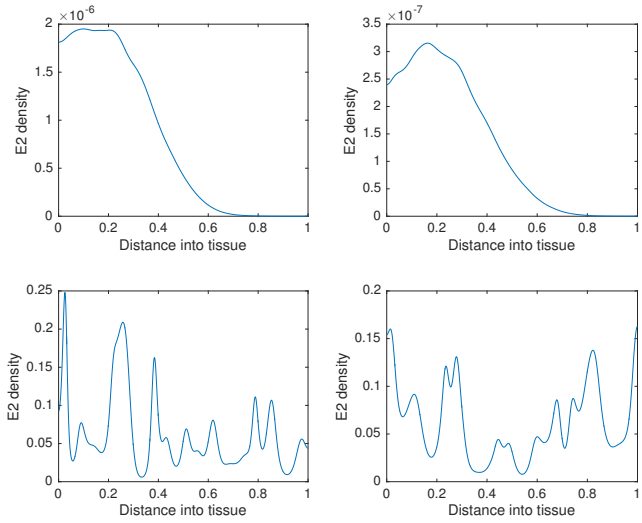

Figure 3.34: *Plots showing the spatial density of E_2 at times 800, 1000, 1500 and 2000 seconds. The figures show heterogeneous travelling waves at $\psi_1 = 2$. This is derived from the same parameter space as the homogeneous system when the Hopf bifurcation is present.*

3.5.2.1 $\psi_3 = 1$

The parameter, ψ_3 has been varied, which determines the recruitment of the E_2 cells when in contact with the T_2 tumour population. Again, there is a Hopf bifurcation in the homogenous system when this parameter is greater than 0.4883. Here the parameter $\psi_1 = 1$, to reflect the results in the homogeneous model. Figures 3.35-3.42 represent the cell densities at times 0-2000 seconds. When looking at the figures for the E_2 population, it can be seen that the boost in the saturation level, allows more cells in the domain, subsequently reducing the T_2 tumour density and heterogeneous type waves are present. Moreover, as before, the T_1 and E_1 cells display uninteresting type dynamics, whereby the solutions seem almost stable.

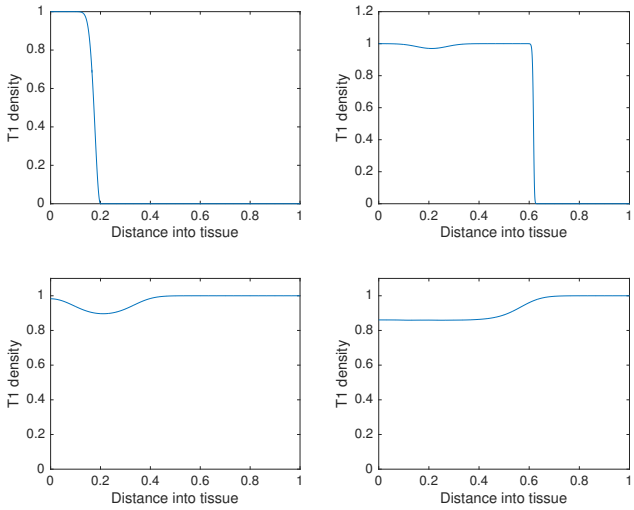

Figure 3.35: *Plots showing the spatial density of T_1 at times 0, 100, 200 and 400 seconds. The figures show heterogeneous travelling waves at $\psi_3 = 1$. This is derived from the same parameter space as the homogeneous system when the Hopf bifurcation is present.*

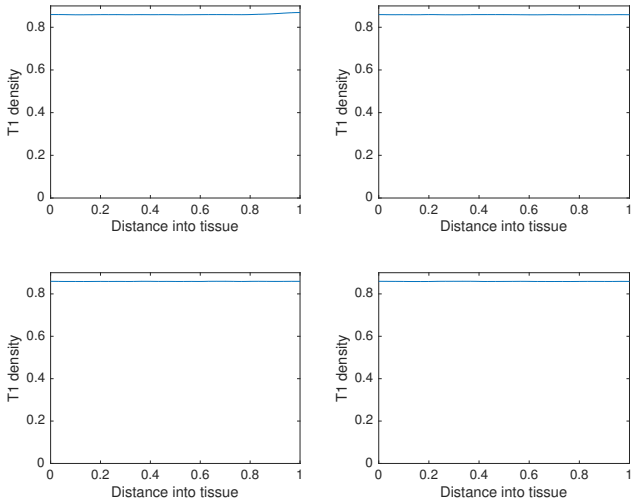

Figure 3.36: *Plots showing the spatial density of T_1 at times 800, 1000, 1500 and 2000 seconds. The figures show heterogeneous travelling waves at $\psi_3 = 1$. This is derived from the same parameter space as the homogeneous system when the Hopf bifurcation is present.*

3.5.3 Discussion

This section has focused on the extension of the homogeneous model into a spatial model. Diffusion terms were added and the results were discussed. The results reflect the findings of the ODE model in that they explore the variation of the parameter s_1, ψ_1 and ψ_3. In s_1 and ψ_1 the T_1, T_2 and E_1 and population showed heterogeneous type waves, driven by the presence of the periodic solutions in the ODE model. ψ_3 showed the T_2 tumour cell population invading the tissue and creating heterogeneous type waves while under attack by the E_1 and E_2 cells. The model will now be extended into 2-D.

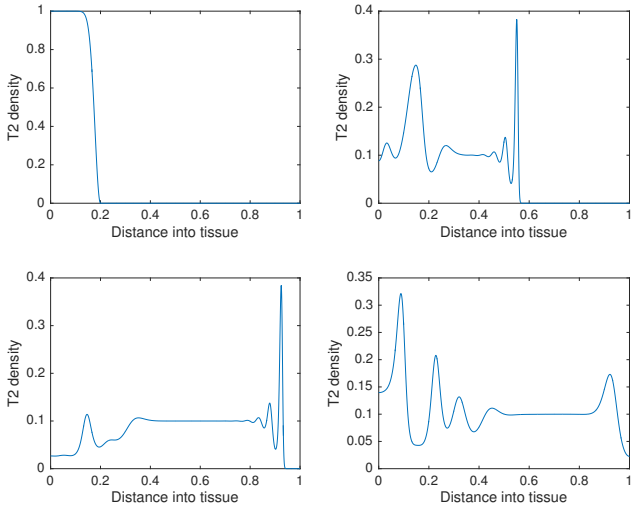

Figure 3.37: *Plots showing the spatial density of T_2 at times 0, 100, 200 and 400 seconds. The figures show heterogeneous travelling waves at $\psi_3 = 1$. This is derived from the same parameter space as the homogeneous system when the Hopf bifurcation is present.*

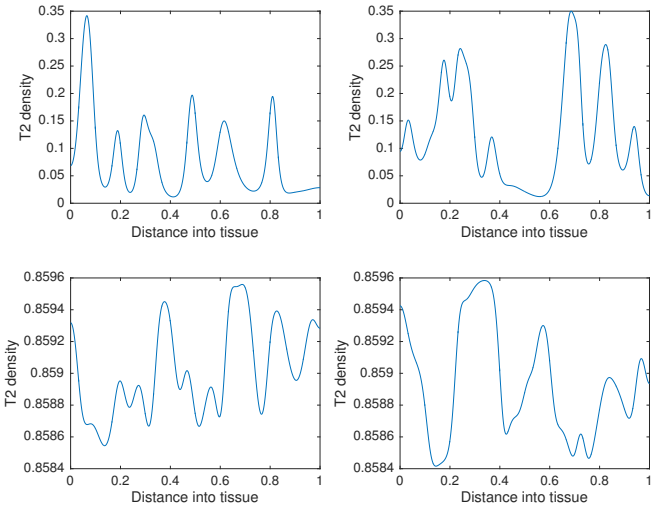

Figure 3.38: *Plots showing the spatial density of T_2 at times 800, 1000, 1500 and 2000 seconds. The figures show heterogeneous travelling waves at $\psi_3 = 1$. This is derived from the same parameter space as the homogeneous system when the Hopf bifurcation is present.*

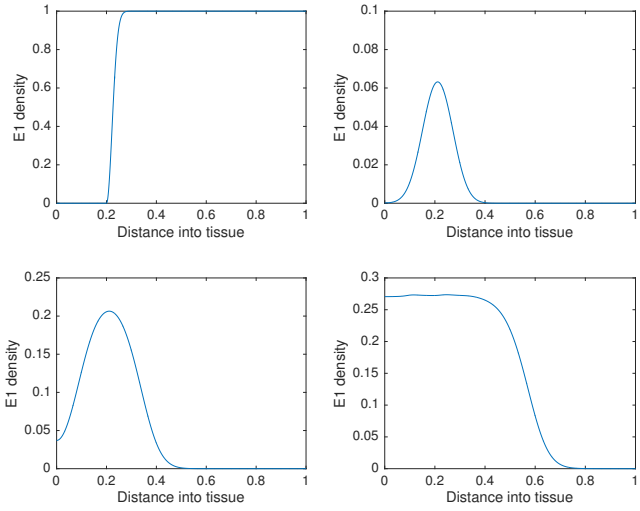

Figure 3.39: *Plots showing the spatial density of E_1 at times 0, 100, 200 and 400 seconds. The figures show heterogeneous travelling waves at $\psi_3 = 1$. This is derived from the same parameter space as the homogeneous system when the Hopf bifurcation is present.*

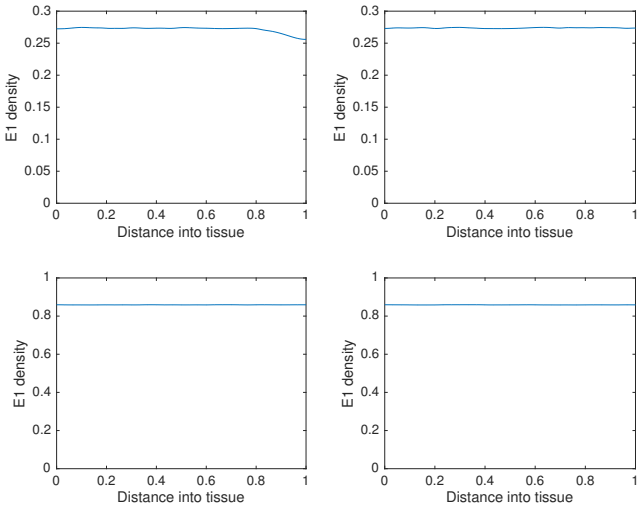

Figure 3.40: *Plots showing the spatial density of E_1 at times 800, 1000, 1500 and 2000 seconds. The figures show heterogeneous travelling waves at $\psi_3 = 1$. This is derived from the same parameter space as the homogeneous system when the Hopf bifurcation is present.*

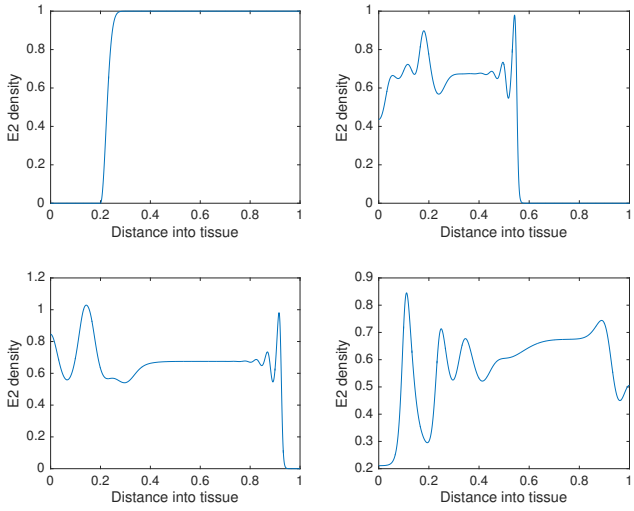

Figure 3.41: *Plots showing the spatial density of E_2 at times 0, 100, 200 and 400 seconds. The figures show heterogeneous travelling waves at $\psi_3 = 1$. This is derived from the same parameter space as the homogeneous system when the Hopf bifurcation is present.*

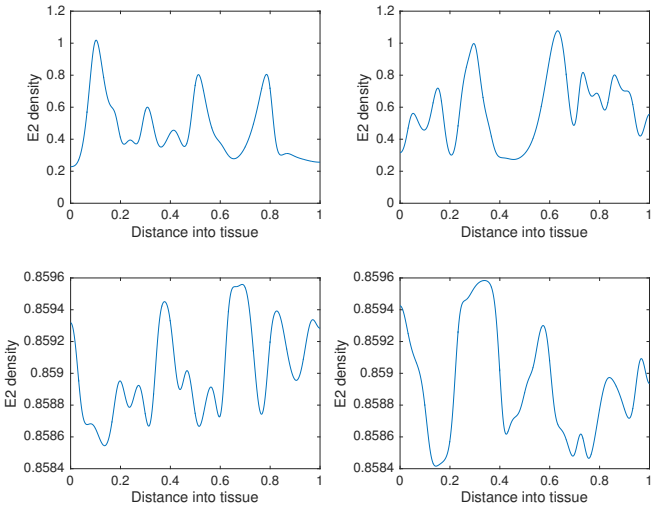

Figure 3.42: *Plots showing the spatial density of E_2 at times 800, 1000, 1500 and 2000 seconds. The figures show heterogeneous travelling waves at $\psi_3 = 1$. This is derived from the same parameter space as the homogeneous system when the Hopf bifurcation is present.*

3.6 2-D spatial model

This section is concerned with extending the spatial model into two dimensions. It is good practice to check whether the system works in higher dimensions to try and ascertain if the model is biologically relevant. The model has been inputted into the computer programme "Comsol", utilised to implement the finite element method in time independent PDE systems, over given domains, to approximate the solutions over a set time. Further details of Comsol are given in Chapter 1.3.

This model utilises a circular domain for each cell type. The initial tumour cell density has been kept constant throughout the domain and the immune cells are set occupy the inside of the domain. This is depicted in Figure 3.43. Moreover, as previously discussed in section 3.5, the chaotic nature of these results is not driven by the initial conditions, but by the presence of the limit cycle in addition to the diffusion of the cells.

3.6.1 Results

In the homogenous model it was found that there is a Hopf bifurcation at $s_1 = 0.225$. This was then investigated in the spatial model by setting s_1 to a value, which is in the same parameter space as when oscillations are present in the homogeneous model, producing heterogeneous travelling waves. Moreover, the parameter s_1 controls the rate of the E_1 cells reaching saturation. In this case the parameter has been decreased, leading to a faster saturation level. In this section, the model has been extended into 2-D and the same parameter has been investigated using a value as when oscillations would be

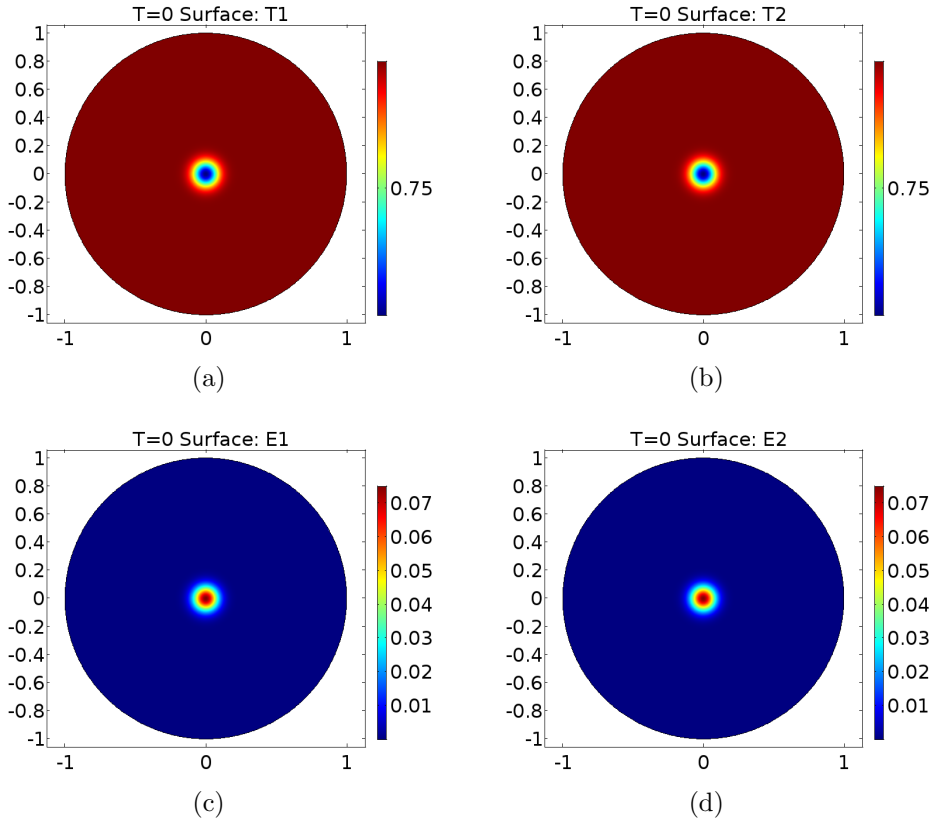

Figure 3.43: *Plots showing initial value plots of tumour and immune cells*

present in the homogeneous model, s_1=0.27. Figures 3.44-3.52 represent the two-dimensional results at times 100, 200, 400, 800, 1000, 1200, 1600 and 2000 seconds. These pictures mimic the results found in the homogenous and one-dimensional spatial cases. The E_1 immune population is seen to be attacking the T_1 tumour population producing heterogeneous dynamics. The waves of immune cell and tumour cells interacting with each other show the oscillatory nature of the system. Moreover, it can be seen that the E_2 immune population is very small and has very little heterogeneity, although it is present. This small population of E_2 cells therefore does not make any significant impact on the T_2 tumour density.

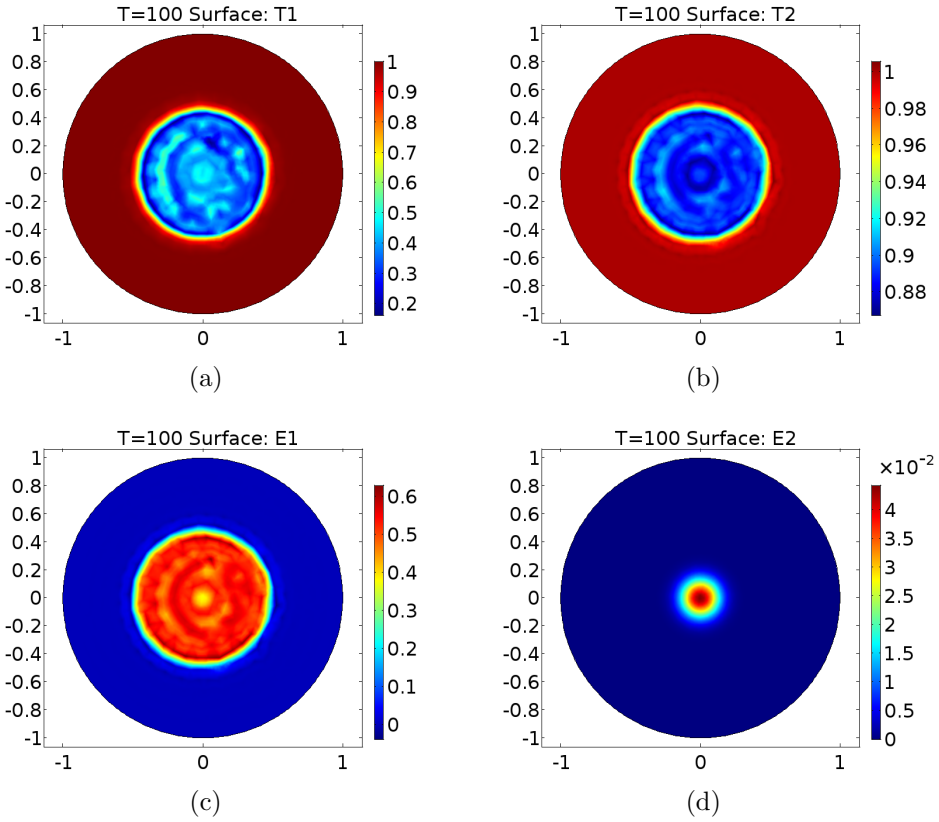

Figure 3.44: *Plots showing two dimensional heterogeneous distribution of tumour and immune cells when $s_1 = 0.27$ at time=100. Figures 3.44(a) and 3.44(b) represent tumour type 1 and 2. Figures 3.44(c) and 3.44(d) represent immune type 1 and 2.*

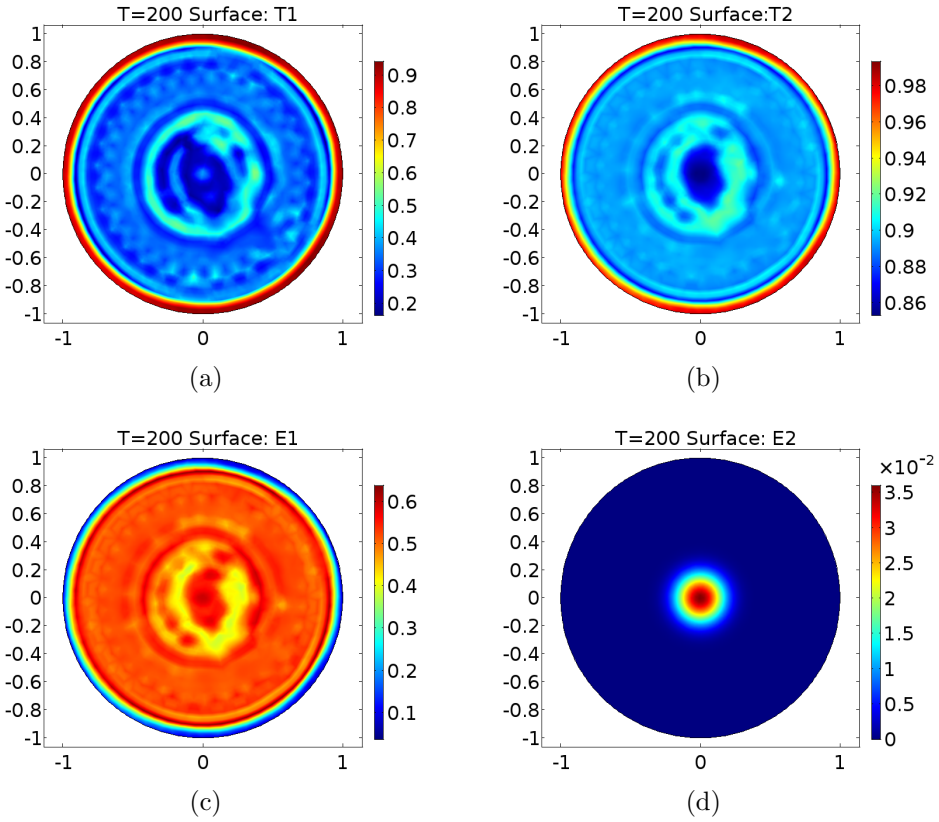

Figure 3.45: *Plots showing two dimensional heterogeneous distribution of tumour and immune cells when $s_1 = 0.27$ at time=200. Figures 3.45(a) and 3.45(b) represent tumour type 1 and 2. Figures 3.45(c) and 3.45(d) represent immune type 1 and 2.*

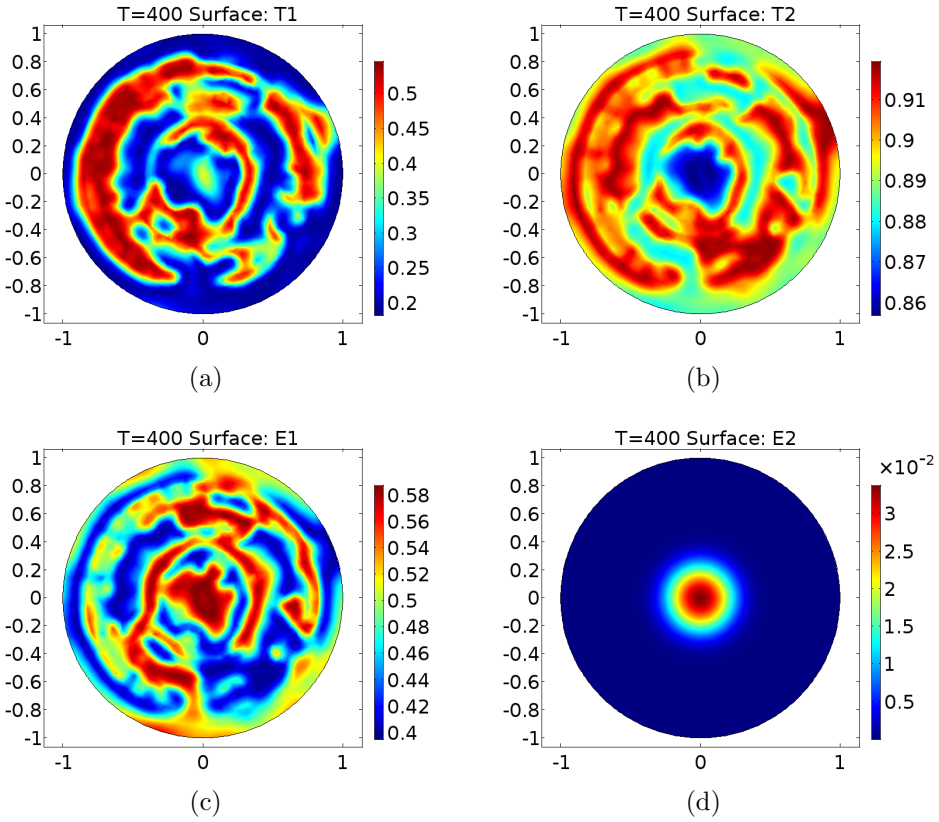

Figure 3.46: *Plots showing two dimensional heterogeneous distribution of tumour and immune cells when $s_1 = 0.27$ at time=400. Figures 3.46(a) and 3.46(b) represent tumour type 1 and 2. Figures 3.46(c) and 3.46(d) represent immune type 1 and 2.*

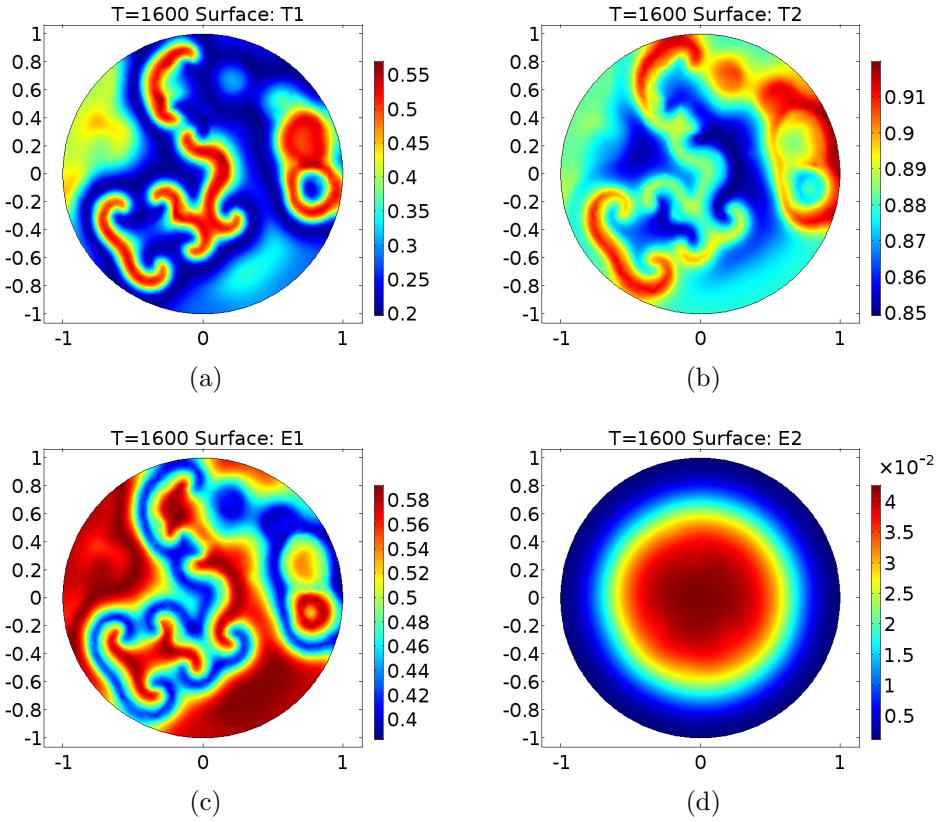

(a) (b) (c) (d)

Figure 3.47: *Plots showing two dimensional heterogeneous distribution of tumour and immune cells when $s_1 = 0.27$ at time=600. Figures 3.47(a) and 3.47(b) represent tumour type 1 and 2. Figures 3.47(c) and 3.47(d) represent immune type 1 and 2.*

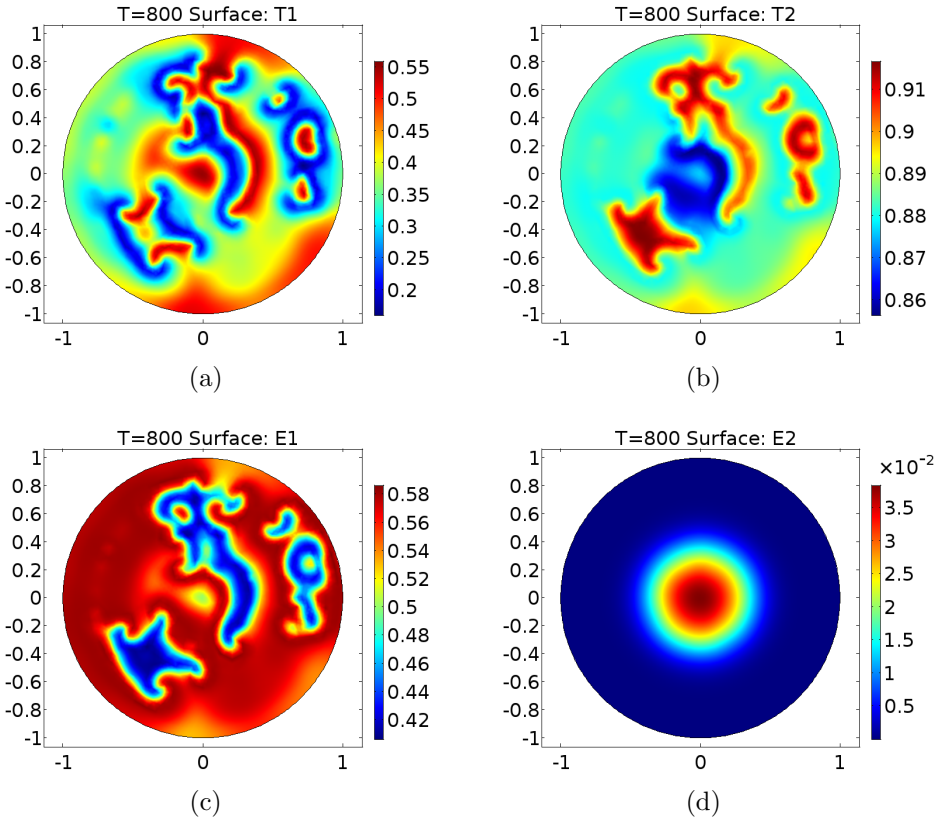

Figure 3.48: *Plots showing two dimensional heterogeneous distribution of tumour and immune cells when $s_1 = 0.27$ at time=800. Figures 3.48(a) and 3.48(b) represent tumour type 1 and 2. Figures 3.48(c) and 3.48(d) represent immune type 1 and 2.*

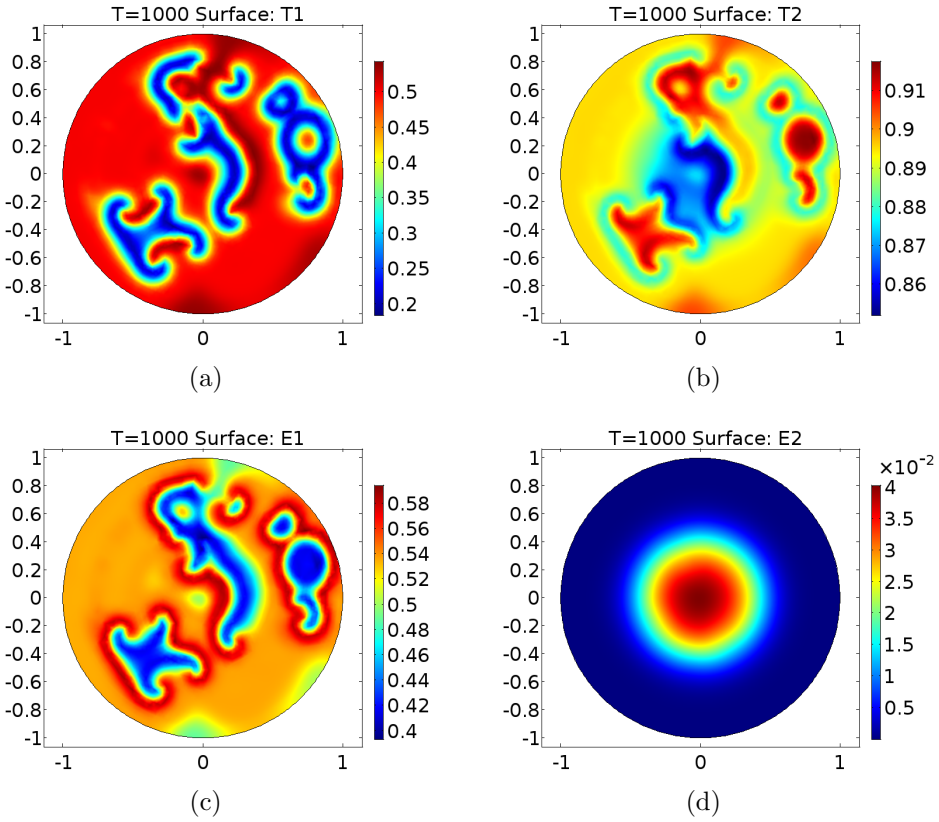

Figure 3.49: *Plots showing two dimensional heterogeneous distribution of tumour and immune cells when* $s_1 = 0.27$ *at time=1000. Figures 3.49(a) and 3.49(b) represent tumour type 1 and 2. Figures 3.49(c) and 3.49(d) represent immune type 1 and 2.*

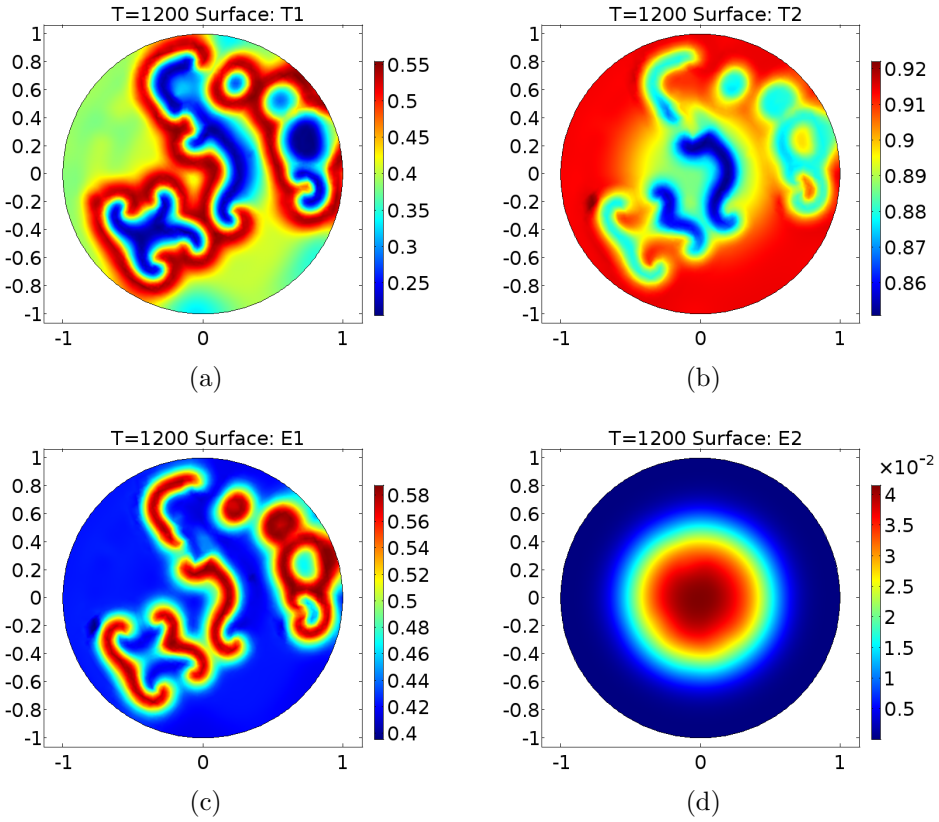

Figure 3.50: *Plots showing two dimensional heterogeneous distribution of tumour and immune cells when* $s_1 = 0.27$ *at time=1200. Figures 3.50(a) and 3.50(b) represent tumour type 1 and 2. Figures 3.50(c) and 3.50(d) represent immune type 1 and 2.*

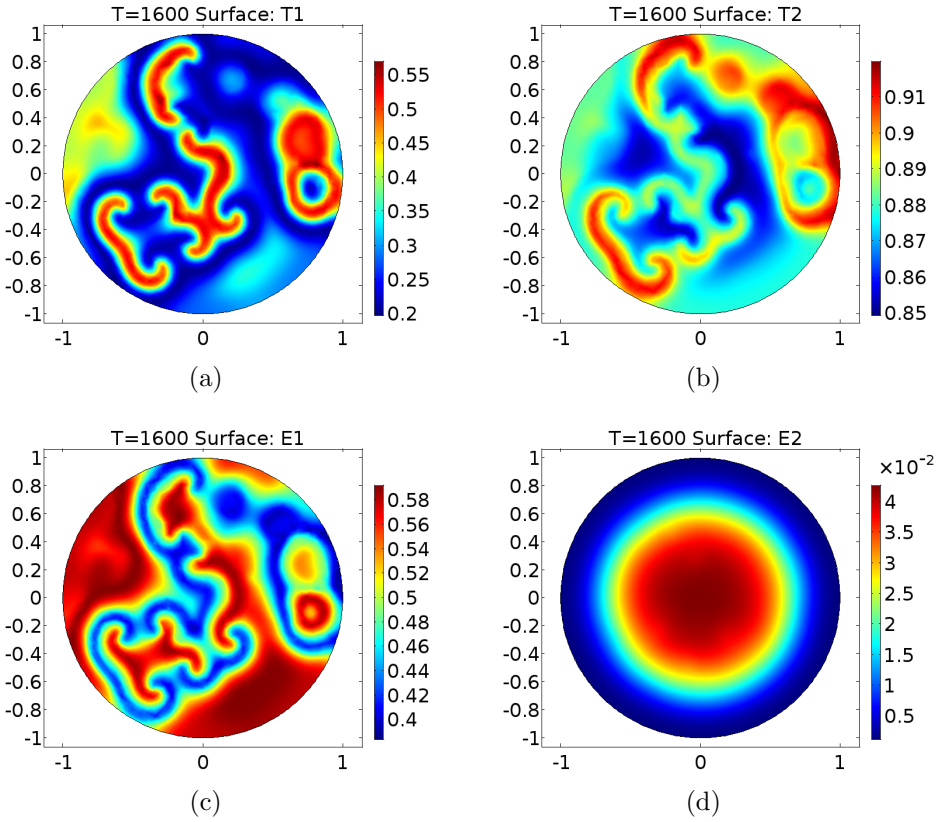

Figure 3.51: *Plots showing two dimensional heterogeneous distribution of tumour and immune cells when* $s_1 = 0.27$ *at time=1600. Figures 3.51(a) and 3.51(b) represent tumour type 1 and 2. Figures 3.51(c) and 3.51(d) represent immune type 1 and 2.*

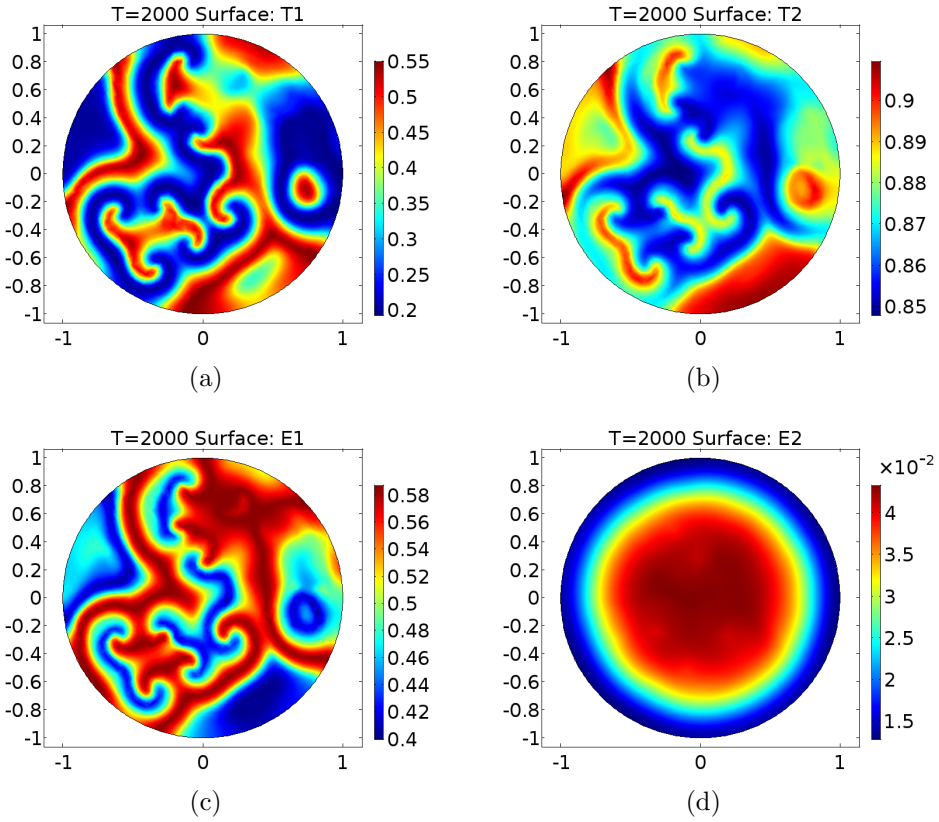

Figure 3.52: *Plots showing two dimensional heterogeneous distribution of tumour and immune cells when* $s_1 = 0.27$ *at time=2000. Figures 3.52(a) and 3.52(b) represent tumour type 1 and 2. Figures 3.52(c) and 3.52(d) represent immune type 1 and 2.*

In the homogeneous model it was found that there is a Hopf bifurcation at $\psi_1 = 0.8287$. This was then investigated in the spatial model by setting ψ_1 to a value, which is in the same parameter space as when oscillations are present in the homogeneous model, producing heterogeneous travelling waves. Figures 3.53-3.61 show the dynamics of the 2-D system when the parameter ψ_1 has been set at 0.08288. This parameter controls the saturation level of the E_1 cells and as it has been increased, from the original parameter value found in section 3.4.2, more E_1 cells are recruited into the domain. The result of this is a decreased T_1 tumour cell density. The figures depict that the system again displays heterogeneity in E_1, T_1 and T_2, whereby the E_1 cells are keeping the T_1 and T_2 (although at a much lower rate) tumour cells in check. Furthermore, in the homogenous case the E_2 cells were not able to provide suitable surveillance of the E_2 tumour cell population resulting in a high T_2 tumour cell density. Moreover, just as in the homogeneous and 1-D spatial case the E_2 cells do not exhibit a lot of heterogeneity but it is present.

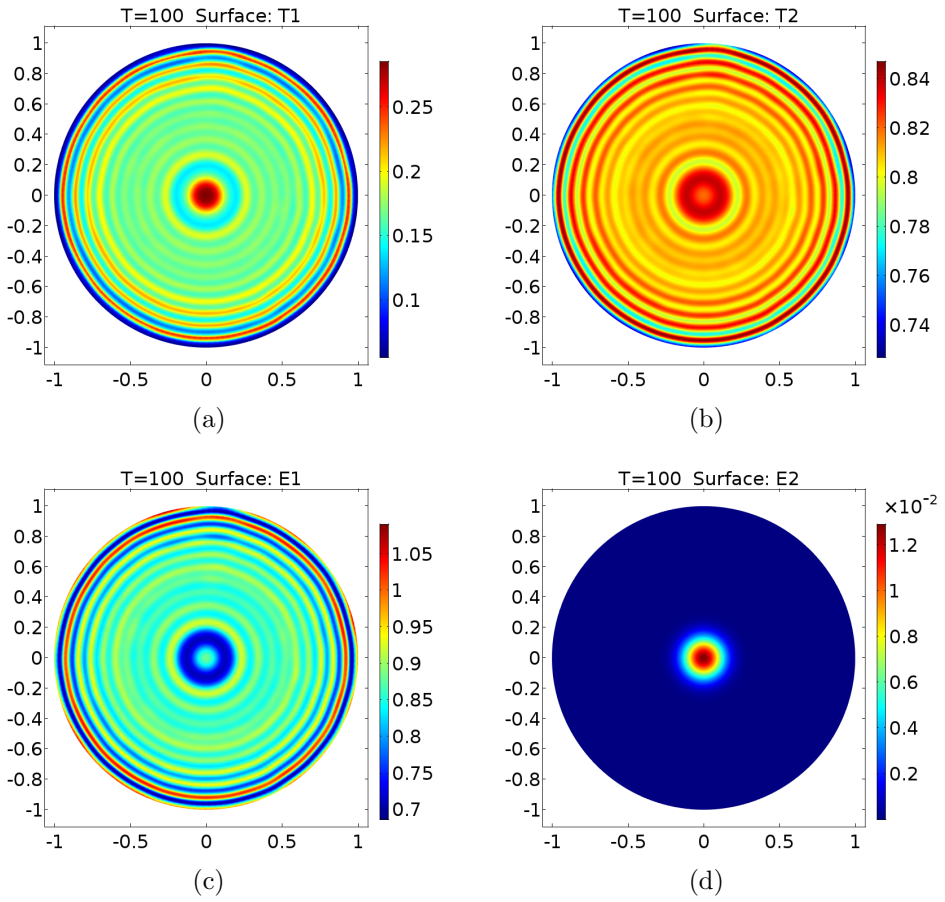

Figure 3.53: *Plots showing two dimensional heterogeneous distribution of tumour and immune cells when* $\psi_1 = 0.8288$ *at time=100. Figures 3.53(a) and 3.53(b) represent tumour type 1 and 2. Figures 3.53(c) and 3.53(d) represent immune type 1 and 2.*

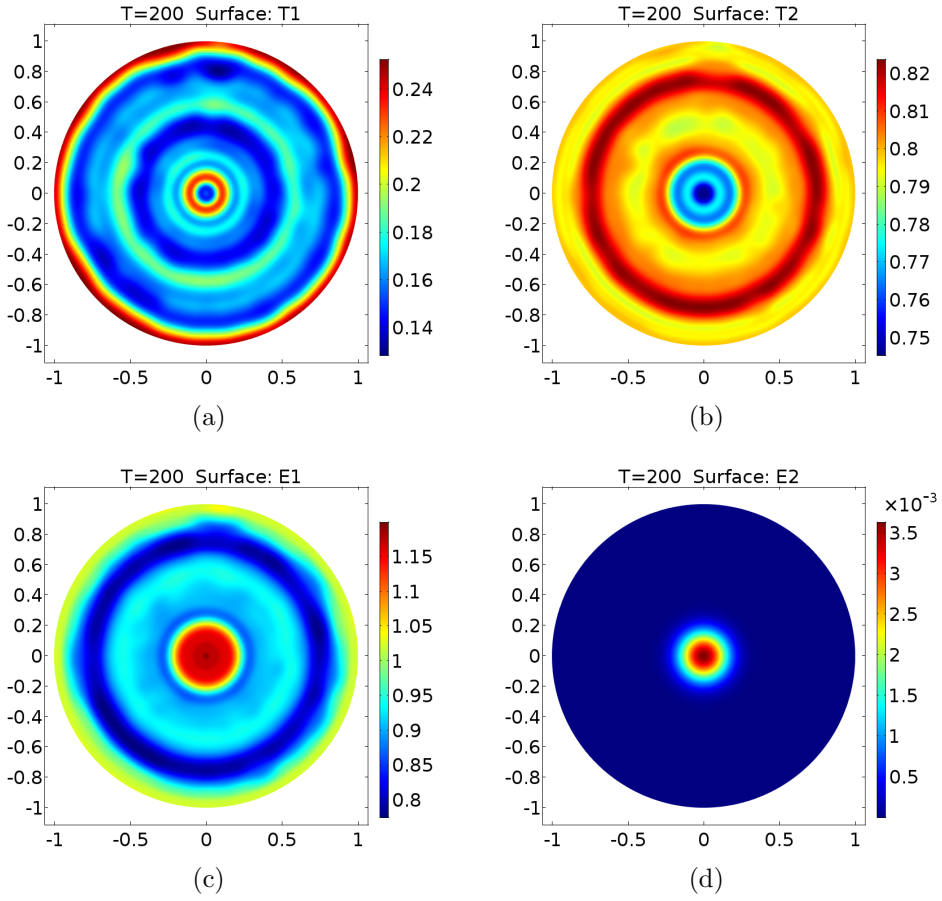

Figure 3.54: *Plots showing two dimensional heterogeneous distribution of tumour and immune cells when* $\psi_1 = 0.8288$ *at time=200. Figures 3.54(a) and 3.54(b) represent tumour type 1 and 2. Figures 3.54(c) and 3.54(d) represent immune type 1 and 2.*

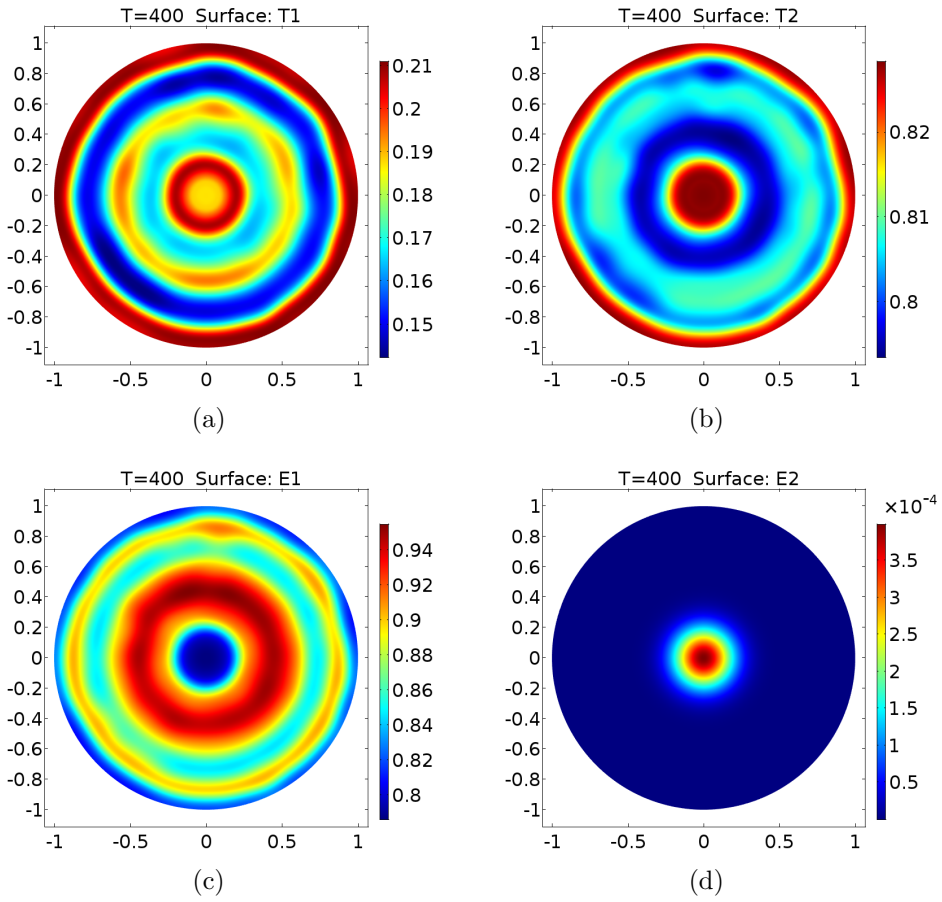

Figure 3.55: *Plots showing two dimensional heterogeneous distribution of tumour and immune cells when* $\psi_1 = 0.8288$ *at time=400. Figures 3.55(a) and 3.55(b) represent tumour type 1 and 2. Figures 3.55(c) and 3.55(d) represent immune type 1 and 2.*

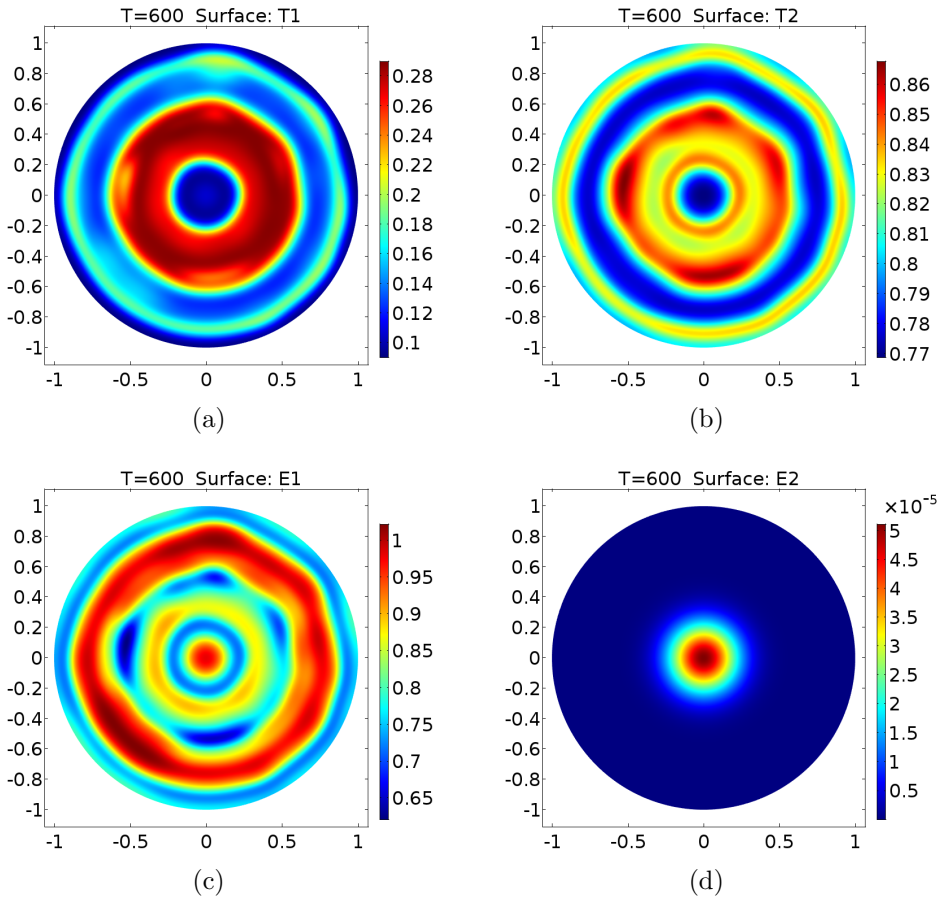

Figure 3.56: *Plots showing two dimensional heterogeneous distribution of tumour and immune cells when* $\psi_1 = 0.8288$ *at time=600. Figures 3.56(a) and 3.56(b) represent tumour type 1 and 2. Figures 3.56(c) and 3.56(d) represent immune type 1 and 2.*

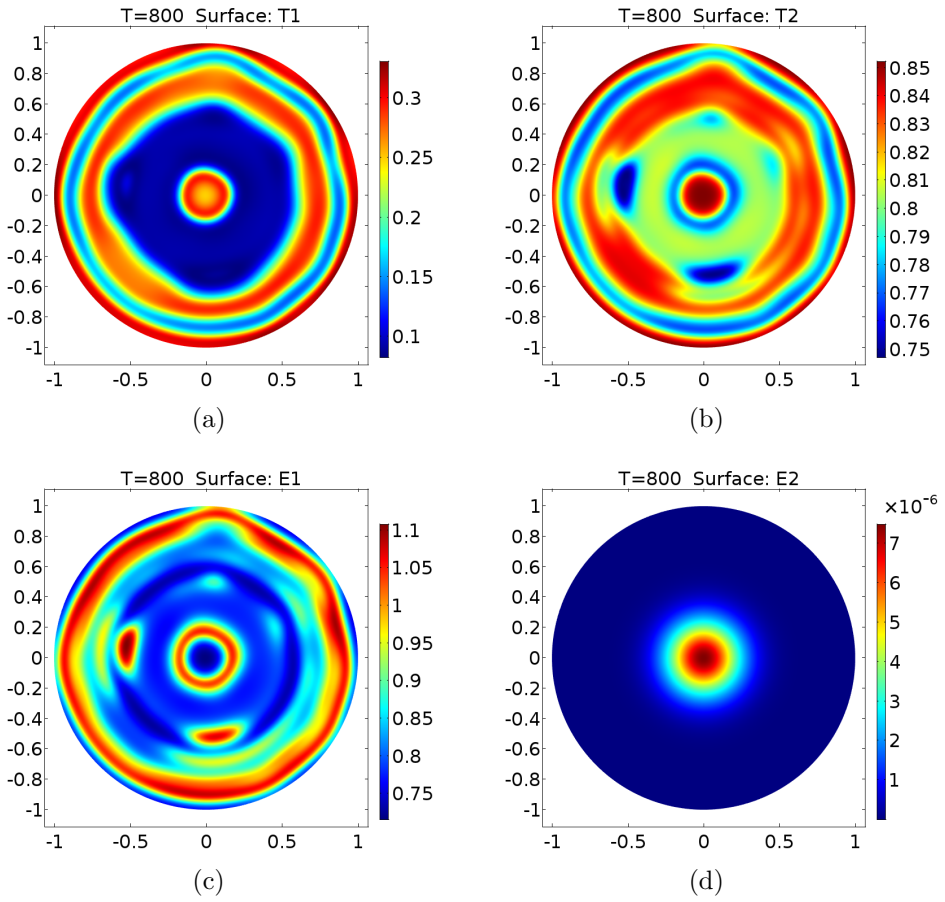

Figure 3.57: *Plots showing two dimensional heterogeneous distribution of tumour and immune cells when* $\psi_1 = 0.8288$ *at time=800. Figures 3.57(a) and 3.57(b) represent tumour type 1 and 2. Figures 3.57(c) and 3.57(d) represent immune type 1 and 2.*

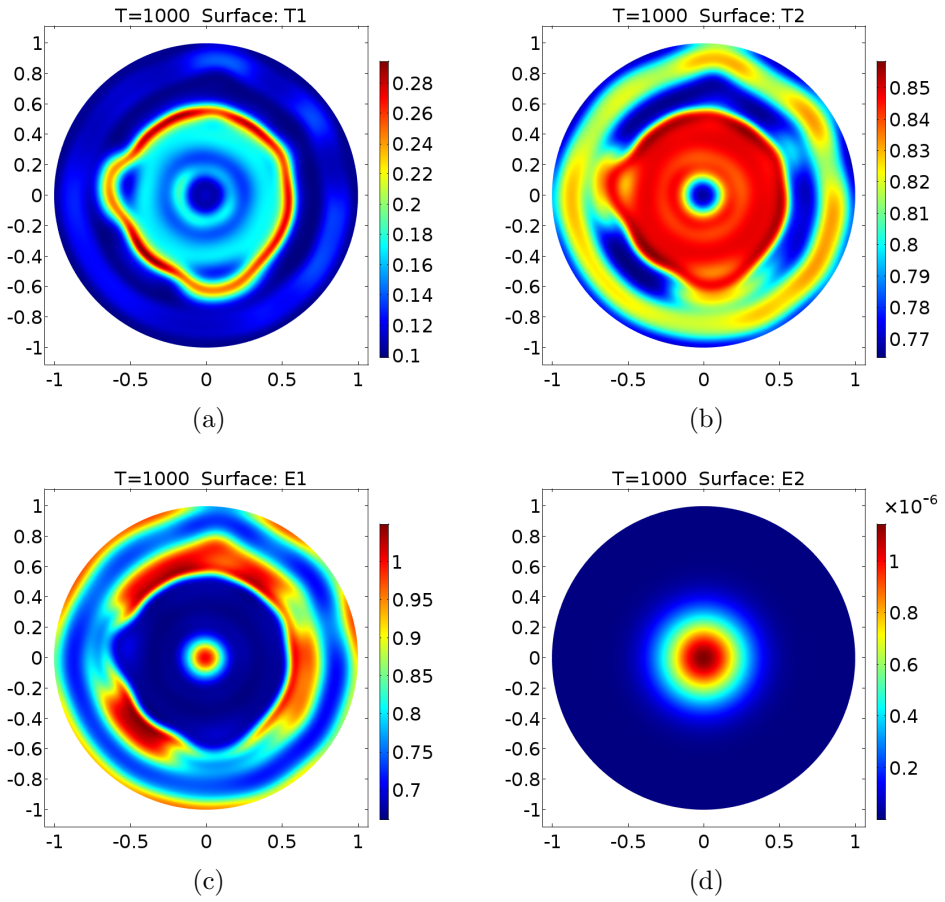

Figure 3.58: *Plots showing two dimensional heterogeneous distribution of tumour and immune cells when* $\psi_1 = 0.8288$ *at time=1000. Figures 3.58(a) and 3.58(b) represent tumour type 1 and 2. Figures 3.58(c) and 3.58(d) represent immune type 1 and 2.*

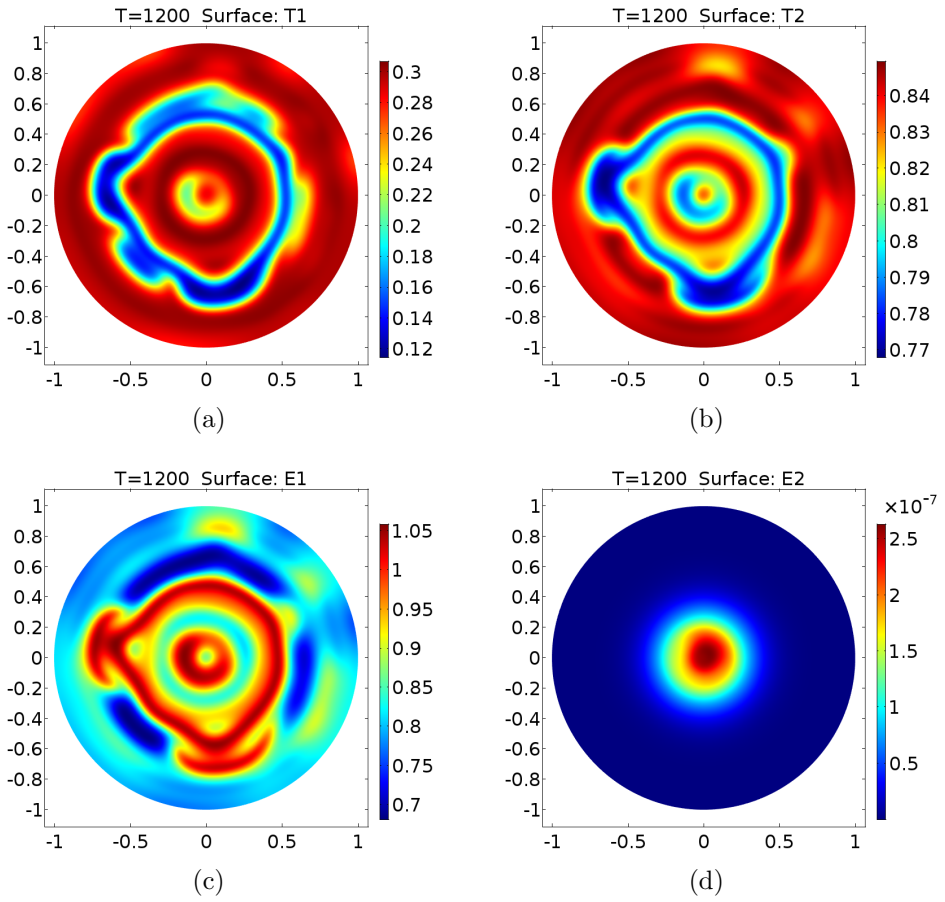

Figure 3.59: *Plots showing two dimensional heterogeneous distribution of tumour and immune cells when* $\psi_1 = 0.8288$ *at time=1200. Figures 3.59(a) and 3.59(b) represent tumour type 1 and 2. Figures 3.59(c) and 3.59(d) represent immune type 1 and 2.*

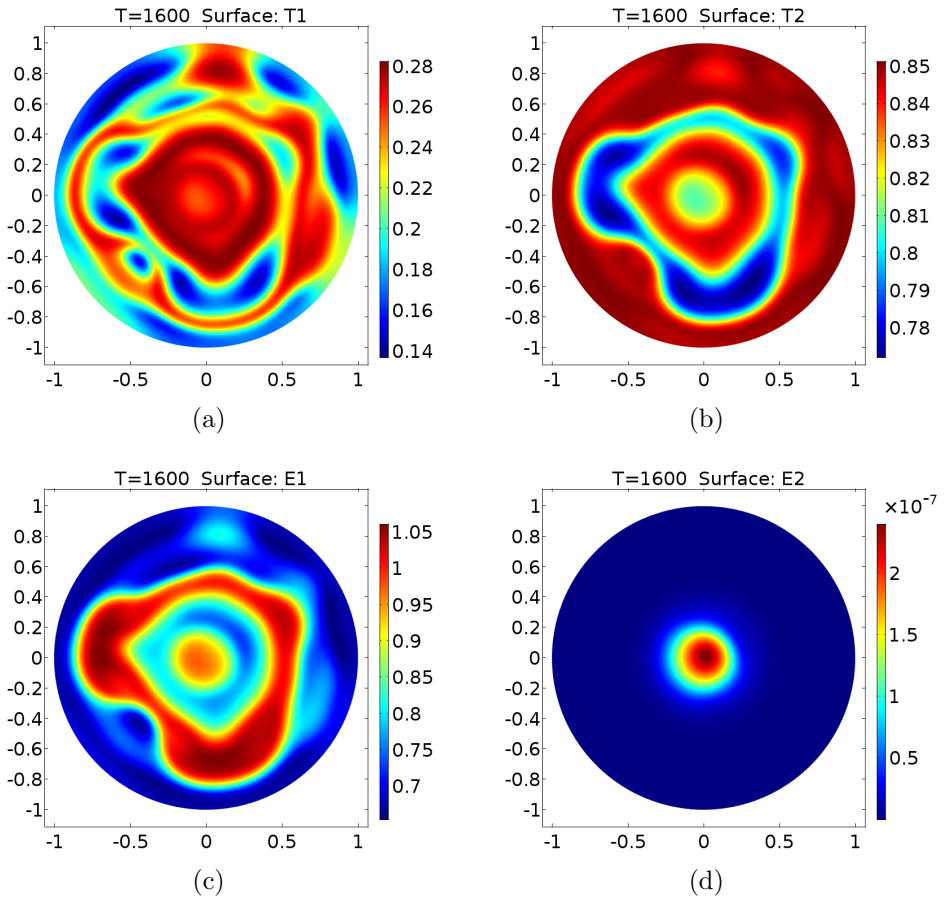

Figure 3.60: *Plots showing two dimensional heterogeneous distribution of tumour and immune cells when* $\psi_1 = 0.8288$ *at time=1600. Figures 3.60(a) and 3.60(b) represent tumour type 1 and 2. Figures 3.60(c) and 3.60(d) represent immune type 1 and 2.*

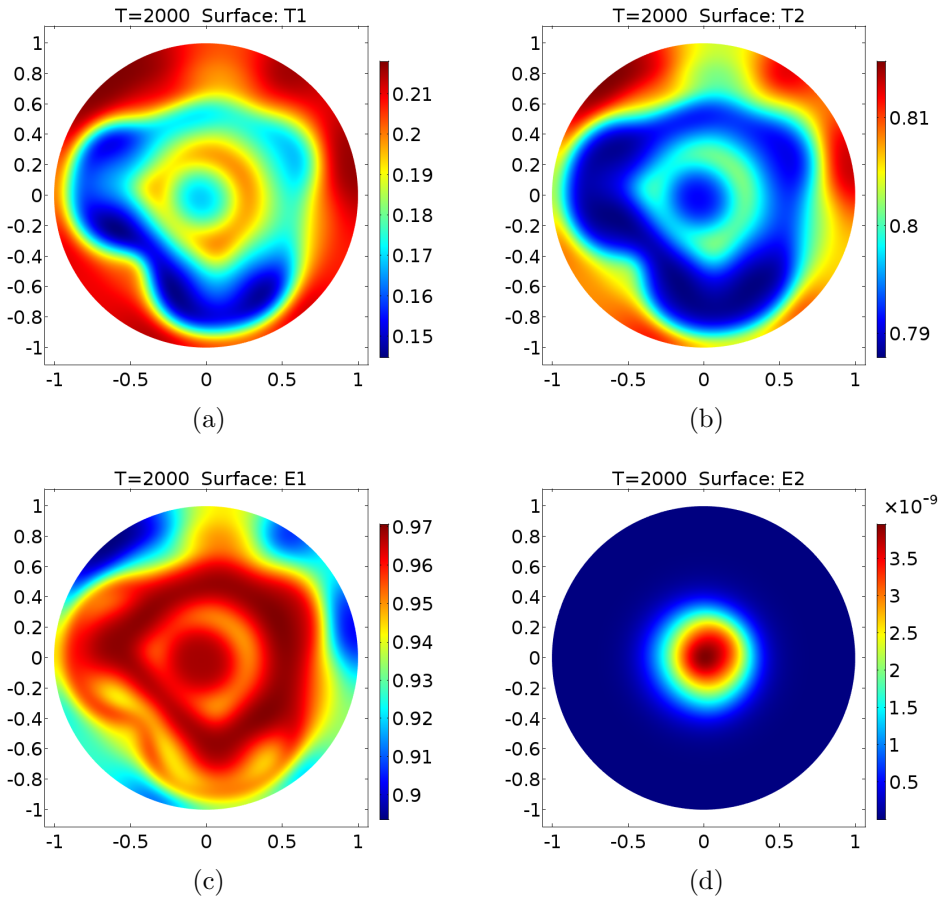

Figure 3.61: *Plots showing two dimensional heterogeneous distribution of tumour and immune cells when* $\psi_1 = 0.8288$ *at time=2000. Figures 3.61(a) and 3.61(b) represent tumour type 1 and 2. Figures 3.61(c) and 3.61(d) represent immune type 1 and 2.*

In the homogenous model it was found that there is a Hopf bifurcation at $\psi_3 = 0.4883$. This was then investigated in the spatial model by setting ψ_3 to a value which is in the same parameter space as when oscillations are present in the homogeneous model, producing heterogeneous travelling waves. Here the parameter ψ_3 has been investigated, which determines the saturation level of the E_2 immune cells. Here the parameter has been increased allowing more E_2 cells to be recruited into the system. Figures 3.62-3.66 represent 2-D simulations for all cell types at times, 100, 400, 800, 1200 and 2000 seconds. Again, just as in the homogeneous and 1-D spatial model, the figures show that the increased recruitment of the E_2 cells results in a decreased T_2 tumour cell density and the E_1 and T_1 populations remain largely unaffected. These figures, although showing very small heterogeneity has not given the best results. When increasing this parameter the model struggled to converge and therefore, the value of the ψ_3 that had to be used in this instance was very close to the bifurcation value in the homogenous case, which produces very small oscillations.

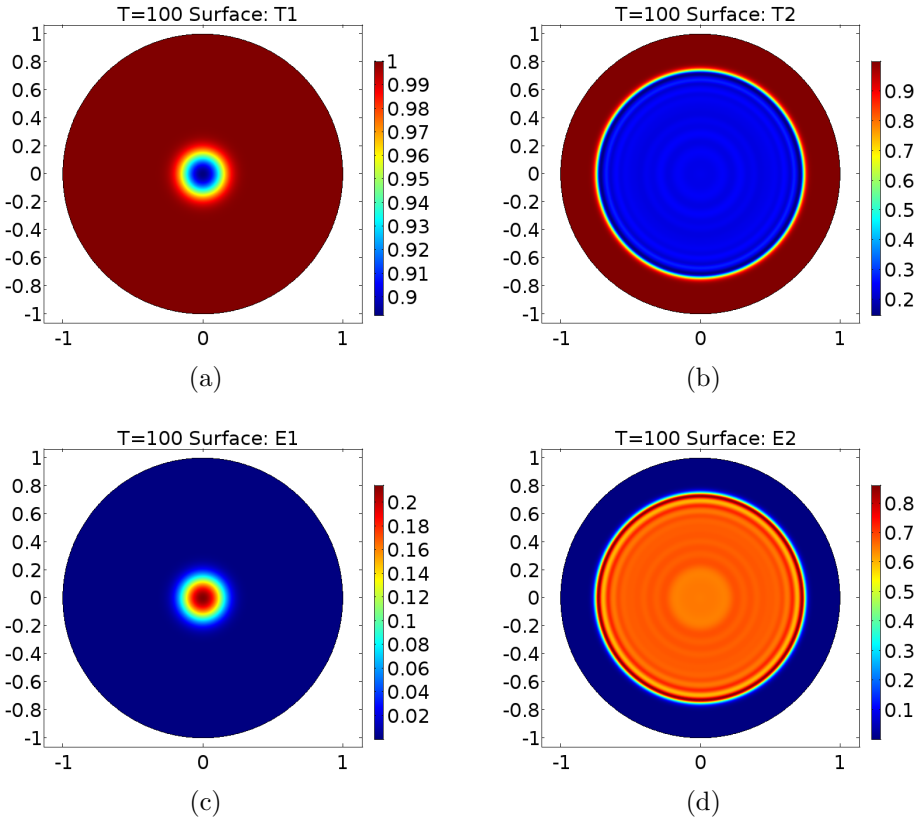

Figure 3.62: *Plots showing two dimensional heterogeneous distribution of tumour and immune cells when* $\psi_3 = 0.5$ *at time=100. Figures 3.62(a) and 3.62(b) represent tumour type 1 and 2. Figures 3.62(c) and 3.62(d) represent immune type 1 and 2.*

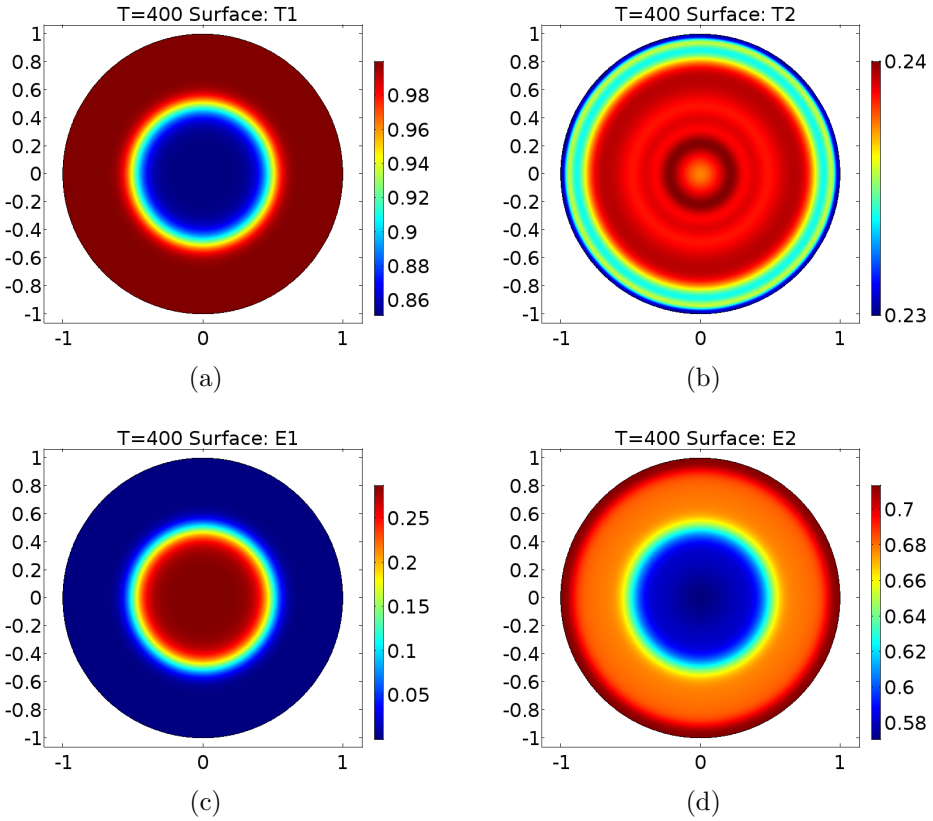

Figure 3.63: *Plots showing two dimensional heterogeneous distribution of tumour and immune cells when* $\psi_3 = 0.5$ *at time=400. Figures 3.63(a) and 3.63(b) represent tumour type 1 and 2. Figures 3.63(c) and 3.63(d) represent immune type 1 and 2.*

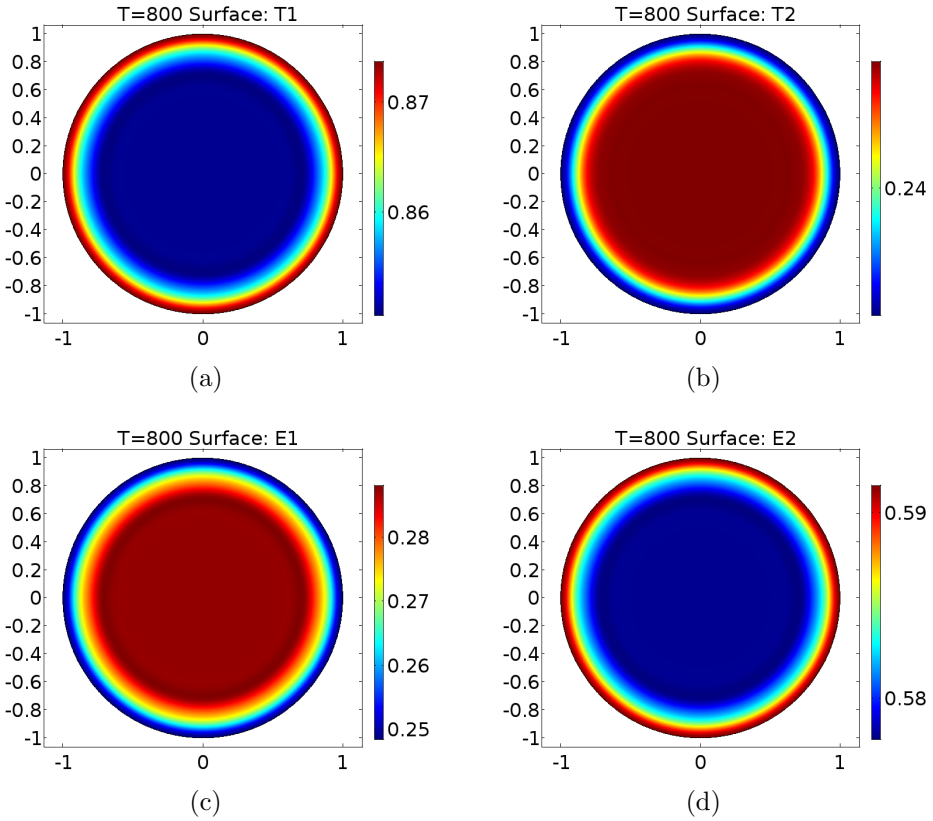

Figure 3.64: *Plots showing two dimensional heterogeneous distribution of tumour and immune cells when* $\psi_3 = 0.5$ *at time=800. Figures 3.64(a) and 3.64(b) represent tumour type 1 and 2. Figures 3.64(c) and 3.64(d) represent immune type 1 and 2.*

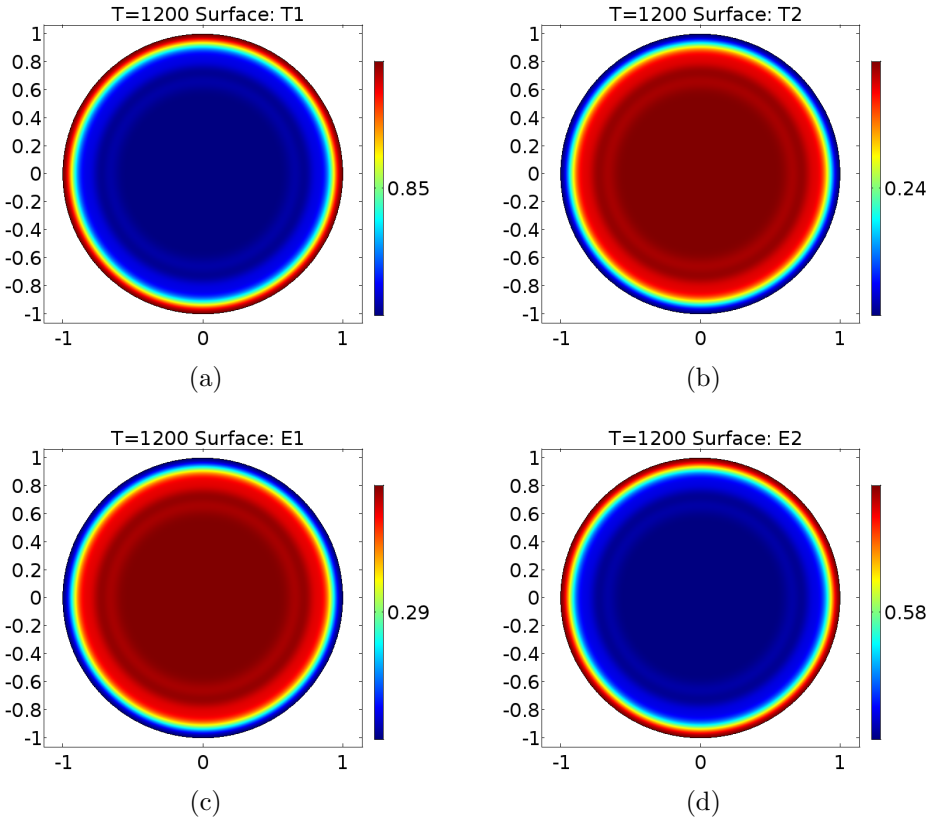

Figure 3.65: *Plots showing two dimensional heterogeneous distribution of tumour and immune cells when* $\psi_3 = 0.5$ *at time=1200. Figures 3.65(a) and 3.65(b) represent tumour type 1 and 2. Figures 3.65(c) and 3.65(d) represent immune type 1 and 2.*

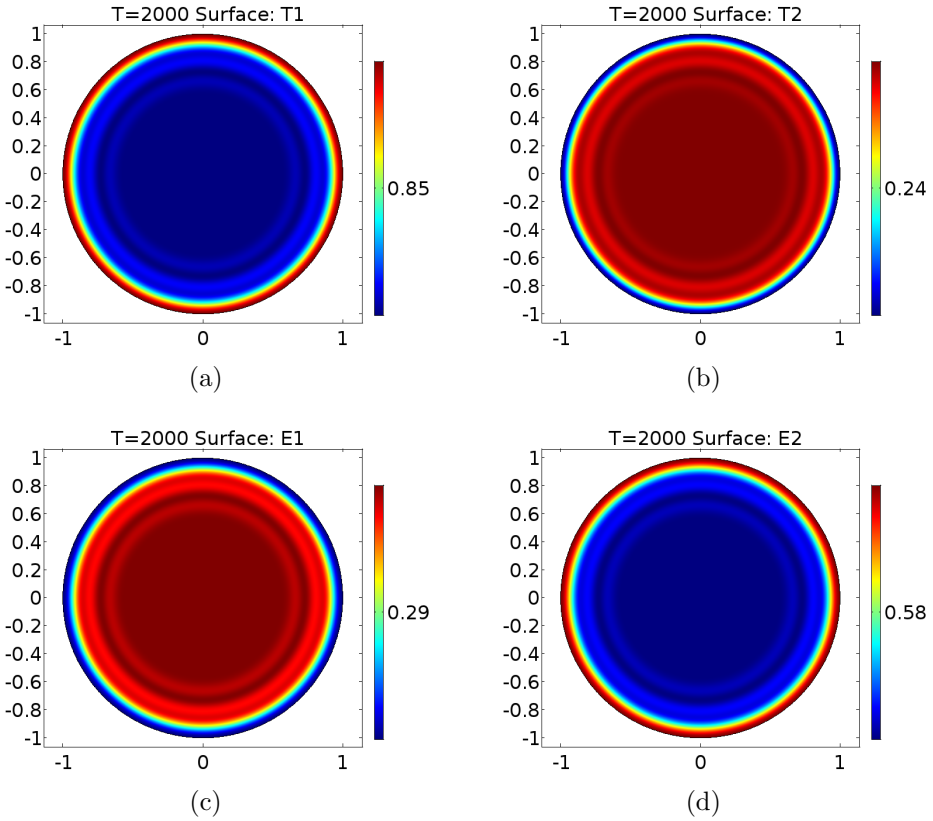

Figure 3.66: *Plots showing two dimensional heterogeneous distribution of tumour and immune cells when $\psi_3 = 0.5$ at time=2000. Figures 3.66(a) and 3.66(b) represent tumour type 1 and 2. Figures 3.66(c) and 3.66(d) represent immune type 1 and 2.*

3.7 Shortened model with supply terms

The next section is concerned with extending the model in section 3.4, whereby the immune supply terms, z_1 and z_2 have been added. This addition will determine if there is any change in the control parameters found in the previous model. Steady states of this system and their stability will be elucidated and bifurcation analysis undertaken. The system still omits the attack of the E_2 tumour cells on the T_2 cells and therefore, $\gamma_4 = 0$ and $\psi_4 = 0$. The non-dimensional system, becomes:

$$\frac{dT_1}{dt} = T_1(1 - T_1) - \gamma_1 \frac{E_1 T_1}{s_1 + T_1} \tag{3.7.1}$$

$$\frac{dT_2}{dt} = \alpha_2 T_2(1 - T_2) - \gamma_2 \frac{E_1 T_2}{s_2 + T_2} - \gamma_3 \frac{E_2 T_2}{s_3 + T_2} \tag{3.7.2}$$

$$\frac{dE_1}{dt} = z_1 + \frac{\psi_1 E_1 T_1}{s_1 + T_1} + \frac{\psi_2 E_1 T_2}{s_2 + T_2} - \omega_1 E_1 \tag{3.7.3}$$

$$\frac{dE_2}{dt} = z_2 + \frac{\psi_3 E_2 T_2}{s_3 + T_2} - \omega_2 E_2 \tag{3.7.4}$$

3.7.1 Steady states and stability

For these parameters there are three semi-trivial steady states and one co-existence steady state. The values of the steady states are:

$$s1 = (0, 0, 0.25, 0.25), \tag{3.7.5}$$

$$s2 = (0, 0.3111, 0.2524, 0.5767)\,, \tag{3.7.6}$$

$$s3 = (0.4199, 0, 0.7980, 0.25)\,, \tag{3.7.7}$$

$$s4 = (0.4147, 0.1783, 0.8012, 0.4011)\,. \tag{3.7.8}$$

The stability of each of these steady states is determined by the sign of their eigenvalues as discussed previously from the Jacobian of the system where J stands for the Jacobian. The eigenvalues are:

$s1 : detJ_{(0,0,0.25,0.25)} - \lambda I = 0$ and

$$\lambda = 0.7008, 0.3675, -0.1778, -0.1333 \tag{3.7.9}$$

$s2 : detJ_{(0,0.3111,0.2524,0.5767)} - \lambda I = 0$ and

$$\lambda = 0.6980, -0.0612 + 0.1545I, -0.1759, -0.0612 - 0.1545I \tag{3.7.10}$$

$s3 : detJ_{(0.4199,0,0.7980,0.25)} - \lambda I = 0$ and

$$\lambda = 0.1240, -0.1240 + 0.1959I, -0.1333, -0.1240 - 0.1959I \tag{3.7.11}$$

$s4 : detJ_{(0.4147,0.1783,0.8012,0.4011)} - \lambda I = 0$

$$\text{and } \lambda = -0.0364 + 0.1123I, -0.1205 + 0.1977I, -0.1205 - 0.1977I, -0.0364 - 0.1124I \tag{3.7.12}$$

Therefore, all the steady states are unstable aside from the coexistence steady

state, s_4.

3.7.2 Results

The model has been numerically solved using ODE45 in Matlab and the bifurcation diagrams have been produced using XPP AUTO. The results will show a reduction in the amount of control parameters, which cause the system to bifurcate. Initial conditions for the model are the same as in section 3.4.

There is a Hopf bifurcation when $s_1 = 0.2537$ and when $s_1 = 0.3899$, shown in Figures 3.67 and 3.68. As previously discussed, s_1 controls the rate at which the E_1 cell reaches saturation. In this case, the parameter has been decreased and therefore, the cells reach saturation at a much quicker rate. s_1 is the only parameter, in this model, that gives rise to stable periodic solutions. The removal of the other two control parameters, which previously displayed Hopf bifurcations, ψ_1 and ψ_3, now no longer exhibit these types of solutions. Figures 3.69-3.72 show the dynamics of the system when $s_1 = 0.33$. When s_1 bifurcated in the previous model, the E_2 population was very close to zero, leaving a high T_2 tumour bulk, however with the addition of the supply terms the E_2 cells are now able to mount an effective attack against the T_2 tumour bulk and displays oscillatory dynamics with a much higher amplitude. The E_1 cells also have an enhanced number and are therefore attributing to the surveillance of the T_2 tumour population, with the E_1 cells, and are mounting a better attack against the T_1 cells. As before, the model will now be extended to include spatial terms.

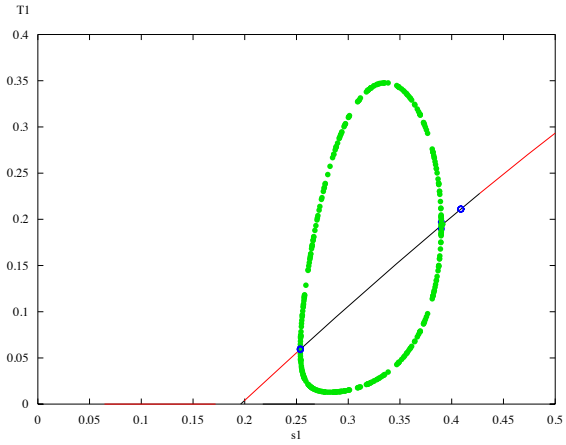

Figure 3.67: *Bifurcation diagram showing a hopf bifurcation in T_1 at $s_1 = 0.2537$. The line in the diagram represents how the steady state changes as s_1 changes. The black part of the line indicates instability of the equilibria and the red, stability. Moreover, green dots indicate that the hopf bifurcation is stable and blue dots represent instability.*

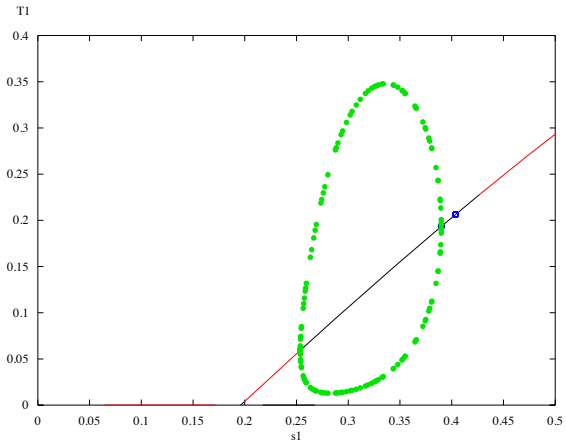

Figure 3.68: *Bifurcation diagram showing a hopf bifurcation in T_1 at $s_1 = 0.3899$. The line in the diagram represents how the steady state changes as s_1 changes. The black part of the line indicates instability of the equilibria and the red, stability. Moreover, green dots indicate that the hopf bifurcation is stable and blue dots represent instability.*

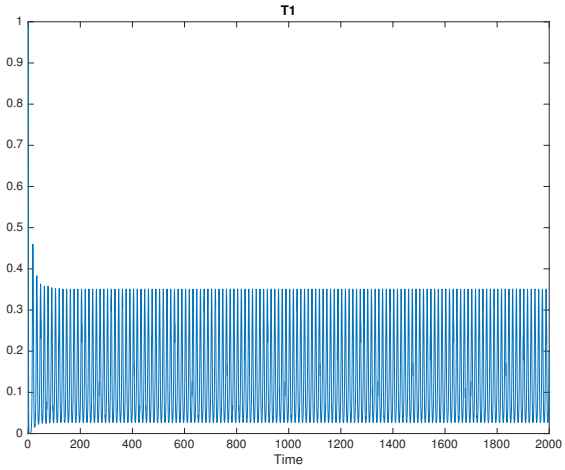

Figure 3.69: *Plot showing T_1 where oscillations are derived from the parameter space when the Hopf bifurcation is present at $s_1 = 0.33$ at times 0 to 2000 seconds.*

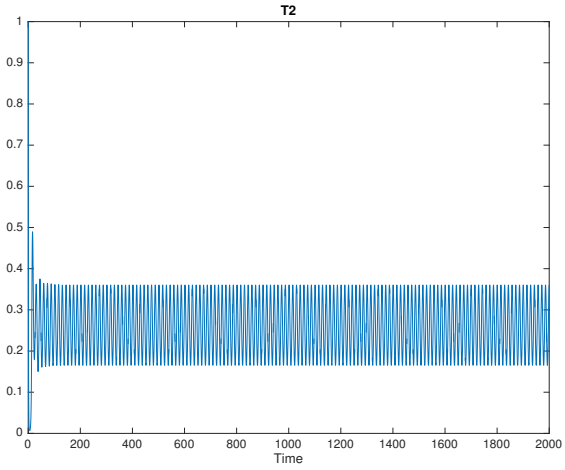

Figure 3.70: *Plot showing T_2 where oscillations are derived from the parameter space when the Hopf bifurcation is present at $s_1 = 0.33$ at times 0 to 2000 seconds.*

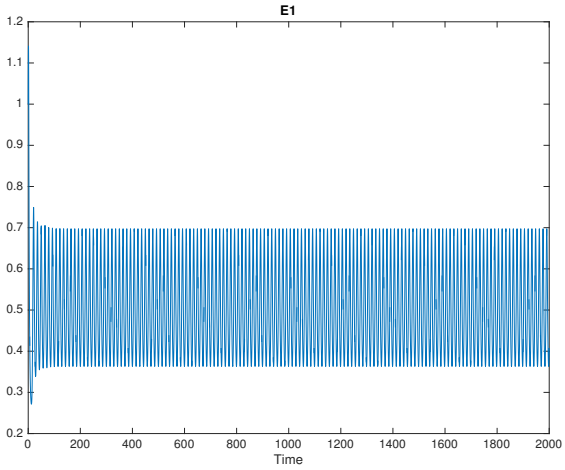

Figure 3.71: *Plot showing E_1 where oscillations are derived from the parameter space when the Hopf bifurcation is present at $s_1 = 0.33$ at times 0 to 2000 seconds.*

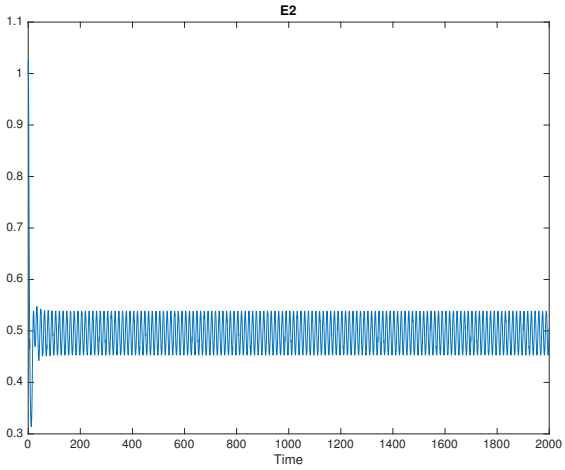

Figure 3.72: *Plot showing E_2 where oscillations are derived from the parameter space when the Hopf bifurcation is present at $s_1 = 0.33$ at times 0 to 2000 seconds.*

3.8 Spatial model

As in section 3.5.2, diffusion terms have been added to the non-dimensional homogeneous model. The diffusion rates, D_1, D_2, D_3 and D_4 are the same

values as before, and the system will be investigated in the same manner.

$$\frac{dT_1}{dt} = D_1\nabla^2 T_1 + T_1(1 - T_1) - \gamma_1 \frac{E_1 T_1}{s_1 + T_1} \tag{3.8.1}$$

$$\frac{dT_2}{dt} = D_2\nabla^2 T_2 + \alpha_2 T_2(1 - T_2) - \gamma_2 \frac{E_1 T_2}{s_2 + T_2} - \gamma_3 \frac{E_2 T_2}{s_2 + T_2} \tag{3.8.2}$$

$$\frac{dE_1}{dt} = D_3\nabla^2 E_1 + z_1 + \frac{\psi_1 E_1 T_1}{s_1 + T_1} + \frac{\psi_2 E_1 T_2}{s_2 + T_2} - \omega_1 E_1 \tag{3.8.3}$$

$$\frac{dE_2}{dt} = D_4\nabla^2 E_2 + z_2 + \frac{\psi_3 E_2 T_2}{s_2 + T_2} - \omega_2 E_2 \tag{3.8.4}$$

3.8.1 Results

The system in this section has again been numerically investigated using PDEPE in Matlab. Again the focus is to try and determine what happens to the system if the parameter value s_1 is set to a value in which there are periodic solutions. Figures 3.73-3.80 show the evolution of the cell densities at times 100, 200, 400, 800, 1200, 1500 and 2000 seconds. Again the time is generic, and could be changed to elucidate more biologically relevant time frames. Initial condition and boundary conditions are the same as in the previous PDE model. The spatial model here again portrays heterogeneous waves of all cell types invading the tissue. Both tumour cell densities have been reduced with the inclusion of more immune cells. In the previous model where the supply terms for the immune cells were omitted, the E_2 cells were

not able to mount an effective attack against the T_2 tumour cells, leading to a high tumour density. However, in this model, the supply term of more E_2 cells into the system has allowed the E_2 cells to mount an effective surveillance against the T_2 tumour cells and therefore they are no longer obsolete.

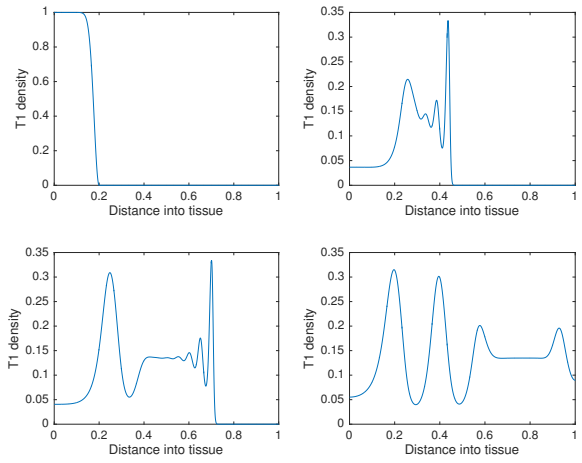

Figure 3.73: *Plots showing the spatial density of T_1 at times 0, 100, 200 and 400 seconds. The figures show heterogeneous travelling waves at $s_1 = 0.33$. This is derived from the same parameter space as the homogeneous system when the Hopf bifurcation is present.*

3.8.2 Discussion

This model has extended the system in 3.4 with the inclusion of immune constant supply terms. The homogeneous system is seen to exhibit periodic solutions, which arise through the presence of Hopf bifurcations, in parameter s_1. The other two terms in the previous model that didn't include supply terms had three control parameters, however the periodic solutions in ψ_1 and ψ_3 have disappeared in this model. The inclusion of the supply terms boosts the numbers of immune cells within the system and therefore the tumour bulk

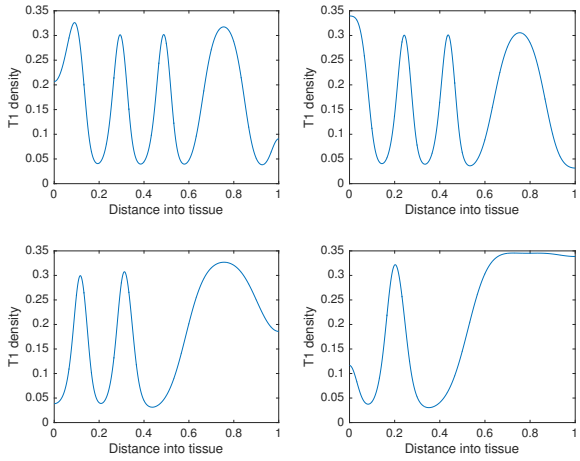

Figure 3.74: *Plots showing the spatial density of T_1 at times 800, 1200, 1500 and 2000 seconds. The figures show heterogeneous travelling waves at $s_1 = 0.33$. This is derived from the same parameter space as the homogeneous system when the Hopf bifurcation is present.*

for both tumour types is reduced. The E_2 cells are also now able to mount an effective attack against the T_2 tumour cells and are no longer obsolete within the system. The spatial model, which was developed by adding diffusion to the homogeneous model, shows heterogeneous type waves that invade the tissue for all cell types. These come to light due to the presence of the Hopf bifurcation in the homogeneous model, provided the parameter s_1 is in the correct range where periodic solutions are exhibited. The model will now be extended to investigate the full system set out in section 3.3.

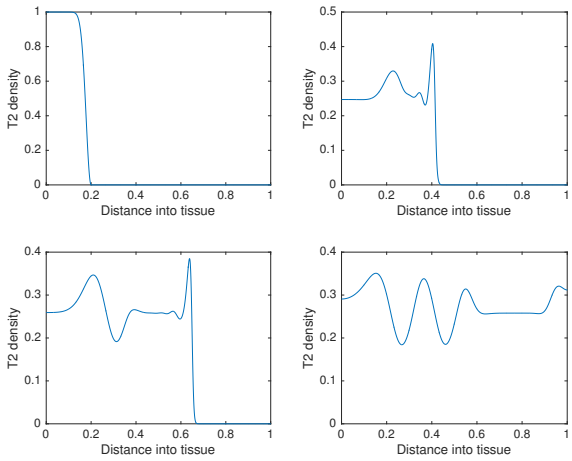

Figure 3.75: *Plots showing the spatial density of T_2 at times 0, 100, 200 and 400 seconds. The figures show heterogeneous travelling waves at $s_1 = 0.33$. This is derived from the same parameter space as the homogeneous system when the Hopf bifurcation is present.*

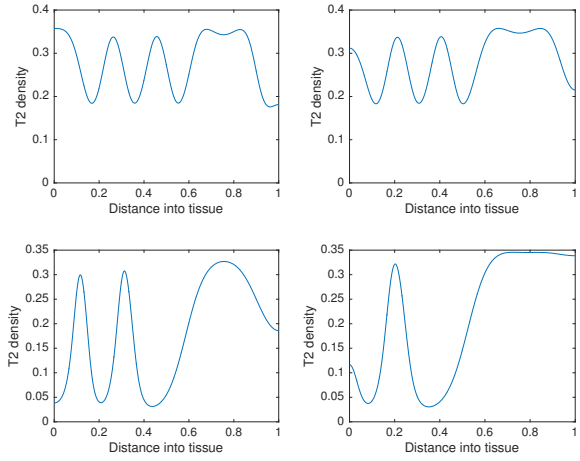

Figure 3.76: *Plots showing the spatial density of T_2 at times 800, 1200, 1500 and 2000 seconds. The figures show heterogeneous travelling waves at $s_1 = 0.33$. This is derived from the same parameter space as the homogeneous system when the Hopf bifurcation is present.*

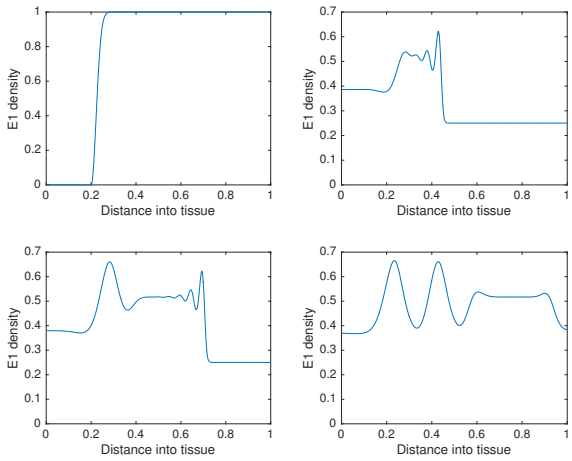

Figure 3.77: *Plots showing the spatial density of E_1 at times 0, 100, 200 and 400 seconds. The figures show heterogeneous travelling waves at $s_1 = 0.33$. This is derived from the same parameter space as the homogeneous system when the Hopf bifurcation is present.*

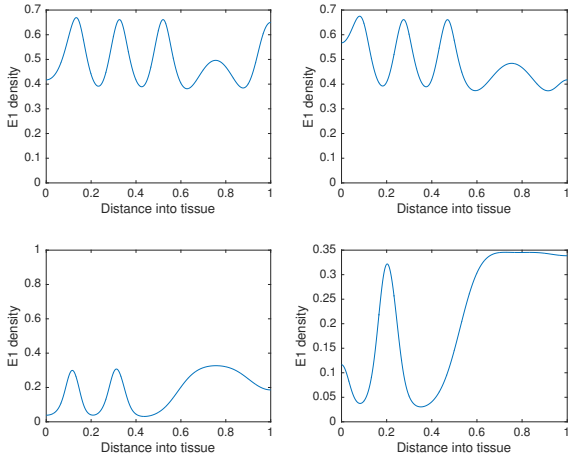

Figure 3.78: *Plots showing the spatial density of E_1 at times 800, 1200, 1500 and 2000 seconds. The figures show heterogeneous travelling waves at $s_1 = 0.33$. This is derived from the same parameter space as the homogeneous system when the Hopf bifurcation is present.*

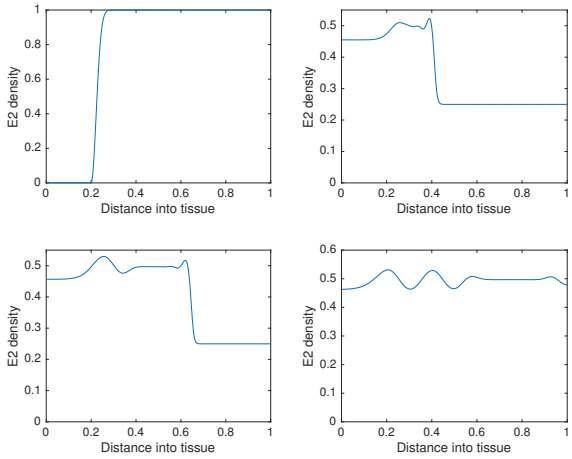

Figure 3.79: *Plots showing the spatial density of E_2 at times 0, 100, 200 and 400 seconds. The figures show heterogeneous travelling waves at $s_1 = 0.33$. This is derived from the same parameter space as the homogeneous system when the Hopf bifurcation is present.*

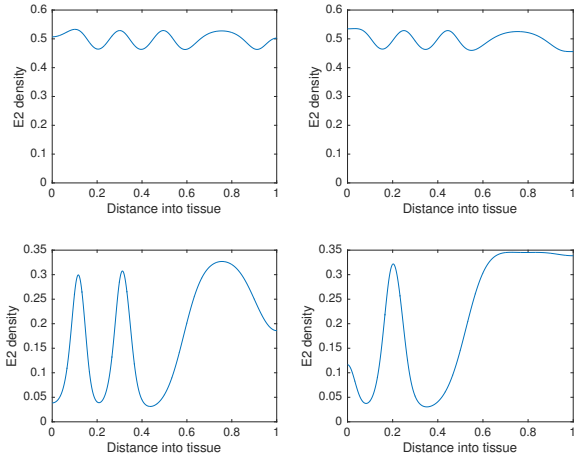

Figure 3.80: *Plots showing the spatial density of E_2 at times 800, 1200, 1500 and 2000 seconds. The figures show heterogeneous travelling waves at $s_1 = 0.33$. This is derived from the same parameter space as the homogeneous system when the Hopf bifurcation is present.*

3.9 Full immune attack

This section will be concerned with investigating the full system in section 3.3. Here, the E_2 cells will be allowed to attack the T_1 cell population, albeit at a lower rate than the E_1 cells. The recruitment of the E_2 cells has also been enhanced by their interaction with the T_2 cells. This model now includes two immune specialists whereby each is better at attacking a specific type of tumour cell and not so good at attacking the other; they both now work together to achieve tumour dormancy. The non-dimensional system is as follows:

$$\frac{dT_1}{dt} = T_1(1 - T_1) - \gamma_1 \frac{E_1 T_1}{s_1 + T_1} - \frac{\gamma_4 E_2 T_1}{s_4 + T_1} \tag{3.9.1}$$

$$\frac{dT_2}{dt} = \alpha_2 T_2(1 - T_2) - \gamma_2 \frac{E_1 T_2}{s_2 + T_2} - \gamma_3 \frac{E_2 T_2}{s_3 + T_2} \tag{3.9.2}$$

$$\frac{dE_1}{dt} = z_1 + \frac{\psi_1 E_1 T_1}{s_1 + T_1} + \frac{\psi_2 E_1 T_2}{s_2 + T_2} - \omega_1 E_1 \tag{3.9.3}$$

$$\frac{dE_2}{dt} = z_2 + \frac{\psi_3 E_2 T_2}{s_3 + T_2} + \frac{\psi_4 E_2 T_1}{s_4 + T_2} - \omega_2 E_2 \tag{3.9.4}$$

As in the previous models, steady states and their stability will be investigated and bifurcation analysis will be undertaken. Furthermore, it is necessary to discover if there is any change in the important parameters in this model as the inclusion of the E_2 attack against the tumour may have an

effect. This will be explored in the results section. All parameter values can be found in section 3.4.2.

3.9.1 Steady states and stability

For these parameters there are three semi-trivial steady states and one co-existence steady state. The numerical values of the steady states are:

$$s1 = (0, 0, 0.25, 0.25), \tag{3.9.5}$$

$$s2 = (0, 0.3111, 0.2524, 0.5767)\,, \tag{3.9.6}$$

$$s3 = (0.4063, 0, 0.7646, 0.25)\,, \tag{3.9.7}$$

$$s4 = (0.3911, 0.1963, 0.7447, 0.4216)\,. \tag{3.9.8}$$

The stability of each of these steady states is determined by the sign of their eigenvalues as discussed previously from the Jacobian of the system where J stands for the Jacobian. The eigenvalues are:

$s1 : detJ_{(0,0,0.25,0.25)} - \lambda I = 0$ and

$$\lambda = 0.6453, 0.3675, -0.1778, -0.1333 \tag{3.9.9}$$

$s2 : detJ_{(0,0.3111,0.2524,0.5767)} - \lambda I = 0$ and

$$\lambda = 0.5698, -0.0612 + 0.1545I, -0.1759, -0.0612 - 0.1545I \tag{3.9.10}$$

$s3 : detJ_{(0.4063,0,.7646,0.25)} - \lambda I = 0$ and

$$\lambda = 0.1389, -0.1171 + 0.1949I, -0.1323, -0.1171 - 0.1949I \tag{3.9.11}$$

$s4 : detJ_{(0.3911,0.1963,0.7447,0.4216)} - \lambda I = 0$ and

$$\lambda = -0.0399 + 0.1158I, -0.1065 + 0.1974I, -0.1065 - 0.1974I, -0.0399 - 0.1158I \tag{3.9.12}$$

Again all the steady states are unstable aside from the coexistence steady state, $s4$.

3.9.2 Results

The results are generated using ODE45 in Matlab and XPP AUTO for the bifurcation diagrams. The focus again will be to try and ascertain the differences between this model and the two previous models, in terms of the oscillatory nature of the system and overall cell bulks.

There is a Hopf bifurcation when $s_1 = 0.3334$. The bifurcation diagrams for T_1 and T_2 are shown in Figures 3.1-3.2 for cells T_1 and T_2 and bifurcation diagrams for the other two cell types can be obtained in a similar fashion. Here, we see the return of a single bifurcation for the parameter set, giving

rise to stable periodic solutions. Figures 3.83-3.86 show the oscillatory nature of the system when $s_1 = 0.35$. As the saturation curve of the E_1 cells is less steep than in the previous homogeneous models, it should be that the T_1 tumour population is lower. However, with the E_2 cells newfound ability against the T_1 tumour cells, the T_1 tumour bulk is lowered. This is also the case for the T_2 cells, as more E_2 cells are being recruited into the system. The amplitude of the oscillations is also much lower, as the immune cells now have a higher base level value and therefore the simulations do not bounce between such high and low levels. The system again has managed to keep the tumour bulk under check, this time keeping the cancer cells at a much lower level than before. It is now prudent to capture the essence of the system in 1-D.

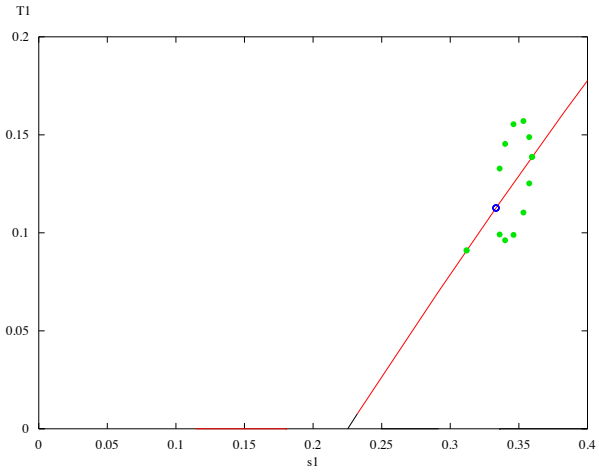

Figure 3.81: *Bifurcation diagram showing a hopf bifurcation in T_1 at $s_1 = 0.3334$. The line in the diagram represents how the steady state changes as s_1 changes. The black part of the line indicates instability of the equilibria and the red, stability. Moreover, green dots indicate that the hopf bifurcation is stable and blue dots represent instability.*

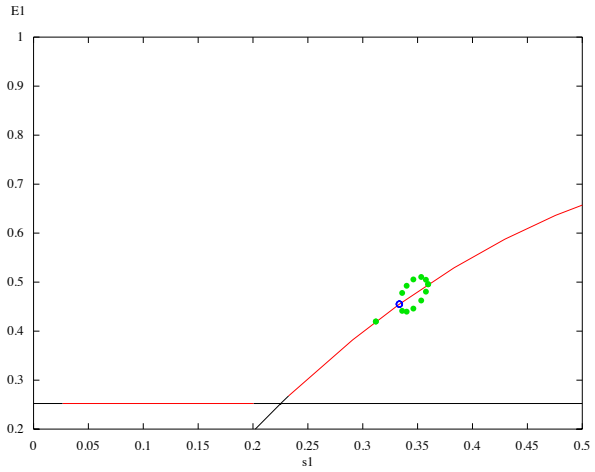

Figure 3.82: *Bifurcation diagram showing a hopf bifurcation in* E_1 *at* $s_1 = 0.3334$*. The line in the diagram represents how the steady state changes as* s_1 *changes. The black part of the line indicates instability of the equilibria and the red, stability. Moreover, green dots indicate that the hopf bifurcation is stable and blue dots represent instability.*

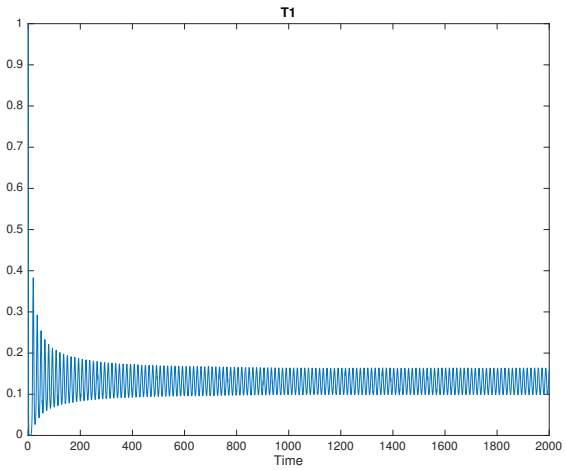

Figure 3.83: *Plot showing* T_1 *where oscillations are derived from the parameter space when the Hopf bifurcation is present at* $s_1 = 0.35$ *at times 0 to 2000 seconds.*

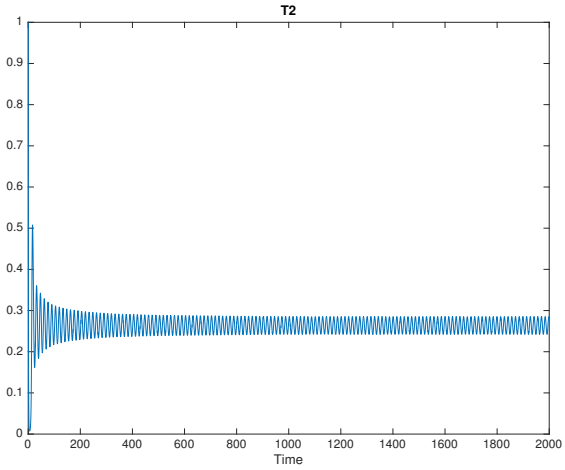

Figure 3.84: *Plot showing T_2 where oscillations are derived from the parameter space when the Hopf bifurcation is present at $s_1 = 0.35$ at times 0 to 2000 seconds.*

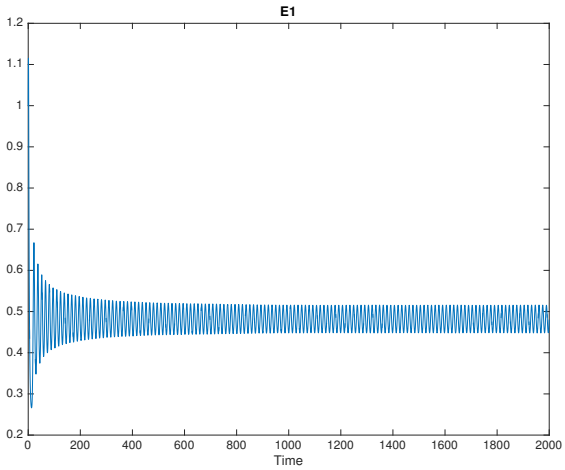

Figure 3.85: *Plot showing E_1 where oscillations are derived from the parameter space when the Hopf bifurcation is present at $s_1 = 0.35$ at times 0 to 2000 seconds.*

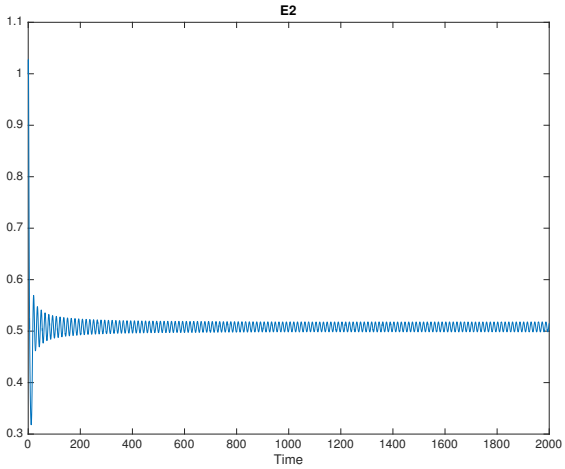

Figure 3.86: *Plot showing E_2 where oscillations are derived from the parameter space when the Hopf bifurcation is present at $s_1 = 0.35$ at times 0 to 2000 seconds.*

3.10 Spatial model of full immune attack

The model in section 3.9 has been extended again by adding diffusion to each of the cell types and their coefficients are the same as in previous models. Furthermore, the results will aim to ascertain a link between the homogenous findings in section 3.9.2 and to discuss differences between the results from previous models. The spatial system is as follows:

$$\frac{dT_1}{dt} = D_1\nabla^2 T_1 + T_1(1-T_1) - \gamma_1\frac{E_1T_1}{s_1+T_1} - \gamma_4\frac{E_2T_1}{s_4+T_1} \tag{3.10.1}$$

$$\frac{dT_2}{dt} = D_2\nabla^2 T_2 + \alpha_2 T_2(1-T_2) - \gamma_2\frac{E_1T_2}{s_2+T_2} - \gamma_3\frac{E_2T_2}{s_2+T_2} \tag{3.10.2}$$

$$\frac{dE_1}{dt} = D_3\nabla^2 E_1 + z_1 + \frac{\psi_1E_1T_1}{s_1+T_1} + \frac{\psi_2E_1T_2}{s_2+T_2} - \omega_1E_1 \tag{3.10.3}$$

$$\frac{dE_2}{dt} = D_4\nabla^2 E_2 + z_2 + \frac{\psi_3E_2T_2}{s_2+T_2} + \psi_4\frac{E_2T_1}{s_4+T_1} - \omega_2E_2 \tag{3.10.4}$$

3.10.1 Results

The results in this section have been numerically explored using PDEPE in Matlab. In the homogeneous model it was found that the inclusion of the E_2 cells attacking the T_2 cells and the improved recruitment of the T_2 cells reduced the overall tumour cell bulks. There was a Hopf bifurcation present when parameter $s_1 = 0.3334$ and, therefore the results will explore the impact this has in the spatial case.

Figures 3.87-3.94 represent the spatial density of cells at times 100, 200, 400, 800, 1200, 1500 and 2000 seconds. Parameter $s_1 = 0.35$ as this falls within the periodic solutions of the homogeneous model. The rest of the parameter values are kept the same. Again, each cell type is exhibiting heterogeneous type waves, whereby the tumour cells are invading the tissue and are attacked by the immune population. It can be seen that the tumour cell densities have been further decreased, compared to the results in the previous model, in section 3.8.1, even though the E_1 cells reach saturation at a slower rate. The results here are less heterogeneous than in the previous model, as the periodic solutions show in the homogeneous case, due to a higher level of immune cells within the system.

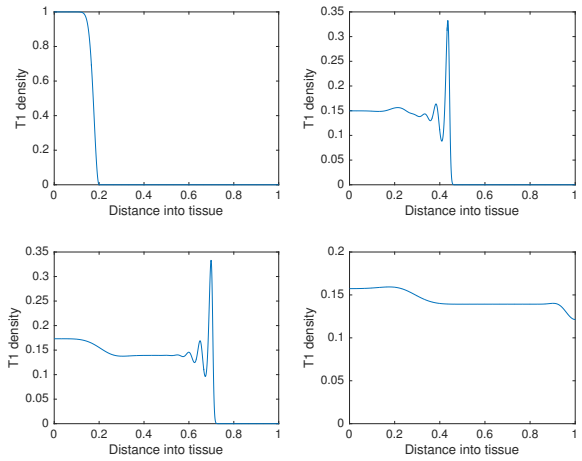

Figure 3.87: *Plots showing the spatial density of T_1 at times 0, 100, 200 and 400 seconds. The figures show heterogeneous travelling waves at $s_1 = 0.35$. This is derived from the same parameter space as the homogeneous system when the Hopf bifurcation is present.*

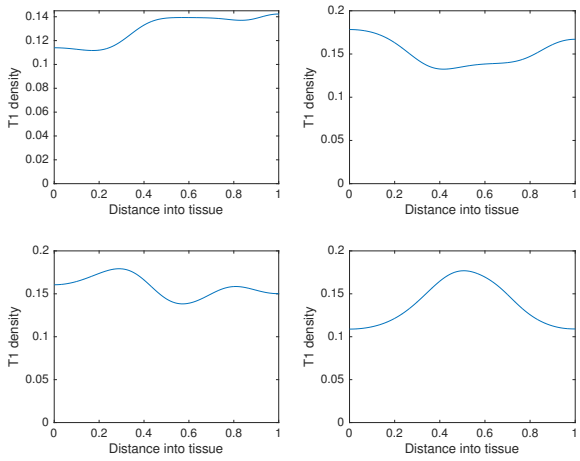

Figure 3.88: *Plots showing the spatial density of T_1 at times 800, 1200, 1500 and 2000 seconds. The figures show heterogeneous travelling waves at $s_1 = 0.35$. This is derived from the same parameter space as the homogeneous system when the Hopf bifurcation is present.*

3.10.2 Discussion

This section has modelled the full system first set out in section 3.4. The homogenous case saw the rise of stable periodic solutions by way of varying s_1 and discovering a Hopf bifurcation. The inclusion of the E_2 cells attack against the T_2 cells, as well as their enhanced recruitment, has allowed both tumour bulks to be lowered, even though s_1 has not been reduced as much as in previous models. The spatial model again exhibited heterogeneous waves of tumour and immune cell densities and showed reduced heterogeneity in the system.

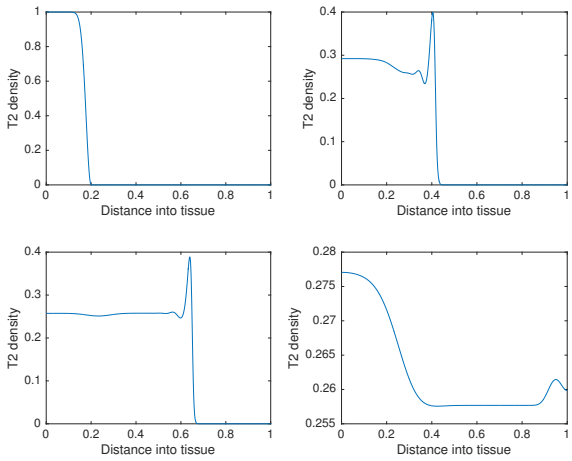

Figure 3.89: *Plots showing the spatial density of T_2 at times 0, 100, 200 and 400 seconds. The figures show heterogeneous travelling waves at $s_1 = 0.35$. This is derived from the same parameter space as the homogeneous system when the Hopf bifurcation is present.*

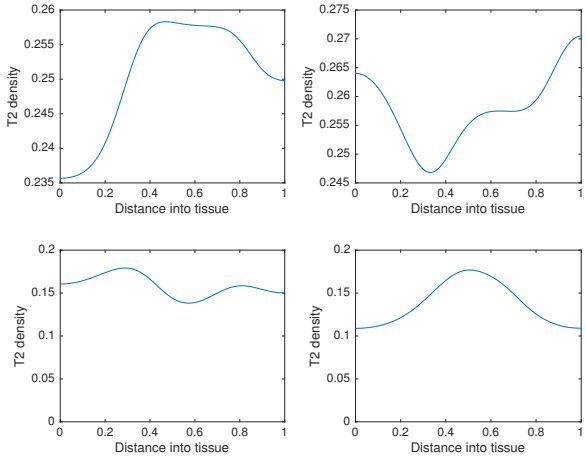

Figure 3.90: *Plots showing the spatial density of T_2 at times 800, 1200, 1500 and 2000 seconds. The figures show heterogeneous travelling waves at $s_1 = 0.35$. This is derived from the same parameter space as the homogeneous system when the Hopf bifurcation is present.*

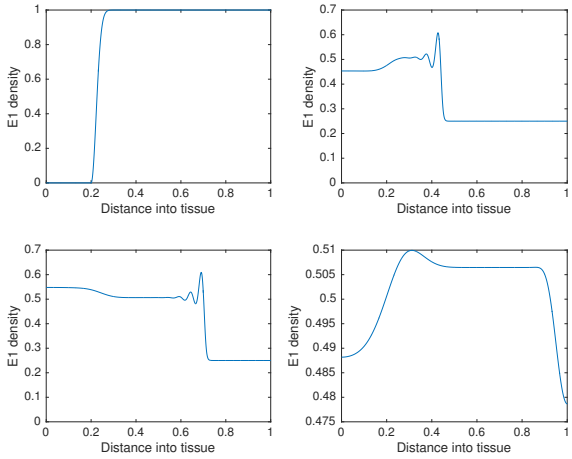

Figure 3.91: *Plots showing the spatial density of E_1 at times 0, 100, 200 and 400 seconds. The figures show heterogeneous travelling waves at $s_1 = 0.35$. This is derived from the same parameter space as the homogeneous system when the Hopf bifurcation is present.*

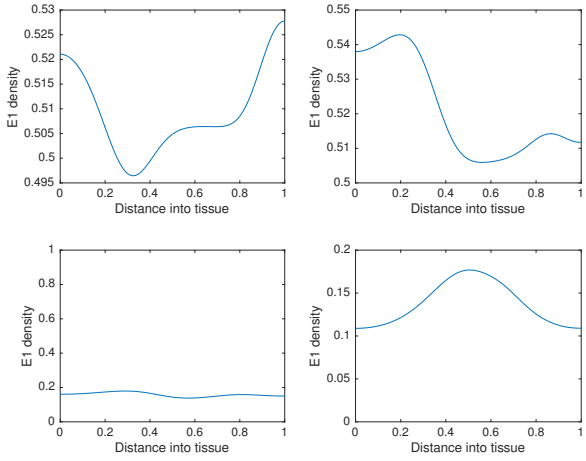

Figure 3.92: *Plots showing the spatial density of E_1 at times 800, 1200, 1500 and 2000 seconds. The figures show heterogeneous travelling waves at $s_1 = 0.35$. This is derived from the same parameter space as the homogeneous system when the Hopf bifurcation is present.*

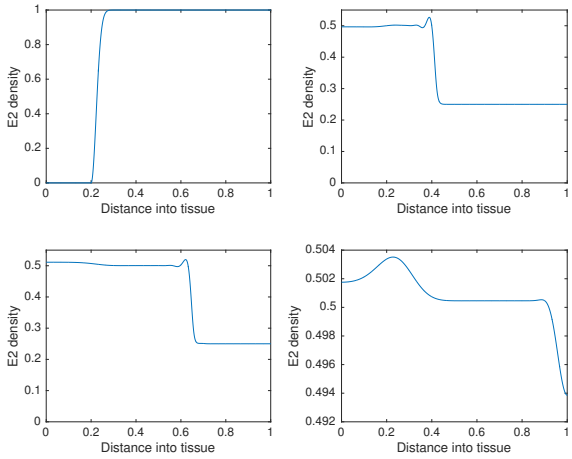

Figure 3.93: *Plots showing the spatial density of E_2 at times 0, 100, 200 and 400 seconds. The figures show heterogeneous travelling waves at $s_1 = 0.35$. This is derived from the same parameter space as the homogeneous system when the Hopf bifurcation is present.*

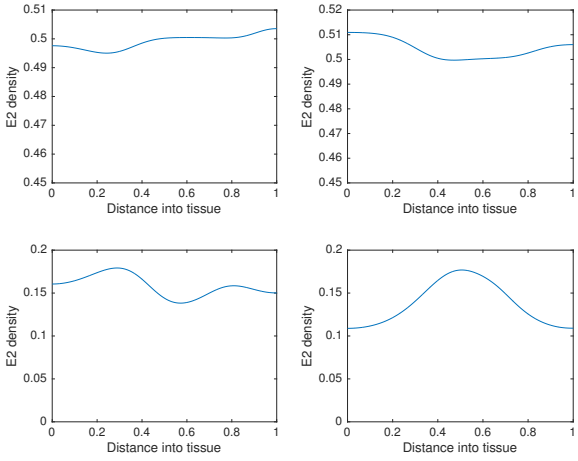

Figure 3.94: *Plots showing the spatial density of E_2 at times 800, 1200, 1500 and 2000 seconds. The figures show heterogeneous travelling waves at $s_1 = 0.35$. This is derived from the same parameter space as the homogeneous system when the Hopf bifurcation is present.*

3.11 Conclusion

In this Chapter, two models have been undertaken. The first model, in section 3.2, was based on de Pillis et al. [2005] where, the system tried to ascertain the dynamics between $CD4^+$ T-cells, $CD8^+$ T-cells, a tumour population and antigen presenting cells, in a homogeneous model. The model used Michaelis Mention dynamics to describe the recruitment of the immune cells, which was enhanced by their interactions with the tumour population. Moreover, the model also included the action of APCs whereby loaded APCs activated the $CD4^+$ T-cells; an extra recruitment term. A fractional kill response term was used for the killing of the tumour population by the $CD8^+$ T-cells, derived in de Pillis et al. [2005], whereas the $CD4^+$ T-cells used a simple product term. Moreover, the tumour population could also kill the immune cells, described again by a product term. Unfortunately, bifurcation analysis remained elusive and the model was scrapped for the time being. Another more generic model was then developed in this Chapter.

The second model tried to encapsulate the dynamics of a system with two tumour populations interacting with two immune populations. The system was developed using generic parameter values and utilises some of the methods from both Matzavinos et al. [2004] and de Pillis et al. [2005]. The homogenous model, in section 3.3, portrays the dynamics of the system where the terms describing the immune cells attacking the tumour cells are surmised using Michaelis Menten dynamics. This interaction then creates extra recruitment for the immune cells. The tumour cells do not kill the immune cells. The model was then split into two shortened models before analysing

the full system.

The first reduced model, in section 3.4, omitted the supply terms for the immune cells, as well as the E_2 cells attack against the T_1 tumour cell population. Steady states and their stability were explored and bifurcation analysis was undertaken. This showed nine steady states of which only the coexistence steady state was stable. The system was then solved using the computer programme XPP AUTO to try and find bifurcations. This model was seen to exhibit periodic solutions arising from Hopf bifurcations when varying three parameters: s_1, controlling the rate at which the E_1 population reaches saturation when in interaction with the T_1 cell population; ψ_1, the saturation point of E_1 when in interaction with the T_1 population; and ψ_3, the saturation point of E_2 when interaction with the T_2 population. The system was then investigated using Matlab to show the oscillatory dynamics of the system.

The reduction of the parameter s_1 allowed the system to exhibit stable periodic solutions. This lowered the T_1 tumour bulk, however E_1 and T_1 exhibited large oscillations. The E_2 cells were not able to sufficiently gain enough momentum to mount an effective surveillance against the T_2 cells and therefore, this lead to a higher T_2 tumour bulk, which was only kept in check by the E_1 population. When varying parameter ψ_1, the amount of E_1 cells was increased, therefore lowering the T_1 cells. Again, the E_2 cells were unable to overcome their decay rate, due to lysis, leading to an almost unchecked T_2 tumour bulk. The last parameter to cause periodic solutions when varied was ψ_3. Here, E_1 and T_1 remained largely unaltered, but the E_2 cells, due to their enhanced recruitment, were now able to keep the T_2

cells under check. The model was then extended into 1-D by the inclusion of diffusion terms. The results explored the system by varying the same parameter values as in the homogeneous model. The results for s_1 show a heterogeneous type distribution of cells throughout the domain for E_1, T_1 and T_2, with an almost obsolete density of E_2 cells. Moreover, parameter ψ_1 showed similar results, whereby waves of E_1 cells are seen to attack both tumour cells and the E_2 population remains obsolete. The varying of ψ_3 shows heterogeneity in E_2 and T_2, but not in E_1 and T_1, due to the enhanced recruitment of the E_2 cells. The model was then extended into 2-D using Comsol, which showed similar heterogeneity when varying all three control parameters as in the 1-D case.

Biologically, the system was developed with the aim to investigate a more potent tumour phenotype in the form of the T_1 population. With the removal of the E_2 cells surveillance on the T_1 population, the T_1 cells should thrive, however as Michaelis mention dynamics are used these terms cause the system to exhibit some different dynamics. When removing the supply term and extra recruitment term for E_2, they become almost obsolete within the system, when s_1 is decreased and ψ_1 is increased. The removal of the E_2 cells recruitment when in interaction with T_2 seems to have the biggest effect on their performance, however the increasing of the saturation level of the cells, ψ_3, can combat this to a certain degree. The homogeneous model was then extended, in section 3.7, to include more elements of the immune-tumour microenvironment.

The supply terms for both immune types, z_1 and z_2, were added and the model was investigated in the same way. Steady states, their stability and

bifurcations were analysed, and the system exhibited two Hopf bifurcations when s_1 was varied. The results show stable periodic solutions. Due to the introduction of the supply terms, the E_2 cells are now able to mount an attack against the T_2 population. The enhanced recruitment and supply of both immune cells results in lower tumour bulks. This model was then extended into a PDE model and again, the system exhibited waves of cells, creating a spatially heterogeneous density throughout the domain. Moreover, the E_2 cells also exhibited this, whereas in the previous model, when varying s_1, they did not. Here, the inclusion of the supply terms has not allowed the T_1 cells to become the dominant cancer cell, as the extra recruitment of the E_1 cells prevents this.

The full system was then examined in section 3.9 and again steady states and bifurcation analysis was undertaken. Again, the parameter s_1 made the system bifurcate but now only at one point. The inclusion of the E_2 cells attack against the T_1 cells lowered the overall tumour cell bulk due to increased recruitment. Furthermore, the system was then extended into a 1-D spatial model, where the results show a train of waves invading the tissue, causing a spatial heterogeneous density throughout the domain, which is met with a host immune system. Moreover, the T_2 cell is again the dominant cancer cell. The recruitment of the E_1 cells is higher, therefore allowing the T_2 cells to become the more potent tumour phenotype. Future discussions on this model and its findings can be found in Chapter 5.

Chapter 4

Individual-Based Model of "Multiple Cell Types"

4.1 Introduction

The next chapter will focus on an avascular tumour, which elicits a response from a host immune system. Most tumours at this stage are harmless and grow to around 10^6 cells in volume (Matzavinos et al. [2004]), whereby cells at the centre of the tumour die off due to a lack of nutrients and oxygen and become "necrotic" (Alberts et al. [2008]). However, the prevention of the tumour mass gaining a regulatory network is paramount in preventing full-blown cancer spread. It seems prudent, therefore, to delve into the underlying kinetics of a nascent tumour microenvironment, to try and understand how to boost an immune cell response, in order to kill the cancer while at the stage when it poses little threat and can be destroyed. Along with the obvious issues that reside here, such as lack of accurate machinery and screening,

which can detect cancer at this small level, there is much discussion as to how the immune system actually attacks a small tumour mass. As discussed in Chapter 1.1, the theory of immune surveillance, and subsequently the new idea of immunoediting, try to describe and portray the way in which cancer can either be cleared by the immune system, lie dormant or promote tumour growth. Tumour cells can often harness the immune cells by changing their phenotype when in a hypoxic state, promoting the growth of a regulatory blood network. More information can be found in section 1.1.3. This chapter will use elements of the model and dynamics exhibited in Chapter 2 and section 3.7. The aim of the model is to try and again detect the three Es of immunoediting, however this time extending the number of immune and cancer cells. The model will then proceed to investigate the impact that the "Warburg Effect", discussed in section 1.1.4, may have on tumour growth.

4.2 Mathematical Model

This section is an extension to Chapter 2. This chapter concerns an investigation of two immune cells and two tumour cells interacting with one another in a discrete model using, the previously discussed, CompuCell3D; an open source software concerned with numerically solving cellular potts models. In the previous chapter, three models were proposed each with their own set of differing interactions and results. Here, the second shortened model will be investigated, from sections 3.7 and 3.8, whereby an immune system is in interaction with different phenotypes of tumour cells. The non-dimensionalised spatial system from the previous section 3.8 is as follows:

$$\frac{dT_1}{dt} = D_1\nabla^2 T_1 + T_1(1-T_1) - \gamma_1\frac{E_1T_1}{s_1+T_1}, \tag{4.2.1}$$

$$\frac{dT_2}{dt} = D_2\nabla^2 T_2 + \alpha_2 T_2(1-T_2) - \gamma_2\frac{E_1T_2}{s_2+T_2} - \gamma_3\frac{E_2T_2}{s_2+T_2}, \tag{4.2.2}$$

$$\frac{dE_1}{dt} = D_3\nabla^2 E_1 + z_1 + \frac{\psi_1E_1T_1}{s_1+T_1} + \frac{\psi_2E_1T_2}{s_2+T_2} - \omega_1E_1, \tag{4.2.3}$$

$$\frac{dE_2}{dt} = D_4\nabla^2 E_2 + z_2 + \frac{\psi_3E_2T_2}{s_2+T_2} - \omega_2E_2. \tag{4.2.4}$$

The above model, (4.2.1)-(4.2.4), describes, mathematically, two tumour cells being attacked by two immune cells. Tumour type one (T_1) is only attacked by immune type one (E_1), whereas tumour type two (T_2) is killed by both (E_1 and E_2). This is to try and investigate the idea that a tumour, when in interaction with a host immune system, can become less immunogenic. The idea stems from the hypothesis of immunoediting. As tumour cells are not homogeneous and are of mixed type, it is thought that the immune system actively kills cells that are more immunogenic, allowing cells that are less immunogenic access to more nutrients and oxygen. Hence, the tumour mass evades "immune destruction" and can secrete growth factors to gain a blood network. However, unlike in the previous CompuCell3D model in Chapter 2, here the tumour cells do not attack the immune cells. This simplification is to aid in the understanding of the kinetics of this model that will eventually lead to immune success or failure. The results of section

3.8 show that there are conditions, whereby a tumour dormant state can exist where heterogeneous waves are seen throughout the 1-D domain. To fully investigate the new model, different modelling techniques of Chapters 2 and 3.1 have been used. Again, the hope is to enrich the results that were found in the previous section 3.8 by using a discrete type model, whereby more biologically relevant information can be inputted and computed.

The model in this chapter, however, will extend (4.2.1)-(4.2.4) by adding in some new kinetics. Here, as in the previous CompuCell3D model in Chapter 2, a host immune system is eliciting a response to a nascent tumour before the tumour cells can secrete growth factors, stimulating an angiogenic reaction. The immune cell-tumour cell interactions are represented by three different probabilities to try and mimic the model. The immune cells, like the model above, do not attack the tumour cells. Immune cell death is calculated by adding in an age term. They are removed from the model if they have been there for a certain number of MCS.

The model in this chapter has a similar set up to the previous CompuCell3D model. Again, different aspects of CompuCell3D will be utilised to try and mimic the results found in section 3.8. In this model, as previously discussed, there are two tumour cell types and two immune cell types. Medium cells again represent healthy tissue, which is considered to be homogeneous. This is a simplification of the microenvironment to try and understand the underlying kinetics involved in the model. A cell is considered to be between $10\mu m$-$20\mu m$ in diameter (Alberts et al. [2008]), however here a 2-D representation is used. Cells are initially determined to be $10\mu m$ and divide at $20\mu m$. A newly divided cell is determined to be 5×5 pixels and each pixel

represents a square element of a cell that is $2\mu m$ x $2\mu m$, giving a total area of $4\mu m^2$. As in the previous CompuCell3D model, the tumour is represented by a central 5×5 cell mass, however this time it contains two randomly placed tumour types: type 1 and type 2. Initially, four immune cells of either type one or type two are also randomly placed throughout the domain. A generic type of nutrient feeds the cells in this model, which could be something such as oxygen or glucose, and is also modelled just as in Chapter 2. Each cell type has its own random cellular motility and chemotaxis has been omitted.

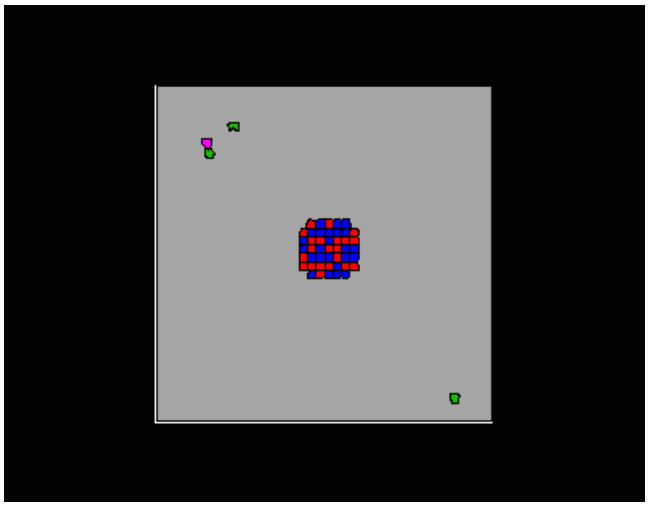

Figure 4.1: *Plot showing the start of the simulation. The domain size is 200×200 pixel grid with each cell being 5×5 pixels. A central initial mass of tumour cells of type 1 (red) and type 2 (blue) are randomly placed in the initial MCS. The simulation begins with four immune cells randomly selected from either type 1 (green) or type 2 (magenta). The tissue is represented by the grey block of cells called medium cells.*

Mitosis is determined in exactly the same way as the previous CompuCell3D model, in that each cell type has an adhesion parameter that determines how strongly each cell type binds to other cell types. Growth is determined by how much nutrient is available and the tumour growth rate

(TGR) determined at every MCS is governed by:

$$TGR = 0.1 \times \text{concentration of nutrient at tumour core.} \tag{4.2.5}$$

Both tumour types divide into two daughter cells when they reach $50\mu m$, $20\mu m$ in diameter. Quiescent cells of both tumour types form when the nutrient goes below a certain threshold. They then become necrotic when there is no oxygen left to support them. When in contact with the medium, the necrotic cells disintegrate into the "healthy tissue". Immune cells do not divide and are supplied to the domain at a constant rate of 25MCS, however this time there is a random probability as to which type of immune cell is introduced into the domain.

Cell migration is the same as in Chapter 2 and has a random orientation for each individual cell type with immune cells having a faster capability than tumour cells. Quiescent and necrotic cells do not move unless pushed by a different cell type or by adhesion.

In this model, adhesion is similar, but now has to work with more cell types. Immune cells of type one and two have a very weak adhesion to one another and to their own cell type. Proliferating tumour cells of type one and two adhere together but not as strongly as immune cells of both types adhere to proliferating tumour cells of type one and two. Immune cells of both types do not adhere to quiescent or necrotic cells, however tumour cells do, but weakly. This is to try and allow the two tumour cell types to branch off and form new local secondary tumour sites.

As before, nutrient is supplied to the domain at a constant rate, secreted

by the medium cells. Diffusion in the domain is "zero flux" at the boundary and is modelled by the PDE:

$$\frac{\partial c}{\partial t} = D\nabla^2 c - kc + secrection,$$

where D is the diffusion rate and k is the decay rate. k represents the uptake of nutrient in a given cell with rates:

$$k = \begin{cases} 0.5, & \text{in the tumour type 1 and 2 cells,} \\ 0.25, & \text{in the quiescent type 1 and 2 cells,} \\ 0.5, & \text{in the immune type 1 and 2 cells,} \\ 0, & \text{in the necrotic cells.} \end{cases} \tag{4.2.6}$$

Within proliferating tumour and immune cells of both types, the uptake of nutrient is much higher than quiescent tumour cells of both types. The tissue, as before, does not uptake nutrient, but instead secretes it. Necrotic cells do not uptake nutrient. Hypoxic and necrotic effects of cells are not taken into consideration.

Cell death is one area where this model differs from the previous CompuCell3D model. Before, when an immune cell came into contact with a proliferating tumour cell there were two different outcomes: the proliferating tumour cell was killed by the immune cell or the immune cell was killed by the tumour cell. However, in this model, it is only the immune cells that are able to kill the tumour cells, the tumour cells do not kill. To incorpo-

rate immune death, an age factor has been introduced, which is user defined. The age is associated with how many MCS an immune cell can survive for. After this time, an immune cell is deemed to be "dead" and is turned into a necrotic cell. The dead cell is then allowed to disintegrate, again only when in contact with the medium. In biology, differing immune cells have different life expectancies, and within this model this has been incorporated. A generic immune cell death time frame for each cell type was devised and has been investigated to show qualitative results, in order to try to mimic the results found in the homogeneous and spatial model from sections 3.7 and 3.8.

To integrate the immune attack against the proliferative tumour cells the same technique has been used as in the previous CompuCell3D model. In Matzavinos et al. [2004], a control parameter p was utilised and again has been introduced into this model. Before, there was only one interaction and therefore only one probability associated with immune success. This time there are three interactions stemming from these terms from system (4.2.1)-(4.2.4):

$$\bullet \text{ in equation } \frac{\partial T_1}{\partial t}, \text{ the term } \frac{E_1 T_1}{s_1 + T_1}; \tag{4.2.7}$$

$$\bullet \text{ in equation} \frac{\partial T_2}{\partial t}, \frac{E_1 T_2}{s_2 + T_2} \text{ and } \frac{E_2 T_2}{s_3 + T_2}. \tag{4.2.8}$$

To model these interactions within CompuCell3D, three probabilities have been introduced. These are:

- the probability of immune 1 killing proliferative tumour 1, $E_1 T_1$,

- the probability of immune 1 killing proliferative tumour 2, E_1T_2,
- the probability of immune 2 killing proliferative tumour 2, E_2T_2.

The aim of the model is to try and qualitatively model aspects of immunoediting, and by modelling cell death in this way it gives the user a good overall control in order to fully investigate the system. Each probability is varied and is discussed in the results section.

The simulations run for a user-defined amount of Montecarlo steps (MCS), laid out in the results section. As before, the simulations will stop if the immune cells kill all of the tumour cells and there are no quiescent cells left. It will also stop if there are no immune cells left in the domain, due to cells of other types fully saturating it. Moreover, time can be implemented in a number of different ways. The most appropriate way for this model to include time would be to take into consideration the average mitotic rate of a cancer cell. This is in the region of around 18-34 hours. The age of the tumour cells does not come into consideration, as one of the main trademarks of cancer is that tumour cell death is averted by mutations. Time however is generic in this model.

4.3 Results

The results in this section try to accurately portray the oscillatory dynamics found in section 3.8, by extending the spatial model into a cellular potts model, using the computer software package, CompuCell3D. In the homogeneous model in section 3.7, a co-existence steady state was identified. By

varying parameter s_1, oscillatory dynamics were found, resulting from a hopf bifurcation. The model was then extended spatially, by adding in random motility. Here, heterogeneous waves exist showing the oscillatory nature of the system. The oscillations represent conditions whereby the immune system can engage the tumour cells and keep them under check, albeit in a dormant situation. Due to the nature of a PDE model, more intricate details cannot be introduced. In the spatial model, as tumour type 2 was attacked by two types of immune cells, the hope was for this population to be cleared. However, the Michaelis Menten dynamics of the system prevented this. This model will aim to rectify this, producing a coexistence steady state where the T_2 cells are at a lower density than the T_1 cells. Moreover, in the PDE model, quiescent cells and nutrients are not taken into consideration. This makes it hard to assess how to increase the potency of the tumour cells.

The discrete model begins with a central tumour mass of randomly placed tumour cells of type one and two, and four randomly selected immune cells of type one and two. Immune cells do not grow or divide and, as before, the tumour cells are allowed to grow in relation to how much nutrient is available at their core. The tumour cells at the rim of the tumour mass, therefore, will grow much faster than those at the centre, as no nutrient is available to them, preventing growth. The cells are deemed to turn quiescent when they fall below a certain threshold value of nutrient level at their core. Then, the quiescent cells either turn back to being proliferative, if the local tumour environment improves, or necrotic if the nutrient levels are no longer sufficient to support it. This creates a "proliferative rim" of very fast growing tumour cells, with a quiescent zone and a necrotic core.

Immune cells of type one and two are randomly introduced into the system at a constant rate of 25MCS. The immune cells have a user defined life expectancy and the tumour cells do not mount an immune attack in this model. By introducing an age value for the immune cells, their numbers will grow to a threshold value, once the life span of the first immune cells has been reached. This number will stay roughly constant throughout the whole model, allowing for small differences, due to the model picking a random immune type to introduce into the domain every 25MCS. When an immune cell and tumour cell come into contact, their random motility is switched off, as is their ability to bind to another cell. This means that the immune cells can only interact with one tumour cell at a time. Each individual reaction type, depending on which tumour cell is interacting with which immune cell, has a probability associated with it. In this model, if, for example, an immune cell has a 10% chance of killing a tumour cell, this means that it will roughly kill a tumour cell one in every ten MCS. This is provided that it is in contact with the tumour cell for the whole time. Again, it should be noted that tumour type one is only attacked by immune type one whereas, tumour type two is attacked by both immune types. Moreover, since this modelling technique is stochastic, results will vary every time a new simulation is undertaken.

As in Chapter 2, this model was used to explore the idea of immunoediting. The probabilities of each of the tumour-immune interactions have been examined in order to try and model the three Es of immunoediting; elimination, equilibrium and escape. Each of the three Es will be identified and conditions under which they occur will be investigated. The results are split

into subsections that reflect the type of immune-tumour interaction, which has been varied, and then will be sub-sectioned according to which immunoediting stage they represent.

While undertaking simulations using this model, it became apparent very quickly that it was necessary to change two of the immune success rates at one time, rather than just one, as it was difficult to ascertain any results otherwise. A control set of parameters was very difficult to attain and therefore, this requires more study into achieving a more structured way of showing how a change in the parameter values dictates a change in the results of the model. However, this chapter has been able to qualitatively show that it is possible to simulate the three Es of immunoediting.

4.3.1 E_1T_1 interactions

As discussed previously, there are three different immune-tumour interactions: tumour one and immune one, E_1T_1 for simplicity; tumour two and immune one, E_1T_2; and tumour two and immune two, E_2T_2. This section will focus on the interactions between immune one and tumour one. As tumour cell one only has immune one attacking it, whereas tumour cell two has both, it was recognised early on that the immune success rate would need to be reasonably high for equilibrium or elimination of the tumour mass to occur.

4.3.1.1 Cancer cell escape

The simulation in this section was run for 20,000 MCS with the probability of E_1T_2 and E_2T_2 at 22% and 77% respectively. The simulations will stop if there are no tumour cells, immune cells or quiescent cells left in the domain. The value of E_1T_1 has been varied between $70 - 89\%$ in order to investigate the effect of changing immune cell success rate on the tumour cells. Immune cell death occurs when the immune cell has been in the domain for 1000 MCS. By looking at Figures 4.2-4.15, concentrations of E_1, E_2, T_1 and T_2 can be seen in graphical representation in Figures 4.2-4.5 and 4.8-4.13. Here, T_1 is represented by the red line, T_2 by the blue line, E_1 by the green line and E_2 by the pink line. The spatial representations for $E_1T_1 = 77\%$ and $E_1T_1 = 88\%$ can be seen in Figures 4.6 and 4.14, where all cell types are depicted. In the spatial pictures, proliferative tumour type 1 (T_1) cells are red, quiescent tumour type 1 cells are salmon, proliferative tumour type 2 (T_2) are blue, quiescent tumour type 2 cells are light blue, necrotic cells are black, medium cells are grey, immune type 1 cells (E_1) are green and immune type 2 (E_2) are magenta. The nutrient concentrations for $E_1T_1 = 77\%$ and $E_1T_1 = 88\%$ are depicted in Figures 4.7 and 4.15, where the bar at the side of the figure shows the nutrient concentration in the domain. Looking at Figures 4.2-4.15, initially the tumour cells and immune cells grow in number. By 1000 MCS the immune cells start to level off at a rough concentration of 50, 25 of each type, in the domain.

The results show that the T_2 cells are killed off very quickly by the immune cells or, if they do survive, they are kept at a level close to zero. Indeed, this

was expected as the T_2 cells have double the amount of immune cells attacking them than the T_1 cells. This allows more space and nutrient for T_1 to invade the domain and actively evade immune attack. The clearing of the more immunogenic cells is discussed is discussed in Chapter 1.1. Here, T_2 cells are acting as the more immunogenic cells i.e. cells which are more easily found by the immune system. As T_2 is killed, this allows the less immunogenic (T_1) cells to grow and evade immune destruction. Moreover, the initial makeup of the tumour mass is also important, as T_2 cells that are on the outside of the tumour mass at the start of the simulation are often killed quickly. If there are T_2 cells present throughout the whole simulation, it is often due to them hiding as quiescent cells in among proliferating or quiescent T_1 cells. This is portrayed in Figures 4.6 and 4.14. T_2 may have small oscillations in this case, as shown, for example, in Figure 4.13 (top). This is due to the T_2 cells either managing to migrate to an area where there is little space for an immune cell to invade, or if T_1 encases the quiescent T_2 cells. In the latter case, as the protective layer of T_1 cells are invaded by E_1, this allows more nutrients for T_2, enabling them to turn from their quiescent state back into a proliferative state. However, this is short lived, and the T_2 cells generally lose numbers and lower in peak concentration with every oscillation.

Furthermore, it can be seen, that oscillations are occurring in T_1. This is not due to the immune attack, but rather the oscillatory nature of the T_1 cells seems to be reliant on the clearance of the necrotic cells. This is depicted in Figures 4.6 and 4.14. This is interesting as it has often been found that the introduction of inflammatory immune cells into a tumour microenvironment can often have negative effects and actually promote tumour growth,

discussed in Chapter 1.1. Moreover, the necrotic cells often provide a barrier for tumour cells against an immune attack, allowing them to grow. Once the necrotic cells come into contact with the medium they start to disintegrate, freeing up space and vital nutrient for the tumour cells to regain their former glory. However, the immune cells are able to clear T_2.

Once the immune cells have successfully killed the T_2 cells, E_2 become obsolete within the system and now serve to hinder the E_1 attack against T_1. This can be attributed to the randomness of immune cell supply every 25MCS. On a smaller scale, the immune cells also provide a physical barrier as, if they are close to one another, and are not attracted by a tumour cell, they will often adhere to one another. E_2 may also adhere to T_1, which it is not potent to, creating a small barrier for T_1.

Looking at the downward trend of E_1 success rate, Figures 4.2-4.14 show that there is no clearance of the T_1 cells and full infiltration of the domain will ensue, albeit over a greater number of MCS than shown here, in some of the simulations. Indeed, even if the immune success rate is raised further, it does not have a big impact on tumour cell clearance or tumour bulk. The simulations that stop before 20,000MCS, such as Figure 4.5 (top), do have a single oscillation, but, however, this is due to the tumour cells flooding the domain, using up the nutrients and therefore turning necrotic. Looking at the figures, T_2 does not survive for very long, even if the success rate of the E_1T_1 interactions is further dropped. This would be counterintuitive however, as the T_1 cells are then allowed to grow much faster due to a smaller immune success rate giving the T_2 cells less nutrient and space to survive. Moreover, there is no apparent downward pattern in tumour bulk of T_1 cells even if the

success rate of E_1 is lowered. One of the ways to combat this is to increase the number of immune cells in the domain. To do this, more immune cells could be introduced at a constant rate, however varying the amount of time the immune cells are in the domain has been investigated. More simulations can be found in Appendix 6.1, whereby the E_1T_1 immune success rate has been lowered, showing no significant effect.

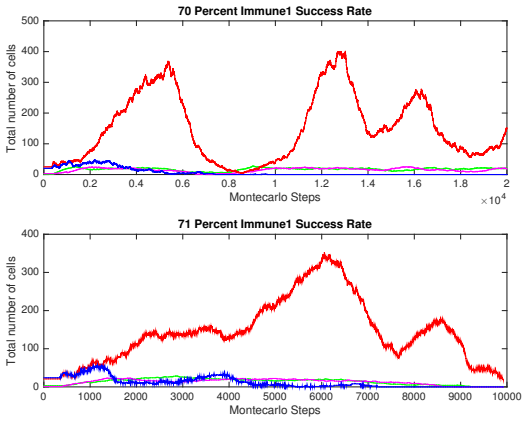

Figure 4.2: *Plots showing the total number of tumour and immune cells for* $70 - 71\%$ *immune 1 kill rate when in interaction with tumour cell type 1, tumour type 2 and immune type 1 at* 22% *and tumour type 2 and immune type 2 at* 77%*. Tumour cell 1 is represented by the red line, tumour cell 2 is represented by the blue line, immune cell 1 is represented by the green line and immune cell 2 by the pink line. These plots show cancer escape*

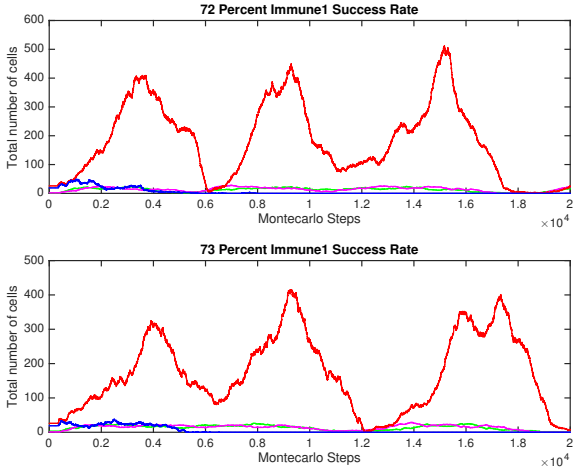

Figure 4.3: *Plots showing the total number of tumour and immune cells for* $72 - 73\%$ *immune 1 kill rate when in interaction with tumour cell type 1, tumour type 2 and immune type 1 at* 22% *and tumour type 2 and immune type 2 at* 77%*. Tumour cell 1 is represented by the red line, tumour cell 2 is represented by the blue line, immune cell 1 is represented by the green line and immune cell 2 by the pink line. These plots show cancer escape.*

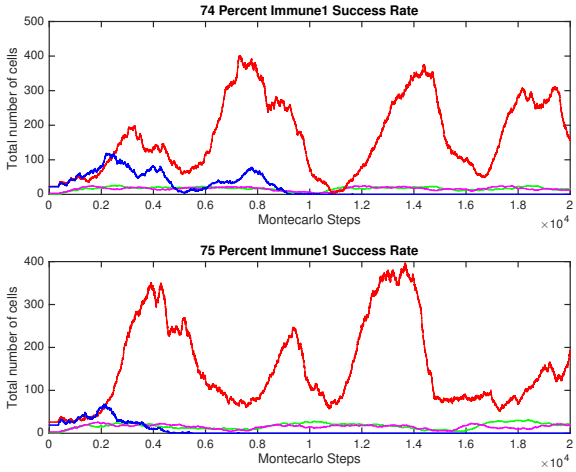

Figure 4.4: *Plots showing the total number of tumour and immune cells for* $74 - 75\%$ *immune 1 kill rate when in interaction with tumour cell type 1, tumour type 2 and immune type 1 at* 22% *and tumour type 2 and immune type 2 at* 77%*. Tumour cell 1 is represented by the red line, tumour cell 2 is represented by the blue line, immune cell 1 is represented by the green line and immune cell 2 by the pink line. These plots show cancer escape.*

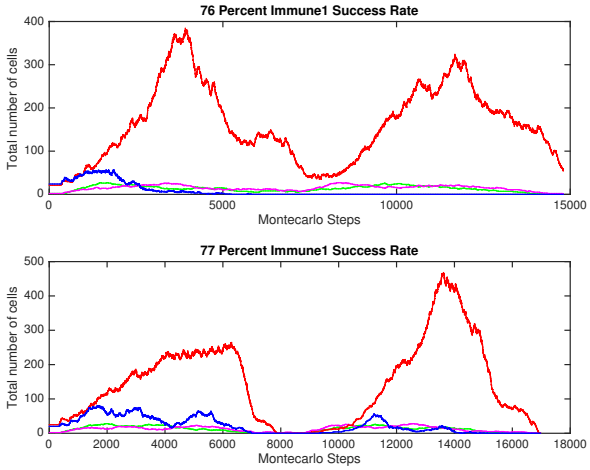

Figure 4.5: *Plots showing the total number of tumour and immune cells for* $76 - 77\%$ *immune 1 kill rate when in interaction with tumour cell type 1, tumour type 2 and immune type 1 at* 22% *and tumour type 2 and immune type 2 at* 77%*. Tumour cell 1 is represented by the red line, tumour cell 2 is represented by the blue line, immune cell 1 is represented by the green line and immune cell 2 by the pink line. These plots show cancer escape*

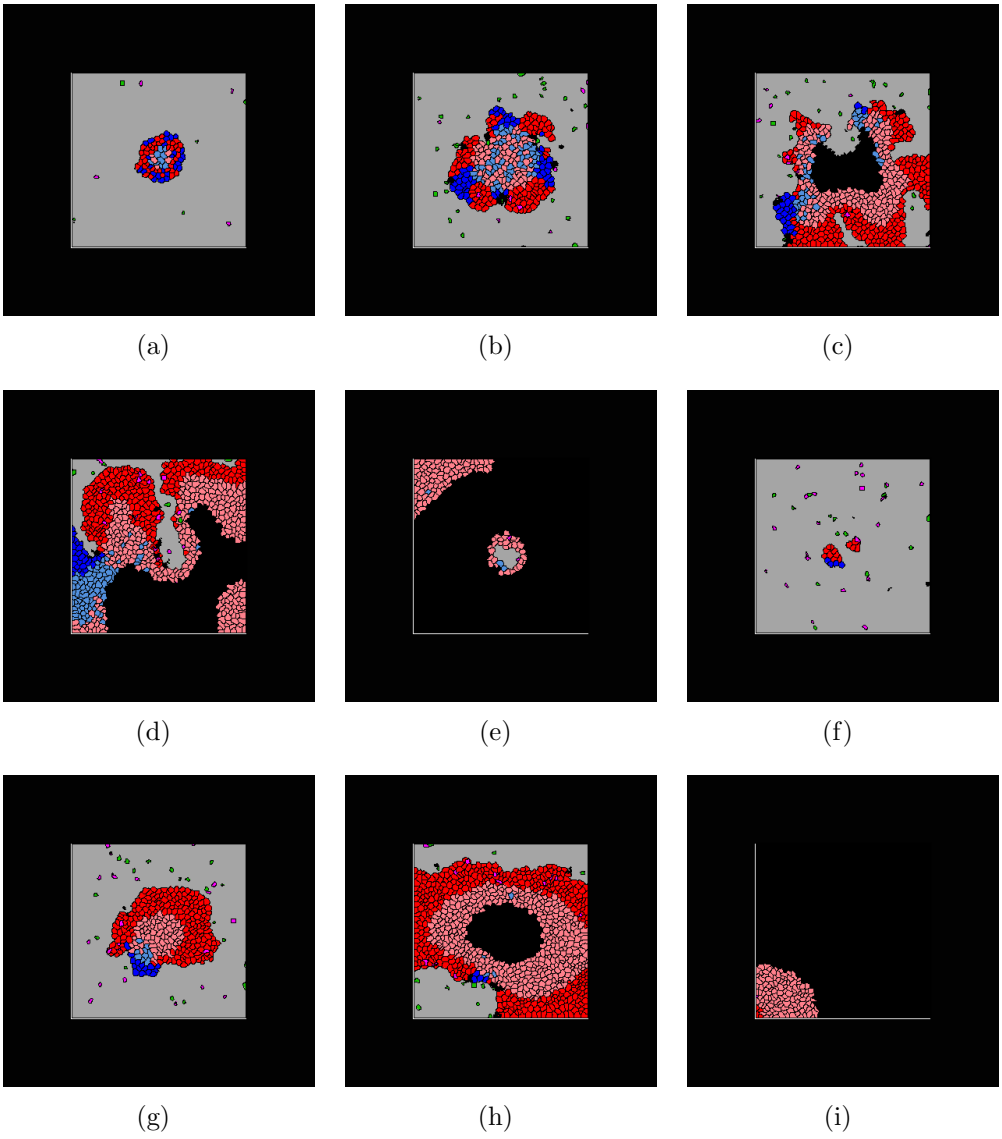

Figure 4.6: *Plots showing the growth of a tumour mass interacting with a host immune system at 1000MCS immune death rate. The types of cells and their corresponding colours in Figures 4.6(a)-4.6(i) are as follows: proliferative tumour type 1 cells in red, quiescent tumour type 1 cells in salmon, proliferative tumour type 2 in blue, quiescent tumour type 2 cells in light blue, necrotic cells in black, medium cells in grey, immune type 1 cells in green, immune type 2 in magenta. The immune success rates are as follows: tumour type 1 and immune type 1 at* 77%*, tumour type 2 and immune type 1 at* 22% *and tumour type 2 and immune type 2 at* 77%*. Figures 4.6(a)-4.6(i) represent the model at 2000MCS, 4000MCS, 6000MCS, 8000MCS, 10000MCS, 12000MCS, 14000MCS, and 16900MCS respectively. The figures show cancer escape and correspond to Figure 4.5 (bottom).*

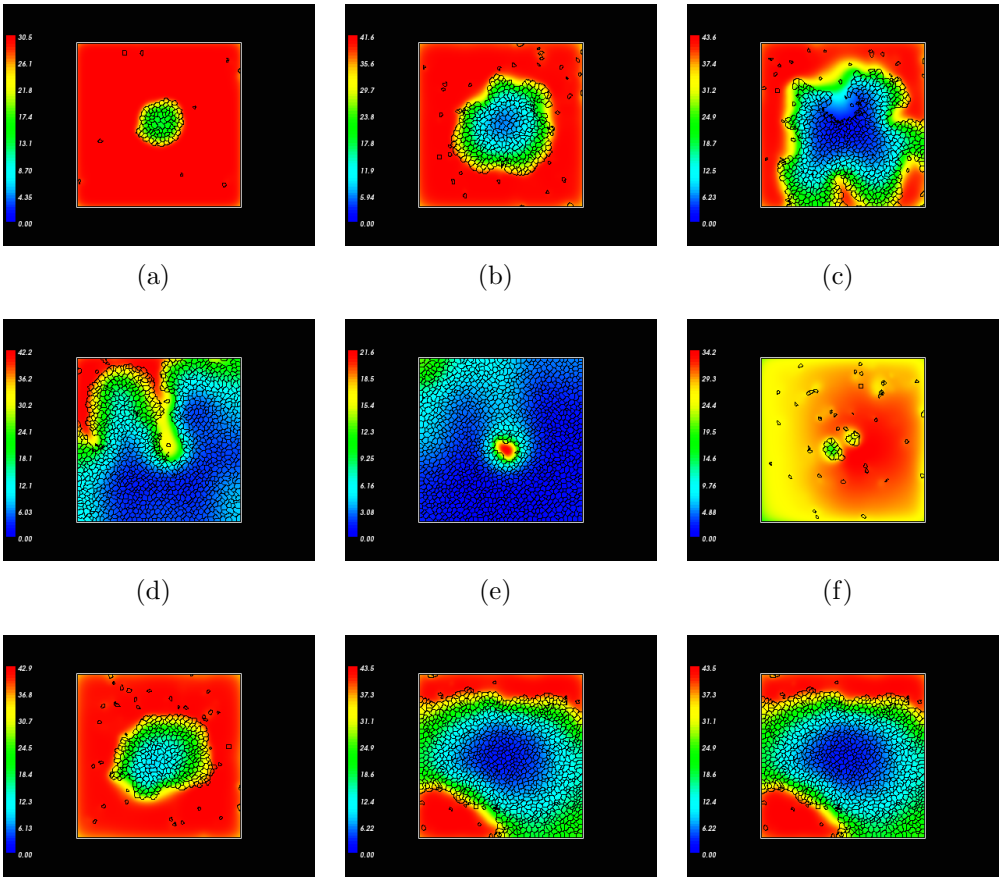

Figure 4.7: *Plots showing the nutrient concentration at times 2000MCS, 4000MCS, 6000MCS, 8000MCS, 10000MCS, 12000MCS, 14000MCS, and 16900MCS. The immune success rates are as follows: tumour type 1 and immune type 1 at 77%, tumour type 2 and immune type 1 at 22% and tumour type 2 and immune type 2 at 77%, corresponding to Figure 4.5 (bottom). The oxygen concentration is high when it is red and low when it is blue. A bar on the left hand side of each picture represents the oxygen concentration. This plot corresponds to Figure 4.5 (bottom). Oxygen is used up by the immune, tumour and quiescent cells leaving areas where tumour cells can longer be supported leading to necrosis. Once the necrotic cells have disintegrated oxygen can flow into the area again via medium cells.*

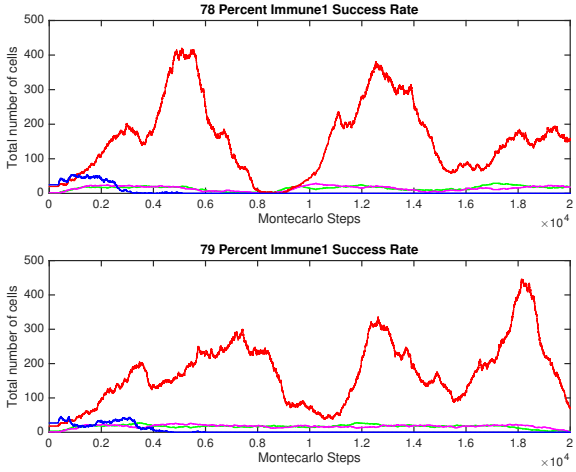

Figure 4.8: *Plots showing the total number of tumour and immune cells for* $78 - 79\%$ *immune 1 kill rate when in interaction with tumour cell type 1, tumour type 2 and immune type 1 at* 22% *and tumour type 2 and immune type 2 at* 77%*. Tumour cell 1 is represented by the red line, tumour cell 2 is represented by the blue line, immune cell 1 is represented by the green line and immune cell 2 by the pink line.*

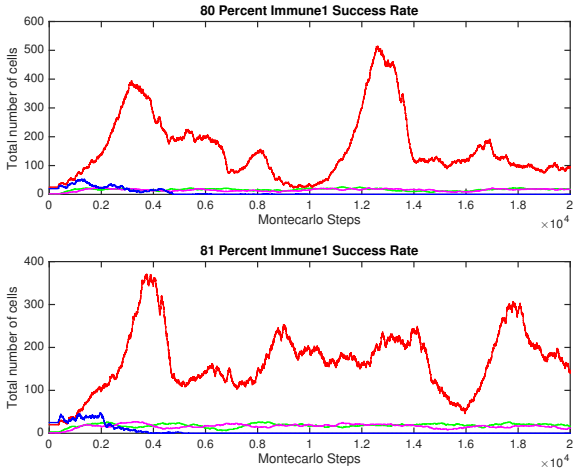

Figure 4.9: *Plots showing the total number of tumour and immune cells for* $80 - 81\%$ *immune 1 kill rate when in interaction with tumour cell type 1, tumour type 2 and immune type 1 at* 22% *and tumour type 2 and immune type 2 at* 77%*. Tumour cell 1 is represented by the red line, tumour cell 2 is represented by the blue line, immune cell 1 is represented by the green line and immune cell 2 by the pink line. These plots show cancer escape.*

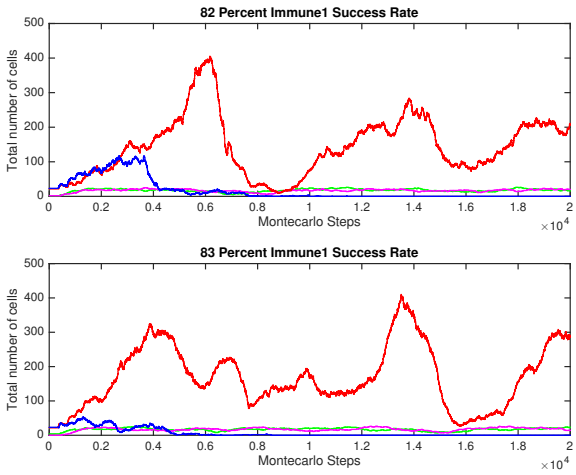

Figure 4.10: *Plots showing the total number of tumour and immune cells for* $82-83\%$ *immune 1 kill rate when in interaction with tumour cell type 1, tumour type 2 and immune type 1 at* 22% *and tumour type 2 and immune type 2 at* 77%*. Tumour cell 1 is represented by the red line, tumour cell 2 is represented by the blue line, immune cell 1 is represented by the green line and immune cell 2 by the pink line. These plots show cancer escape.*

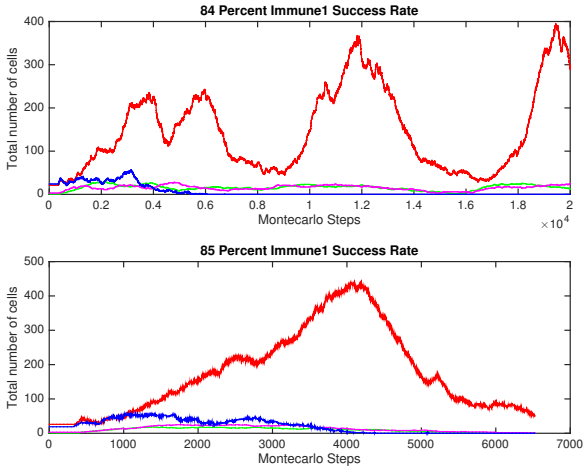

Figure 4.11: *Plots showing the total number of tumour and immune cells for* $84-85\%$ *immune 1 kill rate when in interaction with tumour cell type 1, tumour type 2 and immune type 1 at* 22% *and tumour type 2 and immune type 2 at* 77%*. Tumour cell 1 is represented by the red line, tumour cell 2 is represented by the blue line, immune cell 1 is represented by the green line and immune cell 2 by the pink line. These plots show cancer escape.*

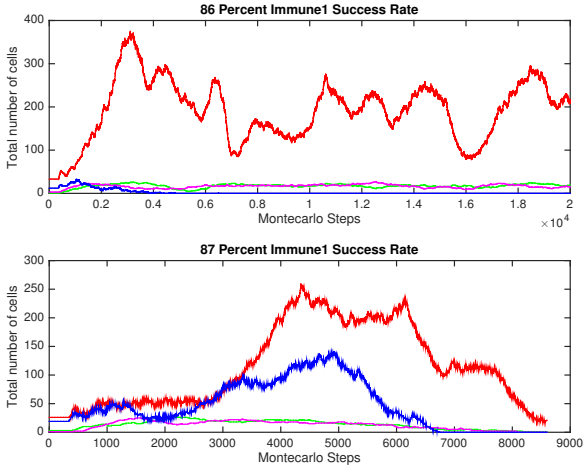

Figure 4.12: *Plots showing the total number of tumour and immune cells for* $86 - 87\%$ *immune 1 kill rate when in interaction with tumour cell type 1, tumour type 2 and immune type 1 at* 22% *and tumour type 2 and immune type 2 at* 77%*. Tumour cell 1 is represented by the red line, tumour cell 2 is represented by the blue line, immune cell 1 is represented by the green line and immune cell 2 by the pink line. These plots show cancer escape.*

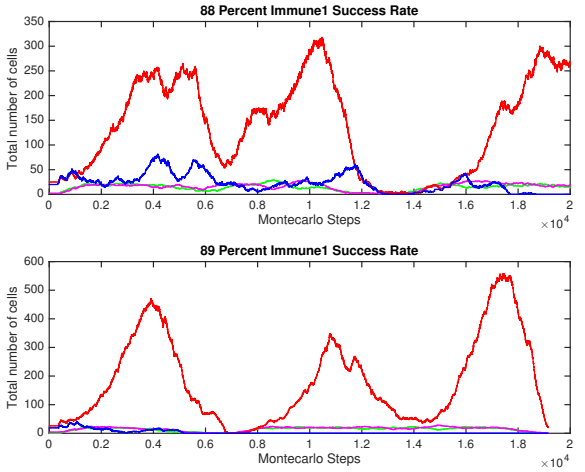

Figure 4.13: *Plots showing the total number of tumour and immune cells for* $88 - 89\%$ *immune 1 kill rate when in interaction with tumour cell type 1, tumour type 2 and immune type 1 at* 22% *and tumour type 2 and immune type 2 at* 77%*. Tumour cell 1 is represented by the red line, tumour cell 2 is represented by the blue line, immune cell 1 is represented by the green line and immune cell 2 by the pink line. These plots show cancer escape.*

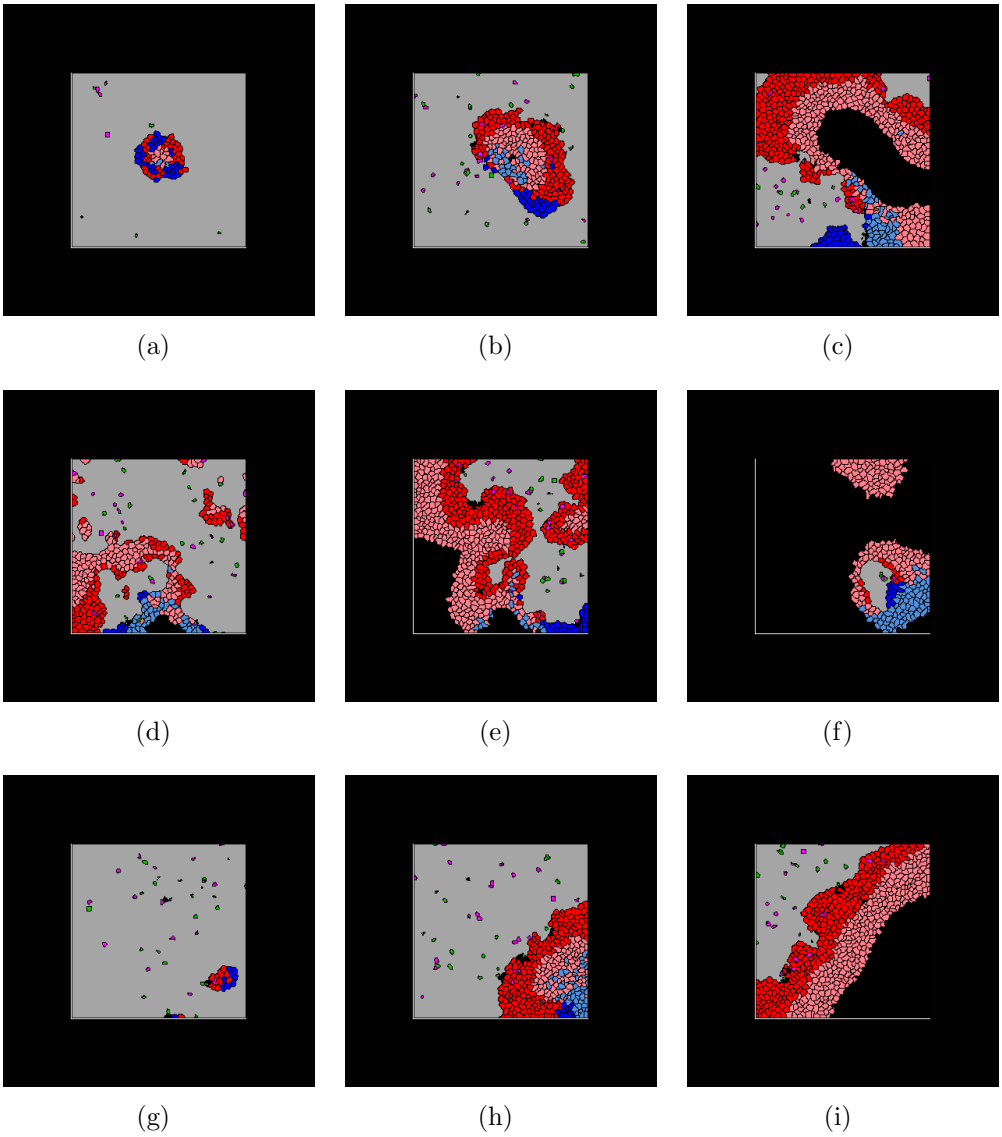

Figure 4.14: *Plots showing the growth of a tumour mass interacting with a host immune system at 1000MCS immune death rate. The types of cells and their corresponding colours in Figures 4.14(a)-4.14(i) are as follows: proliferative tumour type 1 cells in red, quiescent tumour type 1 cells in salmon, proliferative tumour type 2 in blue, quiescent tumour type 2 cells in light blue, necrotic cells in black, medium cells in grey, immune type 1 cells in green, immune type 2 in magenta. The immune success rates are as follows: tumour type 1 and immune type 1 at 88%, tumour type 2 and immune type 1 at 22% and tumour type 2 and immune type 2 at 77%. Figures 4.14(a)-4.14(i) represent the model at 500MCS, 2500MCS, 5000MCS, 7500MCS, 10000MCS, 12500MCS, 15000MCS, 17500MCS, and 20000MCS respectively. These figures show cancer escape and correspond to Figure 4.13 (top).*

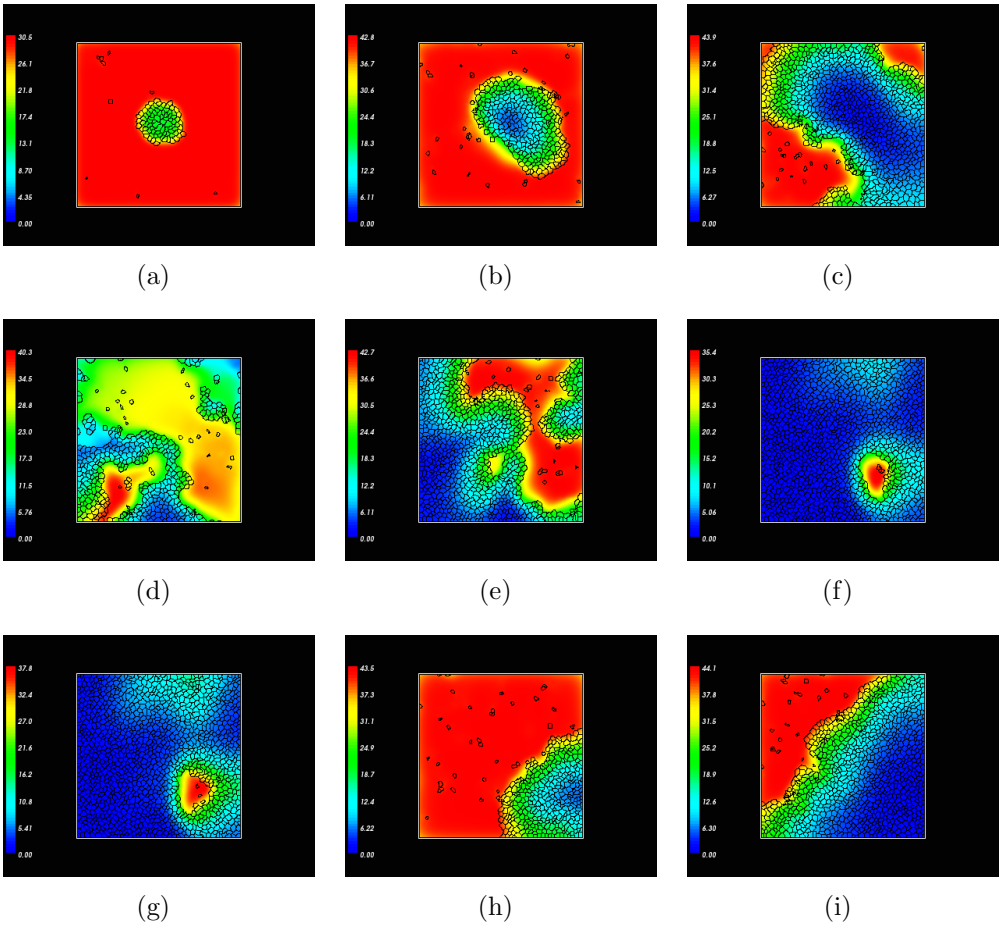

(a) (b) (c)

(d) (e) (f)

(g) (h) (i)

Figure 4.15: *Plots showing the nutrient concentration at times 500MCS, 2500MCS, 5000MCS, 7500MCS, 10000MCS, 12500MCS, 15000MCS, 17500MCS, and 20000MCS, repectively. The immune success rates are as follows: tumour type 1 and immune type 1 at* 77%*, tumour type 2 and immune type 1 at* 22% *and tumour type 2 and immune type 2 at* 77%*, corresponding to Figure 4.13 (top). The oxygen concentration is high when it is red and low when it is blue. A bar on the left hand side of each picture represents the oxygen concentration. Oxygen is used up by the immune, tumour and quiescent cells leaving areas where tumour cells can longer be supported leading to necrosis. Once the necrotic cells have disintegrated oxygen can flow into the area again via medium cells.*

4.3.1.2 Coexistence

The next section is concerned with trying to find an equilibrium state of immune and tumour cells. Here, the tumour and immune cells should exist over a long period of time. In section 4.3.1.1, it was identified that in order to do this, the immune cell concentrations in the domain would need to be increased. This entails increasing the amount of time the immune cells are present in the domain i.e. increasing their life expectancy.

In this section, the immune cell rate was increased from 1000MCS to 2500MCS. This means the immune cells are in the domain for 2500MCS before they are deemed dead, turned into necrotic cells and then allowed to disintegrate into the medium. The success rates of each of the individual reactions of the tumour and immune cells, E_1T_1, E_1T_2 and E_2T_2, are $90-99\%$, 22% and 77%, respectively. The simulations are run for 20,000MCS and again will stop if there are no immune, tumour or quiescent cells left in the domain.

By increasing the amount of immune cells, the host immune system is now able to provide a good immune cell attack against the tumour cells. In Figures 4.16-4.22, the results show that dynamic equilibrium is possible. More specifically, Figure 4.17 shows the spatial distribution of tumour, immune, quiescent, medium and necrotic cells in the domain at $E_1T_1 = 90\%$. In the spatial figures, the immune cells now have a much bigger presence and the tumour cells are kept at bay. Figure 4.18 shows the nutrient concentration at $E_1T_1 = 90\%$. As an aside, in Figure 4.17 it can be seen that the immune cells are adhering to one another when tumour cells are not present in the local area, an observation discussed in section 4.3.1.1. Interestingly, the T_2

tumour cells are now not able to hide among the T_1 tumour and quiescent cells and, therefore, there are no instances of the T_2 cells lasting throughout the entire simulation. As can be seen from Figures 4.16-4.22, the oscillations are now not driven by the clearance of necrotic cells, however this still plays a part, allowing the tumour cell bulk to come back. If the death of the immune cells is lowered further to 3500MCS, a general trend towards elimination can be seen, whereby the immune cells are able to clear the tumour bulk. To guarantee tumour cell clearance however, the immune death rate needs to be lowered. Simulations for the immune death rate at 3500MCS can be found in the appendix in section 6.2.

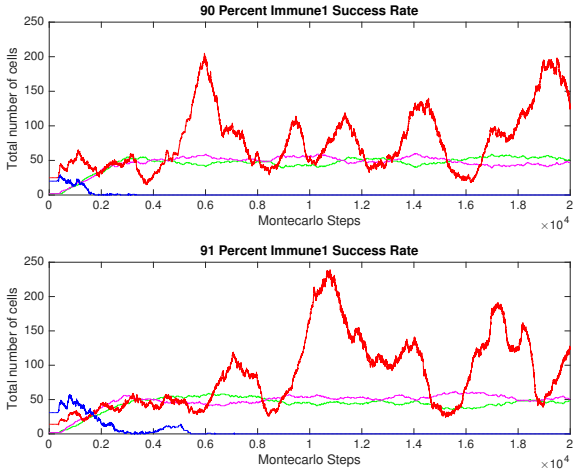

Figure 4.16: *Plots showing the total number of tumour and immune cells for* $90 - 91\%$ *immune 1 kill rate when in interaction with tumour cell type 1, tumour type 2 and immune type 1 at* 22% *and tumour type 2 and immune type 2 at* 77%*. Tumour cell 1 is represented by the red line, tumour cell 2 is represented by the blue line, immune cell 1 is represented by the green line and immune cell 2 by the pink line.*

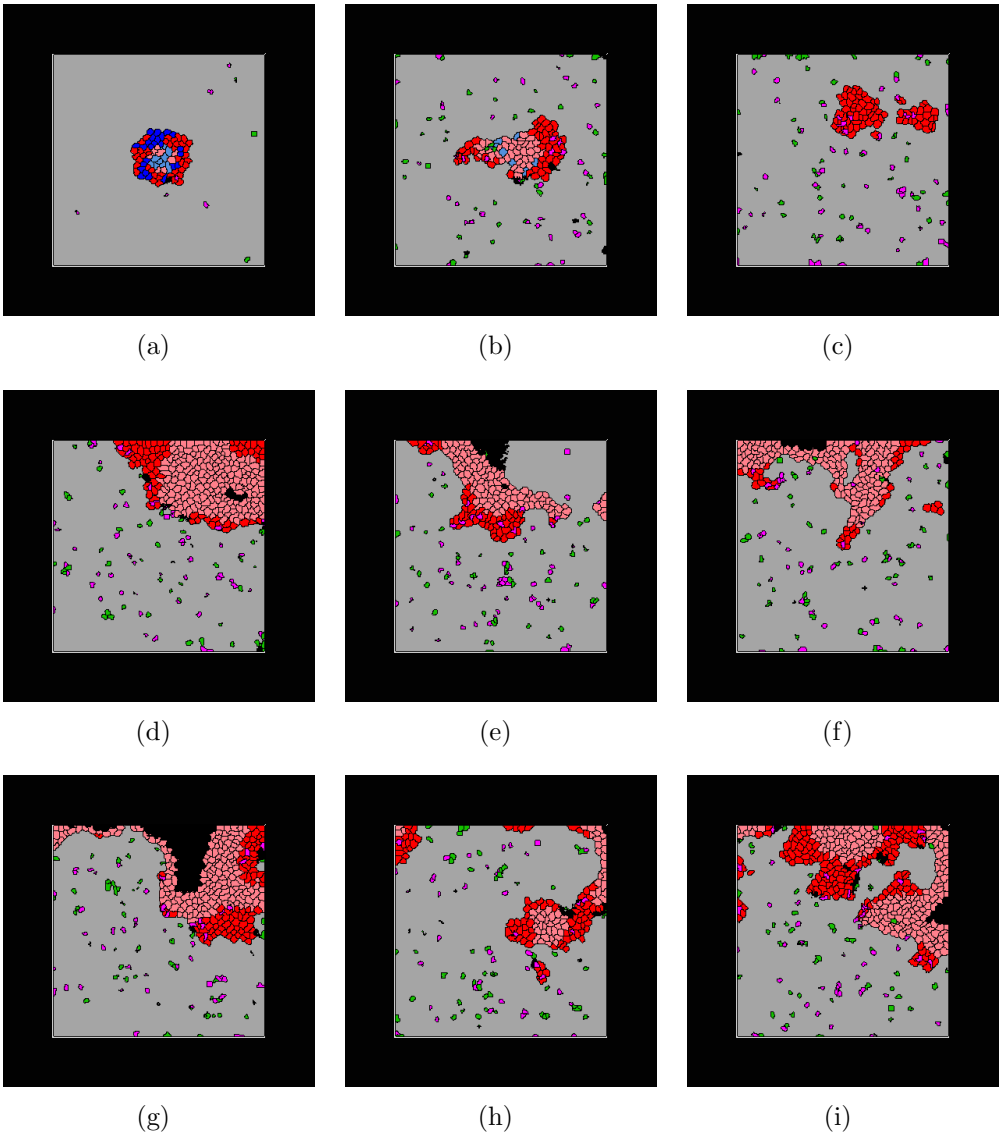

Figure 4.17: *Plots showing the growth of a tumour mass interacting with a host immune system at 2500MCS immune death rate. The types of cells and their corresponding colours in Figures 4.17(a)-4.17(i) are as follows: proliferative tumour type 1 cells in red, quiescent tumour type 1 cells in salmon, proliferative tumour type 2 in blue, quiescent tumour type 2 cells in light blue, necrotic cells in black, medium cells in grey, immune type 1 cells in green, immune type 2 in magenta. The immune success rates are as follows: tumour type 1 and immune type 1 at* 90%*, tumour type 2 and immune type 1 at* 22% *and tumour type 2 and immune type 2 at* 77%*, corresponding to Figure 4.16 (top). Moreover, the immune death rate is now set to 2500MCS to try and achieve coexistence. Figures 4.17(a)-4.17(i) represent the model at 500MCS, 2500MCS, 5000MCS, 7500MCS, 10000MCS 12500MCS, 15000MCS, 175000MCS and 20000MCS respectively.*

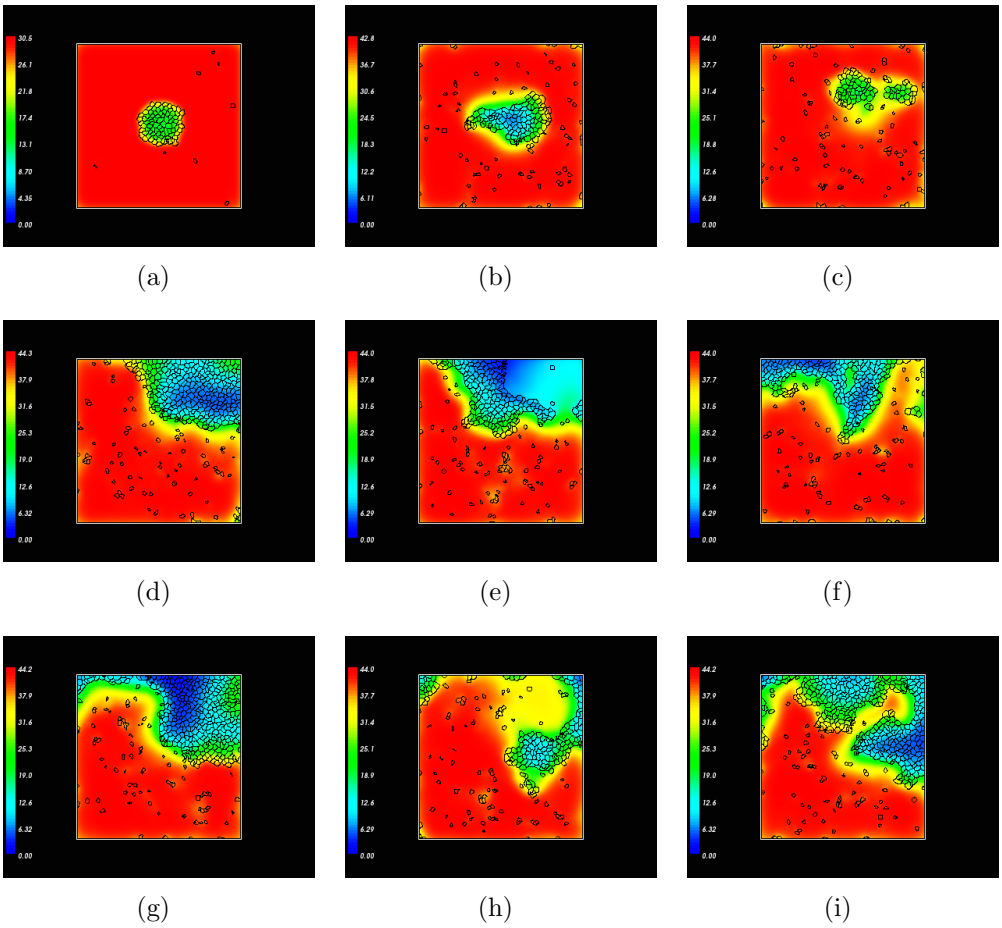

(a) (b) (c)

(d) (e) (f)

(g) (h) (i)

Figure 4.18: *Plots showing the nutrient concentration at times 500MCS, 2500MCS, 5000MCS, 7500MCS, 10000MCS 12500MCS, 15000MCS, 175000MCS and 20000MCS, respectively. The immune success rates are as follows: tumour type 1 and immune type 1 at* 90%*, tumour type 2 and immune type 1 at* 22% *and tumour type 2 and immune type 2 at* 77%*, corresponding to Figure 4.16 (top). The oxygen concentration is high when it is red and low when it is blue. Moreover, the immune death rate is now set to 2500MCS to try and achieve coexistence. A bar on the left hand side of each picture represents the oxygen concentration. Oxygen is used up by the immune, tumour and quiescent cells leaving areas where tumour cells can longer be supported leading to necrosis. Once the necrotic cells have disintegrated oxygen can flow into the area again via medium cells.*

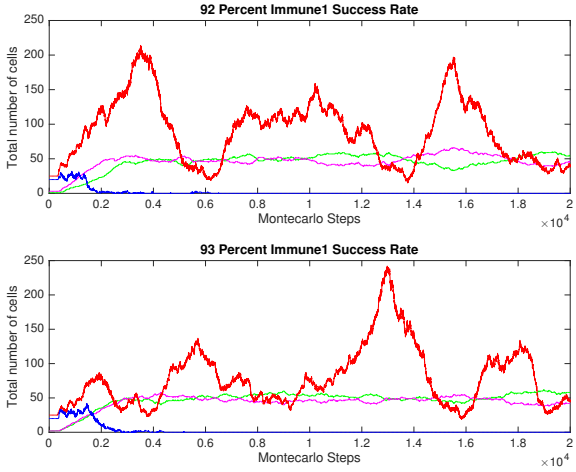

Figure 4.19: *Plots showing the total number of tumour and immune cells for* $92-93\%$ *immune 1 kill rate when in interaction with tumour cell type 1, tumour type 2 and immune type 1 at* 22% *and tumour type 2 and immune type 2 at* 77%*. Tumour cell 1 is represented by the red line, tumour cell 2 is represented by the blue line, immune cell 1 is represented by the green line and immune cell 2 by the pink line.*

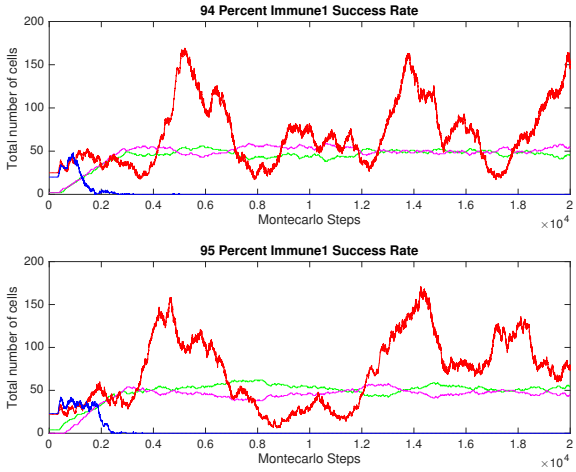

Figure 4.20: *Plots showing the total number of tumour and immune cells for* $94-95\%$ *immune 1 kill rate when in interaction with tumour cell type 1, tumour type 2 and immune type 1 at* 22% *and tumour type 2 and immune type 2 at* 77%*. Tumour cell 1 is represented by the red line, tumour cell 2 is represented by the blue line, immune cell 1 is represented by the green line and immune cell 2 by the pink line.*

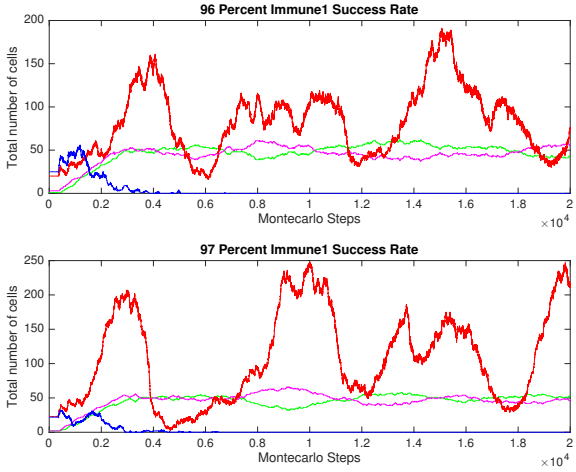

Figure 4.21: *Plots showing the total number of tumour and immune cells for* $96-97\%$ *immune 1 kill rate when in interaction with tumour cell type 1, tumour type 2 and immune type 1 at* 22% *and tumour type 2 and immune type 2 at* 77%*. Tumour cell 1 is represented by the red line, tumour cell 2 is represented by the blue line, immune cell 1 is represented by the green line and immune cell 2 by the pink line.*

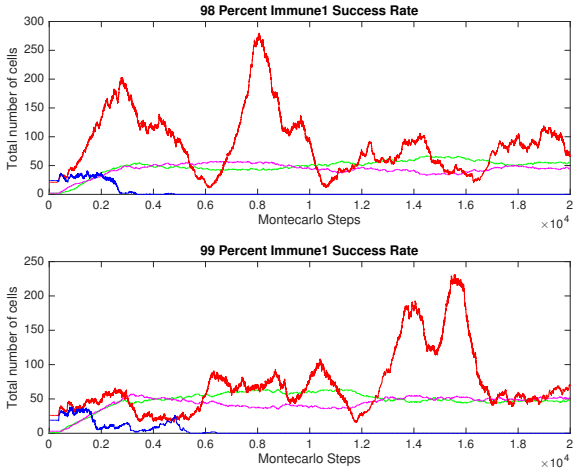

Figure 4.22: *Plots showing the total number of tumour and immune cells for* $98-99\%$ *percent immune 1 kill rate when in interaction with tumour cell type 1, tumour type 2 and immune type 1 at* 22% *and tumour type 2 and immune type 2 at* 77%*. Tumour cell 1 is represented by the red line, tumour cell 2 is represented by the blue line, immune cell 1 is represented by the green line and immune cell 2 by the pink line.*

4.3.1.3 Tumour elimination

In this section cancer destruction by the idealised host immune system is possible. This is known as the first "E" of immunoediting called "Elimination". The immune cell death rate in the following simulations has been decreased further to 5000MCS i.e. the immune cells will reside in the domain for 5000MCS before they are killed. Figures 4.23-4.29 show the immune cells clearing the tumour mass, aside from when the success rate of E_1T_1 is at 99%. Figures 4.23 (top figure), 4.24 and 4.25 show the E_1T_1 success rate at 90%. In Figure 4.23 (top figure) the overall concentrations of immune and tumour cells can be seen with the tumour cells winning out at 11400MCS. Figure 4.24 depicts the spatial distribution of all cell types and Figure 4.25 shows the nutrient concentration throughout the domain. The tumour mass is surviving in Figures 4.24(a)-4.24(d), but by 4000MCS the immune cells have already nearly wiped out the resident T_2 tumour population, as well as cutting into the T_1 population. By 6000MCS, in Figure 4.24(f) it has become apparent that the E_1 cells are not allowing the T_1 cell's concentration to pose a threat. Figures 4.24(g)-4.24(h) show E_1 overcoming the tumour cells. Finally, the simulation ends when there are no tumour cells left, depicted in Figure 4.24(i).

As the simulation is stochastic in nature, fluctuations in the simulations are to be expected. This also corresponds to what happened in the elimination section in the previous CompuCell3D model in Chapter 2. Again, the idea is to try and find a spectrum of results where tumour clearance is nearly always possible. In this model, the tumour cell population has not

won out at 99% but is still in equilibrium. This could be attributed to the adhesion of the tumour cells being set at a low enough level to allow for the tumour cells to branch off and create new tumour masses locally, evading the immune system.

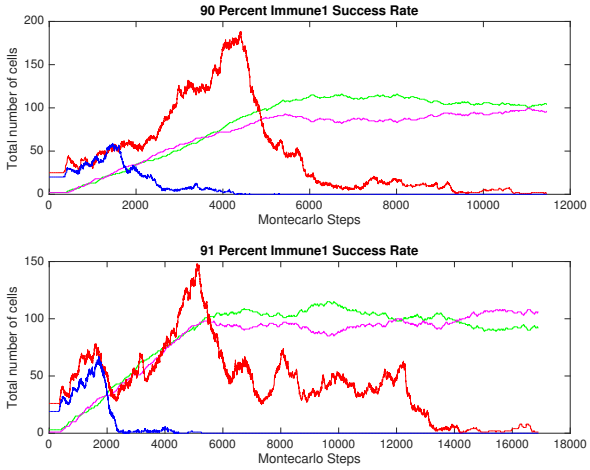

Figure 4.23: *Plots showing the total number of tumour and immune cells for* $90 - 91\%$ *immune 1 kill rate when in interaction with tumour cell type 1, tumour type 2 and immune type 1 at* 22% *and tumour type 2 and immune type 2 at* 77%*. Tumour cell 1 is represented by the red line, tumour cell 2 is represented by the blue line, immune cell 1 is represented by the green line and immune cell 2 by the pink line.*

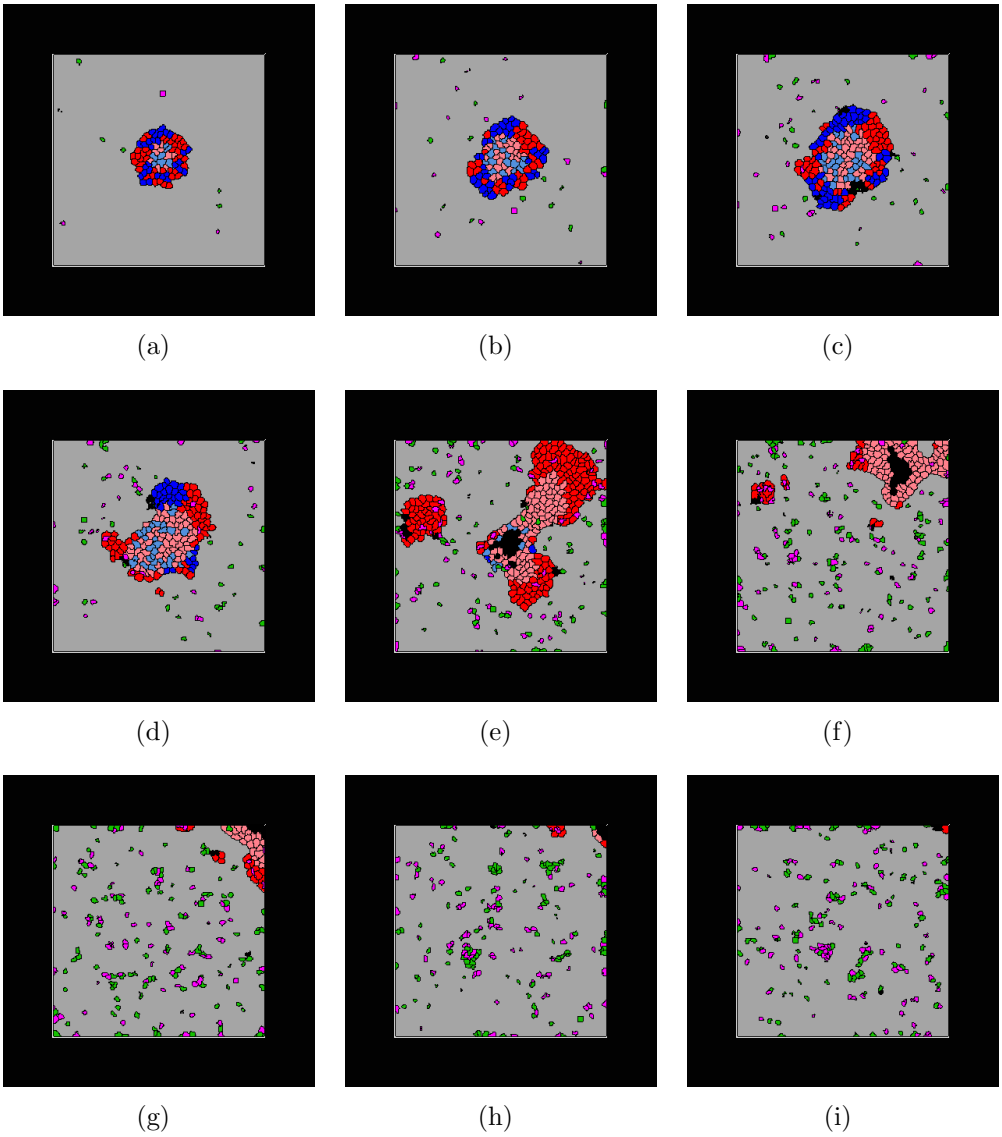

Figure 4.24: *Plots showing the growth of a tumour mass interacting with a host immune system at 5000MCS immune death rate. The types of cells and their corresponding colours in Figures 4.24(a)-4.24(i) are as follows: proliferative tumour type 1 cells in red, quiescent tumour type 1 cells in salmon, proliferative tumour type 2 in blue, quiescent tumour type 2 cells in light blue, necrotic cells in black, medium cells in grey, immune type 1 cells in green, immune type 2 in magenta. The immune success rates are as follows: tumour type 1 and immune type 1 at* 90%*, tumour type 2 and immune type 1 at* 22% *and tumour type 2 and immune type 2 at* 77%*, corresponding to Figure 4.23 (top). Figures 4.24(a)-4.24(i) represent the model at 500MCS, 1000MCS, 2000MCS, 4000MCS, 6000MCS, 8000MCS, 10000MCS and 11400MCS respectively.*

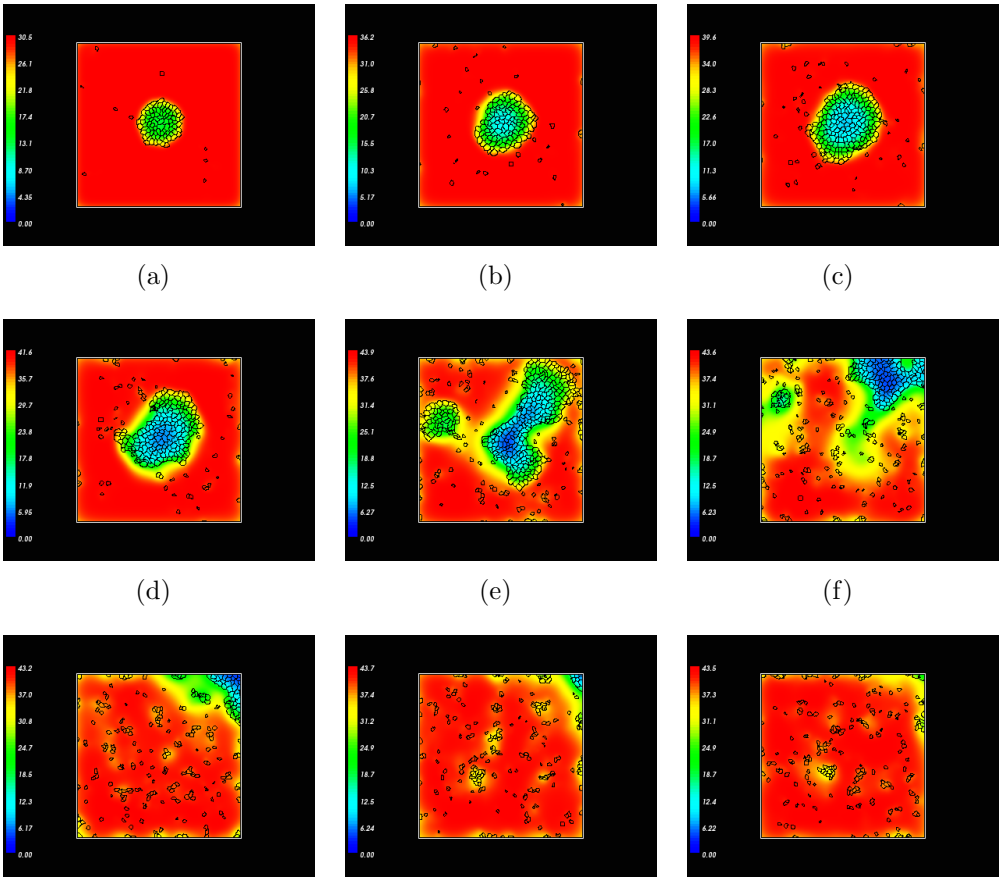

(a) (b) (c)

(d) (e) (f)

(g) (h) (i)

Figure 4.25: *Plots showing the nutrient concentration at times 500MCS, 1000MCS, 2000MCS, 4000MCS, 6000MCS, 8000MCS, 10000MCS and 11400MCS, respectively. The immune success rates are as follows: tumour type 1 and immune type 1 at* 90%*, tumour type 2 and immune type 1 at* 22% *and tumour type 2 and immune type 2 at* 77%*, corresponding to Figure 4.23 (top). The oxygen concentration is high when it is red and low when it is blue. A bar on the left hand side of each picture represents the oxygen concentration. Oxygen is used up by the immune, tumour and quiescent cells leaving areas where tumour cells can longer be supported leading to necrosis. Once the necrotic cells have disintegrated oxygen can flow into the area again via medium cells.*

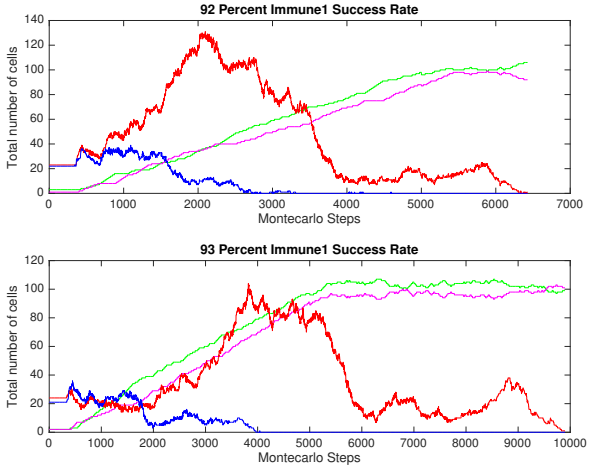

Figure 4.26: *Plots showing the total number of tumour and immune cells for* $92 - 93\%$ *immune 1 kill rate when in interaction with tumour cell type 1, tumour type 2 and immune type 1 at* 22% *and tumour type 2 and immune type 2 at* 77%*. Tumour cell 1 is represented by the red line, tumour cell 2 is represented by the blue line, immune cell 1 is represented by the green line and immune cell 2 by the pink line.*

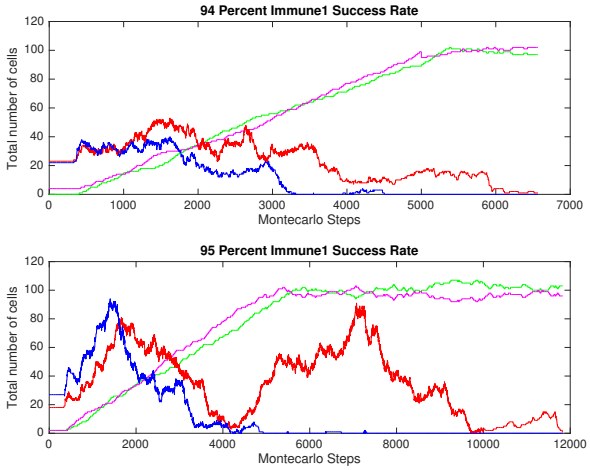

Figure 4.27: *Plots showing the total number of tumour and immune cells for* $94 - 95\%$ *immune 1 kill rate when in interaction with tumour cell type 1, tumour type 2 and immune type 1 at* 22% *and tumour type 2 and immune type 2 at* 77%*. Tumour cell 1 is represented by the red line, tumour cell 2 is represented by the blue line, immune cell 1 is represented by the green line and immune cell 2 by the pink line.*

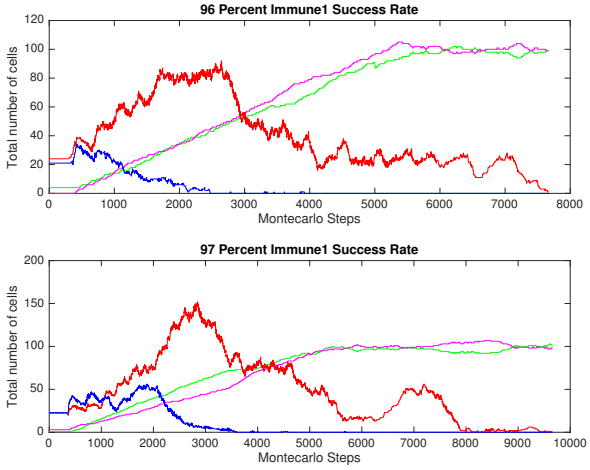

Figure 4.28: *Plots showing the total number of tumour and immune cells for* $96 - 97\%$ *immune 1 kill rate when in interaction with tumour cell type 1, tumour type 2 and immune type 1 at* 22% *and tumour type 2 and immune type 2 at* 77%*. Tumour cell 1 is represented by the red line, tumour cell 2 is represented by the blue line, immune cell 1 is represented by the green line and immune cell 2 by the pink line.*

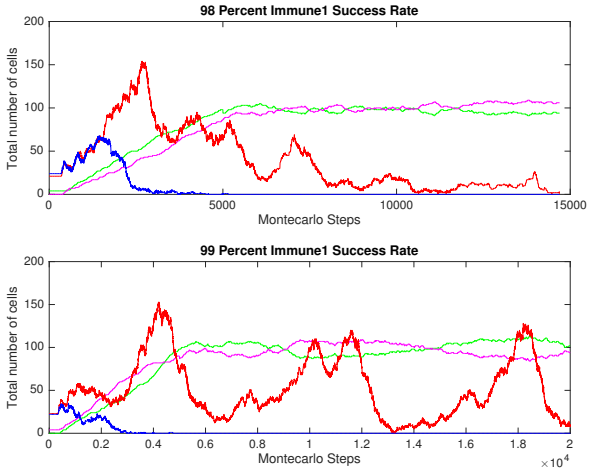

Figure 4.29: *Plots showing the total number of tumour and immune cells for* $98 - 99\%$ *immune 1 kill rate when in interaction with tumour cell type 1, tumour type 2 and immune type 1 at* 22% *and tumour type 2 and immune type 2 at* 77%*. Tumour cell 1 is represented by the red line, tumour cell 2 is represented by the blue line, immune cell 1 is represented by the green line and immune cell 2 by the pink line.*

4.3.2 E_2T_2 interactions

In section 4.3.1, many different observations became apparent from varying the success rate of E_1 when interaction with T_1. Firstly, it can be seen that either the T_2 tumour cells are killed very quickly in the domain or they hide among the T_1 quiescent and tumour cells, allowing them to exist through the whole simulation, albeit close to zero. Moreover, the T_1 cells are seen to oscillate, driven by clearance of the necrotic cells when the immune life expectancy is low. Furthermore, in section 4.3.1, the simulations were able to model each of the three "Es" of immunoediting, by lowering the immune death rate.

This section will focus on the interactions of the E_2 immune cells with T_2 tumour cells. To try and allow the T_2 cells to grow, the success rate of the E_2 cells when in interaction with T_2 cells has been lowered (E_2T_2). As before, this section will be split into the three different categories for immunoediting.

4.3.2.1 Tumour escape

To increase the potency of the T_2 tumour cells, the percentage of E_2T_2 has been decreased. The simulations here run for a period of 20,000MCS and, as before, the simulations will stop if there are no tumour cells, immune cells or quiescent cells left in the domain. The values of each of the interactions are as follows: $E_1T_1 = 95\%$, $E_1T_2 = 22\%$ and $E_2T_2 = 40 - 45\%$. The success rate of E_1T_1 has been kept high to try and deplete the T_1 cells along with the hope that the lowered success rate of E_2T_2 will allow the T_2 cells to grow. Immune cell death for both types occurs at 1000MCS. As in the previous

investigation into E_1T_1 in section 4.3.1, the total cell concentration figures, such as Figure 4.30, show T_1 represented by the red line, T_2 by the blue line, E_1 by the green line and E_2 by the pink line. The spatial representation can be seen in figures such as Figure 4.31, where all cell types are depicted. In the spatial pictures, proliferative tumour type 1 (T_1) cells are red, quiescent tumour type 1 cells are salmon, proliferative tumour type 2 (T_2) cells are blue, quiescent tumour type 2 cells are light blue, necrotic cells are black, medium cells are grey, immune type 1 cells (E_1) are green and immune type 2 (E_2) are magenta.

Looking at Figures 4.30-4.35, it is clear to see that the T_1 tumour population has an oscillatory pattern, such as in Figure 4.30 (top) at 40% E_2T_2 success rate, which is again driven by the clearance of necrotic cells. This time they are also able to fully invade the domain, such as in Figure 4.30 (bottom) where E_2T_2 is at 41% success rate. The lowering of the E_2T_2 success rate seems to have allowed more space for the T_1 cells, as they seem more potent than when the E_2T_2 success rate was almost double. The T_2 cells unfortunately have not been able to mount a full attack and are roughly at the same level as what they were in section 4.3.1.1, where $E_1T_1 = 95\%$ and immune death was set at 1000MCS. Decreasing the percentage of E_1T_1 has little effect on T_2 and just increases the T_1 tumour bulk. For these simulations see Appendix 3 in section 6.3. T_2 does however seem to be occasionally able to last for the whole simulation. In Figures 4.31-4.32, the spatial progression of E_2T_2 at 40% can be seen. Here, as discussed in 4.3.1.1, the initial makeup of the tumour mass seems to be important. Before, in 4.3.1.1, when the percentage of E_2T_2 was higher, the T_2 cells were picked off at a faster

rate. Now, by looking at Figure 4.31, the T_2 cells are able to mount an attack on the immune cells and are able to grow into separate entities away from the T_1 cells and even are able to stay in the system through to the end of the simulation as shown in Figure 4.32.

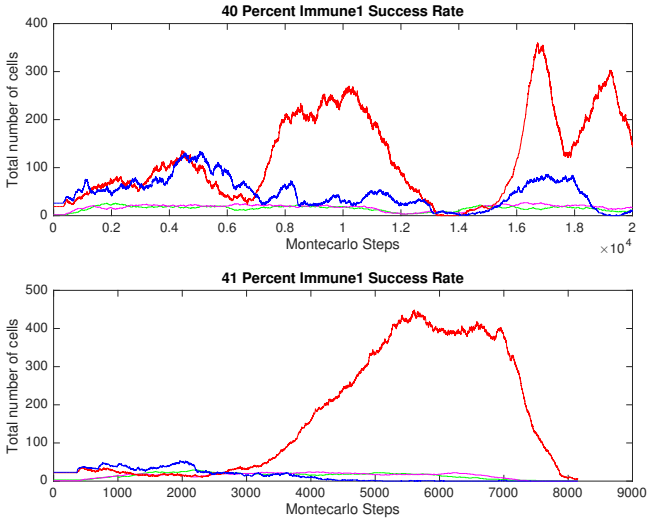

Figure 4.30: *Plots showing the total number of tumour and immune cells for* $40 - 41\%$ *immune 2 kill rate when in interaction with tumour cell type 2, tumour type 1 and immune type 1 at* 95% *and tumour type 2 and immune type 1 at* 22%*. Tumour cell 1 is represented by the red line, tumour cell 2 is represented by the blue line, immune cell 1 is represented by the green line and immune cell 2 by the pink line.*

Figure 4.33 shows the progression of all cells in a spatial setting when E_2T_2 is at 41% immune success rate. Here, T_1 has fully invaded the domain and T_2 has not been able to grow enough to evade the immune cells. The initial composition seems to need the T_2 cells to be placed around the outside of the tumour bulk and even then it may just be luck that the T_2 are able to gain enough momentum to grow. Again, it is necessary for the immune cell death rate to be lowered in order to exhibit dormancy and elimination.

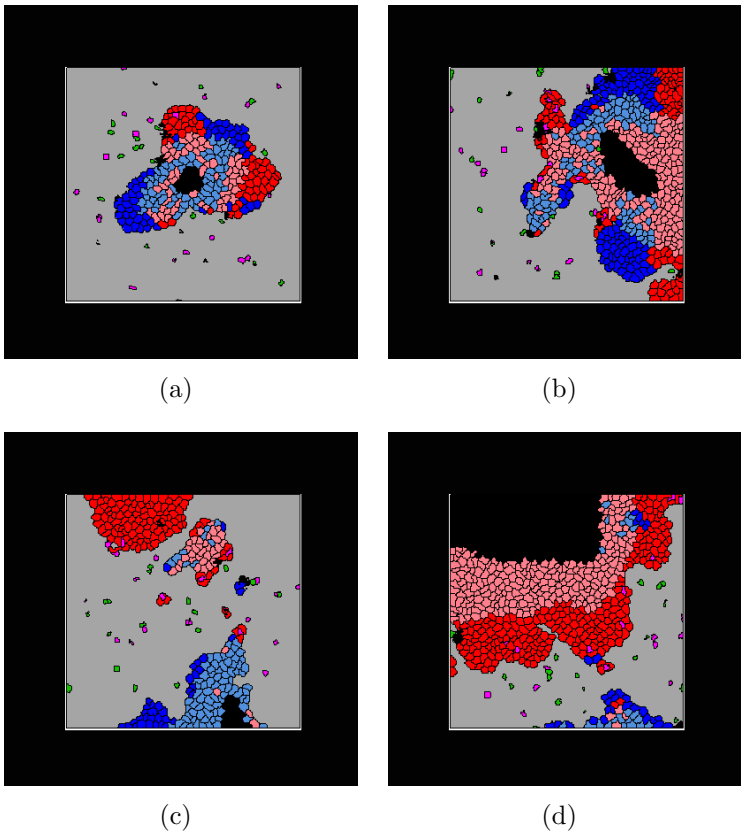

(a) (b)

(c) (d)

Figure 4.31: *Plots showing the growth of a tumour mass interacting with a host immune system at 1000MCS immune death rate. The types of cells and their corresponding colours in Figures 4.31(a)-4.31(d) are as follows: proliferative tumour type 1 cells in red, quiescent tumour type 1 cells in salmon, proliferative tumour type 2 in blue, quiescent tumour type 2 cells in light blue, necrotic cells in black, medium cells in grey, immune type 1 cells in green, immune type 2 in magenta. The immune success rates are as follows: tumour type 1 and immune type 1 at* 90%*, tumour type 2 and immune type 1 at* 22% *and tumour type 2 and immune type 2 at* 40%*, corresponding to Figure 4.30 (top). Figures 4.31(a)-4.31(d) represent the model at 2500MCS, 5000MCS, 7500MCS and 10000MCS respectively and show cancer escape.*

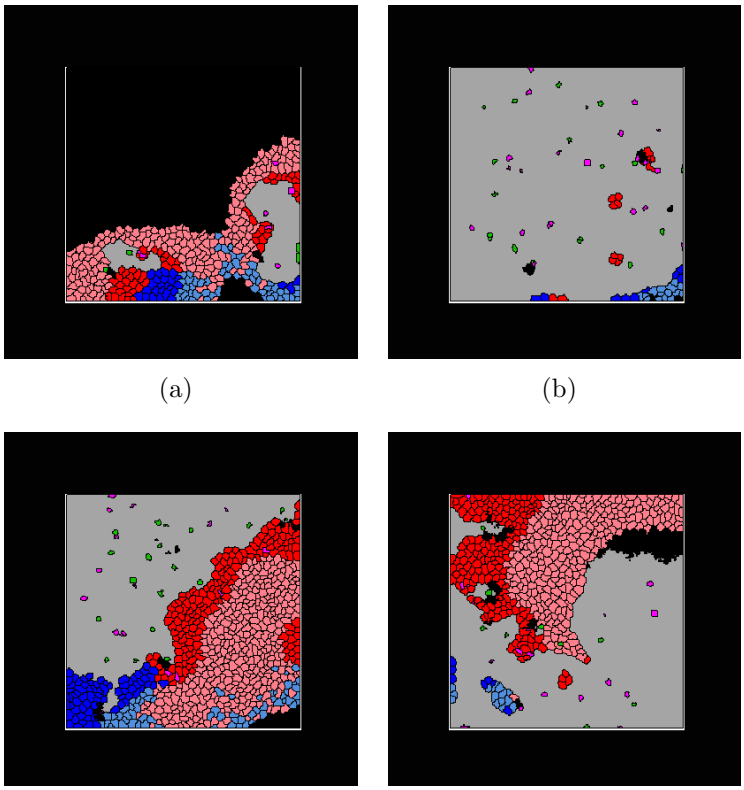

(a) (b)

(c) (d)

Figure 4.32: *Plots showing the growth of a tumour mass interacting with a host immune system at 1000MCS immune death rate. The types of cells and their corresponding colours in Figures 4.32(a)-4.32(d) are as follows: proliferative tumour type 1 cells in red, quiescent tumour type 1 cells in salmon, proliferative tumour type 2 in blue, quiescent tumour type 2 cells in light blue, necrotic cells in black, medium cells in grey, immune type 1 cells in green, immune type 2 in magenta. The immune success rates are as follows: tumour type 1 and immune type 1 at* 90%*, tumour type 2 and immune type 1 at* 22% *and tumour type 2 and immune type 2 at* 40%*, corresponding to Figure 4.30 (top). Figures 4.32(a)-4.32(d) represent the model at 12500MCS, 15000MCS, 17500MCS and 19900MCS respectively and show cancer escape.*

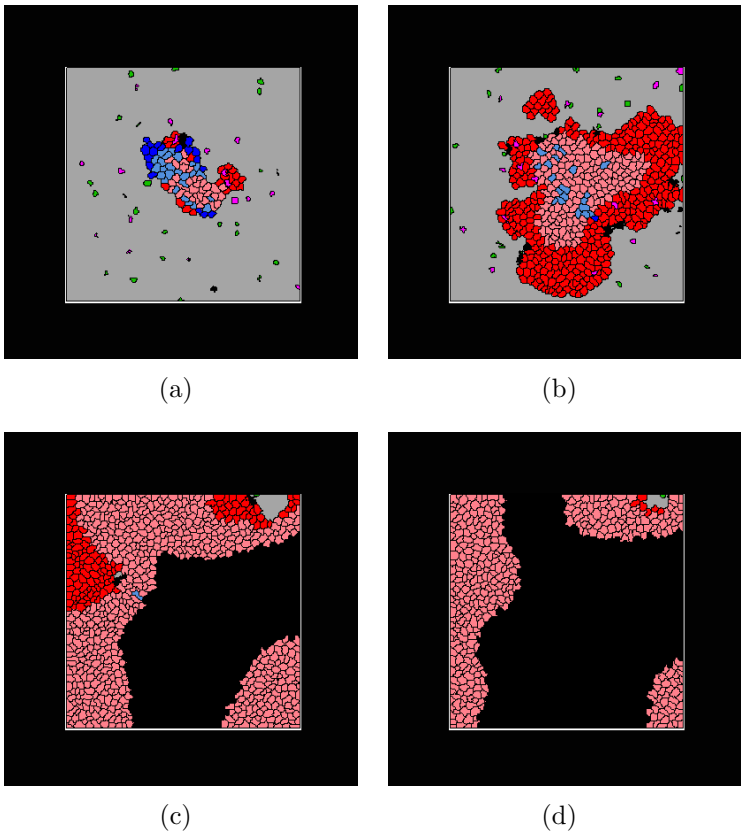

(a) (b)

(c) (d)

Figure 4.33: *Plots showing the growth of a tumour mass interacting with a host immune system at 1000MCS immune death rate. The types of cells and their corresponding colours in Figures 4.33(a)-4.33(d) are as follows: proliferative tumour type 1 cells in red, quiescent tumour type 1 cells in salmon, proliferative tumour type 2 in blue, quiescent tumour type 2 cells in light blue, necrotic cells in black, medium cells in grey, immune type 1 cells in green, immune type 2 in magenta. The immune success rates are as follows: tumour type 1 and immune type 1 at* 90%*, tumour type 2 and immune type 1 at* 22% *and tumour type 2 and immune type 2 at* 41%*, corresponding to Figure 4.30 (bottom). Figures 4.33(a)-4.33(d) represent the model at 2500MCS, 5000MCS, 7500MCS and 8100MCS respectively and show cancer escape.*

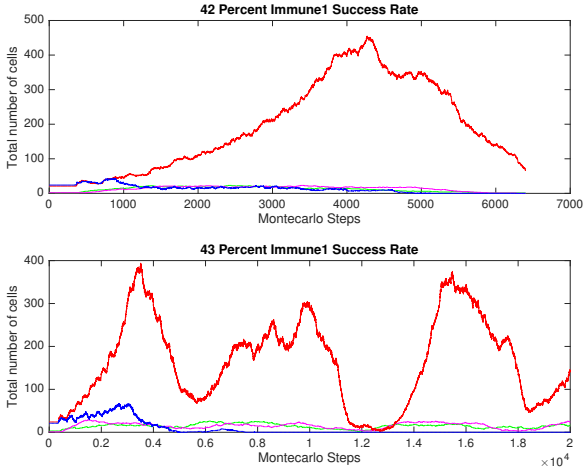

Figure 4.34: *Plots showing the total number of tumour and immune cells for* $42 - 43\%$ *immune 2 kill rate when in interaction with tumour cell type 2, tumour type 1 and immune type 1 at* 95% *and tumour type 2 and immune type 1 at* 22%*. Tumour cell 1 is represented by the red line, tumour cell 2 is represented by the blue line, immune cell 1 is represented by the green line and immune cell 2 by the pink line.*

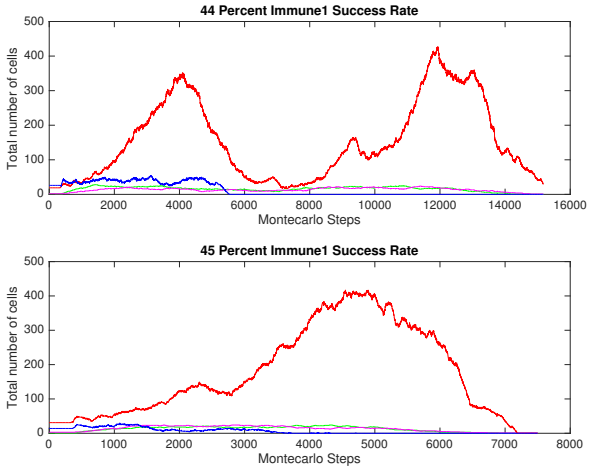

Figure 4.35: *Plots showing the total number of tumour and immune cells for* $44 - 45\%$ *immune 2 kill rate when in interaction with tumour cell type 2, tumour type 1 and immune type 1 at* 95% *and tumour type 2 and immune type 1 at* 22%*. Tumour cell 1 is represented by the red line, tumour cell 2 is represented by the blue line, immune cell 1 is represented by the green line and immune cell 2 by the pink line.*

4.3.2.2 Coexistence

By increasing the amount of time the immune cells are allowed in the domain, an equilibrium state can be found. Even though the value of E_2T_2 has been changed, the dynamics of this section are very similar to section 4.3.1. E_2T_2 has been lowered and varied over $30-36\%$ and the simulation has been run for 40,000MCS, double the amount of time of the previous simulations in section 4.3.1. Extra simulations have also been run for the standard 20,000MCS, which can be found in the appendix in section 6.4

Figures 4.36-4.45 show equilibrium in most cases, but have also produced tumour clearance in others. More specifically, when $E_2T_2 = 32\%$ there is a tumour clearance, which can be seen in Figure 4.37 (top). Initially, both tumour cell types rise, however after 2000MCS the immune cells begin to make an attack. This can be seen more closely in Figure 4.38. At 1000MCS, depicted in Figure 4.38(b), the tumour mass is still growing, however by 2000-4000MCS, shown in Figures 4.38(d)-4.38(f), the immune cells are mounting an effective defence, and by 6000MCS the tumour cells have been wiped out. Figure 4.39 shows the nutrient concentration over time where, even though the domain is flooded with nutrient, the immune cells are mounting an effective attack against the tumour cells preventing nutrient uptake.

Conversely, in Figure 4.37 (bottom) the T_1, E_1 and E_2 cells are in equilibrium. Here, the immune cells are not able to clear the T_1 cells, but are able to keep them at a steady state level. Looking more closely at this particular simulation, the spatial description in Figures 4.40 and 4.42 show that again the T_2 cells are depleted almost completely by 5000MCS, pictured in

sub figure 4.40(d). The nutrient concentration over time, for $E_2T_2 = 33\%$, is depicted in Figures 4.41 and 4.43. As the simulation progresses, both T_1 and T_2 tumour cells grow into the space where nutrient is available. After the T_2 tumour cells are depleted by the immune cells, the space left by these cells is able to produce more nutrient and can therefore support more cells. Subsequently this gives the T_1 cells more space to grow and divide. Moreover, if the T_1 cells are already close to this area, it allows them to branch off and fully proliferate into a new part of the domain. If the immune cell death is decreased further to 3500MCS, then the simulations tend towards an "elimination" phase, however equilibrium is still present. These simulations can be found in the appendix in section 6.5.

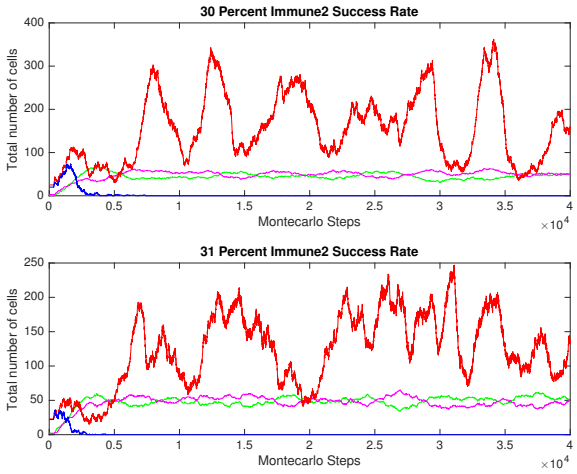

Figure 4.36: *Plots showing the total number of tumour and immune cells for* $30 - 31\%$ *immune 2 kill rate when in interaction with tumour cell type 2, tumour type 1 and immune type 1 at* 95% *and tumour type 2 and immune type 1 at* 22%*. Tumour cell 1 is represented by the red line, tumour cell 2 is represented by the blue line, immune cell 1 is represented by the green line and immune cell 2 by the pink line.*

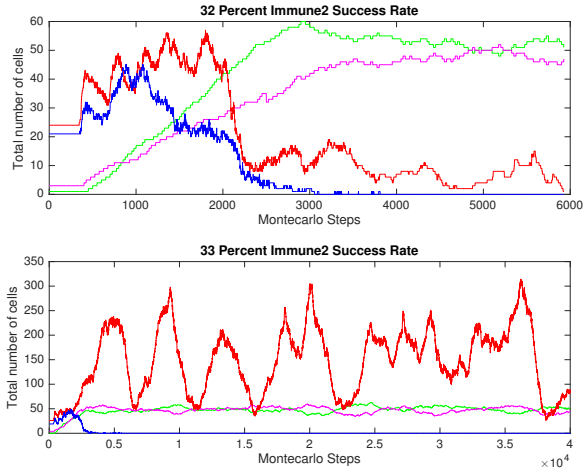

Figure 4.37: *Plots showing the total number of tumour and immune cells for* $32 - 33\%$ *immune 2 kill rate when in interaction with tumour cell type 2, tumour type 1 and immune type 1 at* 95% *and tumour type 2 and immune type 1 at* 22%*. Tumour cell 1 is represented by the red line, tumour cell 2 is represented by the blue line, immune cell 1 is represented by the green line and immune cell 2 by the pink line.*

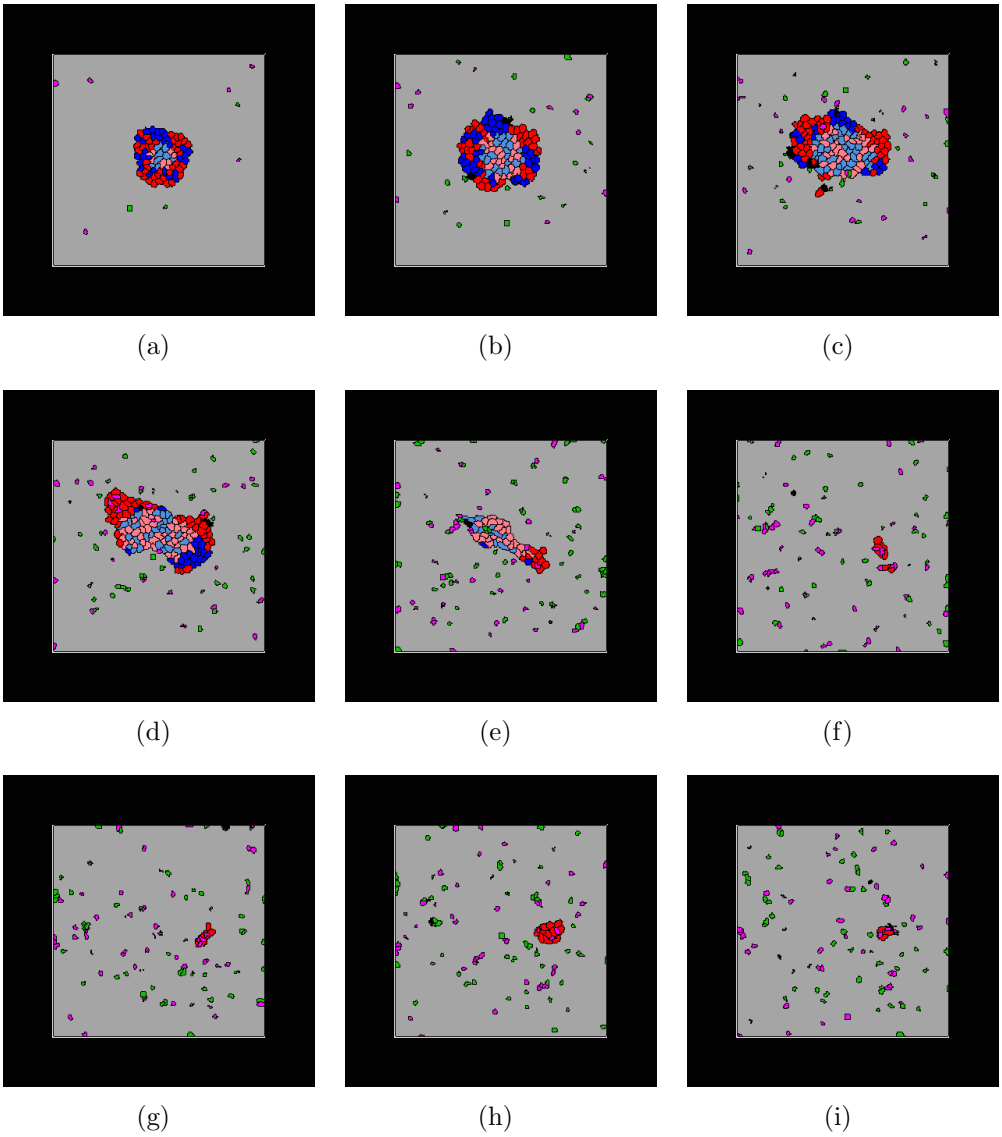

Figure 4.38: *Plots showing the growth of a tumour mass interacting with a host immune system at 2500MCS immune death rate. The types of cells and their corresponding colours in Figures 4.38(a)-4.38(i) are as follows: proliferative tumour type 1 cells in red, quiescent tumour type 1 cells in salmon, proliferative tumour type 2 in blue, quiescent tumour type 2 cells in light blue, necrotic cells in black, medium cells in grey, immune type 1 cells in green, immune type 2 in magenta. The immune success rates are as follows: tumour type 1 and immune type 1 at* 95%*, tumour type 2 and immune type 1 at* 22% *and tumour type 2 and immune type 2 at* 32%*, corresponding to Figure 4.37 (top). Figures 4.38(a)-4.38(i) represent the model at 500MCS, 1000MCS, 1500MCS, 2000MCS, 3000MCS, 4000MCS, 5000MCS, 5500MCS and 5900MCS respectively.*

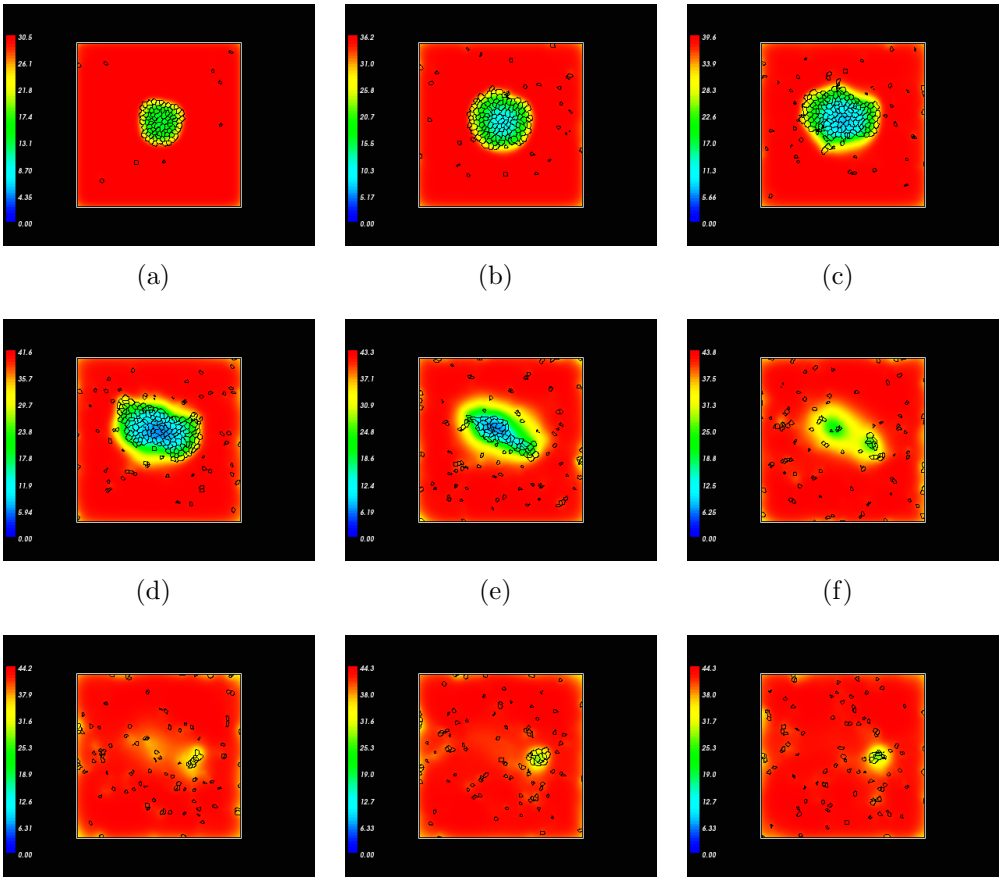

(a) (b) (c)

(d) (e) (f)

(g) (h) (i)

Figure 4.39: *Plots showing the nutrient concentration at times 500MCS, 1000MCS, 1500MCS, 2000MCS, 3000MCS, 4000MCS, 5000MCS, 5500MCS and 5900MCS, respectively. The immune success rates are as follows: tumour type 1 and immune type 1 at* 95%*, tumour type 2 and immune type 1 at* 22% *and tumour type 2 and immune type 2 at* 32%*, corresponding to Figure 4.37 (top). The oxygen concentration is high when it is red and low when it is blue. A bar on the left hand side of each picture represents the oxygen concentration. Oxygen is used up by the immune, tumour and quiescent cells leaving areas where tumour cells can longer be supported leading to necrosis. Once the necrotic cells have disintegrated oxygen can flow into the area again via medium cells.*

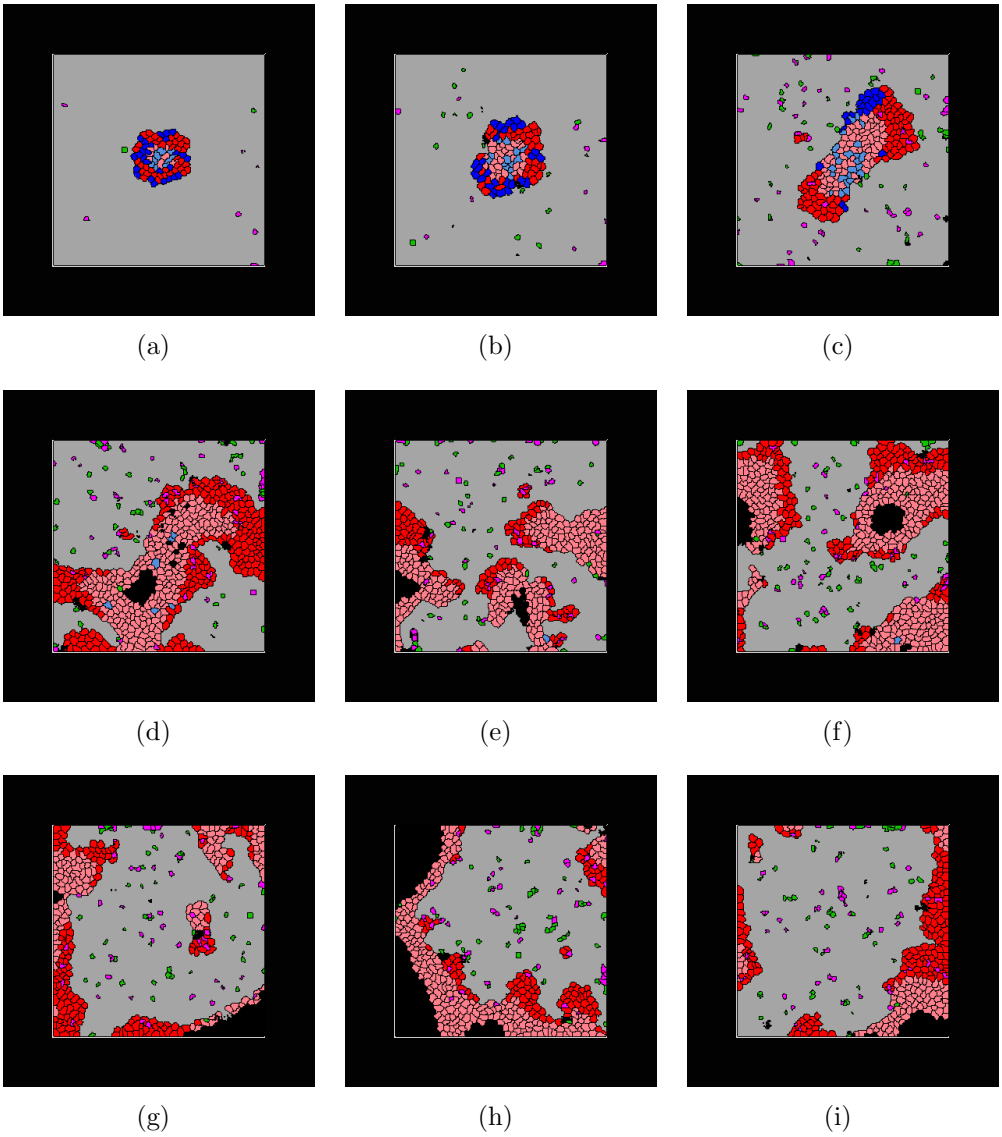

Figure 4.40: *Plots showing the growth of a tumour mass interacting with a host immune system at 2500MCS immune death rate. The types of cells and their corresponding colours in Figures 4.40(a)-4.40(i) are as follows: proliferative tumour type 1 cells in red, quiescent tumour type 1 cells in salmon, proliferative tumour type 2 in blue, quiescent tumour type 2 cells in light blue, necrotic cells in black, medium cells in grey, immune type 1 cells in green, immune type 2 in magenta. The immune success rates are as follows: tumour type 1 and immune type 1 at* 95%*, tumour type 2 and immune type 1 at* 22% *and tumour type 2 and immune type 2 at* 33%*, corresponding to Figure 4.37 (bottom). Figures 4.40(c)-4.42(a) represent the model at 500MCS, 1000MCS, 2500MCS, 5000MCS, 7500MCS, 10000MCS 12500MCS, 15000MCS and 17500MCS respectively.*

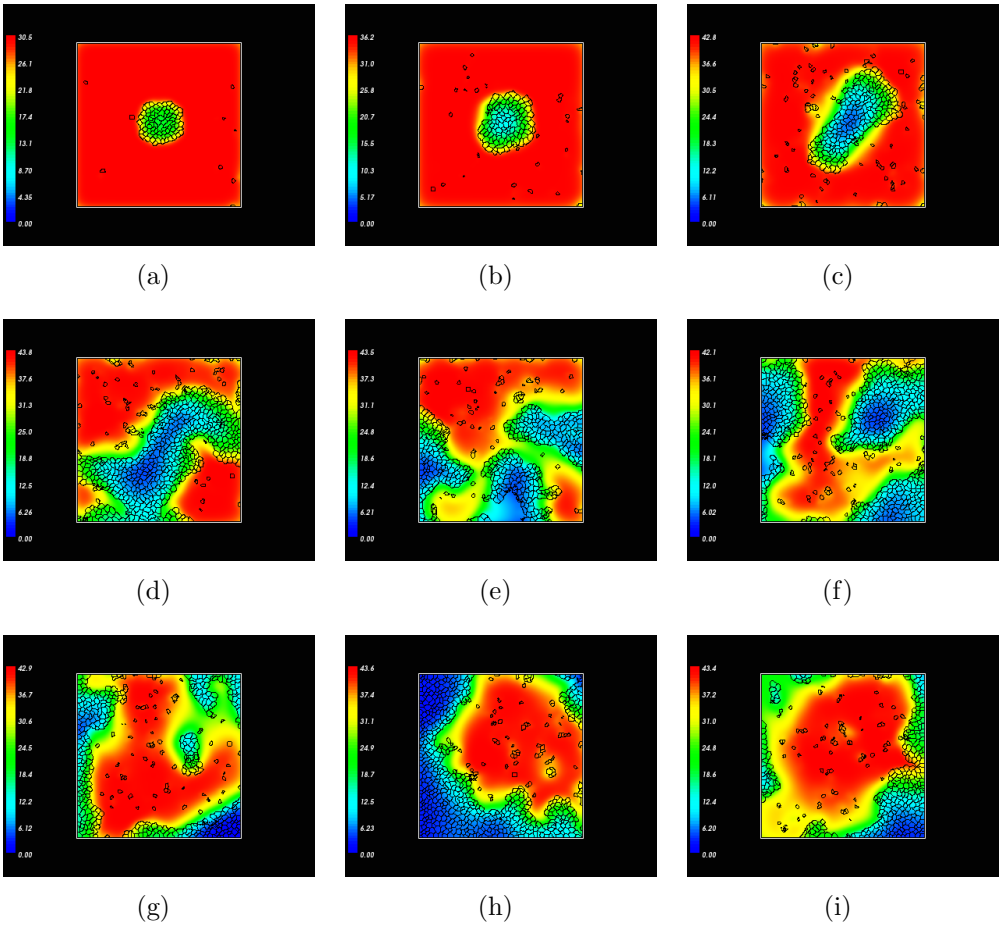

(a) (b) (c)

(d) (e) (f)

(g) (h) (i)

Figure 4.41: *Plots showing the nutrient concentration at times 500MCS, 1000MCS, 2500MCS, 5000MCS, 7500MCS, 10000MCS, 12500MCS, 15000MCS and 17500MCS, respectively. The immune success rates are as follows: tumour type 1 and immune type 1 at* 95%*, tumour type 2 and immune type 1 at* 22% *and tumour type 2 and immune type 2 at* 33%*, corresponding to Figure 4.37 (bottom). The oxygen concentration is high when it is red and low when it is blue. A bar on the left hand side of each picture represents the oxygen concentration. Oxygen is used up by the immune, tumour and quiescent cells leaving areas where tumour cells can longer be supported leading to necrosis. Once the necrotic cells have disintegrated oxygen can flow into the area again via medium cells.*

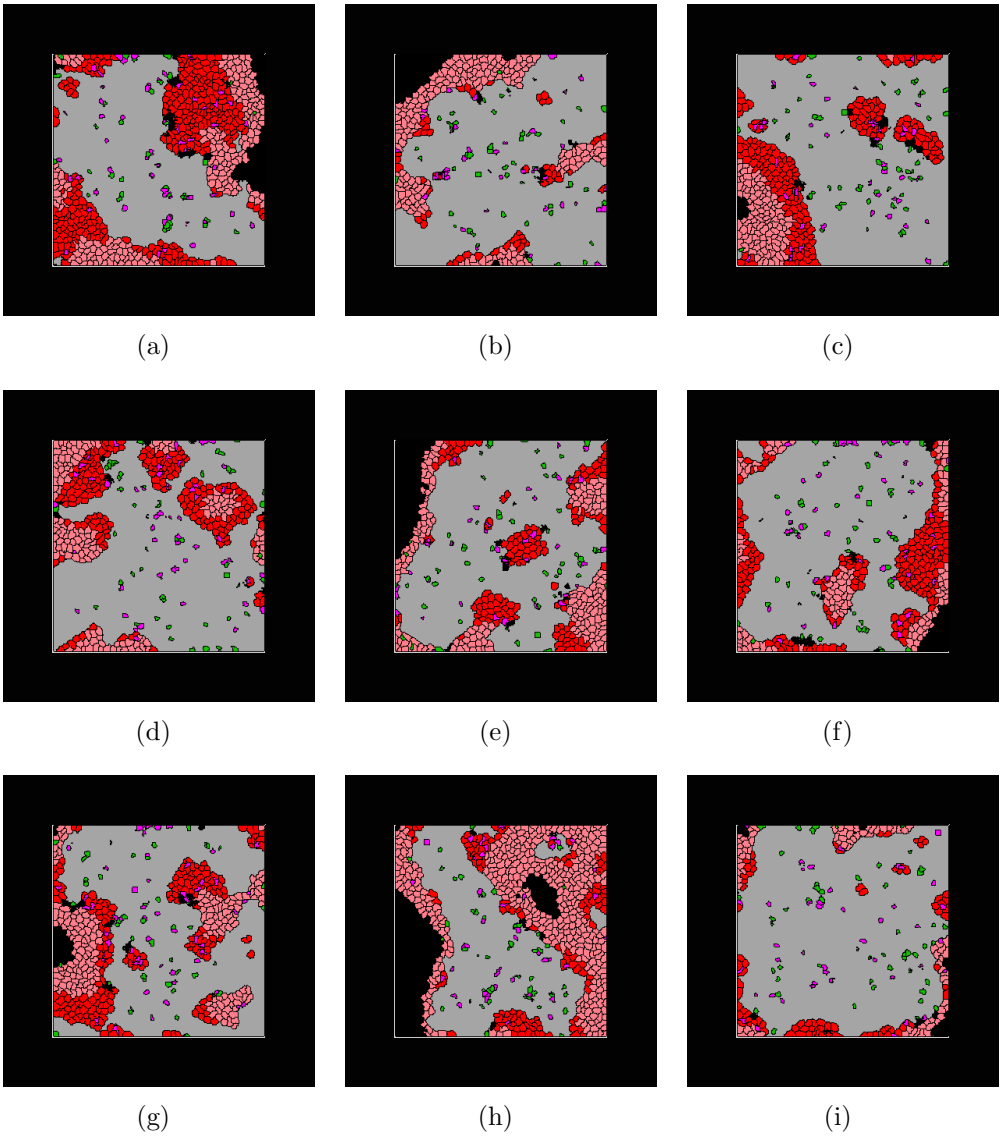

Figure 4.42: *Plots showing the growth of a tumour mass interacting with a host immune system at 2500MCS immune death rate. The types of cells and their corresponding colours in Figures 4.42(a)-4.42(i) are as follows: proliferative tumour type 1 cells in red, quiescent tumour type 1 cells in salmon, proliferative tumour type 2 in blue, quiescent tumour type 2 cells in light blue, necrotic cells in black, medium cells in grey, immune type 1 cells in green, immune type 2 in magenta. The immune success rates are as follows: tumour type 1 and immune type 1 at* 95%*, tumour type 2 and immune type 1 at* 22% *and tumour type 2 and immune type 2 at* 33% *corresponding to Figure 4.37 (bottom). Figures 4.42(a)-4.42(i) represent the model at 20000MCS, 22500MCS, 25000MCS, 27500MCS, 3000MCS, 32500MCS 35000MCS, 37500MCS and 40000MCS respectively.*

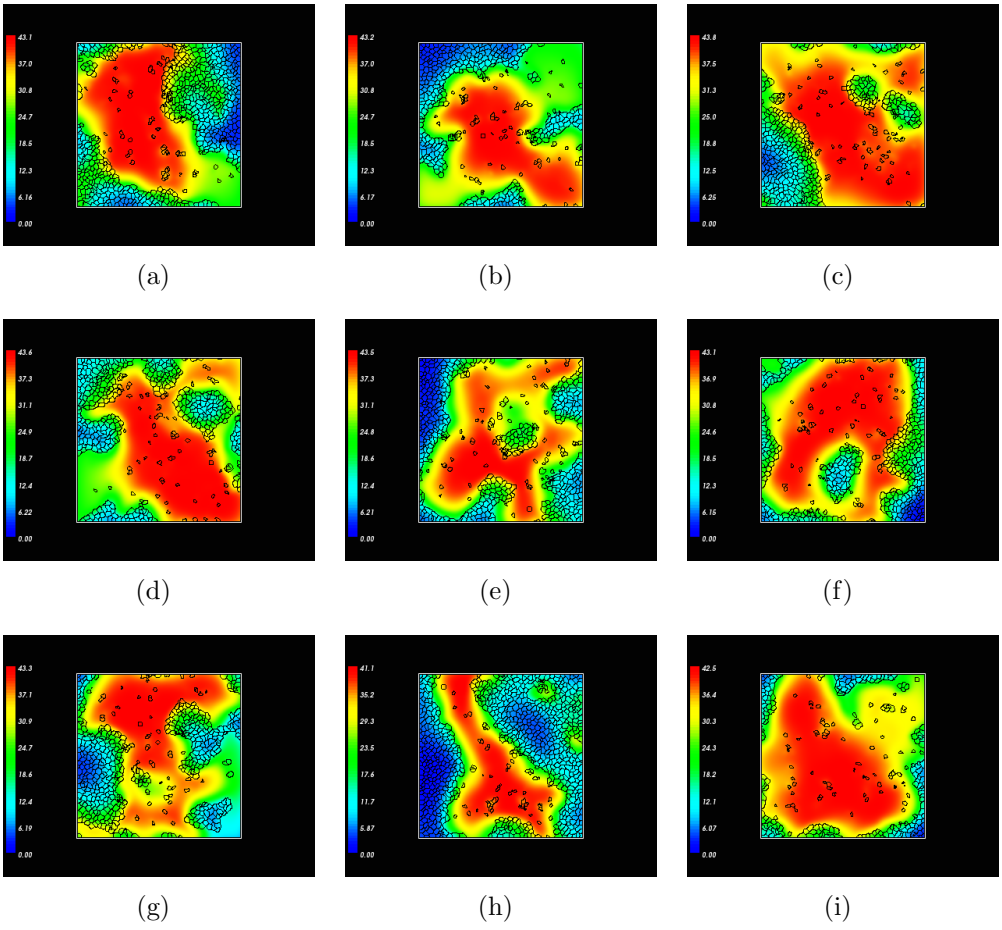

(a) (b) (c)

(d) (e) (f)

(g) (h) (i)

Figure 4.43: *Plots showing the nutrient concentration at times 20000MCS, 22500MCS, 25000MCS, 27500MCS, 30000MCS, 32500MCS, 35000MCS, 37500MCS and 40000MCS, respectively. The immune success rates are as follows: tumour type 1 and immune type 1 at* 95%*, tumour type 2 and immune type 1 at* 22% *and tumour type 2 and immune type 2 at* 33% *corresponding to Figure 4.37 (bottom). The oxygen concentration is high when it is red and low when it is blue. A bar on the left hand side of each picture represents the oxygen concentration. Oxygen is used up by the immune, tumour and quiescent cells leaving areas where tumour cells can longer be supported leading to necrosis. Once the necrotic cells have disintegrated oxygen can flow into the area again via medium cells.*

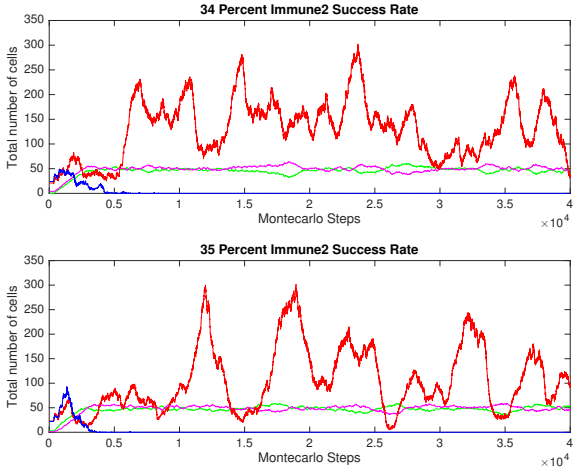

Figure 4.44: *Plots showing the total number of tumour and immune cells for* $34 - 35\%$ *immune 2 kill rate when in interaction with tumour cell type 2, tumour type 1 and immune type 1 at* 95% *and tumour type 2 and immune type 1 at* 22%*. Tumour cell 1 is represented by the red line, tumour cell 2 is represented by the blue line, immune cell 1 is represented by the green line and immune cell 2 by the pink line.*

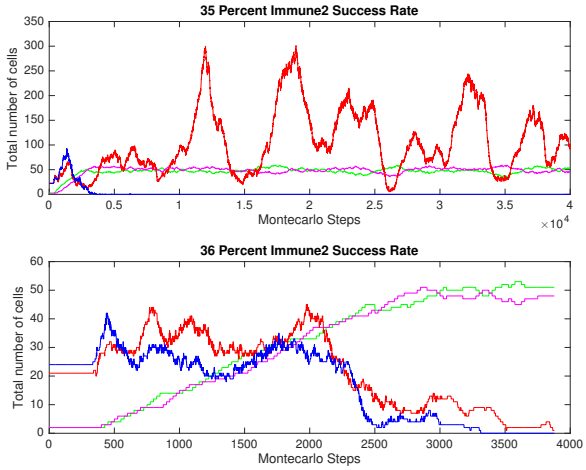

Figure 4.45: *Plots showing the total number of tumour and immune cells for* $36 - 37\%$ *immune 2 kill rate when in interaction with tumour cell type 2, tumour type 1 and immune type 1 at* 95% *and tumour type 2 and immune type 1 at* 22%*. Tumour cell 1 is represented by the red line, tumour cell 2 is represented by the blue line, immune cell 1 is represented by the green line and immune cell 2 by the pink line.*

4.3.2.3 Tumour elimination

This section is concerned with tumour elimination i.e. immune cell destruction of the tumour cells. Here, the simulations have been run for 20,000MCS, again unless there are no tumour, quiescent or immune cells left in the domain, in which case the simulation will stop. Section 4.3.2.1 focused on the evasion of the immune destruction by T_1 and, in some cases, T_2. Section 4.3.2.2 described the simulations that showed steady state dynamics in T_1, E_1 and E_2 cells. Equilibrium was found by increasing the amount of time the immune cells of both types were in the domain. In order to allow the immune cells to have a proficient enough attack against the tumour cells to fully eradicate them, in the given amount of monte-carlo steps, the immune cell death rate has again been decreased to 5000MCS. The percentage of immune success rate for the interactions between E_1T_1, E_1T_2 and E_2T_2 have been kept the same as in section 4.3.2.2, in order to show a direct comparison.

Figures 4.46-4.51 show that for each individual success rate for E_2T_2, ranging from $30-39\%$, the immune cells are able to destroy the tumour cell populations. Figure 4.47 focuses on the spatial dynamics of the simulation for 30% E_1T_2 immune success rate. In this figure, the immune cells are seen to flood the domain fairly quickly by 5000MCS, shown in Figure 4.47(b), however in Figure 4.47(d), representing 10,000MCS, the T_1 cells are trying to grow a new tumour mass. This is short lived, and is eradicated by the immune cells by 12900MCS, shown in Figure 4.47(f).

Even though section 4.3.2 has managed to show tumour escape, tumour-immune equilibrium and tumour elimination, it has not managed to mimic

the coexistence dynamics from the previous section 3.8 i.e. allowing the T_2 to grow so that equilibrium can be found among both tumour and immune types.

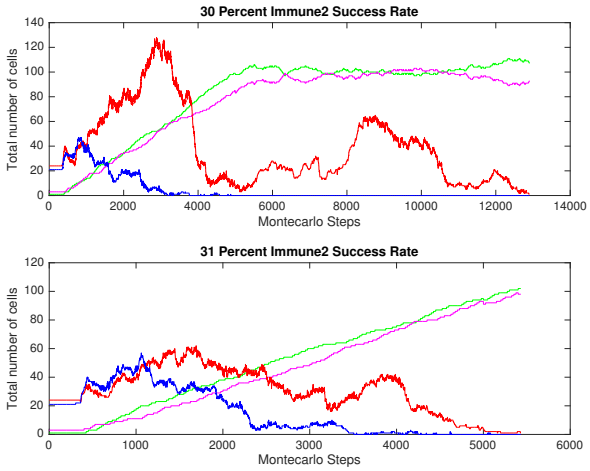

Figure 4.46: *Plots showing the total number of tumour and immune cells for* $30 - 31\%$ *immune 2 kill rate when in interaction with tumour cell type 2, tumour type 1 and immune type 1 at* 95% *and tumour type 2 and immune type 1 at* 22%*. Tumour cell 1 is represented by the red line, tumour cell 2 is represented by the blue line, immune cell 1 is represented by the green line and immune cell 2 by the pink line.*

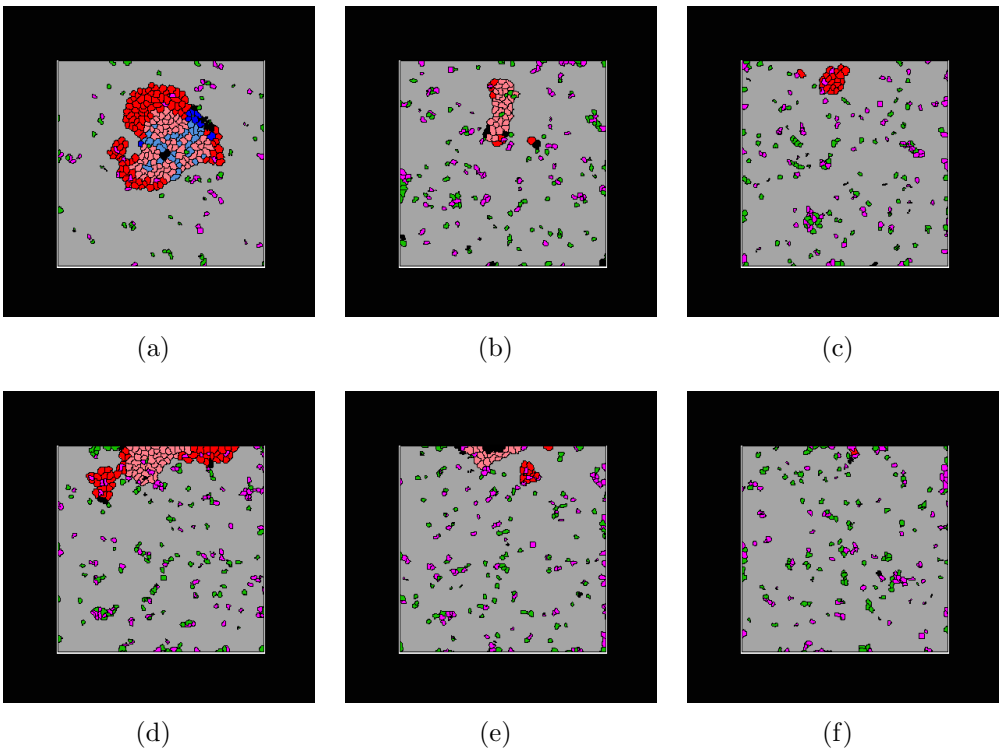

(a) (b) (c)

(d) (e) (f)

Figure 4.47: *Plots showing the growth of a tumour mass interacting with a host immune system at 5000MCS immune death rate. The types of cells and their corresponding colours in Figures 4.47(a)-4.47(d) are as follows: proliferative tumour type 1 cells in red, quiescent tumour type 1 cells in salmon, proliferative tumour type 2 in blue, quiescent tumour type 2 cells in light blue, necrotic cells in black, medium cells in grey, immune type 1 cells in green, immune type 2 in magenta. The immune success rates are as follows: tumour type 1 and immune type 1 at* 90%*, tumour type 2 and immune type 1 at* 22% *and tumour type 2 and immune type 2 at* 30%*, corresponding to Figure 4.46. Figures 4.47(a)-4.47(d) represent the model at 2500MCS, 5000MCS, 7500MCS, 10000MCS, 11000MCS, 12900MCS respectively and show tumour elimination.*

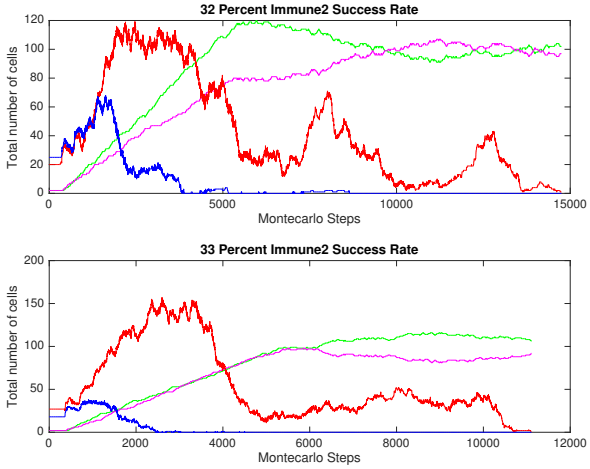

Figure 4.48: *Plots showing the total number of tumour and immune cells for* $32 - 33\%$ *immune 2 kill rate when in interaction with tumour cell type 2, tumour type 1 and immune type 1 at* 95% *and tumour type 2 and immune type 1 at* 22%*. Tumour cell 1 is represented by the red line, tumour cell 2 is represented by the blue line, immune cell 1 is represented by the green line and immune cell 2 by the pink line.*

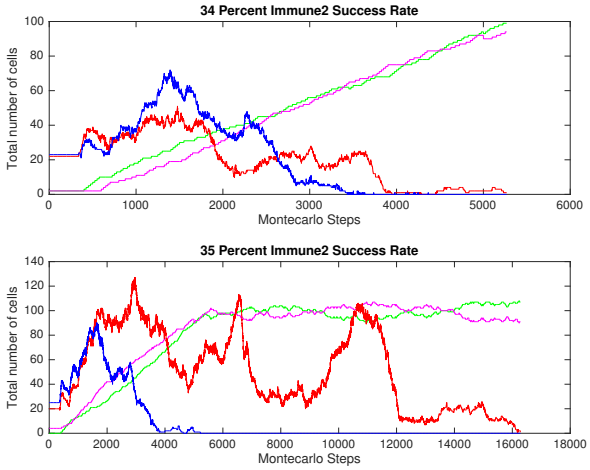

Figure 4.49: *Plots showing the total number of tumour and immune cells for* $34 - 35\%$ *immune 2 kill rate when in interaction with tumour cell type 2, tumour type 1 and immune type 1 at* 95% *and tumour type 2 and immune type 1 at* 22%*. Tumour cell 1 is represented by the red line, tumour cell 2 is represented by the blue line, immune cell 1 is represented by the green line and immune cell 2 by the pink line.*

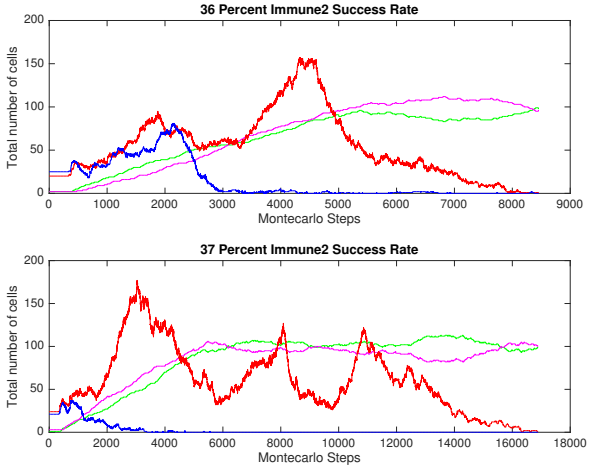

Figure 4.50: *Plots showing the total number of tumour and immune cells for* $36-37\%$ *immune 2 kill rate when in interaction with tumour cell type 2, tumour type 1 and immune type 1 at* 95% *and tumour type 2 and immune type 1 at* 22%*. Tumour cell 1 is represented by the red line, tumour cell 2 is represented by the blue line, immune cell 1 is represented by the green line and immune cell 2 by the pink line.*

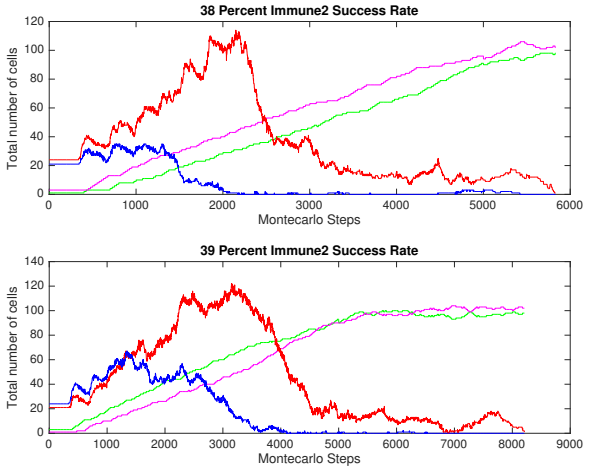

Figure 4.51: *Plots showing the total number of tumour and immune cells for* $38-39\%$ *immune 2 kill rate when in interaction with tumour cell type 2, tumour type 1 and immune type 1 at* 95% *and tumour type 2 and immune type 1 at* 22%*. Tumour cell 1 is represented by the red line, tumour cell 2 is represented by the blue line, immune cell 1 is represented by the green line and immune cell 2 by the pink line.*

4.3.3 E_1T_2 interactions

In this section, dynamic equilibrium is sought between tumour and immune cells of both types. Therefore, this section will be only concerned with trying to get a steady state range of values for the interactions between cells. Again, the amount of time the immune cells are in the domain is varied, as well as lowering the success rates of the immune cells, when in contact with the tumour populations.

4.3.3.1 Coexistence

To try and find a coexistence steady state, the immune success rate of E_1T_2 and E_2T_2 has been lowered. The thinking behind this is to try and give the T_2 cells a fighting chance against the dominance of the T_1 cells, in order to understand the dynamics that govern the coexistence steady state. In Figures 4.52-4.56, $E_1T_1 = 90\%$, $E_2T_2 = 20\%$ and E_1T_2 is varied from 10% to 20%. Both immune cell types die after being in the domain for 3500MCS and the simulations have been run for 10,000MCS. It was recognised that this strategy, judging by the simulations in section 4.3.1 and 4.3.2, would be exposed quickly if it failed to work and, therefore, the shorter simulation time would be prudent here.

When running the simulations, unfortunately there does not seem to be any impact on the T_2 tumour cell population. There may be more tumour bulk or less tumour bulk depending on each individual interaction, but finding a equilibrium in this instance seems to be elusive. The amount of time the immune cells are in the domain has been further decreased to 3000MCS,

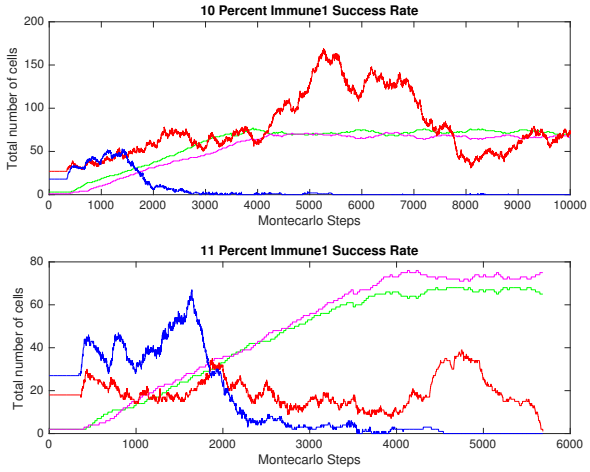

Figure 4.52: *Plots showing the total number of tumour and immune cells for* $10-11\%$ *immune 1 kill rate when in interaction with tumour cell type 2, tumour type 1 and immune type 1 at* 95% *and tumour type 2 and immune type 2 at* 20%*. Tumour cell 1 is represented by the red line, tumour cell 2 is represented by the blue line, immune cell 1 is represented by the green line and immune cell 2 by the pink line.*

which can be seen in the appendix in section 6.6, which again has no impact on the length of time the T_2 cells are involved.

The next strategy was to try to split the immune death rates i.e. give each of them a different value. It seemed prudent to give E_1 the highest chance possible of killing the T_1 tumour population, therefore the immune death for T_1 was set at 5000MCS. Conversely, the T_2 immune death rate was set very low, with E_2 immune cells dying after 500MCS. Again this had no effect, and only pushed the results of the simulations into a displaying dynamics for the tumour "elimination" stage. This can be seen in Figures 4.57-4.60, where the interactions between the tumour and immune cells have the same immune success rates, but E_1T_2 has only been varied between $10-17\%$. Therefore, a new strategy is needed to allow the T_2 cells to grow.

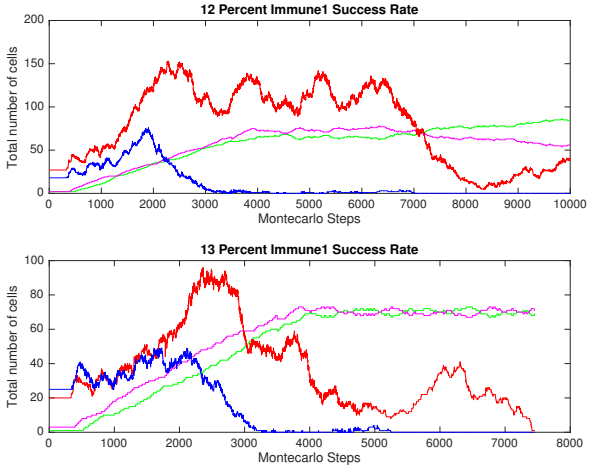

Figure 4.53: *Plots showing the total number of tumour and immune cells for* $12 - 13\%$ *immune 1 kill rate when in interaction with tumour cell type 2, tumour type 1 and immune type 1 at* 95% *and tumour type 2 and immune type 2 at* 20%*. Tumour cell 1 is represented by the red line, tumour cell 2 is represented by the blue line, immune cell 1 is represented by the green line and immune cell 2 by the pink line.*

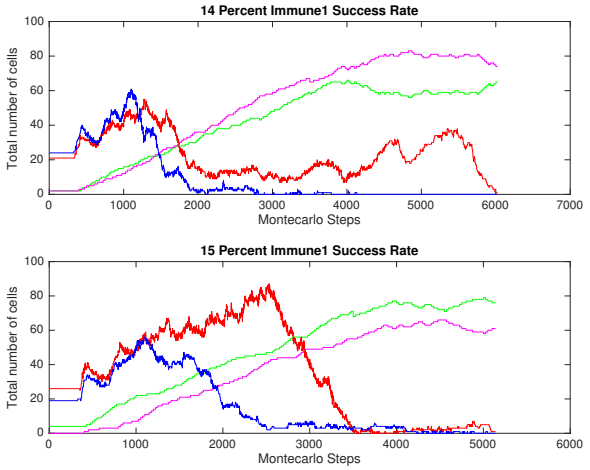

Figure 4.54: *Plots showing the total number of tumour and immune cells for* $14 - 15\%$ *immune 1 kill rate when in interaction with tumour cell type 2, tumour type 1 and immune type 1 at* 95% *and tumour type 2 and immune type 2 at* 20%*. Tumour cell 1 is represented by the red line, tumour cell 2 is represented by the blue line, immune cell 1 is represented by the green line and immune cell 2 by the pink line.*

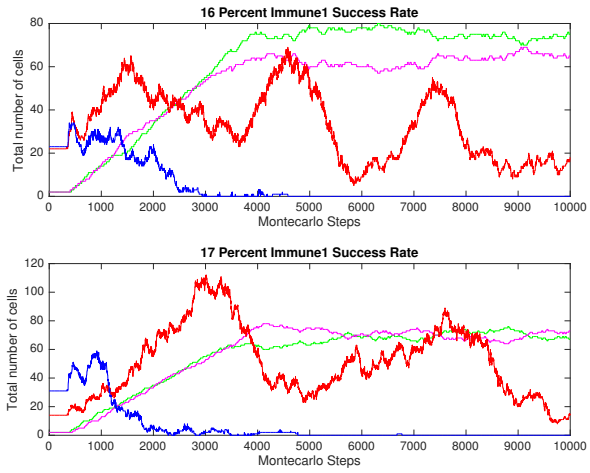

Figure 4.55: *Plots showing the total number of tumour and immune cells for* $16-17\%$ *immune 1 kill rate when in interaction with tumour cell type 2, tumour type 1 and immune type 1 at* 95% *and tumour type 2 and immune type 2 at* 20%*. Tumour cell 1 is represented by the red line, tumour cell 2 is represented by the blue line, immune cell 1 is represented by the green line and immune cell 2 by the pink line.*

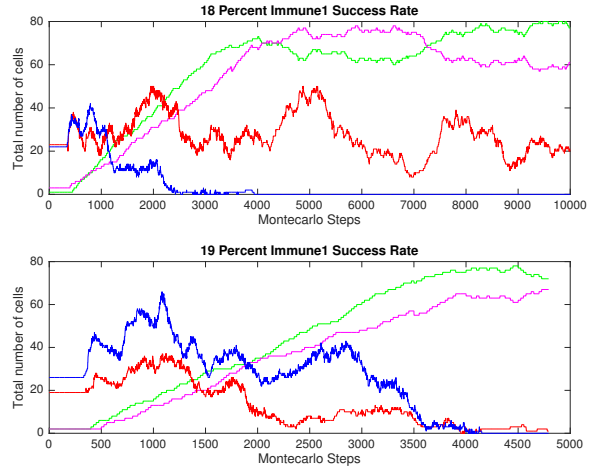

Figure 4.56: *Plots showing the total number of tumour and immune cells for* $18-19\%$ *immune 1 kill rate when in interaction with tumour cell type 2, tumour type 1 and immune type 1 at* 95% *and tumour type 2 and immune type 2 at* 20%*. Tumour cell 1 is represented by the red line, tumour cell 2 is represented by the blue line, immune cell 1 is represented by the green line and immune cell 2 by the pink line.*

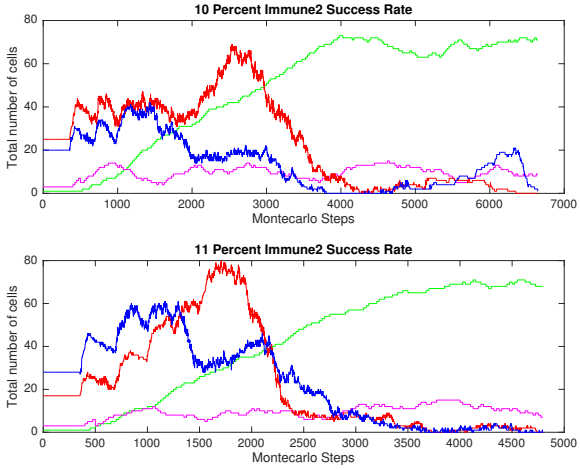

Figure 4.57: *Plots showing the total number of tumour and immune cells for* $10-11\%$ *immune 1 kill rate when in interaction with tumour cell type 2, tumour type 1 and immune type 1 at* 95% *and tumour type 2 and immune type 2 at* 20%*. Tumour cell 1 is represented by the red line, tumour cell 2 is represented by the blue line, immune cell 1 is represented by the green line and immune cell 2 by the pink line.*

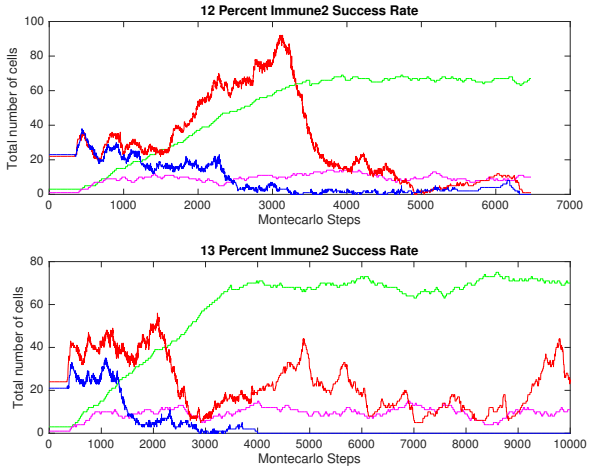

Figure 4.58: *Plots showing the total number of tumour and immune cells for* $12-13\%$ *immune 1 kill rate when in interaction with tumour cell type 2, tumour type 1 and immune type 1 at* 95% *and tumour type 2 and immune type 2 at* 20%*. Tumour cell 1 is represented by the red line, tumour cell 2 is represented by the blue line, immune cell 1 is represented by the green line and immune cell 2 by the pink line.*

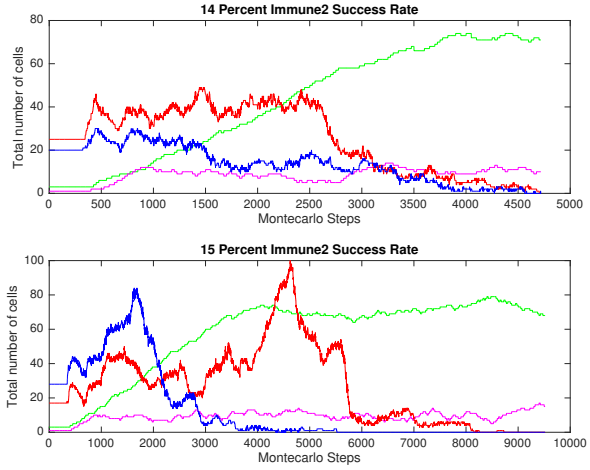

Figure 4.59: *Plots showing the total number of tumour and immune cells for* $14-15\%$ *immune 1 kill rate when in interaction with tumour cell type 2, tumour type 1 and immune type 1 at* 95% *and tumour type 2 and immune type 2 at* 20%*. Tumour cell 1 is represented by the red line, tumour cell 2 is represented by the blue line, immune cell 1 is represented by the green line and immune cell 2 by the pink line.*

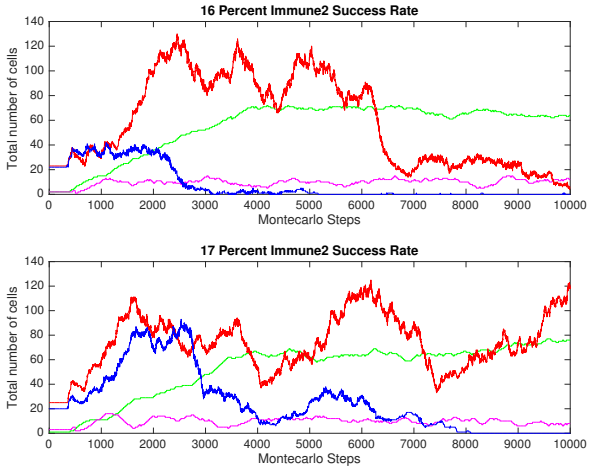

Figure 4.60: *Plots showing the total number of tumour and immune cells for* $16-17\%$ *immune 1 kill rate when in interaction with tumour cell type 2, tumour type 1 and immune type 1 at* 95% *and tumour type 2 and immune type 2 at* 20%*. Tumour cell 1 is represented by the red line, tumour cell 2 is represented by the blue line, immune cell 1 is represented by the green line and immune cell 2 by the pink line.*

4.3.4 The Warburg Effect

In section 4.3.1, 4.3.3 and 4.3.2, the T_2 cells are killed by both types of immune cells. Even at a very small rate of immune success, the T_2 cells are killed off very quickly by the immune cells, and it was hard to promote tumour growth. Although the promotion of tumour proliferation seems counter intuitive, it is necessary in order to understand what causes uncontrollable growth, even in the presence of a strong immune response. The idea of modelling some form of the Warburg effect seemed prudent in this situation.

The model has been altered to try and imitate some of the hallmarks of the Warburg Effect. In this model, as in section 4.3, the nutrient is generic. If the nutrient here is treated in a similar way, in that it contains oxygen and glucose, some aspects of the Warburg Effect can be modelled. The T_1 cells will still undergo nutrient uptake by way of oxidative mitochondrial phosphorylation. In the presence of hypoxia the T_1 cells will, as in section 4.3, go quiescent, and then necrotic, if the nutrient goes below a critical level. However, the T_2 cells will no longer exhibit quiescence if in a hypoxic region.

The T_2 cells will now uptake energy through glycolysis. In an oxidised environment this is called aerobic glycolysis, however in a hypoxic zone it is called anaerobic glycolysis. As previously discussed in section 1.1.4, there are many reasons as to why a tumour cell may favour anaerobic glycolysis over OXPHOS. In this section, the hypoxic activation of glycolysis will be studied. As the T_2 cells no longer turn quiescent in a limited oxygen environment, the cells that are at the centre of the tumour mass will still grow. Moreover, in the necrotic zone, the nutrient is low, stifling tumour growth, however, this

does not kill the T_2 tumour cells under these new circumstances. In a way, the T_2 cells lay in wait until the other cell types around it die off or are killed by a tumour cell. This will allow it to gain a link to the available nutrient in the space, in order to continue its uncontrollable growth. The other aspects of the model, such as cell motility and adhesion, will remain the same.

The aim of this section is to try and focus on evolving the model to show the three Es of immunoediting. In the following results observations and conclusions will be drawn as to whether this has been successful. More importantly, the realisation of a coexistence state through tumour dormancy has been the outlook of the discrete model from the beginning, and this extension will hopefully portray it.

4.3.4.1 Tumour escape

When utilising the Warburg Effect for the T_2 cells, it is hoped that they will be able to thrive even in the presence of low oxygen. For the results in this section both immune types have a death rate of 1000MCS, i.e. the immune cells die after they have been in the domain for 1000MCS, and the simulations run for 20,000MCS. The interactions between tumour and immune cells are still described by the same terms as in sections 4.3.1, 4.3.2 and 4.3.3. Figures 4.61 - 4.67 show the results when $E_1T_1 = 95\%$, $E_1T_2 = 22\%$ and E_2T_2 is varied between $30-39\%$. These figures have been chosen to try and portray the same values as in section 4.3.2. As before, overall concentrations of immune and tumour cells can be seen in figures such as 4.61. The spatial distribution of all cells can be seen in Figure 4.62, and the nutrient concentration can be seen in Figure 4.63. What is apparent from these figures, is the T_2 cells have

now managed to promote their growth. With the switch to glycolysis, by means of the turning off of the quiescent/necrotic pathways, the T_2 cells are able to survive in a hostile environment. Furthermore, the figures show that not only do they survive in the domain, but often out strip the T_1 tumour cells. It should also be noted that as the T_2 cells now completely over run the domain before the simulation has finished. It is still apparent that the oscillatory dynamics here are determined by the clearance of the necrotic cells for both tumour types.

Looking more closely at the spatial domain in Figure 4.62, showing the evolution of the cells at certain time steps, the figures show the oscillatory nature of the tumour cells. In Figure 4.62(d) the tumour cells seem to be filling the domain, but by Figure 4.62(e) the necrotic cells have been cleared, which allows the tumour cells to begin to proliferate into the medium again. Figure 4.63 shows the nutrient concentration in the domain at certain time steps. Here, as the T_1 cells turn quiescent the T_2 cells maintain their proliferative state, allowing growth even when there is no or very little nutrient available. The T_2 cells are therefore able to "hide" from the immune cells and lie in wait until the T_1 cells are either killed or die off due to lack of nutrient. Once the T_2 cells are able to to gain access to more nutrient, they may be the dominant cell type. Here, the T_1 cells may have been killed a the lack of nutrient therefore can no longer compete for space with so many T_2 cells. This is apparent in Figure 4.61 (bottom).

The tumour cells here are evading immune detection just as in the previous model, however as discussed above, the introduction of the Warburg Effect allows the T_2 cells to thrive in a low oxygen environment. It has

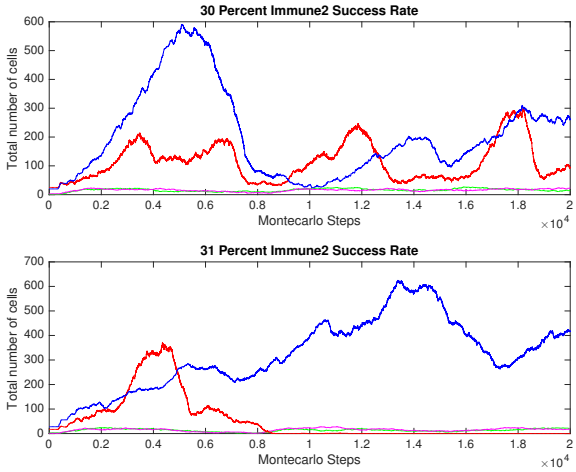

Figure 4.61: *Plots showing the total number of tumour and immune cells for* 22% *immune 1 kill rate when in interaction with tumour cell type 2, tumour type 1 and immune type 1 at* 95% *and tumour type 2 and immune type 2 at* $30-31\%$*. Tumour cell 1 is represented by the red line, tumour cell 2 is represented by the blue line, immune cell 1 is represented by the green line and immune cell 2 by the pink line.*

not shown however, dynamic equilibrium for all cells and therefore, further investigations into this system will need to be performed to elucidate this.

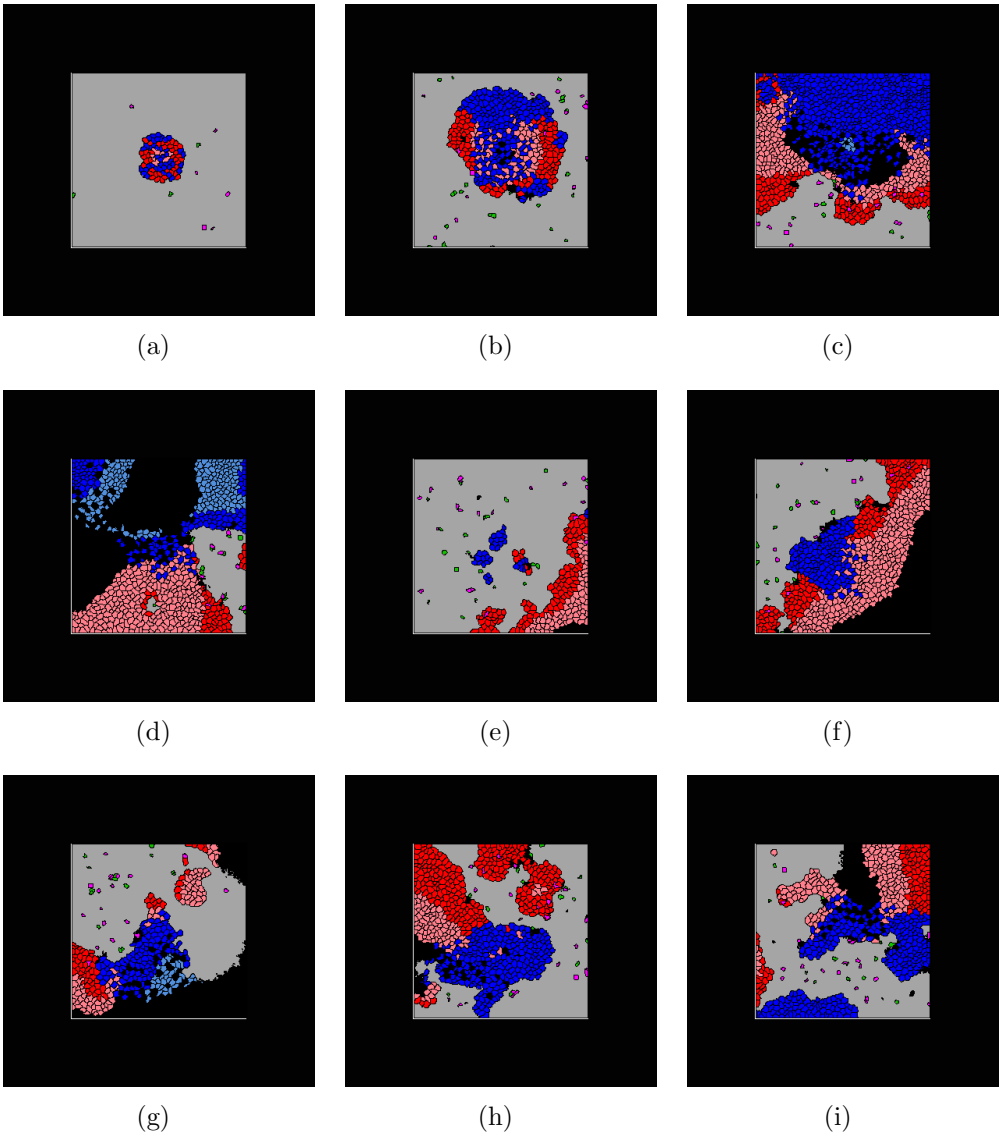

Figure 4.62: *Plots showing the growth of a tumour mass interacting with a host immune system at 1000MCS immune death rate. The types of cells and their corresponding colours in Figures 4.62(a)-4.62(i) are as follows: proliferative tumour type 1 cells in red, quiescent tumour type 1 cells in salmon, proliferative tumour type 2 in blue, quiescent tumour type 2 cells in light blue, necrotic cells in black, medium cells in grey, immune type 1 cells in green, immune type 2 in magenta. The immune success rates are as follows: tumour type 1 and immune type 1 at* 30%*, tumour type 2 and immune type 1 at* 22% *and tumour type 2 and immune type 2 at* 77%*, corresponding to Figure 4.61 (top). Figures 4.62(a)-4.62(i) represent the model at 500MCS, 2500MCS, 5000MCS, 7500MCS and 10000MCS, 12500MCS, 15000MCS, 17500MCS, 20000MCS respectively and show tumour escape.*

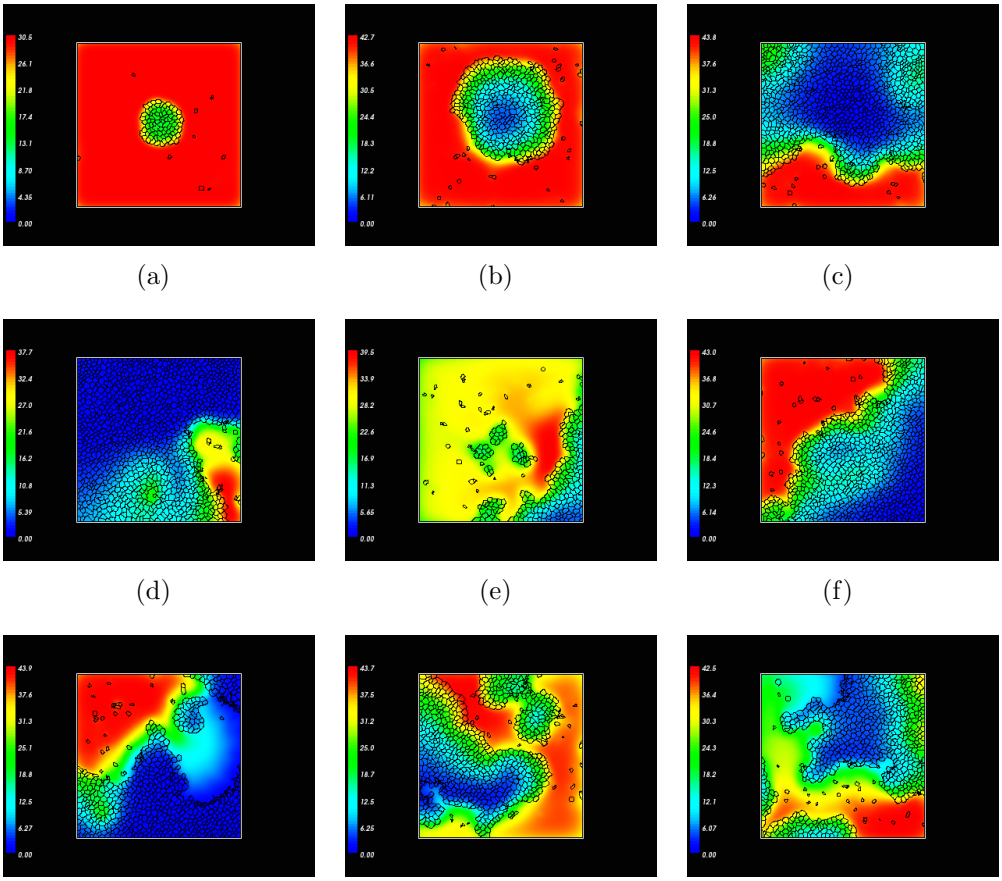

(a) (b) (c)

(d) (e) (f)

(g) (h) (i)

Figure 4.63: *Plots showing the nutrient concentration at times 500MCS, 2500MCS, 5000MCS, 7500MCS, 10000MCS 12500MCS, 15000MCS, 17500MCS and 20000MCS, respectively. The immune success rates are as follows: tumour type 1 and immune type 1 at* 95%*, tumour type 2 and immune type 1 at* 22% *and tumour type 2 and immune type 2 at* 30%*, corresponding to Figure 4.61 (top). The oxygen concentration is high when it is red and low when it is blue. A bar on the left hand side of each picture represents the oxygen concentration. Oxygen is used up by the immune, tumour and quiescent cells leaving areas where tumour cells can longer be supported leading to necrosis. Once the necrotic cells have disintegrated oxygen can flow into the area again via medium cells.*

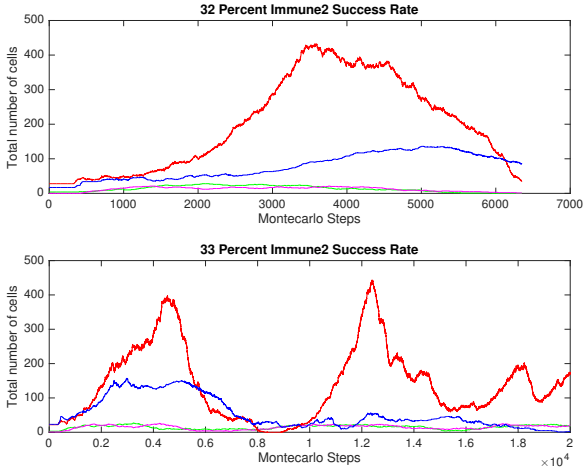

Figure 4.64: *Plots showing the total number of tumour and immune cells for 22% immune 1 kill rate when in interaction with tumour cell type 2, tumour type 1 and immune type 1 at 95% and tumour type 2 and immune type 2 at 32 – 33%. Tumour cell 1 is represented by the red line, tumour cell 2 is represented by the blue line, immune cell 1 is represented by the green line and immune cell 2 by the pink line.*

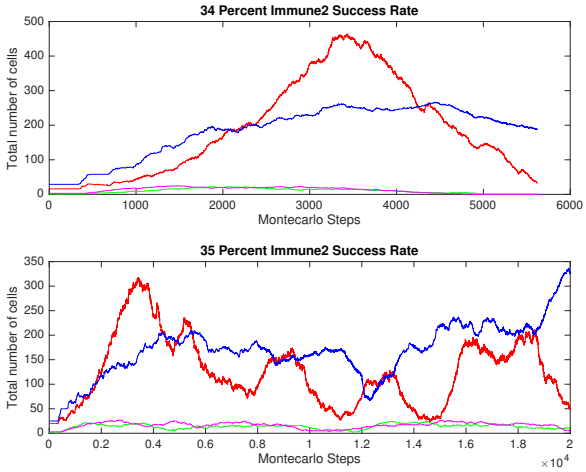

Figure 4.65: *Plots showing the total number of tumour and immune cells for 22% immune 1 kill rate when in interaction with tumour cell type 2, tumour type 1 and immune type 1 at 95% and tumour type 2 and immune type 2 at 34 – 35%. Tumour cell 1 is represented by the red line, tumour cell 2 is represented by the blue line, immune cell 1 is represented by the green line and immune cell 2 by the pink line.*

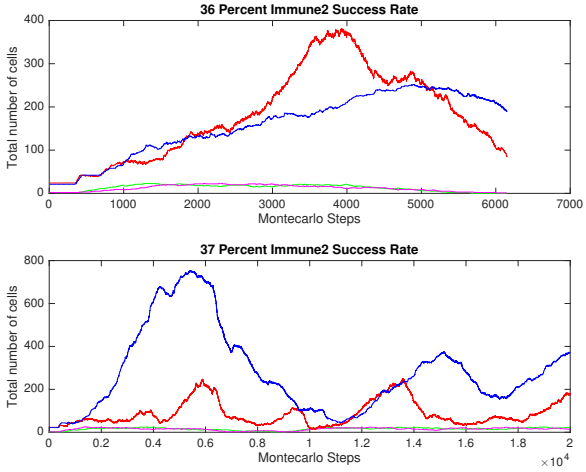

Figure 4.66: *Plots showing the total number of tumour and immune cells for* 22% *immune 1 kill rate when in interaction with tumour cell type 2, tumour type 1 and immune type 1 at* 95% *and tumour type 2 and immune type 2 at* $36-37\%$*. Tumour cell 1 is represented by the red line, tumour cell 2 is represented by the blue line, immune cell 1 is represented by the green line and immune cell 2 by the pink line.*

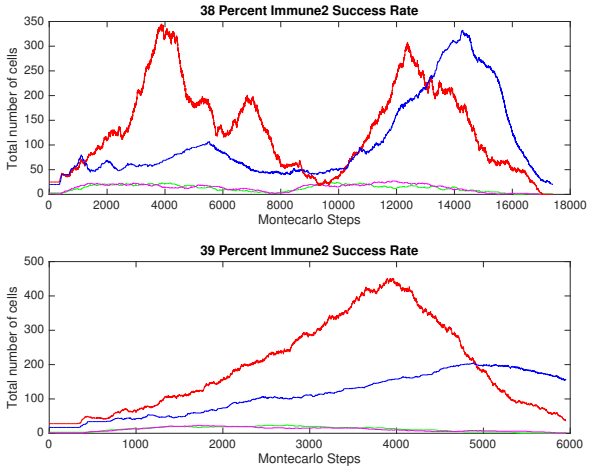

Figure 4.67: *Plots showing the total number of tumour and immune cells for* 22% *immune 1 kill rate when in interaction with tumour cell type 2, tumour type 1 and immune type 1 at* 95% *and tumour type 2 and immune type 2 at* $38-39\%$*. Tumour cell 1 is represented by the red line, tumour cell 2 is represented by the blue line, immune cell 1 is represented by the green line and immune cell 2 by the pink line.*

4.3.4.2 Coexistence

To try and portray the results found in section 3.8, a few different modelling techniques have been utilised. The changing of parameter values and the addition of the Warburg effect has tried to show accurately the coexistence state, found in the ODE/PDE models in sections 3.7 and 3.8. In this section, the simulations will again run for 20,000MCS. Each immune type has been given a different death rate. E_1 cells will be killed in the domain at 2500MCS from when they were introduced, whereas E_2 cells will be killed by 500MCS. This change has been introduced to give the T_2 cells a fighting chance, while upping the amount of E_1 cells in the domain, to try and achieve equilibrium. The percentage of the tumour immune interactions has also been adjusted. While, $E_1T_1 = 95\%$ as before, $E_1T_2 = 10\%$ and E_2T_2 will vary between $12 - 20\%$. This lowering of the immune cell success rate for E_1T_2 and E_2T_2 had very little impact in section 4.3.4.1, however the hope is that the T_2 cells will be able to survive even though the E_1 cells will have a high concentration.

The lowering of the immune success interaction terms along with the changing of the immune death has made an impact on the model, in fact the model now becomes quite changeable. At $E_2T_2 = 12\%$ and $E_2T_2 = 13\%$, shown in Figure 4.68, the dynamics are very similar to sections 4.3.1.2 and 4.3.2.2, although the immune cells are now mounting an effective attack on the tumour cells causing oscillations. Looking at the spatial domain in Figure 4.69, it is apparent that the immune cells, even when they have a small success rate, have killed off the T_2 cells very quickly. Figure 4.69(a)-4.69(b) show the T_2 cells actually manage, initially, to break off from the

main tumour group and form a new mass. However, this exposes them to immune attack and they are quickly killed off by 5000MCS, shown in Figure 4.69(c). The nutrient concentration can be seen in Figure 4.70. Looking at both of the spatial figures, while the T_2 cells still maintain their proliferative state in the presence of low nutrient, the T_1 cells turn quiescent and then necrotic.

When E_2T_2 has been furthered increased to 15%, depicted in Figure 4.71 (bottom), the picture is quite different. In this simulation the T_2 cells have managed to out manoeuvre the T_1 cells and have become the dominant tumour phenotype. This would seem odd as the immune cells percentage success rate has been increased. However, looking at the spatial description in Figure 4.72, the T_2 have been placed more so around the outer rim of the tumour allowing its growth to exceed that of the T_1 cells. In the fight for nutrient, as seen in Figure 4.73, the T_2 cells, due to their close proximity to the T_1 cells, use up more nutrient as they do not turn quiescent, starving the T_1 cells. Their numbers are far greater by 2500MCS, depicted in Figure 4.72(d), and the T_1 cells are picked off by the immune cells and the lack of nutrient.

At 16% E_2T_2 success rate, in Figure 4.74 (top), the tumour and immune cells seem to be living in equilibrium. There is an oscillatory like nature to the tumour cells as the immune cells begin to attack them. This continues through the whole simulation. Figure 4.75 shows this oscillatory like nature in a spatial setting. The existence of all four cell types is now realised. The nutrient concentration is also portrayed in Figure 4.76. When $E_2T_2 =$ 17%, the immune cells have managed to kill the tumour cells however, the

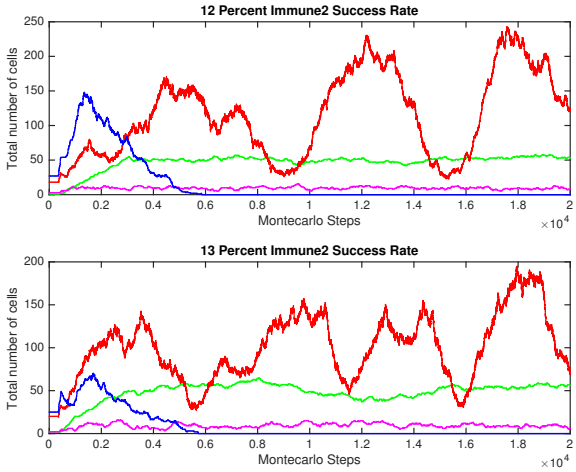

Figure 4.68: *Plots showing the total number of tumour and immune cells for* 10% *immune 1 kill rate when in interaction with tumour cell type 2, tumour type 1 and immune type 1 at* 95% *and tumour type 2 and immune type 2 at* $12-13\%$*. Tumour cell 1 is represented by the red line, tumour cell 2 is represented by the blue line, immune cell 1 is represented by the green line and immune cell 2 by the pink line.*

concentration of immune cells will need to be further increased in order for the immune system to fully eradicate the cancer cells.

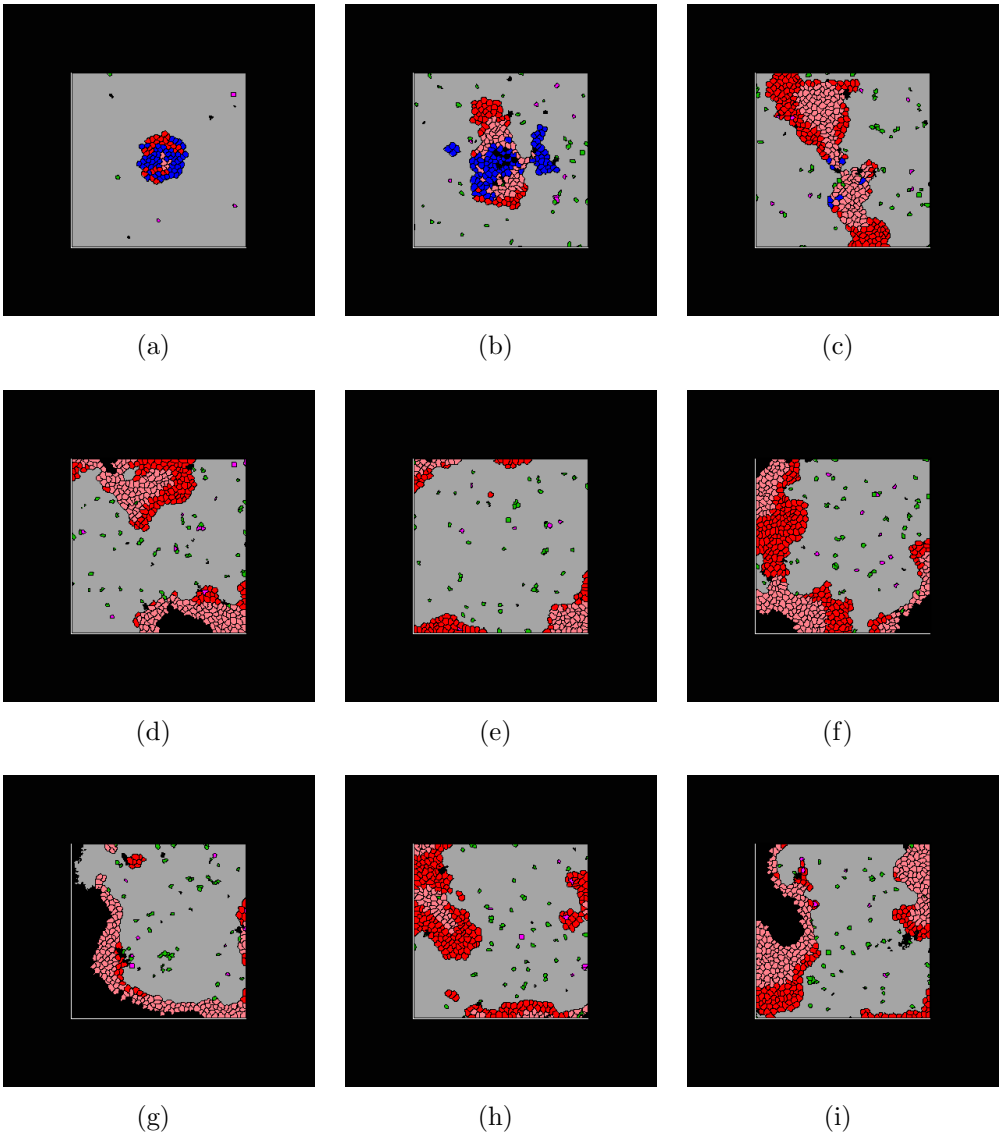

Figure 4.69: *Plots showing the growth of a tumour mass interacting with a host immune system at 2500MCS E_1 immune death rate and 500MCS E_2 immune death rate. The types of cells and their corresponding colours in Figures 4.69(a)-4.69(i) are as follows: proliferative tumour type 1 cells in red, quiescent tumour type 1 cells in salmon, proliferative tumour type 2 in blue, quiescent tumour type 2 cells in light blue, necrotic cells in black, medium cells in grey, immune type 1 cells in green, immune type 2 in magenta. The immune success rates are as follows: tumour type 1 and immune type 1 at* 95%*, tumour type 2 and immune type 1 at* 10% *and tumour type 2 and immune type 2 at* 12%*, corresponding to Figure 4.68 (top). Figures 4.69(a)-4.69(i) represent the model at 500MCS, 2500MCS, 5000MCS, 7500MCS and 10000MCS, 12500MCS, 15000MCS, 17500MCS, 20000MCS respectively.*

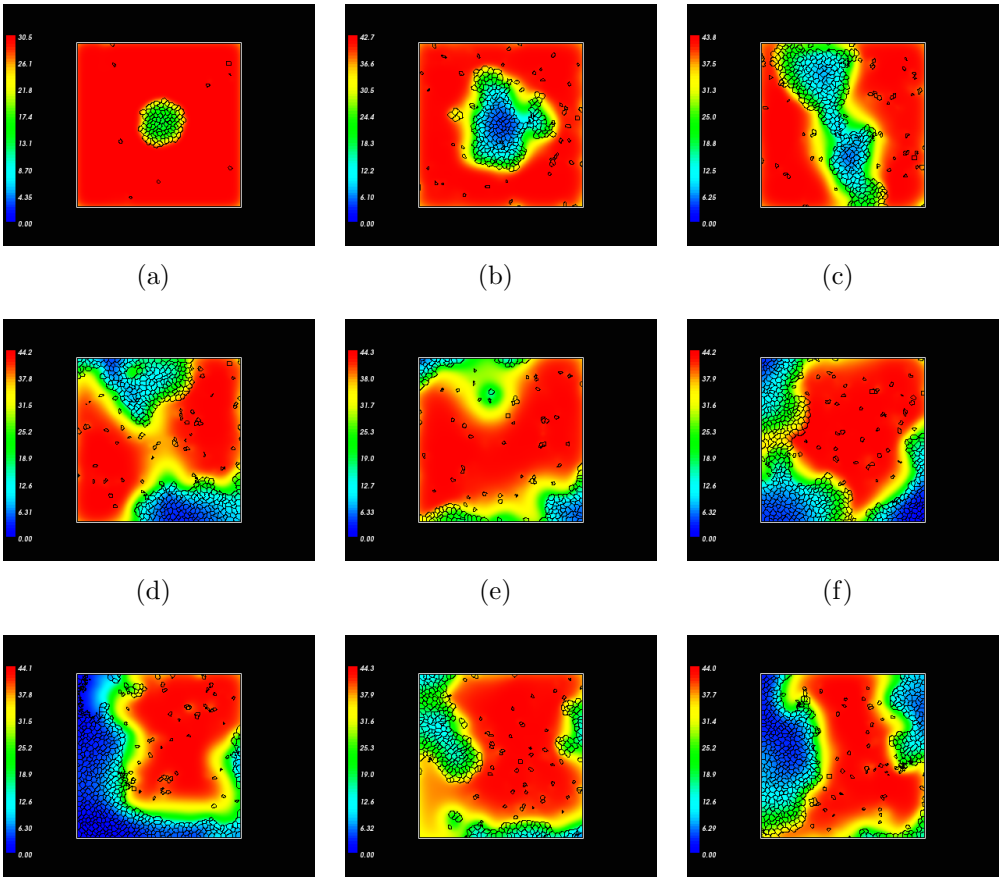

(a) (b) (c)

(d) (e) (f)

(g) (h) (i)

Figure 4.70: *Plots showing the nutrient concentration at times 500MCS, 2500MCS, 5000MCS, 7500MCS, 10000MCS 12500MCS, 15000MCS, 17500MCS and 20000MCS, respectively. The immune success rates are as follows: tumour type 1 and immune type 1 at* 95%*, tumour type 2 and immune type 1 at* 10% *and tumour type 2 and immune type 2 at* 12%*, corresponding to Figure 4.68 (top). The oxygen concentration is high when it is red and low when it is blue. A bar on the left hand side of each picture represents the oxygen concentration. Oxygen is used up by the immune, tumour and quiescent cells leaving areas where tumour cells can longer be supported leading to necrosis. Once the necrotic cells have disintegrated oxygen can flow into the area again via medium cells.*

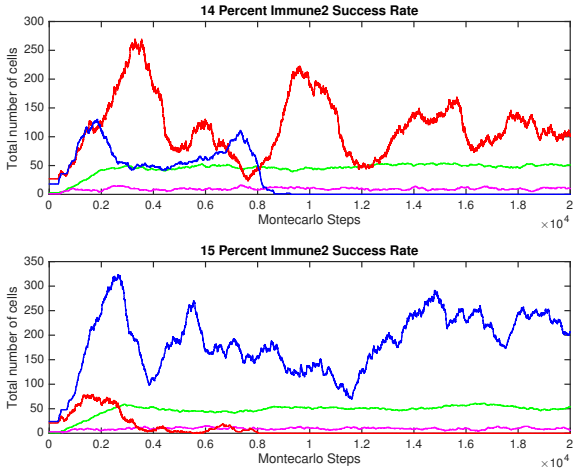

Figure 4.71: *Plots showing the total number of tumour and immune cells for* 10% *immune 1 kill rate when in interaction with tumour cell type 2, tumour type 1 and immune type 1 at* 95% *and tumour type 2 and immune type 2 at* $14-15\%$*. Tumour cell 1 is represented by the red line, tumour cell 2 is represented by the blue line, immune cell 1 is represented by the green line and immune cell 2 by the pink line.*

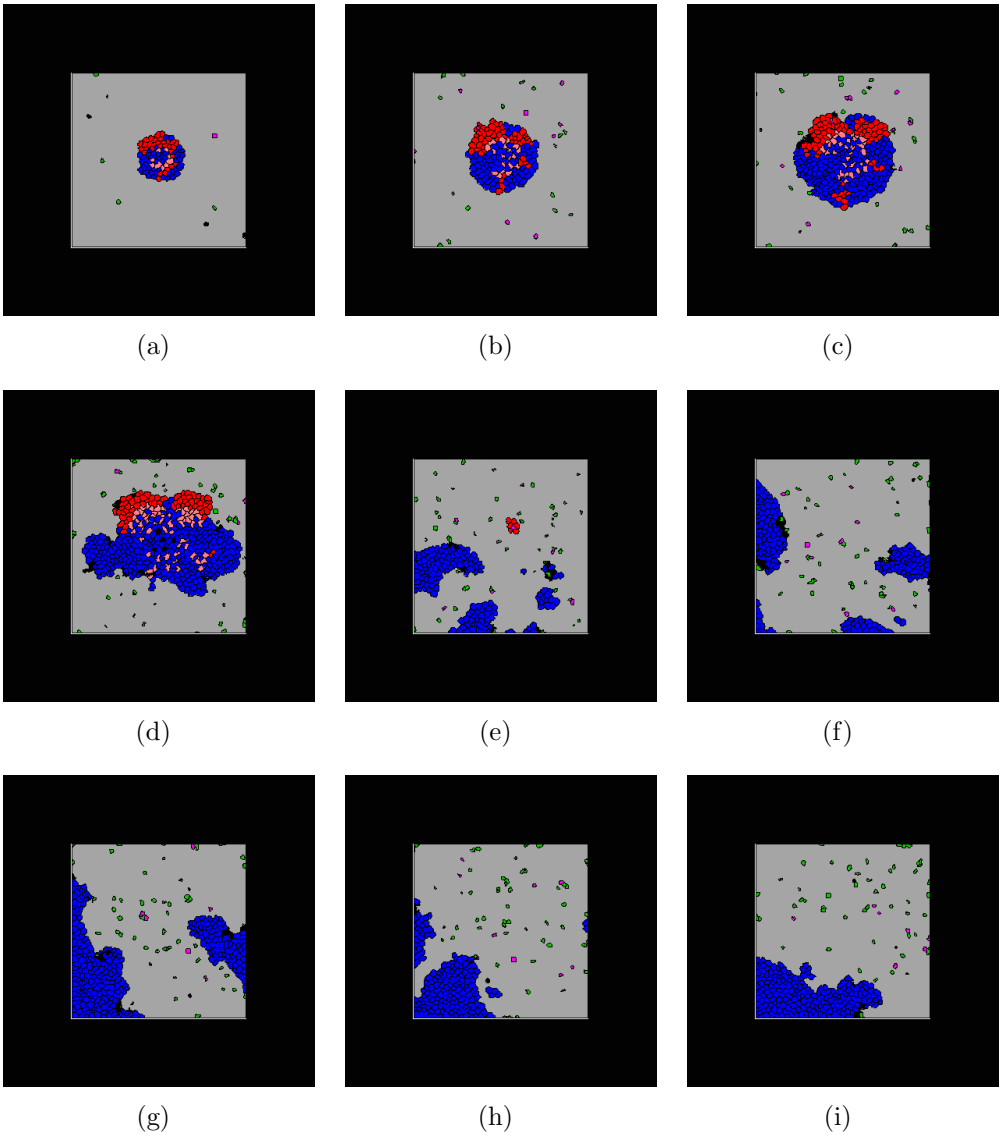

Figure 4.72: *Plots showing the growth of a tumour mass interacting with a host immune system at 2500MCS E_1 immune death rate and 500MCS E_2 immune death rate. The types of cells and their corresponding colours in Figures 4.72(a)-4.72(i) are as follows: proliferative tumour type 1 cells in red, quiescent tumour type 1 cells in salmon, proliferative tumour type 2 in blue, quiescent tumour type 2 cells in light blue, necrotic cells in black, medium cells in grey, immune type 1 cells in green, immune type 2 in magenta. The immune success rates are as follows: tumour type 1 and immune type 1 at* 95%*, tumour type 2 and immune type 1 at* 10% *and tumour type 2 and immune type 2 at* 15%*, corresponding to Figure 4.71 (bottom). Figures 4.72(a)-4.72(i) represent the model at 500MCS, 1000MCS, 1500MCS, 2500MCS 2500MCS, 7500MCS, 12500MCS, 15000MCS, 17500MCS, 20000MCS respectively.*

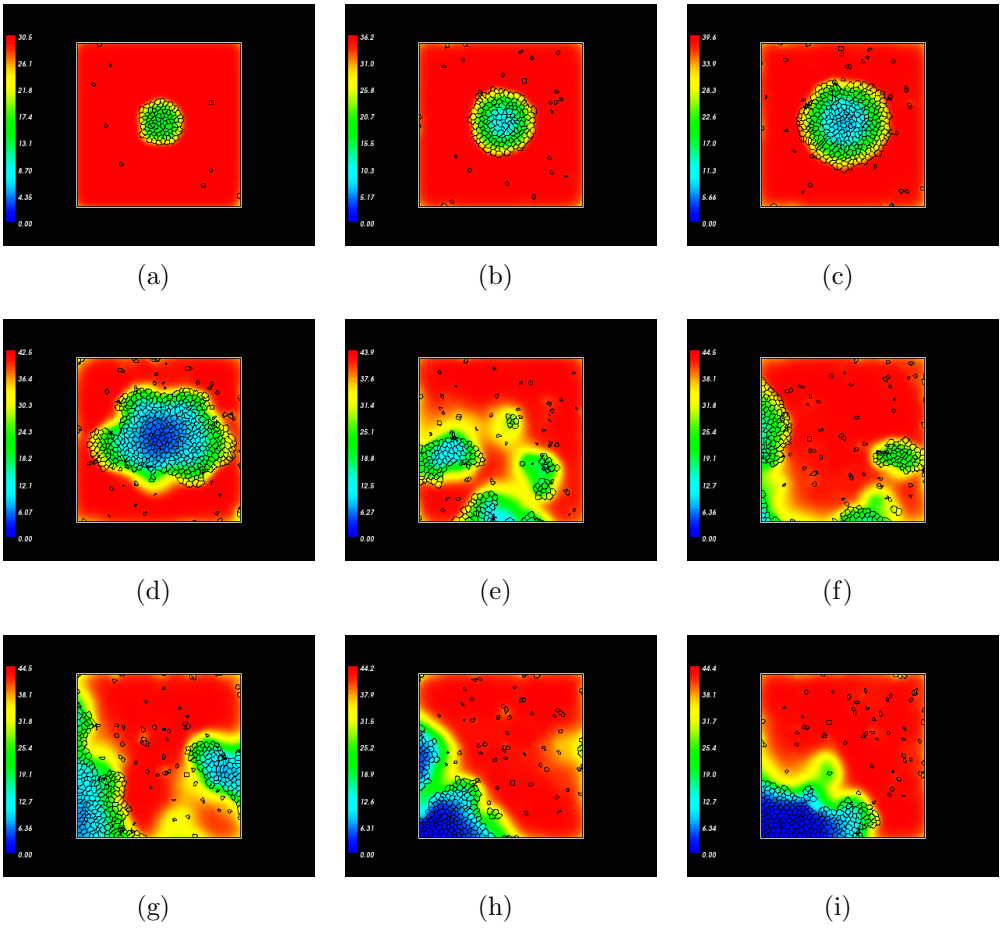

(a) (b) (c)

(d) (e) (f)

(g) (h) (i)

Figure 4.73: *Plots showing the nutrient concentration at times 500MCS, 2500MCS, 5000MCS, 7500MCS, 10000MCS 12500MCS, 15000MCS, 17500MCS and 20000MCS, respectively. The immune success rates are as follows: tumour type 1 and immune type 1 at* 95%*, tumour type 2 and immune type 1 at* 10% *and tumour type 2 and immune type 2 at* 15%*, corresponding to Figure 4.71 (bottom). The oxygen concentration is high when it is red and low when it is blue. A bar on the left hand side of each picture represents the oxygen concentration. Oxygen is used up by the immune, tumour and quiescent cells leaving areas where tumour cells can longer be supported leading to necrosis. Once the necrotic cells have disintegrated oxygen can flow into the area again via medium cells.*

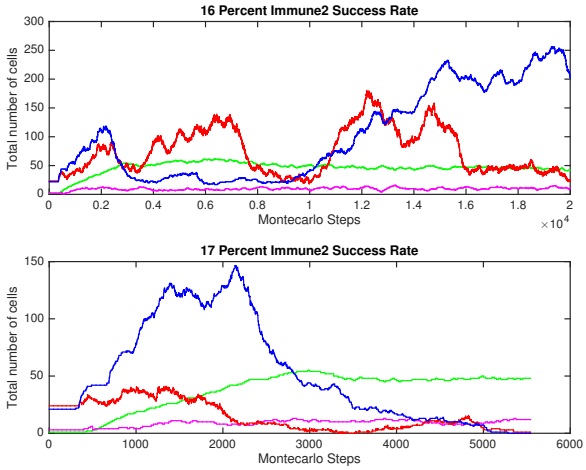

Figure 4.74: *Plots showing the total number of tumour and immune cells for* 10% *immune 1 kill rate when in interaction with tumour cell type 2, tumour type 1 and immune type 1 at* 95% *and tumour type 2 and immune type 2 at* $16-17\%$*. Tumour cell 1 is represented by the red line, tumour cell 2 is represented by the blue line, immune cell 1 is represented by the green line and immune cell 2 by the pink line.*

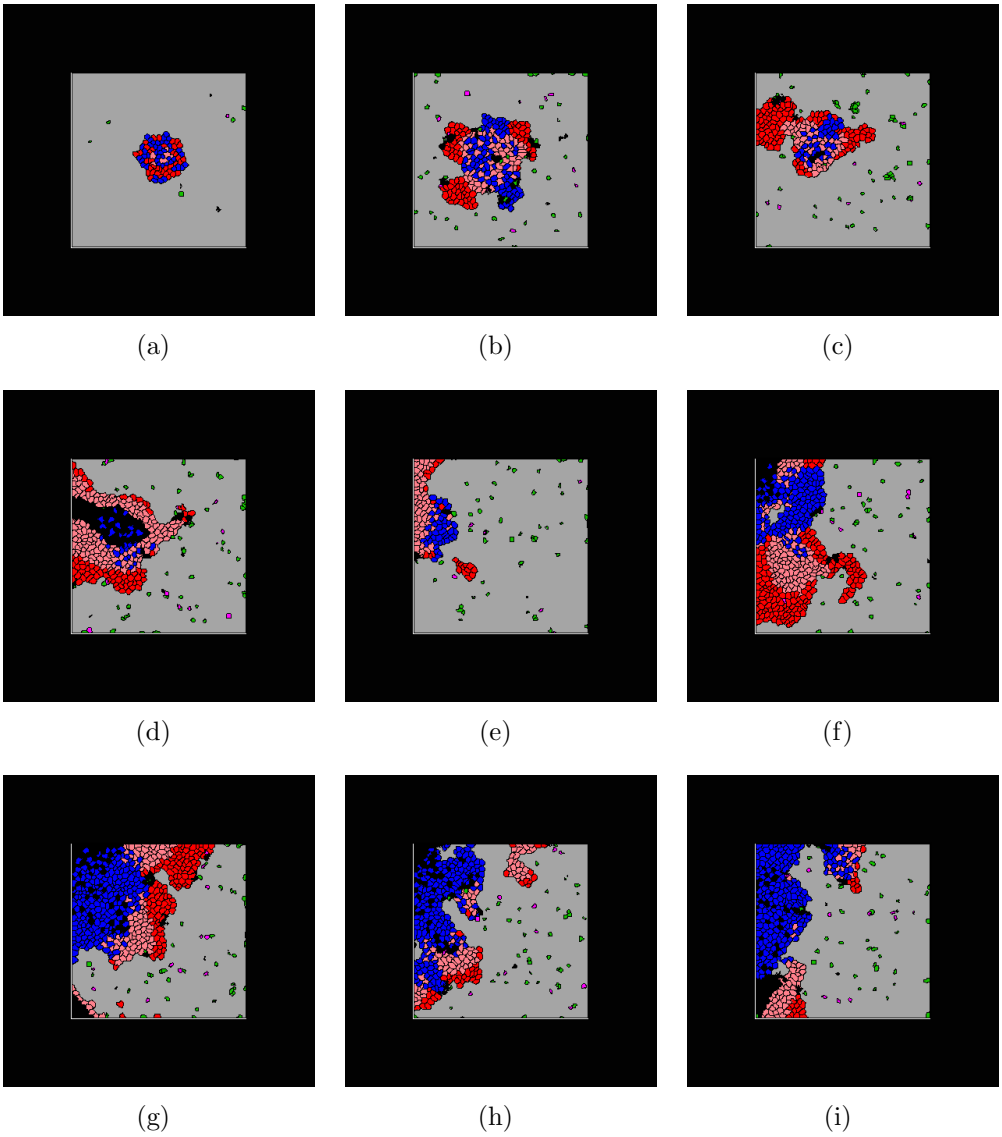

Figure 4.75: *Plots showing the growth of a tumour mass interacting with a host immune system at 2500MCS E_1 immune death rate and 500MCS E_2 immune death rate. The types of cells and their corresponding colours in Figures 4.75(a)-4.75(i) are as follows: proliferative tumour type 1 cells in red, quiescent tumour type 1 cells in salmon, proliferative tumour type 2 in blue, quiescent tumour type 2 cells in light blue, necrotic cells in black, medium cells in grey, immune type 1 cells in green, immune type 2 in magenta. The immune success rates are as follows: tumour type 1 and immune type 1 at* 95%*, tumour type 2 and immune type 1 at* 10% *and tumour type 2 and immune type 2 at* 16%*, corresponding to Figure 4.74 (top). Figures 4.75(a)-4.75(i) represent the model at 500MCS, 2500MCS, 5000MCS, 7500MCS and 10000MCS, 12500MCS, 15000MCS, 17500MCS, 20000MCS respectively.*

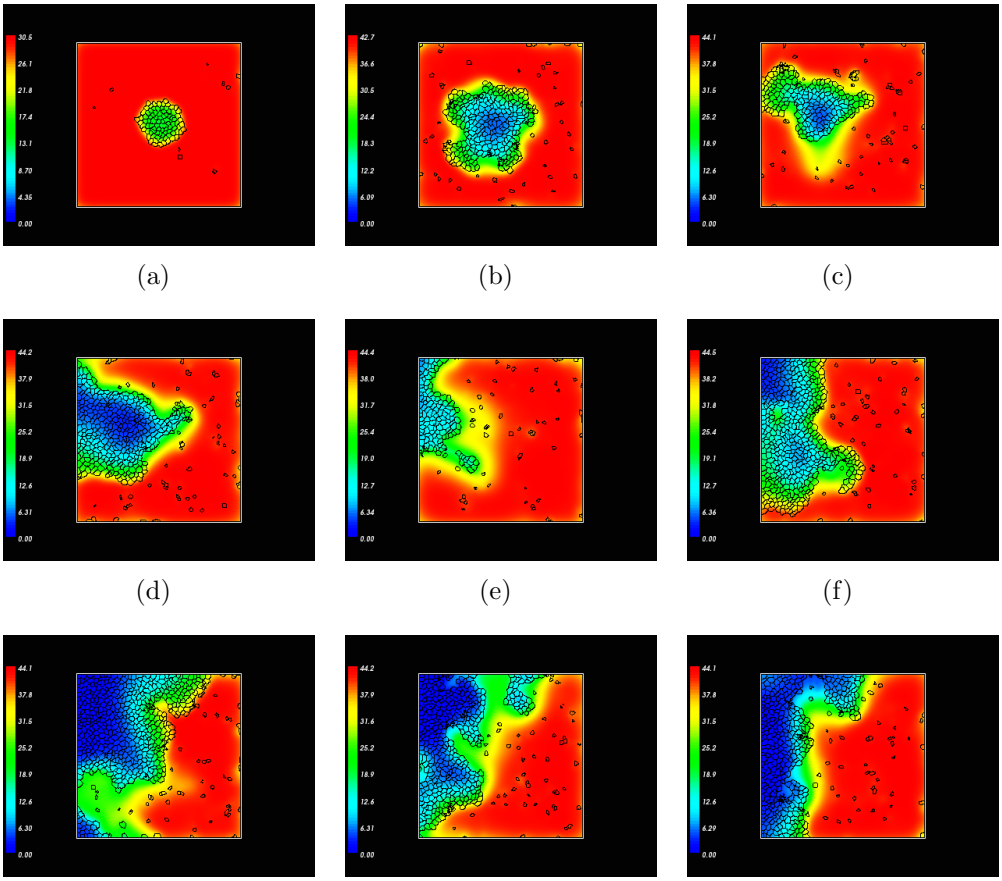

(a) (b) (c)

(d) (e) (f)

(g) (h) (i)

Figure 4.76: *Plots showing the nutrient concentration at times 500MCS, 2500MCS, 5000MCS, 7500MCS, 10000MCS 12500MCS, 15000MCS, 17500MCS and 20000MCS, respectively. The immune success rates are as follows: tumour type 1 and immune type 1 at* 95%*, tumour type 2 and immune type 1 at* 10% *and tumour type 2 and immune type 2 at* 16%*, corresponding to Figure 4.74 (top). The oxygen concentration is high when it is red and low when it is blue. A bar on the left hand side of each picture represents the oxygen concentration. Oxygen is used up by the immune, tumour and quiescent cells leaving areas where tumour cells can longer be supported leading to necrosis. Once the necrotic cells have disintegrated oxygen can flow into the area again via medium cells.*

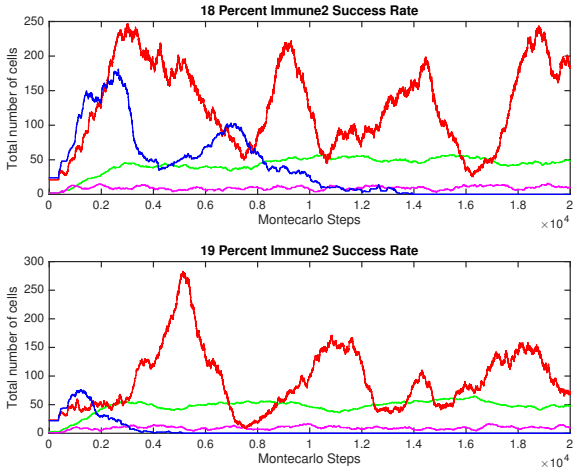

Figure 4.77: *Plots showing the total number of tumour and immune cells for* 10% *immune 1 kill rate when in interaction with tumour cell type 2, tumour type 1 and immune type 1 at* 95% *and tumour type 2 and immune type 2 at* $18-19\%$*. Tumour cell 1 is represented by the red line, tumour cell 2 is represented by the blue line, immune cell 1 is represented by the green line and immune cell 2 by the pink line.*

4.3.4.3 Tumour elimination

In order to realise the third E of immunoediting, Elimination, the immune concentrations must be increased. Both immune types have now had their death rates decreased to 5000MCS. Again, the simulations have been run for 20,000MCS, and the will stop if there are no tumour, quiescent or immune cells left in the domain. The immune cell success rates have been kept the same as section 4.3.4.1. In the previous section the immune cell interaction terms needed to be lowered to achieve equilibrium, however, this time it has been kept the same as section 4.3.4.1: $E_1T_1 = 95\%$, $E_1T_2 = 22\%$ and E_2T_2 is varied between $30 - 39\%$.

The Figures 4.78-4.84 show the results for these set of parameter values. It is clear from these figures that the immune cells now have enough numbers to overcome the tumour cells. This could be realised in real life through many different means, such as, for example, chemotaxis, where local immune cells are drawn towards the tumour cells; or two different immune types whereby one signals more immune cells to exit the blood and flow into the domain. In Figure 4.79 the spatial distribution of all cells is shown. As the tumour cells divides and grows, the immune cell population also increases, as shown in Figures 4.79(a)-4.79(c). In Figures 4.79(d)-4.79(f) the immune cells are killing off the tumour cells and by 13,000MCS, depicted in Figure 4.79(i), the immune cells have cleared the tumour mass. The nutrient concentration can be seen in Figure 4.80.

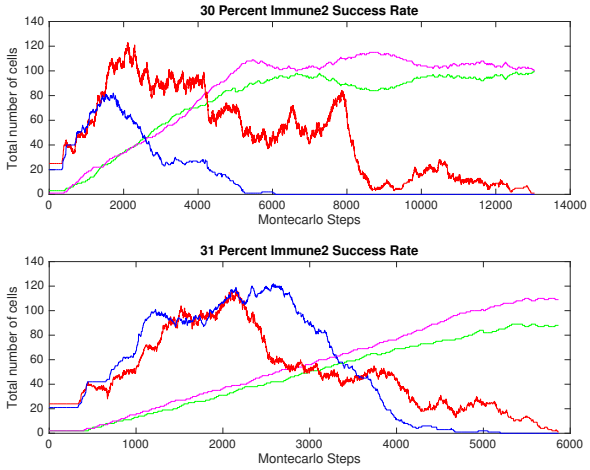

Figure 4.78: *Plots showing the total number of tumour and immune cells for* 22% *immune 1 kill rate when in interaction with tumour cell type 2, tumour type 1 and immune type 1 at* 95% *and tumour type 2 and immune type 2 at* $30-31\%$*. Tumour cell 1 is represented by the red line, tumour cell 2 is represented by the blue line, immune cell 1 is represented by the green line and immune cell 2 by the pink line.*

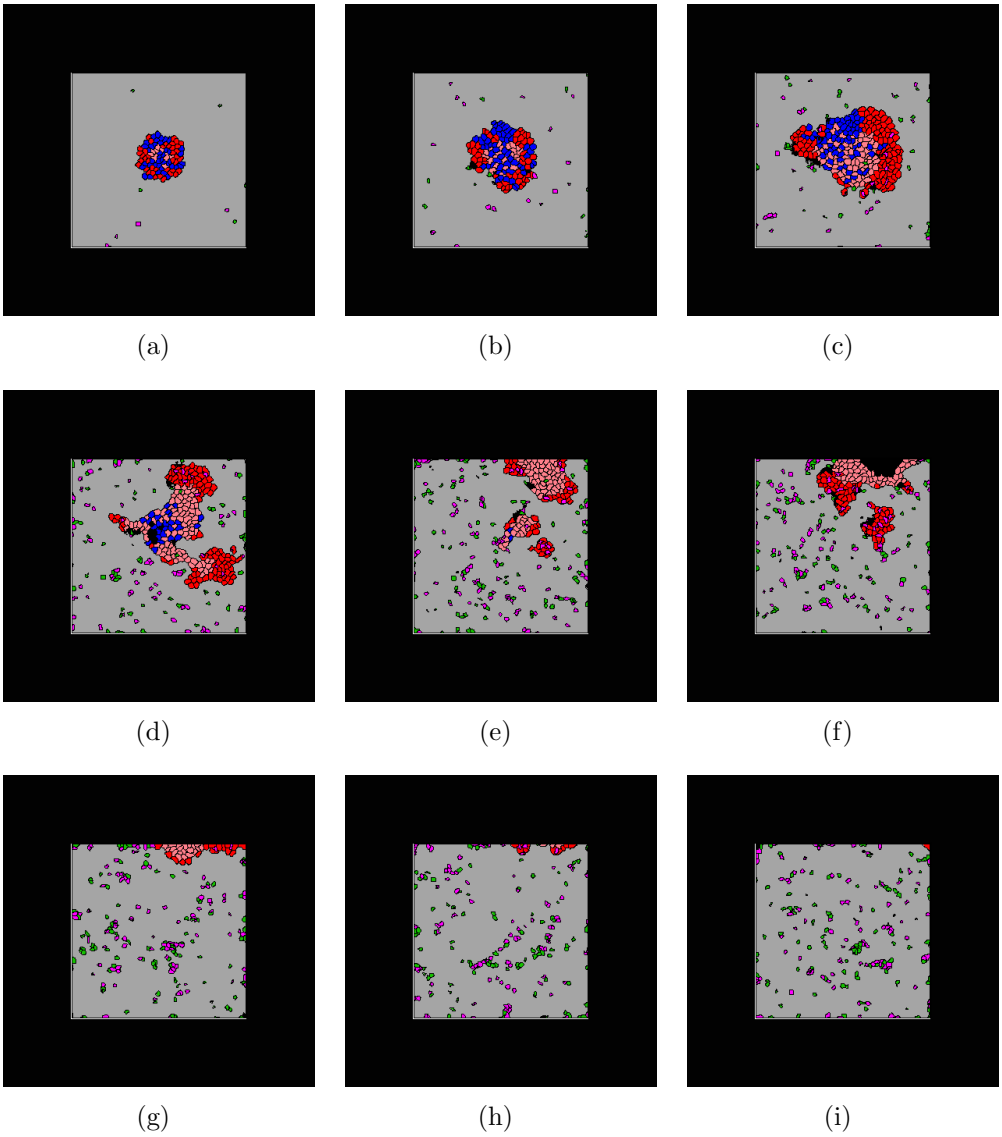

Figure 4.79: *Plots showing the growth of a tumour mass interacting with a host immune system at 5000MCS immune death rate. The types of cells and their corresponding colours in Figures 4.79(b)-4.79(i) are as follows: proliferative tumour type 1 cells in red, quiescent tumour type 1 cells in salmon, proliferative tumour type 2 in blue, quiescent tumour type 2 cells in light blue, necrotic cells in black, medium cells in grey, immune type 1 cells in green, immune type 2 in magenta. The immune success rates are as follows: tumour type 1 and immune type 1 at* 95%*, tumour type 2 and immune type 1 at* 22% *and tumour type 2 and immune type 2 at* 30%*, corresponding to Figure 4.78 (top). Figures 4.79(b)-4.79(i) represent the model at 2500MCS, 5000MCS, 7500MCS and 10000MCS respectively and show tumour elimination.*

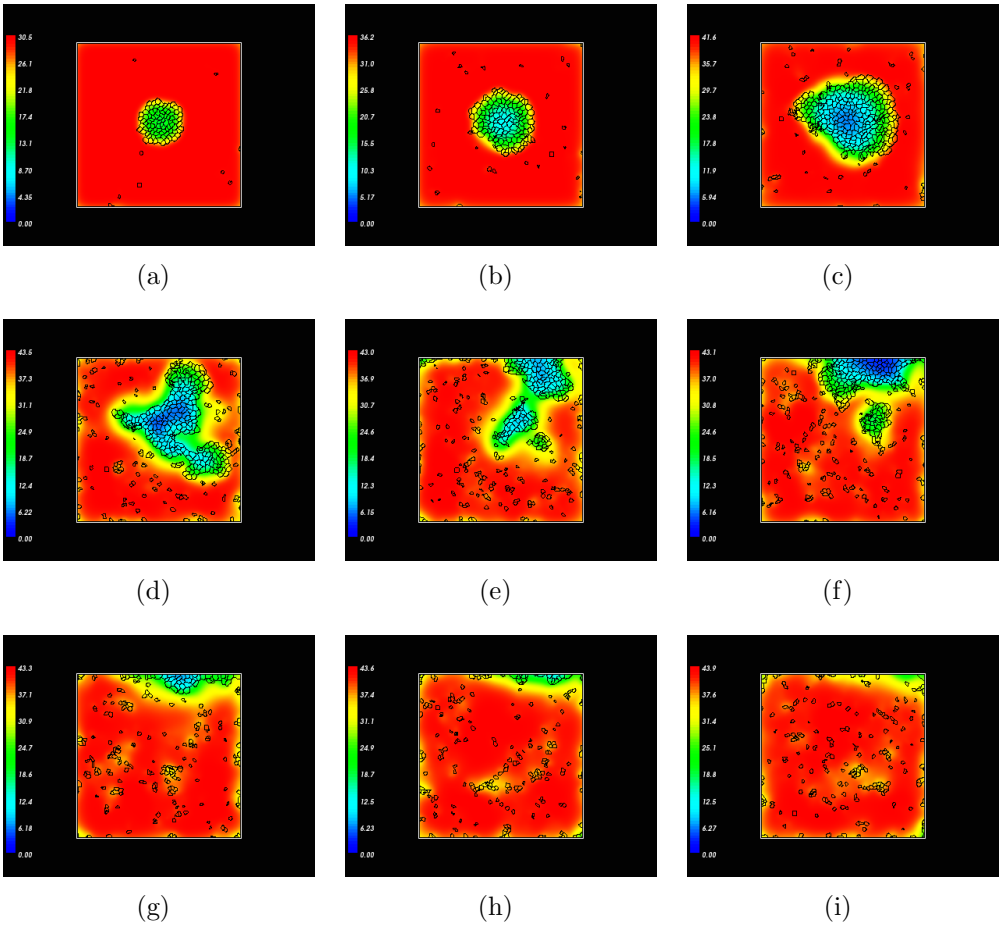

(a) (b) (c)

(d) (e) (f)

(g) (h) (i)

Figure 4.80: *Plots showing the nutrient concentration at times 500MCS, 1000MCS, 2000MCS, 4000MCS, 6000MCS, 8000MCS 10000MCS, 12000MCS, and 13000MCS, respectively. The immune success rates are as follows: tumour type 1 and immune type 1 at* 95%*, tumour type 2 and immune type 1 at* 22% *and tumour type 2 and immune type 2 at* 30%*, corresponding to Figure 4.78 (top). The oxygen concentration is high when it is red and low when it is blue. A bar on the left hand side of each picture represents the oxygen concentration. Oxygen is used up by the immune, tumour and quiescent cells leaving areas where tumour cells can longer be supported leading to necrosis. Once the necrotic cells have disintegrated oxygen can flow into the area again via medium cells.*

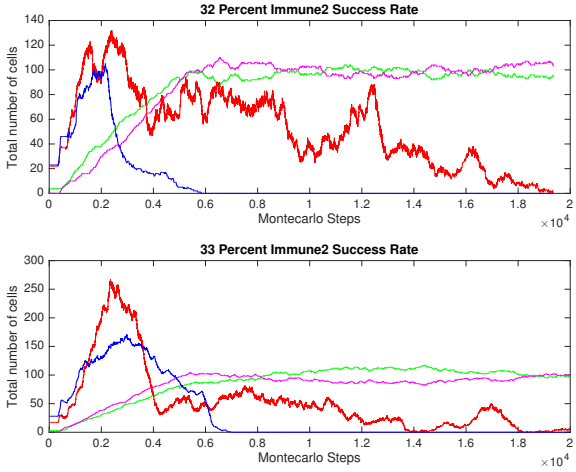

Figure 4.81: *Plots showing the total number of tumour and immune cells for* 22% *immune 1 kill rate when in interaction with tumour cell type 2, tumour type 1 and immune type 1 at* 95% *and tumour type 2 and immune type 2 at* $32-33\%$*. Tumour cell 1 is represented by the red line, tumour cell 2 is represented by the blue line, immune cell 1 is represented by the green line and immune cell 2 by the pink line.*

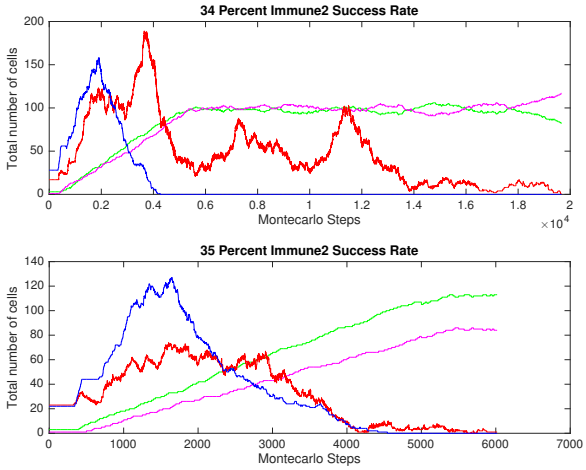

Figure 4.82: *Plots showing the total number of tumour and immune cells for* 22% *immune 1 kill rate when in interaction with tumour cell type 2, tumour type 1 and immune type 1 at* 95% *and tumour type 2 and immune type 2 at* $34-35\%$*. Tumour cell 1 is represented by the red line, tumour cell 2 is represented by the blue line, immune cell 1 is represented by the green line and immune cell 2 by the pink line.*

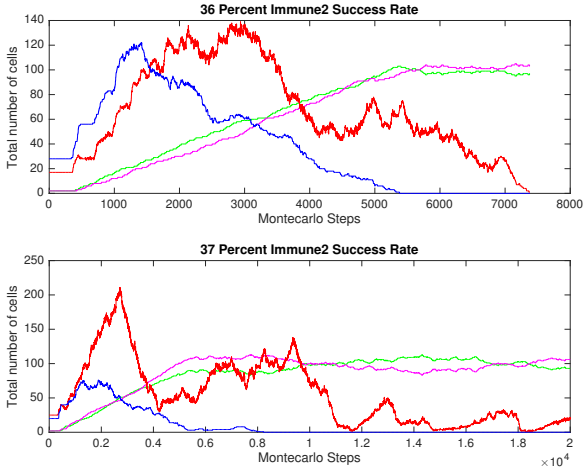

Figure 4.83: *Plots showing the total number of tumour and immune cells for* 22% *immune 1 kill rate when in interaction with tumour cell type 2, tumour type 1 and immune type 1 at* 95% *and tumour type 2 and immune type 2 at* $36-37\%$*. Tumour cell 1 is represented by the red line, tumour cell 2 is represented by the blue line, immune cell 1 is represented by the green line and immune cell 2 by the pink line.*

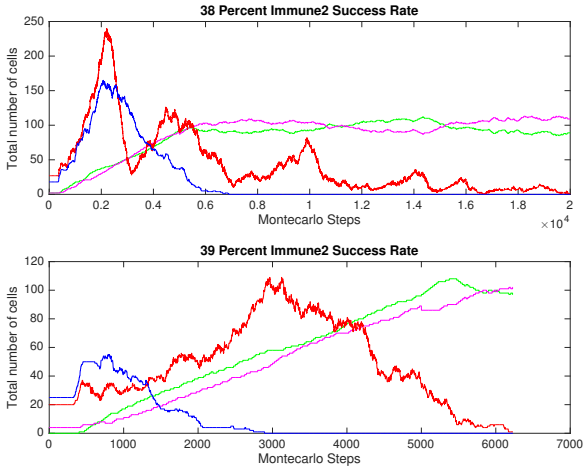

Figure 4.84: *Plots showing the total number of tumour and immune cells for* 22% *immune 1 kill rate when in interaction with tumour cell type 2, tumour type 1 and immune type 1 at* 95% *and tumour type 2 and immune type 2 at* $38-39\%$*. Tumour cell 1 is represented by the red line, tumour cell 2 is represented by the blue line, immune cell 1 is represented by the green line and immune cell 2 by the pink line.*

4.4 Conclusion

This chapter has focused on extending the models from both of the previous chapters. The model utilises a discrete CompuCell3D model to try and surmise the dynamics, which underlie a novel system, whereby two tumour types are interaction with two immune cell types, before the development of a tumour blood regulatory network. The aim was to try and find a co-existence dormant state between all cell types, extending the models in sections 3.7 and 3.8.

The model begins with a central tumour mass containing randomly placed tumour cells of type one and two, surrounded by four randomly placed immune cells. The model utilises the control parameter set out in Matzavinos et al. [2004] to employ the killing method used by the immune cells. However, this time there are three immune-tumour interactions: E_1T_1, E_1T_2 and E_2T_2. These mimic the ODE/PDE model found in sections 3.7 and 3.8. Unlike the previous CompuCell3D model in Chapter 2, the tumour cells no longer pose a threat to the immune cells, therefore an age at which the immune cells die has been implemented. Immune cell death occurs when they have been in the domain for a certain number of MCS, defined by the user. Again different tumour zones can be established, however this time there are two tumour cells, bringing a whole host of new challenges. Moreover, the tumour cells are allowed to divide when they reach a certain number of MCS and both cells have a random motility associated with them.

The model is explored by varying the immune success rates, in order to allow the system to exhibit the three Es of immunoediting. Firstly, the immune

type one success rate when interaction with tumour type one (E_1T_1), was varied. The three Es of immunoediting were realised and some conclusions can be drawn. To gain control over the three different state of immunoediting the amount of time at which the immune cells were in the domain needed to be increased. Increasing the immune success rate in the interaction, E_1T_1 did not provide sufficient enough protection against the T_1 cells, although there was a slight decrease in tumour bulk. Moreover, the T_2 cells did not really propagate through the domain and seemed almost obsolete throughout the system in most simulations. In the dormancy setting, the E_1, T_1 and E_2 cells all exhibited equilibrium, however the T_2 did not and were killed in the domain quickly. The second interaction to be varied was E_2T_2 and again the three Es of immunoediting can be realised in T_1 but not in T_2. Lastly, an investigation on the interaction of E_1T_2 was carried out. This section only focused on trying to get the T_2 cells to become more potent within the system, but this ultimately failed. In order to try and allow the T_2 cells to grow and sustain their mass, a different approach was required. This came in the form of a phenomenon known as the Warburg Effect.

The Warburg effect allows a cancer cell to utilise glycolysis to try and gain sufficient nutrient to sustain itself in an often-hostile environment. To try and promote the growth of the T_2 cells, a novel method for implementing the Warburg effect was employed. When the nutrient level that surrounds the tumour mass begins to be used up, the T_1 cells go quiescent and will eventually die if they are unable to move into an area where nutrient is readily available. However, the T_2 cells in this situation switch to using glycolysis in order to maintain their growth and evade immune destruction.

The three Es of immunoediting have been explored by again varying the immune cells' success rate and age. It was shown that the model is able to generate immune elimination, equilibrium and escape. Moreover, the T_2 cells, aided by their ability to survive in a low nutrient environment, now have sufficient enough numbers to allow them to be present throughout the domain for a longer number of MCS. Furthermore, the model for all cell types can, now demonstrate a dormant state like the one exhibited by the spatial model in 3.8. Further discussions and details on how the model can be extended can be found in Chapter 5.

Chapter 5

Discussion and Future Directions

This Chapter will be concerned with drawing conclusions and providing discussion on possible extensions to the models found in Chapter 2, 3 and 4. It is hoped that these models can eventually provide insightful reasons as to why the dynamics exhibited are present.

The model in Chapter 2, was developed to try and explore the dynamics between $CD8^+$ T-cells and tumour cells. An individual based model was examined in CompuCell3D and the Three Es of immunoediting were exhibited. The model is an extension to the paper Matzavinos et al. [2004], whereby a parameter variation caused the model to exhibit periodic solutions, driven by the presence of a limit cycle. The killing mechanism within Matzavinos et al. [2004] was utilised in the CompuCell3D model, allowing the system to exhibit different stages of cancer growth. Future work with this model is quite extensive. The pursuit of a model that is biologically seamless is almost

impossible, but certain aspects of the tumour-immune environment, as well as more extensive parameter studies, could be added to hopefully make the model more biologically realistic.

Firstly, and the most obvious, chemotaxis can be added to the model. Chemotaxis is when cells move in response to an extracellular chemical gradient. Tumour cells realise these chemicals in order to shape the way the mass will grow. In response, an immune cell is able to recognise these growth factors and subsequently are driven toward the tumour mass. This would be relatively easy to implement within CompuCell3D, with the results probably showing the immune cells combating the tumour much quicker. Moreover, immune cells do not live indefinitely as they do in this model. They have a natural life span, but they also have a limit to how many tumour cells they can kill. The introduction of both chemotaxis and ageing of immune cells would be interesting to input in the model. It is possible that these factors may cancel each other out or the tumour cells may take more of a hold, as the immune cells could be combating a much bigger tumour, due to the ageing of immune cells.

Adhesion could also be changed and studied further. In the current model set up, the immune cells only adhere to one another slightly, however tumour cells adhere together more, allowing them to stay clustered together. Quiescent cells also adhere together more than tumour cells, often creating protective walls around other tumour masses. The idea would be to investigate if tumour cell adhesion had any impact on the model or whether it was a secondary issue that just caused qualitative rather than quantitative changes. The necrotic core also binds together as a mass and is broken down when

in contact with the medium. This gives an area where immune cells are not present, however the area is sucked of nutrient, preventing the tumour mass from growing into that area. This allows the immune cells to re populate and when the tumour is able to grow, they can mount an attack. If chemotaxis was introduced into the model this may have a major impact. However, the presence of hypoxic and necrotic tumour cells also creates issues. These cells will let off growth factors to try and gain a regulatory blood network. Again, this could be implemented using CompuCell3D, but this model is only concerned with an avascular tumour without a blood supply.

There is also the possibility of investigating tumour cell sub populations. This is a proposed phenomenon, discussed in the biology section, during the equilibrium process, where the immune cells and tumour cells oscillate around a certain level, preventing the tumour cells from gaining a blood network. The sub population is created by the tumour cells having multiple interactions with immune cells, killing the immune cells and subsequently changing their phenotype. While other tumour cells die, these cells are less immunogenic. Essentially, this type of tumour cell sub population is able to grow without the immune system driving an effective response, while also becoming more adept at killing. However, this has been implemented in the next two Chapters.

In Chapter 3, two models of immune-tumour interactions were developed. The first model focused on the infiltration of a tumour by $CD8^+$ and $CD4^+$ T-cells, utilising some of the modelling techniques found in de Pillis et al. [2005]. There is much discussion in the literature, such as in Eftimie et al. [2011], whereby it is argues that the modelling of the cancer-immune dynamic should

not solely focus on cytotoxic T-cells, therefore this model was developed to try and understand the important role T-helper cells play in destroying MHC I negative tumours. However, the system exhibited no bifurcations and therefore was shelved. In future, the development of this model could possibly lie in extracting some of the dynamics, making the model simpler. This may allow possible problems to be identified with certain terms. The model was also solved using experimental data values from de Pillis et al. [2005] and Joshi et al. [2009], therefore it may be prudent to use generic values to see if the system does exhibit interesting dynamics. In light of this model, it was determined that it may be interesting to develop a generic model of two different types of immune cells, interacting with two tumour population, with a focus on different tumour phenotypes.

The second model in this chapter developed a system whereby two immune populations are attacking two tumour populations. The model utilises methods from both de Pillis et al. [2005] and Matzavinos et al. [2004]. The system allows two immune cells to attack both cancer cell populations, however each is better at killing one and less so the other. The model was then shortened into two models where certain dynamics were removed. Firstly, the constant supply terms for the immune cells was removed, as well as the E_2 cells' attack on the T_2 population. The system was seen to bifurcate and three control parameters were identified. A spatial model was then developed, which showed heterogeneous type waves throughout the domain. The second model reintroduced the supply terms, and the system was able to now exhibit a periodic coexistence steady state, whereby the immune cells are keeping the tumour cells under check. Within both of these models,

however, the T_2 population remains higher than the T_1 population. This is counter-intuitive as the T_1 population is only attacked by one immune cell type, therefore this should be the dominant cancer cell, however due to the extra recruitment of the E_1 population when interaction with the T_1 cells, the E_1 cells are able to lower the T_1 tumour cell bulk more effectively. Lastly, the full system was modelled, and here the extra recruitment of the T_2 population further reduced the T_2 tumour population. This model can be extended in a number of different ways.

Future work with this model can be quite extensive. First of all, to allow the T_1 cell population to become the dominant cancer cell, certain measures would need to be put in place. The reduction of their recruitment would need to be implemented or the E_2 cells would need to be very good at killing the T_2 cells, increasing their recruitment. Also, the constant supply terms could also be increased, although these parameters do not seem to pose much control over the system. Another, and very obvious way to extend the model, would be to allow both tumour cells to attack the immune cells and terms to describe this behaviour would need to be explored. Moreover, the model is qualitative and therefore it would be prudent to try and retain more biologically relevant solutions by implementing some experimental parameter values. Further analysis can then be carried out biologically on the system. Furthermore, it would be interesting to marry both the main models in this chapter, to try and capture the action of T-helper cells within the environment, along with the evolution of changing tumour phenotypes.

An individual-based model was developed in Chapter 4 to examine the dynamics between two immune populations and two tumour populations in

an avascular tumour, using CompuCell3D. The model extends both models in Chapters 2 and sections 3.7 and 3.8. Both immune cell populations are allowed to attack the T_2 population, however only the E_1 immune cells are able to kill the T_1 cells, making them the dominant cancer cell. Tumour cells are unable to kill the immune cells, however the immune cells die in the model when in the domain for a user defined amount of Monte Carlo Steps. Nutrient is supplied to the model by the medium cells and is generic, containing both oxygen and glucose. The tumour cells are able to grow and divide depending on how much nutrient is available at their core. Tumour cells turn quiescent and then necrotic if the nutrient at their core is insufficient to support proliferation. The dynamics of the model are investigated by introducing three killing terms for the immune cells, and these are varied to try and produce the three Es of immunoediting. Moreover, a further aim in this model was to have all of the cell types exhibiting dynamic equilibrium. When simulating the system, the T_2 cells mostly became obsolete very quickly. This was either due to their destruction by the immune cells or by the exponential growth of T_1 cells, which use up all the available nutrient, preventing T_2 growth. In reality, the cancer cells are thought to undergo the Warburg Effect in order to deal with low nutrient environments and therefore, the introduction of this effect seemed the most appropriate way to increase the T_2 cells in the domain. The T_2 cells were therefore allowed to continue growth unless there was absolutely no nutrient at their core. This had the desired effect and the system was able to produce coexistence. However, many more elements of the tumour immune environment can be explored using this model.

Further extensions to this model could include some major aspects of

cancer growth. Most importantly, the immune cells only decay in the domain due to age, and therefore, the introduction of the tumour attack against the immune cells should be implemented. Moreover, the E_2 cells could be allowed to kill the T_1 cells, just as in the main model in Chapter 3. The dynamics of the T_1 cells could also be extended by allowing them to exhibit the Warburg Effect. Furthermore, chemotaxis could be implemented in the model, whereby cells move in response to an extracellular chemical gradient. Adhesion could also be studied further, with an aim to see if the reduction of the tumour cells' adhesion would enable them to grow more in more sites locally, by breaking off from the main tumour, possibly allowing immune evasion. Tumour cells also secrete growth factors to try and gain a blood network especially when in an area where little oxygen is available, known as hypoxia and again this model could be extended to include this. This list is only a snapshot of extensions this system could model, however, in conclusion, these concepts are the most prudent to implement.

In conclusion, this thesis has aimed to model different aspects of immune-tumour interactions. It has developed two discrete and two classical models of these dynamics to try and better understand the body's natural ability to kill cancer. However, it is of paramount importance that more experimental human data be used when implementing these models to try and enrich and validate the results. It is also important to point out that the complexities of this disease make it impossible to accurately model all aspects of cancer growth. However, mathematical models are an excellent tool to elucidate the underlying dynamics of the disease and could lead to the discovery of the most important biological actions that govern it, with a hope to develop better

treatments to extend the host's life, or to eradicate the cancer completely.

Chapter 6

Appendices

6.1 Appendix 1

Immune 1, tumour 1 varied

The percentages for the immune-tumour interactions, the number of MCS and immune death rate in the following results, are as follows:

$E_1T_2 = 22\%$

$E_2T_2 = 77\%$

$E_1T_1 = 60 - 71\%$

$MCS = 10000$

Immune cell death rate: $1000MCS$

The results are displayed in Figures 6.1-6.8.

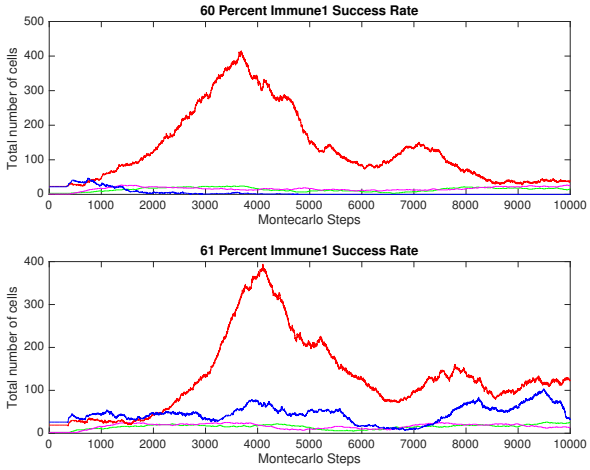

Figure 6.1: *Plots showing the total number of tumour and immune cells for* $60 - 61\%$ *immune 1 kill rate when in interaction with tumour cell type 1, tumour type 2 and immune type 1 at* 22% *and tumour type 2 and immune type 2 at* 77%*. Tumour cell 1 is represented by the red line, tumour cell 2 is represented by the blue line, immune cell 1 is represented by the green line and immune cell 2 by the pink line.*

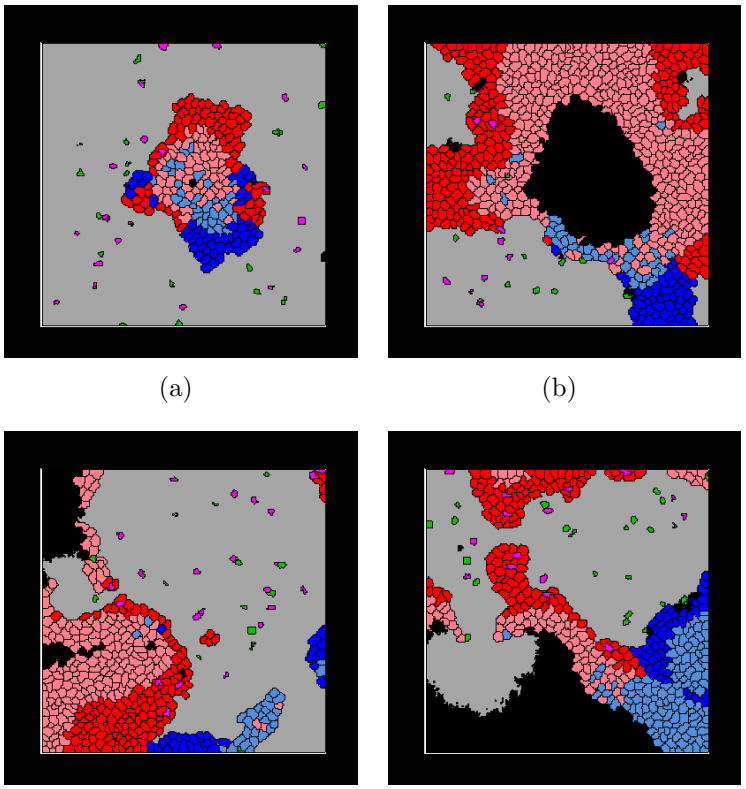

Figure 6.2: *Plots showing the growth of a tumour mass interacting with a host immune system. The types of cells and their corresponding colours in Figures 6.2(a)-6.2(d) are as follows: proliferative tumour type 1 cells in red, quiescent tumour type 1 cells in salmon, proliferative tumour type 2 in blue, quiescent tumour type 2 cells in light blue, necrotic cells in black, medium cells in grey, immune type 1 cells in green, immune type 2 in magenta. The immune success rates are as follows: tumour type 1 and immune type 1 at* 61%*, tumour type 2 and immune type 1 at* 22% *and tumour type 2 and immune type 2 at* 77%*. Figures 6.2(a)-6.2(d) represent the model at 2500MCS, 5000MCS, 7500MCS and 10000MCS respectively.*

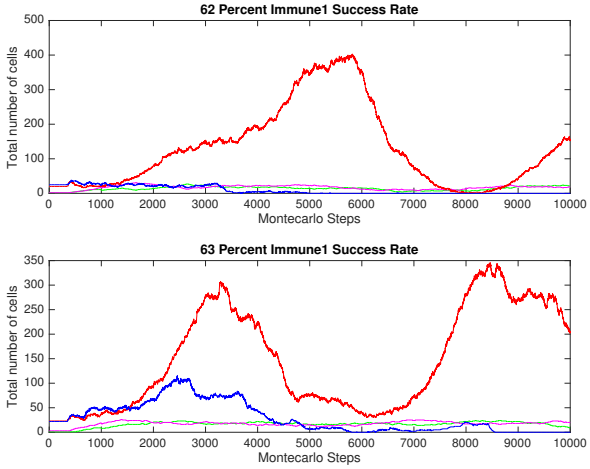

Figure 6.3: *Plots showing the total number of tumour and immune cells for* $62 - 63\%$ *immune 1 kill rate when in interaction with tumour cell type 1, tumour type 2 and immune type 1 at* 22% *and tumour type 2 and immune type 2 at* 77%*. Tumour cell 1 is represented by the red line, tumour cell 2 is represented by the blue line, immune cell 1 is represented by the green line and immune cell 2 by the pink line.*

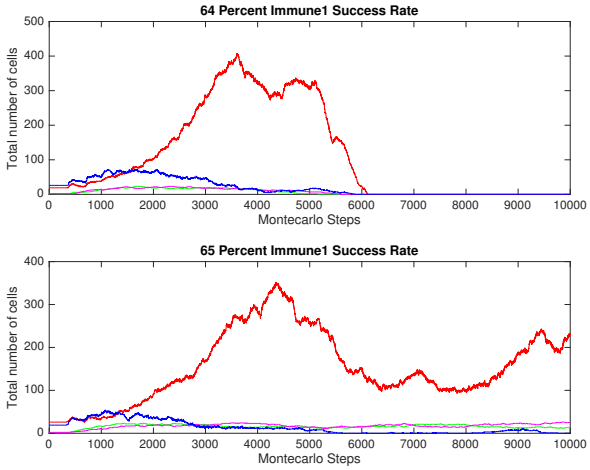

Figure 6.4: *Plots showing the total number of tumour and immune cells for* $64 - 65\%$ *immune 1 kill rate when in interaction with tumour cell type 1, tumour type 2 and immune type 1 at* 22% *and tumour type 2 and immune type 2 at* 77%*. Tumour cell 1 is represented by the red line, tumour cell 2 is represented by the blue line, immune cell 1 is represented by the green line and immune cell 2 by the pink line.*

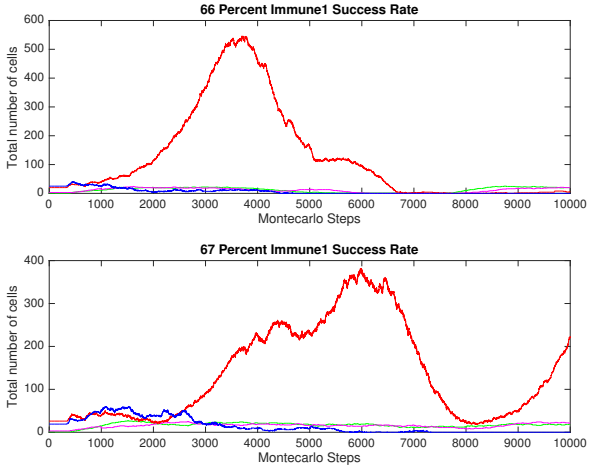

Figure 6.5: *Plots showing the total number of tumour and immune cells for* $66 - 67\%$ *immune 1 kill rate when in interaction with tumour cell type 1, tumour type 2 and immune type 1 at* 22% *and tumour type 2 and immune type 2 at* 77%*. Tumour cell 1 is represented by the red line, tumour cell 2 is represented by the blue line, immune cell 1 is represented by the green line and immune cell 2 by the pink line.*

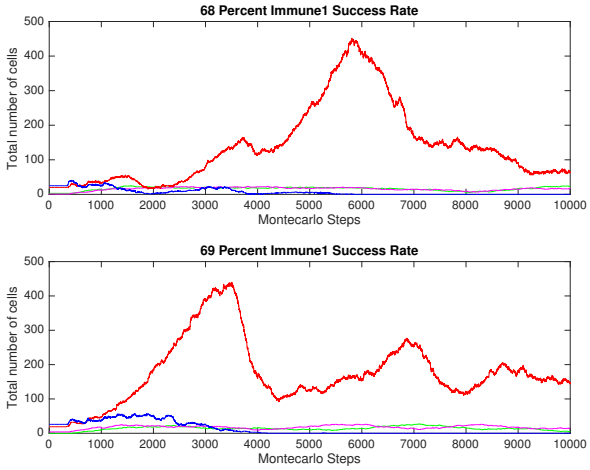

Figure 6.6: *Plots showing the total number of tumour and immune cells for* $68 - 69\%$ *immune 1 kill rate when in interaction with tumour cell type 1, tumour type 2 and immune type 1 at* 22% *and tumour type 2 and immune type 2 at* 77%*. Tumour cell 1 is represented by the red line, tumour cell 2 is represented by the blue line, immune cell 1 is represented by the green line and immune cell 2 by the pink line.*

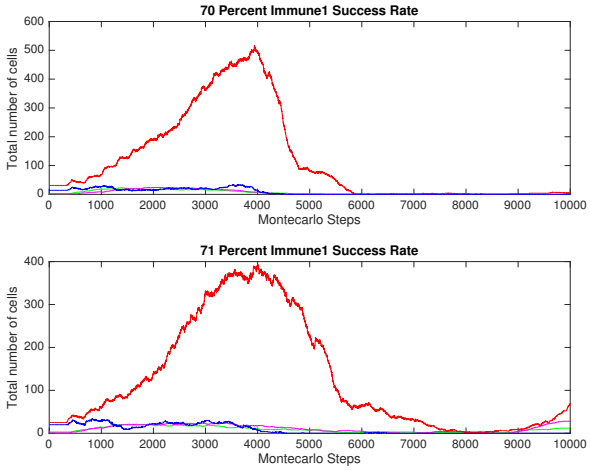

Figure 6.7: *Plots showing the total number of tumour and immune cells for* $70 - 71\%$ *immune 1 kill rate when in interaction with tumour cell type 1, tumour type 2 and immune type 1 at* 22% *and tumour type 2 and immune type 2 at* 77%*. Tumour cell 1 is represented by the red line, tumour cell 2 is represented by the blue line, immune cell 1 is represented by the green line and immune cell 2 by the pink line.*

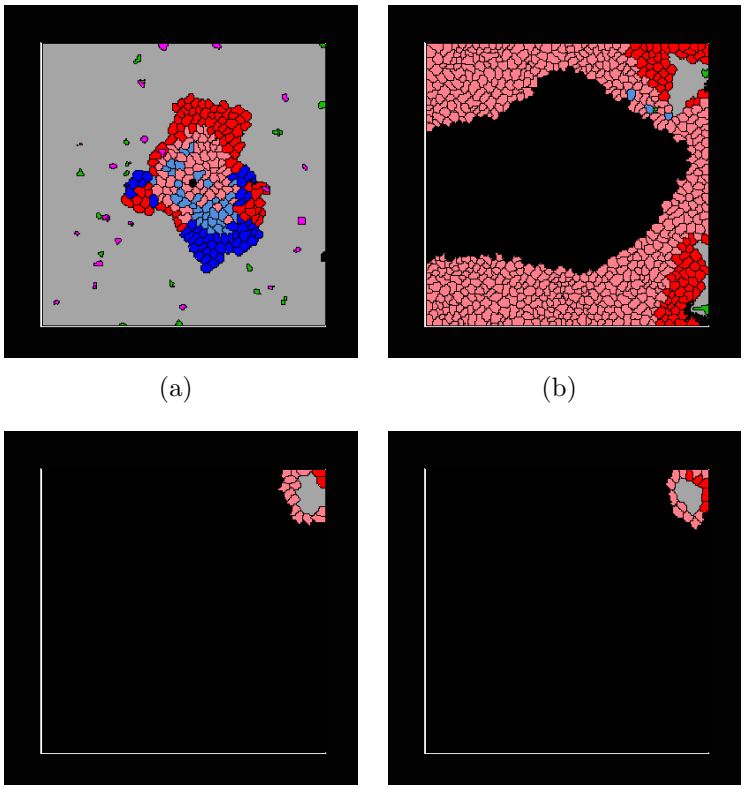

Figure 6.8: *Plots showing the growth of a tumour mass interacting with a host immune system. The types of cells and their corresponding colours in Figures 6.8(a)-6.8(d) are as follows: proliferative tumour type 1 cells in red, quiescent tumour type 1 cells in salmon, proliferative tumour type 2 in blue, quiescent tumour type 2 cells in light blue, necrotic cells in black, medium cells in grey, immune type 1 cells in green, immune type 2 in magenta. The immune success rates are as follows: tumour type 1 and immune type 1 at* 70%*, tumour type 2 and immune type 1 at* 22% *and tumour type 2 and immune type 2 at* 77%*. Figures 6.8(a)-6.8(d) represent the model at 2500MCS, 5000MCS, 7500MCS and 10000MCS respectively.*

6.2 Appendix 2

Immune 1, tumour 1 varied

The percentages for the immune-tumour interactions, the number of MCS and immune death rate in the following results, are as follows:

$E_1T_2 = 22\%$

$E_2T_2 = 77\%$

$E_1T_1 = 90 - 99\%$

$MCS = 10000$

Immune cell death rate: $3500MCS$

The results are displayed in Figures 6.9-6.13.

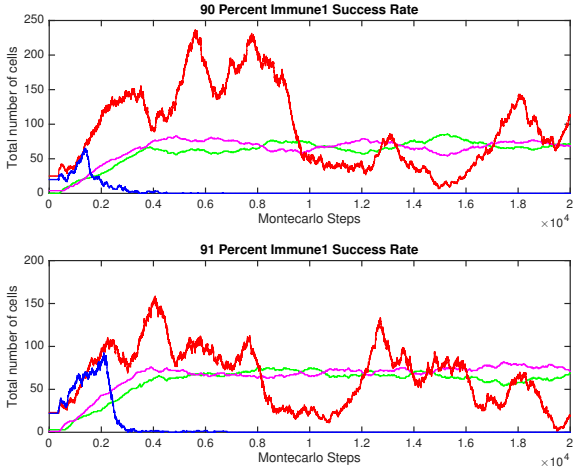

Figure 6.9: *Plots showing the total number of tumour and immune cells for* $90 - 91\%$ *immune 1 kill rate when in interaction with tumour cell type 1, tumour type 2 and immune type 1 at* 22% *and tumour type 2 and immune type 2 at* 77%*. Tumour cell 1 is represented by the red line, tumour cell 2 is represented by the blue line, immune cell 1 is represented by the green line and immune cell 2 by the pink line.*

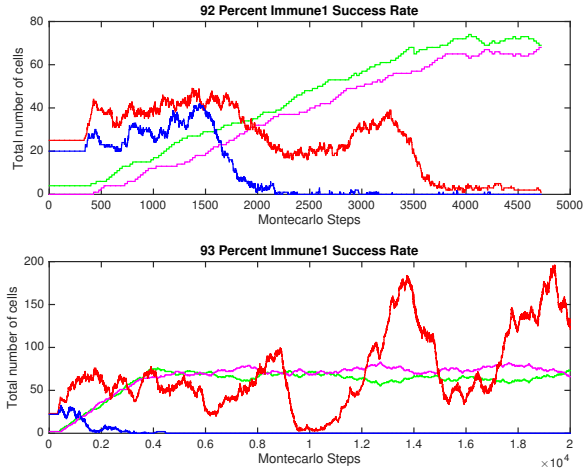

Figure 6.10: *Plots showing the total number of tumour and immune cells for* $92 - 93\%$ *immune 1 kill rate when in interaction with tumour cell type 1, tumour type 2 and immune type 1 at* 22% *and tumour type 2 and immune type 2 at* 77%*. Tumour cell 1 is represented by the red line, tumour cell 2 is represented by the blue line, immune cell 1 is represented by the green line and immune cell 2 by the pink line.*

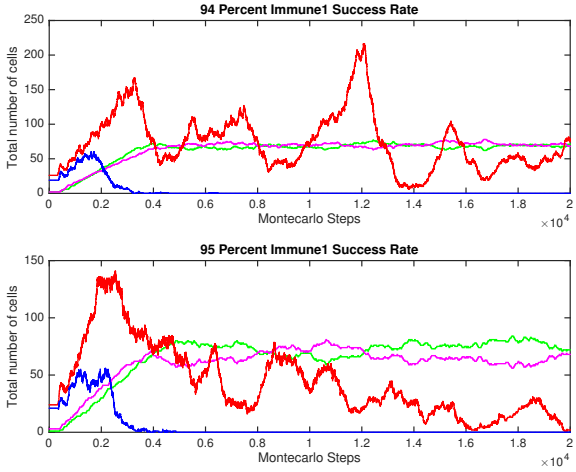

Figure 6.11: *Plots showing the total number of tumour and immune cells for* $94 - 95\%$ *immune 1 kill rate when in interaction with tumour cell type 1, tumour type 2 and immune type 1 at* 22% *and tumour type 2 and immune type 2 at* 77%*. Tumour cell 1 is represented by the red line, tumour cell 2 is represented by the blue line, immune cell 1 is represented by the green line and immune cell 2 by the pink line.*

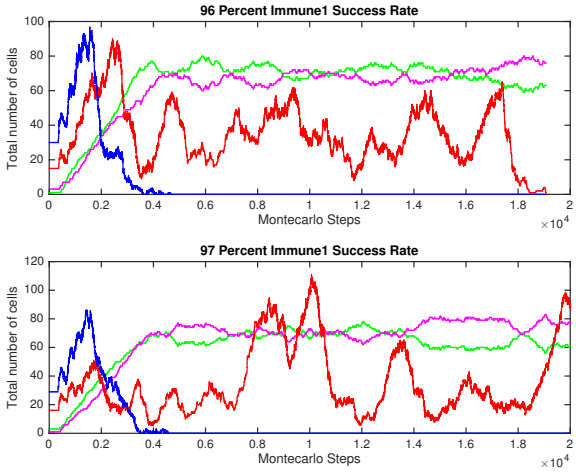

Figure 6.12: *Plots showing the total number of tumour and immune cells for* $96 - 97\%$ *immune 1 kill rate when in interaction with tumour cell type 1, tumour type 2 and immune type 1 at* 22% *and tumour type 2 and immune type 2 at* 77%*. Tumour cell 1 is represented by the red line, tumour cell 2 is represented by the blue line, immune cell 1 is represented by the green line and immune cell 2 by the pink line.*

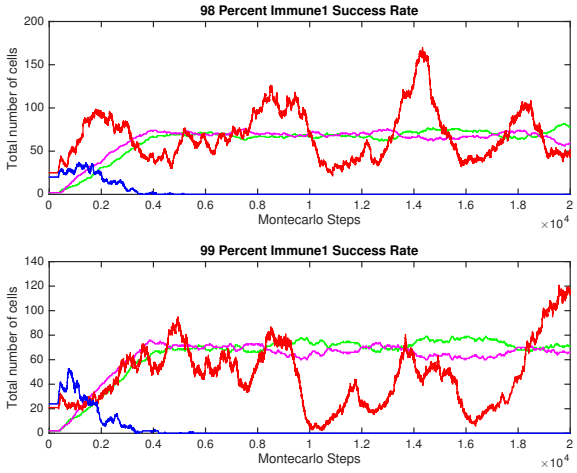

Figure 6.13: *Plots showing the total number of tumour and immune cells for* $98 - 99\%$ *immune 1 kill rate when in interaction with tumour cell type 1, tumour type 2 and immune type 1 at* 22% *and tumour type 2 and immune type 2 at* 77%*. Tumour cell 1 is represented by the red line, tumour cell 2 is represented by the blue line, immune cell 1 is represented by the green line and immune cell 2 by the pink line.*

6.3 Appendix 3

Immune 2, tumour 2 varied

The percentages for the immune-tumour interactions, the number of MCS and immune death rate in the following results, are as follows:

$$E_1T_2 = 22\%$$

$$E_2T_2 = 40 - 43\%$$

$$E_1T_1 = 90\%$$

$$MCS = 20,000$$

$$\text{Immune cell death rate} = 1000MCS$$

The results are displayed in Figures 6.14-6.17.

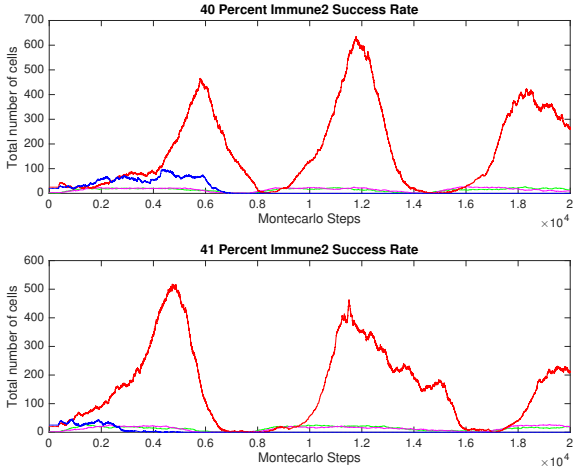

Figure 6.14: *Plots showing the total number of tumour and immune cells for* $40-41\%$ *immune 2 kill rate when in interaction with tumour cell type 2, tumour type 1 and immune type 1 at* 90% *and tumour type 2 and immune type 1 at* 22%*. Tumour cell 1 is represented by the red line, tumour cell 2 is represented by the blue line, immune cell 1 is represented by the green line and immune cell 2 by the pink line.*

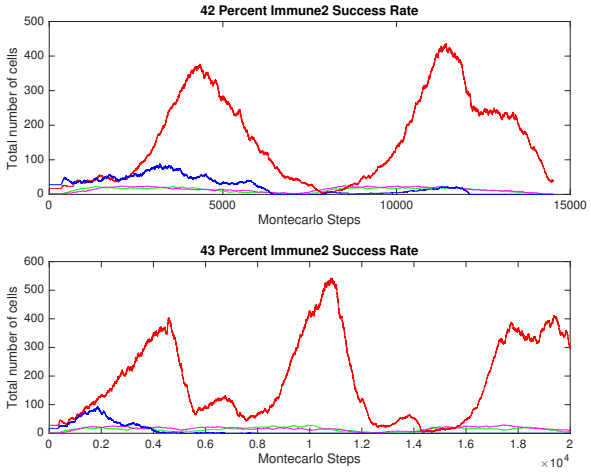

Figure 6.15: *Plots showing the total number off tumour and immune cells for* $42-43\%$ *percent immune 2 kill rate when in interaction with tumour cell type 2, tumour type 1 and immune type 1 at* 90% *and tumour type 2 and immune type 1 at* 22%*. Tumour cell 1 is represented by the red line, tumour cell 2 is represented by the blue line, immune cell 1 is represented by the green line and immune cell 2 by the pink line.*

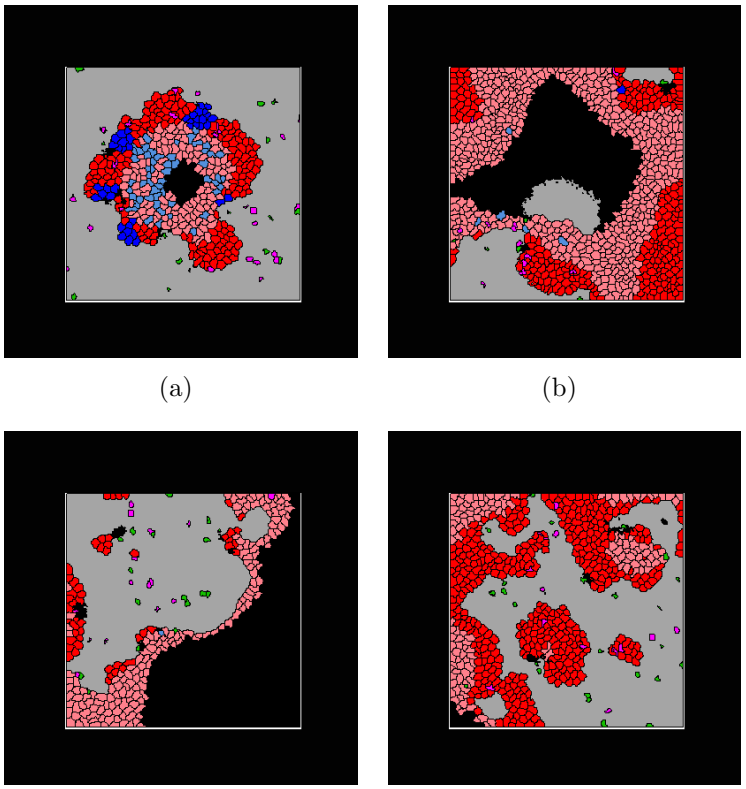

Figure 6.16: *Plots showing the growth of a tumour mass interacting with a host immune system. The types of cells and their corresponding colours in Figures 6.16(a)-6.16(d) are as follows: proliferative tumour type 1 cells in red, quiescent tumour type 1 cells in salmon, proliferative tumour type 2 in blue, quiescent tumour type 2 cells in light blue, necrotic cells in black, medium cells in grey, immune type 1 cells in green, immune type 2 in magenta. The immune success rates are as follows: tumour type 1 and immune type 1 at* 90%*, tumour type 2 and immune type 1 at* 22% *and tumour type 2 and immune type 2 at* 43%*. Figures 6.16(a)-6.16(d) represent the model at 2500MCS, 5000MCS, 7500MCS and 10000MCS respectively.*

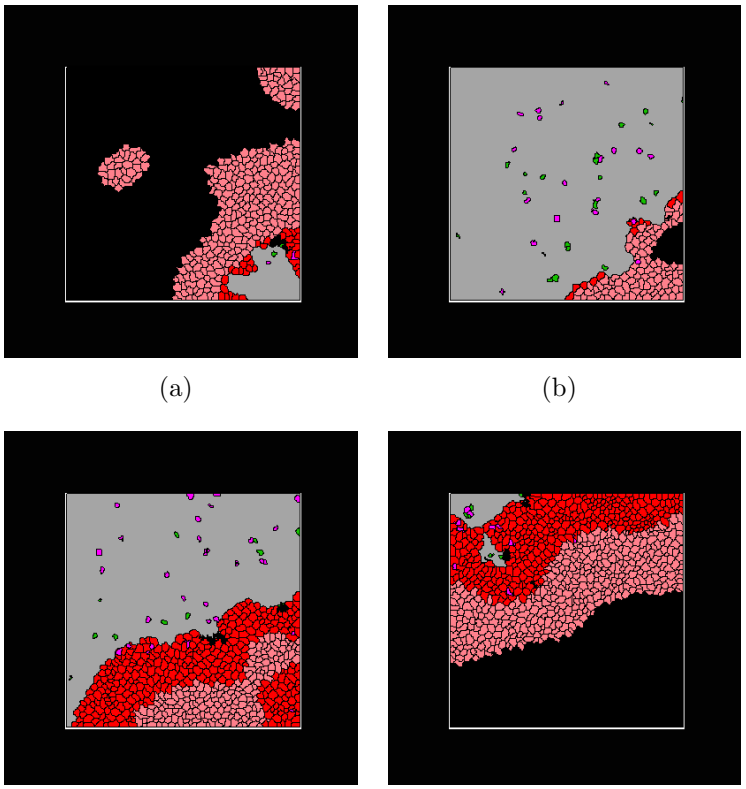

(a) (b)

(c) (d)

Figure 6.17: *Plots showing the growth of a tumour mass interacting with a host immune system. The types of cells and their corresponding colours in Figures 6.17(a)-6.17(d) are as follows: proliferative tumour type 1 cells in red, quiescent tumour type 1 cells in salmon, proliferative tumour type 2 in blue, quiescent tumour type 2 cells in light blue, necrotic cells in black, medium cells in grey, immune type 1 cells in green, immune type 2 in magenta. The immune success rates are as follows: tumour type 1 and immune type 1 at* 90%*, tumour type 2 and immune type 1 at* 22% *and tumour type 2 and immune type 2 at* 43%*. Figures 6.17(a)-6.17(d) represent the model at 12500MCS, 15000MCS, 17500MCS and 20000MCS respectively.*

6.4 Appendix 4

Immune 2, tumour 2 varied

The percentages for the immune-tumour interactions, the number of MCS and immune death rate in the following results, are as follows:

$$E_1T_2 = 22\%$$

$$E_2T_2 = 30 - 39\%$$

$$E_1T_1 = 95\%$$

$$MCS = 20,000$$

$$\text{Immune cell death rate} = 2500MCS$$

The results are displayed in Figures 6.18-6.24.

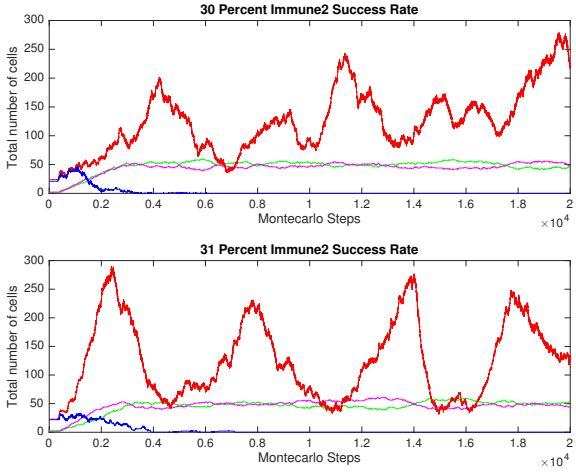

Figure 6.18: *Plots showing the total number of tumour and immune cells for* $30 - 31\%$ *immune 2 kill rate when in interaction with tumour cell type 2, tumour type 1 and immune type 1 at* 95% *and tumour type 2 and immune type 1 at* 22%*. Tumour cell 1 is represented by the red line, tumour cell 2 is represented by the blue line, immune cell 1 is represented by the green line and immune cell 2 by the pink line.*

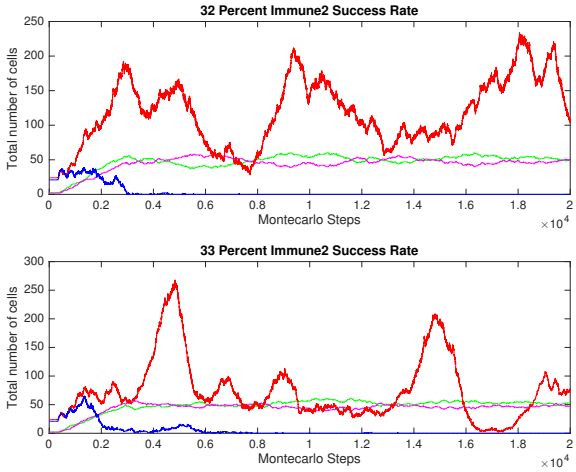

Figure 6.19: *Plots showing the total number of tumour and immune cells for* $32 - 33\%$ *immune 2 kill rate when in interaction with tumour cell type 2, tumour type 1 and immune type 1 at* 95% *and tumour type 2 and immune type 1 at* 22%*. Tumour cell 1 is represented by the red line, tumour cell 2 is represented by the blue line, immune cell 1 is represented by the green line and immune cell 2 by the pink line.*

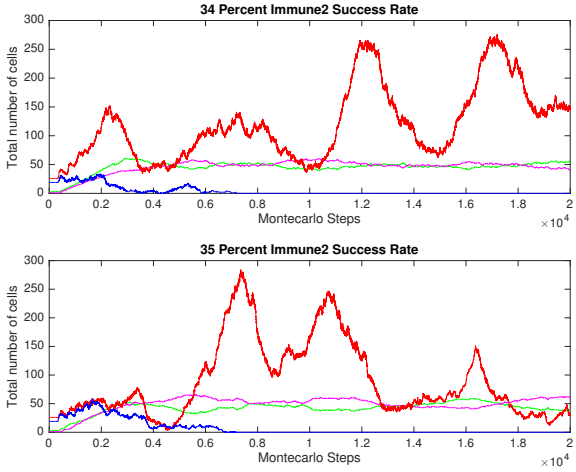

Figure 6.20: *Plots showing the total number of tumour and immune cells for* $34 - 35\%$ *immune 2 kill rate when in interaction with tumour cell type 2, tumour type 1 and immune type 1 at* 95% *and tumour type 2 and immune type 1 at* 22%*. Tumour cell 1 is represented by the red line, tumour cell 2 is represented by the blue line, immune cell 1 is represented by the green line and immune cell 2 by the pink line.*

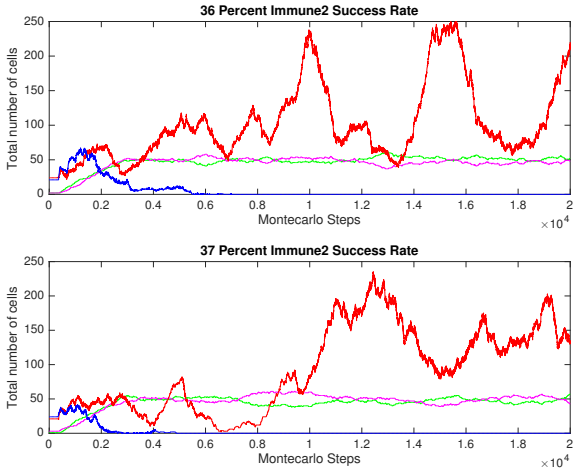

Figure 6.21: *Plots showing the total number of tumour and immune cells for* $36 - 37\%$ *immune 2 kill rate when in interaction with tumour cell type 2, tumour type 1 and immune type 1 at* 95% *and tumour type 2 and immune type 1 at* 22%*. Tumour cell 1 is represented by the red line, tumour cell 2 is represented by the blue line, immune cell 1 is represented by the green line and immune cell 2 by the pink line.*

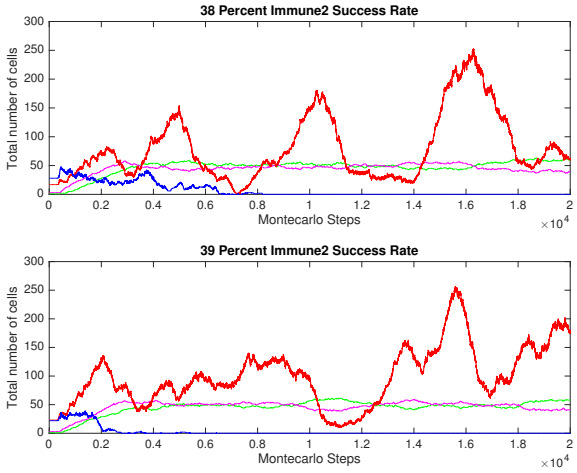

Figure 6.22: *Plots showing the total number of tumour and immune cells for* $38 - 39\%$ *immune 2 kill rate when in interaction with tumour cell type 2, tumour type 1 and immune type 1 at* 95% *and tumour type 2 and immune type 1 at* 22%*. Tumour cell 1 is represented by the red line, tumour cell 2 is represented by the blue line, immune cell 1 is represented by the green line and immune cell 2 by the pink line.*

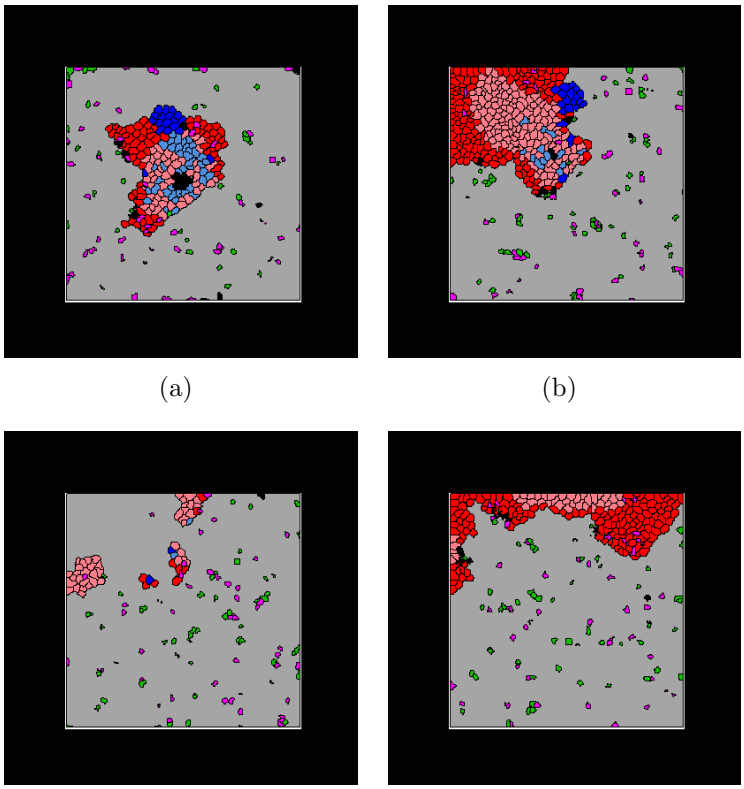

(a) (b)

(c) (d)

Figure 6.23: *Plots showing the growth of a tumour mass interacting with a host immune system. The types of cells and their corresponding colours in Figures 4.47(a)-4.47(d) are as follows: proliferative tumour type 1 cells in red, quiescent tumour type 1 cells in salmon, proliferative tumour type 2 in blue, quiescent tumour type 2 cells in light blue, necrotic cells in black, medium cells in grey, immune type 1 cells in green, immune type 2 in magenta. The immune success rates are as follows: tumour type 1 and immune type 1 at* 90%*, tumour type 2 and immune type 1 at* 22% *and tumour type 2 and immune type 2 at* 38%*. Figures 6.23(a)-6.23(d) represent the model at 2500MCS, 5000MCS, 7500MCS and 10000MCS respectively.*

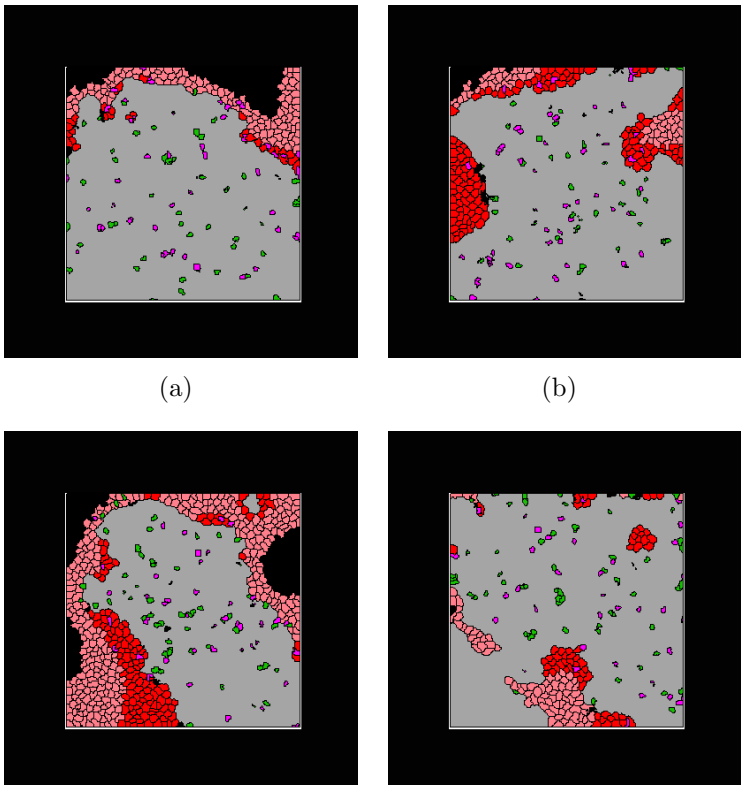

(a) (b)

(c) (d)

Figure 6.24: *Plots showing the total number of interacting with a host immune system. The types of cells and their corresponding colours in Figures 6.24(a)-6.24(d) are as follows: proliferative tumour type 1 cells in red, quiescent tumour type 1 cells in salmon, proliferative tumour type 2 in blue, quiescent tumour type 2 cells in light blue, necrotic cells in black, medium cells in grey, immune type 1 cells in green, immune type 2 in magenta. The immune success rates are as follows: tumour type 1 and immune type 1 at* 90%*, tumour type 2 and immune type 1 at* 22% *and tumour type 2 and immune type 2 at* 38%*. Figures 6.24(a)-6.24(d) represent the model at 12500MCS, 15000MCS, 17500MCS and 20000MCS respectively.*

6.5 Appendix 5

Immune 2, tumour 2 varied

The percentages for the immune-tumour interactions, the number of MCS and immune death rate in the following results, are as follows:

$$E_1T_2 = 22\%$$

$$E_2T_2 = 30 - 39\%$$

$$E_1T_1 = 95\%$$

$$MCS = 20,000$$

$$\text{Immune cell death rate} = 3500MCS$$

The results are displayed in Figures 6.25-6.29.

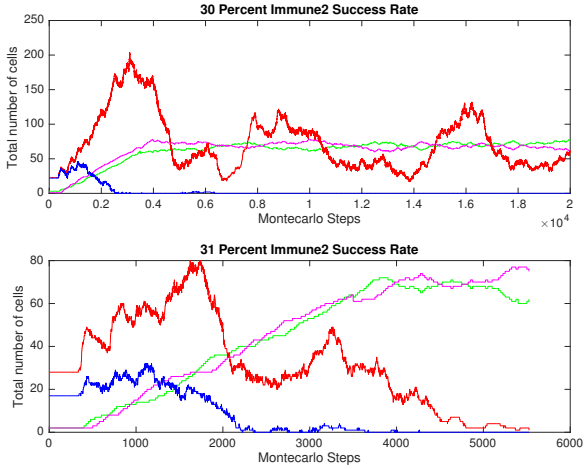

Figure 6.25: *Plots showing the total number of tumour and immune cells for* $30 - 31\%$ *immune 2 kill rate when in interaction with tumour cell type 2, tumour type 1 and immune type 1 at* 95% *and tumour type 2 and immune type 1 at* 22%*. Tumour cell 1 is represented by the red line, tumour cell 2 is represented by the blue line, immune cell 1 is represented by the green line and immune cell 2 by the pink line.*

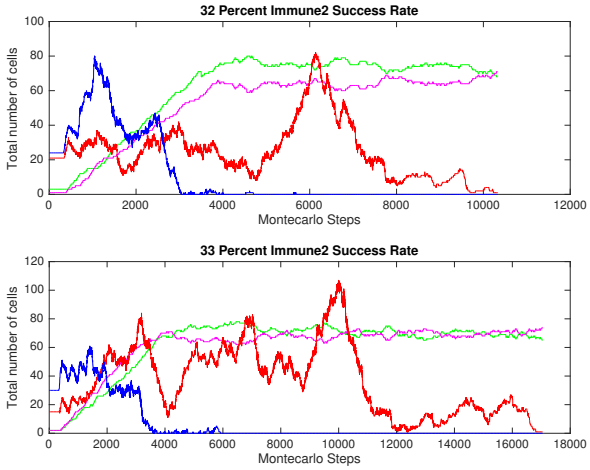

Figure 6.26: *Plots showing the total number of tumour and immune cells for* $32 - 33\%$ *immune 2 kill rate when in interaction with tumour cell type 2, tumour type 1 and immune type 1 at* 95% *and tumour type 2 and immune type 1 at* 22%*. Tumour cell 1 is represented by the red line, tumour cell 2 is represented by the blue line, immune cell 1 is represented by the green line and immune cell 2 by the pink line.*

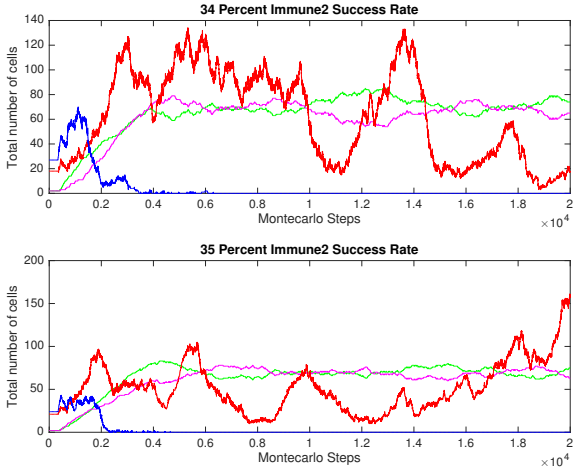

Figure 6.27: *Plots showing the total number of tumour and immune cells for* $34 - 35\%$ *immune 2 kill rate when in interaction with tumour cell type 2, tumour type 1 and immune type 1 at* 95% *and tumour type 2 and immune type 1 at* 22%*. Tumour cell 1 is represented by the red line, tumour cell 2 is represented by the blue line, immune cell 1 is represented by the green line and immune cell 2 by the pink line.*

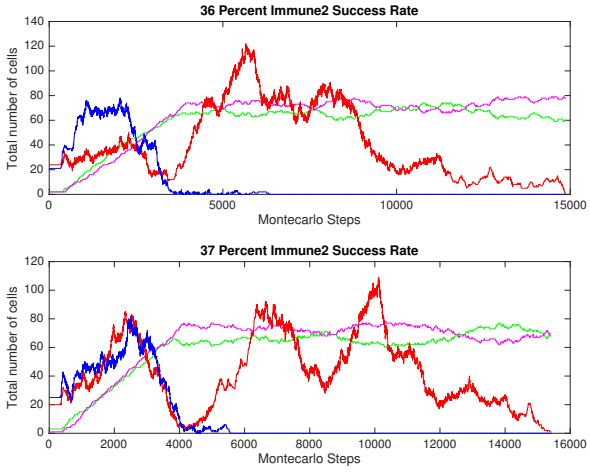

Figure 6.28: *Plots showing the total number of tumour and immune cells for* $36 - 37\%$ *immune 2 kill rate when in interaction with tumour cell type 2, tumour type 1 and immune type 1 at* 95% *and tumour type 2 and immune type 1 at* 22%*. Tumour cell 1 is represented by the red line, tumour cell 2 is represented by the blue line, immune cell 1 is represented by the green line and immune cell 2 by the pink line.*

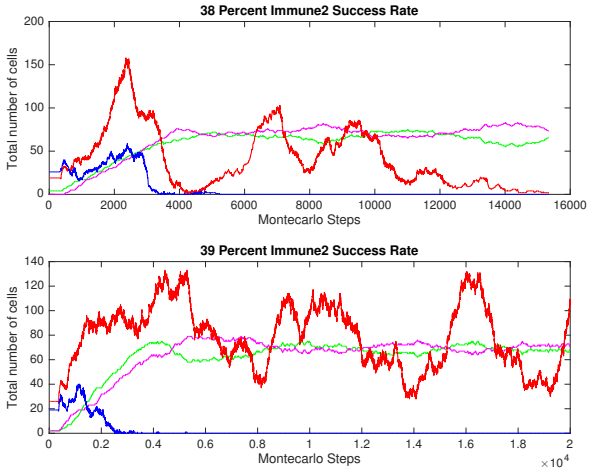

Figure 6.29: *Plots showing the total number of tumour and immune cells for* $38 - 39\%$ *immune 2 kill rate when in interaction with tumour cell type 2, tumour type 1 and immune type 1 at* 95% *and tumour type 2 and immune type 1 at* 22%*. Tumour cell 1 is represented by the red line, tumour cell 2 is represented by the blue line, immune cell 1 is represented by the green line and immune cell 2 by the pink line.*

6.6 Appendix 6

Immune 2, tumour 2 varied

The percentages for the immune-tumour interactions, the number of MCS and immune death rate in the following results, are as follows:

$$E_1T_2 = 22\%$$

$$E_2T_2 = 30 - 39\%$$

$$E_1T_1 = 95\%$$

$$MCS = 20,000$$

$$\text{Immune cell death rate} = 3000MCS$$

The results are displayed in Figures 6.30-6.34.

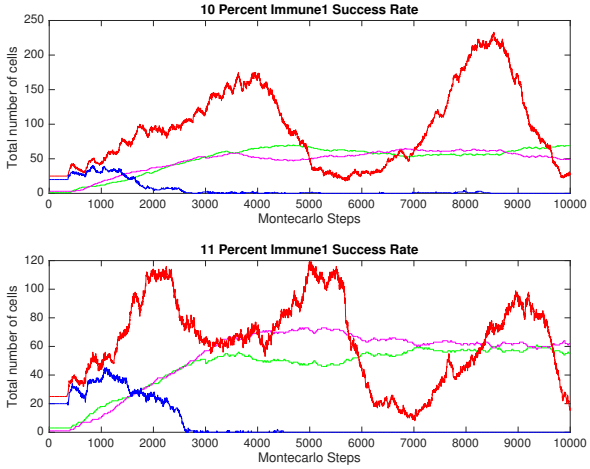

Figure 6.30: *Plots showing the total number of tumour and immune cells for* $10 - 11\%$ *immune 1 kill rate when in interaction with tumour cell type 2, tumour type 1 and immune type 1 at* 95% *and tumour type 2 and immune type 2 at* 20%*. Tumour cell 1 is represented by the red line, tumour cell 2 is represented by the blue line, immune cell 1 is represented by the green line and immune cell 2 by the pink line.*

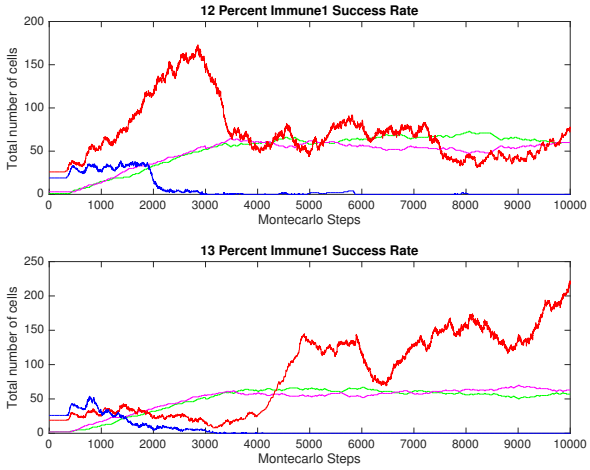

Figure 6.31: *Plots showing the total number of tumour and immune cells for* $12 - 13\%$ *immune 1 kill rate when in interaction with tumour cell type 2, tumour type 1 and immune type 1 at* 95% *and tumour type 2 and immune type 2 at* 20%*. Tumour cell 1 is represented by the red line, tumour cell 2 is represented by the blue line, immune cell 1 is represented by the green line and immune cell 2 by the pink line.*

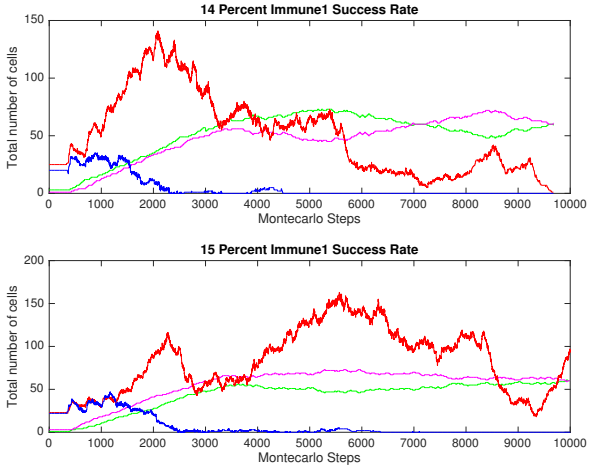

Figure 6.32: *Plots showing the total number of tumour and immune cells for* $14-15\%$ *immune 1 kill rate when in interaction with tumour cell type 2, tumour type 1 and immune type 1 at* 95% *and tumour type 2 and immune type 2 at* 20%*. Tumour cell 1 is represented by the red line, tumour cell 2 is represented by the blue line, immune cell 1 is represented by the green line and immune cell 2 by the pink line.*

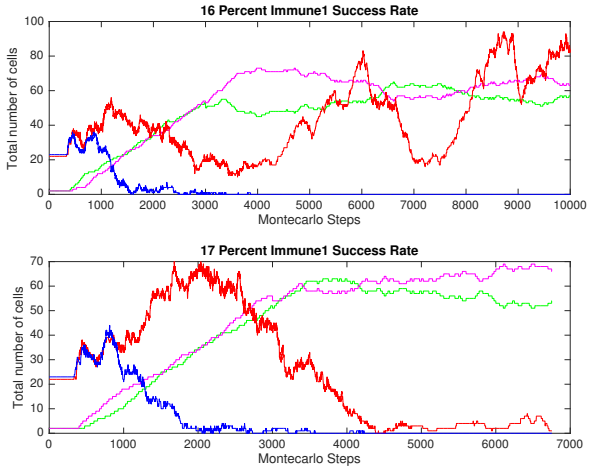

Figure 6.33: *Plots showing the total number of tumour and immune cells for* $16-17\%$ *immune 1 kill rate when in interaction with tumour cell type 2, tumour type 1 and immune type 1 at* 95% *and tumour type 2 and immune type 2 at* 20%*. Tumour cell 1 is represented by the red line, tumour cell 2 is represented by the blue line, immune cell 1 is represented by the green line and immune cell 2 by the pink line.*

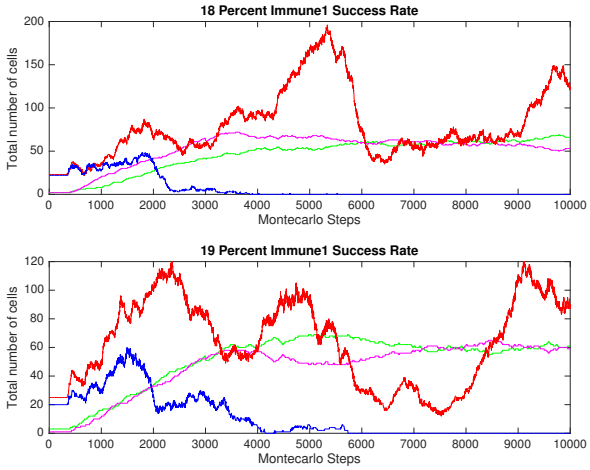

Figure 6.34: *Plots showing the total number of tumour and immune cells for* $18-19\%$ *immune 1 kill rate when in interaction with tumour cell type 2, tumour type 1 and immune type 1 at* 95% *and tumour type 2 and immune type 2 at* 20%*. Tumour cell 1 is represented by the red line, tumour cell 2 is represented by the blue line, immune cell 1 is represented by the green line and immune cell 2 by the pink line.*

Bibliography

Al-Tameemi, M., Chaplain, M. A. J., and d'Onofrio, A. (2012). Evasion of tumours from the control of the immune system: consequences of brief encounters. *Biol. Direct*, 7(31):doi: 10.1186/1745–6150–7–31.

Alberts, B., Johnson, A., Lewis, J., Raff, M., Roberts, K., and Walter, P. (2008). *Molecular Biology of the Cell*. Garland Science, 5th edition.

Andasari, V., Roper, R. T., Swat, M. H., and Chaplain, M. A. J. (2012). Integrating intracellular dynamics using CompuCell3D and bionetsolver: applications to multiscale modelling of cancer cell growth and invasion. *PLoS One*, 7(3):e33726. doi:10.1371/journal.pone.0033726.

Arciero, J. C., Jackson, T. L., and Kirschner, D. E. (2004). A mathematical model of tumor-immune evasion and siRNA treatment. *DCDS-B*, 4(1):39–58.

Bartrons, R. and Caro, J. (2007). Hypoxia, glucose metabolism and the Warburg's effect. *J. Bioenerg. Biomembr.*, 39(3):223–229.

Bauer, A. L., Jackson, T. L., and Hirowaka, Y. (2007). A cell-based model

exhibiting branching and anastomosis during tumor-induced angiogensis. *Biophys. J.*, 92(9):3105–3121.

Bauer, A. L., Jackson, T. L., and Jiang, Y. (2009). Topography of extracellular matrix mediates vascular morphogenesis and migration speeds in angiogenesis. *PLoS Comput. Biol.*, 5(7):e1000445. doi:10.1371/journal.pcbi.1000445.

Boon, T. and van der Bruggen, P. (1996). Human tumor antigens recognized by T lymphocytes. *J. Exp. Med.*, 183(3):725–729.

Bose, T. and Trimper, S. (2009). Stocastic model for tumor growth with immunization. *Phys. Rev. E.*, 79(5):051903 doi:10.1103/PhysRevE.79.051903.

Brooks, G. A. (2009). Cell-cell and intracellular lactate shuttles. *J. Physiol.*, 587(23):5591–5600.

Burnet, F. M. (1957). Cancer-A Biological Approach. *Br. Med. J.*, 1(5023):841–847.

Burnet, F. M. (1964). Immunological factors in the process of carcinogenesis. *Br. Med. Bull.*, 20(154-158).

Burnet, F. M. (1970). The concept of immunological surveillance. *Prog. Exp. Tumour Res.*, 13(1-27).

Byrne, H. M. and Chaplain, M. A. J. (1996). Modelling the role of cell-cell adhesion in the growth and development of carcinomas. *Math. Comp. Modelling*, 24(12):1–17.

Byrne, H. M., Cox, S. M., and Kelly, C. E. (2004). Macrophage-tumour interactions: In vivo dynamics. *DCDS-B*, 4(1):81–98.

Callaway, M. P. and Briggs, J. C. (1989). The incidence of late recurrence (greater than 10 years); an analysis of 536 consecutive cases of cutaneous melanoma. *Br. J. Plast. Surg.*, 42(1):46–49.

Cappuccio, A., Elishmereni, M., and Agur, Z. (2006). Cancer Immunotherapy by Interleukin-21: Potential Treatment Strategies Evaluated in a Mathematical Model. *Cancer Res.*, 66(14):7293–7300.

de Pillis, L. G. and Radunskaya, A. (2001). A Mathematical Tumor Model with Immune Resistance and Drug Therapy: An Optimal Control Approach. *J. Theor. Med.*, 3(2):79–100.

de Pillis, L. G., Radunskaya, A., and Bathe, K. J. (2003). Mathematical model of immune response to tumor invasion. *Comp. Fluid Solid Mech.*, 2:1661–1668.

de Pillis, L. G., Radunskaya, A., and Wiseman, C. (2005). A validated mathematical model of cell-mediated immune response to tumor growth. *Cancer Res.*, 65(17):7950–8.

Deboer, R. J., Hogeweg, P., Dullens, H. F. J., Deweger, R. A., Denotter, W., De Boer, R. J., De Weger, R. A., and Den Otter, W. (1985). Macrophage T lymphocyte interactions in the anti-tumor immune response: a mathematical model. *J. Immunol.*, 134(4):2748–58.

Demicheli, R., Abbattista, A., Miceli, R., Valagussa, P., and Bonadonna, G.

(1996). Time distribution of the recurrence risk for breast cancer patients undergoing mastectomy: Further support about the concept of tumor dormancy. *Breast Cancer Res. Treat.*, 41(2):177–185.

Diefenbach, A., Jensen, E., Jamieson, A., and Raulet, D. (2001). Rae1 and H60 ligands of the NKG2D receptor stimulate tumour immunity. *Nature*, 413(6852):165–171.

Dighe, A. S., Richards, E., Old, L. J., and Schreiber, R. D. (1994). Enhanced in vivo growth resistance to rejection of tumor cells expressing dominant negative IFN receptors. *Immunity*, 1(6):447–56.

d'Onofrio, A. (2008). Metamodeling tumor-immune system interaction, tumor evasion and immunotherapy. *Math. Comp. Modelling*, 47(5-6):614–637.

Dudley, M. E., Wunderlich, J. R., Robbins, P. F., Yang, J. C., Hwu, P., Schwartzentruber, D. J., et al. (2002). Cancer regression and autoimmunity in patients after clonal repopulation with antitumour lymphocytes. *Science*, 298(5594):850–854.

Dunn, G. P., Bruce, A. T., Ikeda, H., Old, L. J., and Schrieber, R. D. (2002). Cancer immunoediting: from immunosurveillence to tumour escape. *Nat. Immunol.*, 3(11):991–998.

Dunn, G. P., Old, L. J., and Schreiber, R. D. (2004a). The immunobiology of cancer immunosurveillence and immunoediting. *Immunity*, 21(2):137–148.

Dunn, G. P., Old, L. J., and Schreiber, R. D. (2004b). The three Es of cancer immunoediting. *Annu. Rev. Immunol*, 22:329–60.

Eftimie, R., Bramson, J., and Earn, D. J. D. (2010). Modeling anti-tumor Th1 and Th2 immunity in the rejection of melanoma. *J. Theor. Biol.*, 265(3):467–480.

Eftimie, R., Bramson, J., and Earn, D. J. D. (2011). Interactions Between the Immune System and Cancer: A Brief Review of Non-spatial Mathematical Models. *Bull. Math. Biol.*, 73(1):2–32.

Ehrlich, P. (1909). Über den jetzigen stand der karzinomforschung. *Ned Tijdschr Geneeskd*, 5:273–290.

Fishman, M. and Perelson, A. (1993). Modeling T Cell-Antigen Presenting Cell Interactions. *J. Theor. Biol.*, 160(3):311–342.

Glazier, J. A., Balter, A., and Poplawski, N. J. (2007). *Single-Cell-Based Models in Biology and Medicine*. Birkhauser, Basel, Boston and Berlin.

Griffiths, D. and Higham, D. J. (2011). *Numerical Methods for Ordinary Differential Equations*. Springer.

Gu, W., de Pillis, L. G., and Radunskaya, A. E. (2006). Mixed immunotherapy and chemotherapy of tumors: modeling, applications and biological interpretations. *J. Theor. Biol.*, 238(4):841–862.

Guckenheimer, J. and Holmes, P. (1983). *Nonlinear Oscillations, Dynamical Systems, and Bifurcations of Vector Fields*, volume 42. Springer.

Haabeth, O. A. W., Tveita, A. A., Fauskanger, M., Schjesvold, F., Lorvid, K. B., Hofgaard, P., Omholt, H., Munthe, L. A., Dembic, Z., Corthay, A., and Bogen, B. (2014). How do CD4+ T cells detect and eliminate tumor cells that either lack or express MHC class II molecules? *Front. Immunol.*, 5(174):doi: 10.3389/fimmu.2014.00174.

Hanahan, D. and Weinberg, R. A. (2000). The hallmarks of cancer. *Cell*, 100(1):57–70.

Hanahan, D. and Weinberg, R. A. (2011). Hallmarks of Cancer: The Next Generation. *Cell*, 144(5):646–674.

Herrlinger, U., Hebart, H., Kanz, L., Dichgans, J., and Weller, M. (2005). Relapse of primary CNS lymphoma after more than 10 years in complete remission. *J. Neurol.*, 252(11):1409–1410.

Hester, S. D., Belmonte, J. M., Gens, J. S., Clendenon, S. G., and Glazier, J. A. (2011). A multi-cell, multi-scale model of vertebrate segmentation and somite formation. *PLoS Comput. Biol.*, 7(10):7(e1002155). doi: 10.1371/journal.pcbi.1002155.

Hung, K., Hayashi, R., Lafond-Walker, A., Lowenstien, C., Paradoll, D., and Levitsky, H. (1998). The central role of CD4+ T cells in the antitumor response. *J. Exp. Med.*, 188(12):2357–2368.

Izaguirre, J. A., Chaturvedi, R., Huang, C., Cickovski, T., Coffland, J., Thomas, G., Forgacs, G., Alber, M., Hentschel, G., Newman, S. A., and Glazier, J. A. (2004). CompuCell, a multi-model framework for simulation of morphogenesis. *Bioinf.*, 20(7):1129–1137.

Joshi, B., Wang, X., Banerjee, S., Tian, H., and Matzavinos, A. (2009). On immunotherapies and cancer vaccination protocols: A mathematical modelling approach. *J. Theor. Biol.*, 259(4):820–827.

Kaplan, D. H., Shankaran, V., Dighe, A. S., Stockert, E., Aguet, M., et al. (1998). Demonstration of an interferon gamma-dependent tumor surveillance system in immunocompetent mice. *Proc. Natl. Acad. Sci. USA*, 95(13):7556–7561.

Kern, D. E., Klarnet, J. P. M., Jensen, M. C., and Greenberg, P. D. (1986). Requirement for recognition of class II molecules and processed tumor antigen for optimal generation of syngeneic tumor-specific class I-restricted CTL. *J. Immunol.*, 136(11):4303–4310.

Khar, A. (1997). Mechanisms involved in natural killer cell mediated target cell death leading to spontaneous tumour regression. *J. Biosci.*, 22(1):23–31.

Kirschner, D. and Panetta, J. C. (1998). Modeling Immunotherapy of the Tumour-Immune Interaction. *J. Math. Biol.*, 37(3):235–252.

Koebel, C., Vermi, W., Swann, J., Zerafa, N., Rodig, S., Old, L., Smyth, M., and Schreiber, R. (2007). Adaptive immunity maintains occult cancer in an equilibrium state. *Nature*, 450(7171):903–907.

Kogan, Y., Forys, U., Shukron, O., Kronik, N., and Agur, Z. (2010). Cellular Immunotherapy for High Grade Gliomas: Mathematical Analysis Deriving Efficacious Infusion Rates Based on Patient Requirements. *SIAM J. Appl. Math.*, 70(6):1953–1976.

Kronik, N., Kogan, Y., Elishmereni, M., Halevi, T., Vuk, P., Agur, Z., and Meuth, S. (2010). Predicting Outcomes of Prostate Cancer Immunotherapy by Personalized Mathematical Models. *PLoS one*, 5(12):e15482. doi: 10.1371/journal.pone.0015482.

Kronik, N., Kogan, Y., Vainstein, V., and Agur, Z. (2008). Improving alloreactive CTL immunotherapy for malignant gliomas using a simulation model of their interactive dynamics. *Cancer Immunol. and Immunother.*, 57(3):425–439.

Kuznetsov, V. (1991). A mathematical model for the interaction between cytotoxic T lymphocytes and tumour cells. Analysis of the growth, stabilization, and regression of a B-cell lymphoma in mice chimeric with respect to the major histocompatibility complex. *Biomed. Sci.*, 2(5):465–476.

Kuznetsov, V., Makalkin, I., Taylor, M., and Perelson, A. (1994). Nonlinear dynamics of immunogenic tumors: Parameter estimation and global bifurcation analysis. *Bull. Math. Biol.*, 56(2):295–321.

Kuznetsov, V. A. and Knott, G. D. (2001). Modeling tumor regrowth and immunotherapy. *Math. Comp. Modelling*, 33(12-13):1275–1287.

Kuznetsov, V. A. and Stepnova, L. A. (1992). Space-time waves and dissipative structures in a model of growth of tumours infiltrated by immune lymphocytes. *Lecture notes of the ICB Seminars Biosystems. (G.I. Marchuk and A. werynski, eds). Warsaw, Poland*, International centre for Biocybernetics:68–111.

Laio, K. L., Bai, X. F., and Friedman, A. (2014). Mathematical Modeling of Interleukin-27 Induction of Anti-Tumor T Cells Response. *PLoS One*, 9(3):e91844. doi: 10.1371/journal.pone.0091844.

Lejeune, O. and El Akili, I. (2008). Oscillations and bistability in the dynamics of cytotoxic reactions mediated by the response of immune cells to solid tumours. *Math. Comp. Modelling*, 47(5-6):649–662.

Liberti, M. V. and Locasale, J. W. (2016). The Warburg Effect: How Does it Benefit Cancer Cells? *Trends Biochem. Sci.*, 41(3):211–218.

Lollini, P., Motta, S., and Pappalardo, F. (2006). Modeling tumour immunology. *Math. Mod. Methods Appl. Sci.*, 16(7S):1091–1124.

Lu, J., Tan, M., and Cai, Q. (2015). The Warburg effect in tumor progression: Mitochondrial oxidative metabolism as an anti-metastasis mechanism. *Cancer Lett.*, 356(2, Pt A):156 – 164.

MacSween, R. N. M. and Whaley, K. (1992). *Muir's Textbook of Pathology*. Arnold, London, 13th edition.

Malet, D. and de Pillis, L. (2006). A cellular automata model of the tumor-immune system interactions. *J. Theor. Biol.*, 239(3):334–350.

Mansury, Y., Diggory, M., and Diesboeck, T. (2006). Evolutionary game theory in an agent-based brain tumor model: exploring the 'Genotype-Phenotype' link. *J. Theor. Biol.*, 238(1):146–156.

Marincola, F. M., Jaffee, E. M., Hicklin, D. J., and Ferrone, S. (2000). Escape

of human solid tumors from T-cell recognition: molecular mechanisms and fuctional significance. *Adv. Immunol.*, 74:181–273.

Matsui, K., Sawa, T., Suzuki, H., Nakagawa, K., Okamoto, N., Tada, T., Nagano, T., and Masuda, N. (2006). Relapse of Stage I Small Cell Lung Cancer Ten or More Years after the Start of Treatment. *Jpn. J. Clin. Oncol.*, 36(7):457–461.

Mattes, J., Hulett, M., Xie, W., Hogan, S., Rothenberg, M. E., Foster, P., and Parish, C. (2003). Immunotherapy of Cytotoxic T Cell-resistant Tumors by T helper 2 Cells: An Eotaxin and STAT-6 dependent Process. *J. Exp. Med.*, 197(3):387–393.

Matzavinos, A. and Chaplain, M. A. J. (2004). Travelling-wave analysis of a model of the immune response to cancer. *C. R. Biol.*, 327(11):995–1008.

Matzavinos, A., Chaplain, M. A. J., and Kuznetsov, V. A. (2004). Mathematical modelling of the spatio-temporal response of cytotoxic T-lymphocytes to a solid tumour. *Math. Med. Biol.*, 21(1):1–34.

Melief, C. J., Toes, R. E., Medema, J. P., van der Burg, S. H., Ossendorp, F., and Offringa, R. (2000). Strategies for immunotherapy of cancer. *Adv. Immunol.*, 75:235–282.

Meng, S., Tripathy, D., Frenkel, E., Shete, S., Naftalis, E., Huth, J., Beitsch, P., Leitch, M., Hoover, S., Euhus, D., Haley, B., Morrison, L., Fleming, T., Herlyn, D., Uhr, J. W., Fehm, T., Tucker, T., Lane, N., and Wang, J. (2004). Circulating Tumor Cells in Patients with Breast Cancer Dormancy. *Clin. Cancer Res.*, 10(24):8152–8162.

Merks, R. M. H. and Glazier, J. A. (2006). Dynamic mechanisms of blood vessel growth. *Nonlinearity*, 19(1):1–10.

Merks, R. M. H., Perryn, E. D., Shirinifard, A., and Glazier, J. A. (2008). Contact-inhibited chemotaxis in de novo and sprouting blood-vessel growth. *PLoS Comput. Biol.*, 4(9):e1000163. doi: 10.1371/journal.pcbi.1000163.

Montagna, D., Maccario, R., Locatelli, F., Montini, E., Pagani, S., Bonetti, F., Daudt, L., Turin, I., Lisini, D., Garavaglia, C., Dellabona, P., and Casorati, G. (2006). Emergence of antitumor cytolytic T cells is associated with maintenance of hematologic remission in children with acute myeloid leukemia. *Blood*, 108(12):3843–3850.

Mumberg, D., Monach, P. A., Wanderling, S., Philip, M., Toledano, A. Y., and Schreiber, H. (1999). CD4(+) T cells eliminate MHC class II-negative cancer cells in vivo by indirect effects of IFN-gamma. *Proc. Natl. Acad. Sci. U. S. A.*, 96(15):8633–8638.

Nelson, B. (2008). The impact of T-cell immunity on ovarian cancer outcomes. *Immunol. Rev.*, 222(1):101–116.

Nishimura, T., Iwakabe, K., Sekimoto, M., Ohmi, Y., Yahata, T., Nakui, M., Sato, T., Habu, S., Tashiro, H., and Ohta, A. (1999). Distinct role of antigen speicific T helper type 1 (Th1) and Th2 cells in tumour eradication in vivo. *J. Exp. Med.*, 190(5):617–627.

Nwabugwu, C. L., Rakhra, K., Felsher, D. W., and Paik, D. S. (2012). Mathematical Modeling of the Interactions between Cellular Programs in Re-

sponse to Oncogene Inactivation. *12th IEEE Int. Conf. on Bioinfor. Bioeng. (BIBE)*, pages 454–459.

Nwabugwu, C. L., Rakhra, K., Felsher, D. W., and Paik, D. S. (2013). A Tumor-Immune Mathematical Model of CD4+ T Helper Cell Dependent Tumor Regression by Oncogene Inactivation. *Conf. Proc. IEEE. Eng. Med. Biol. Soc.*, pages 4529–4532.

O'Byrne, K. J. and Dalgleish, A. G. (2001). Chronic immune activation and inflammation as the cause of malignancy. *Br. J. Cancer*, 85(4):473–483.

Ossendorp, F., Mengede, E., Camps, M., Filius, R., and Melief, C. (1998). Specific T Helper Cell Requirement for Optimal Induction of Cytotoxic T Lymphocytes against Major Histocompatibility Complex Class II Negative Tumors. *J. Exp. Med.*, 187(5):693–702.

Owen, M. and Sherratt, J. (1997). Pattern Formation and Spatiotemporal Irregularity in a Model for Macrophage-Tumour Interactions. *J. Theor. Biol.*, 189(1):63–80.

Owen, M. and Sherratt, J. (1999). Mathematical modelling of marcophage dynamics in tumours. *Math. Mod. Methods Appl. Sci.*, 9(4):513–539.

Owen, M., Stamper, I. J., Muthana, M., Richardson, G., Dobson, J., Lewis, C., and Byrne, H. (2011). Mathematical Modeling Predicts Synergistic Antitumor Effects of Combining a Macrophage-Based, Hypoxia-Targeted Gene Therapy with Chemotherapy. *Cancer Res.*, 71(8):2826–2837.

Owen, M. R. and Sherratt, J. A. (1998). Modelling the macrophage invasion

of tumours: effects on growth and composition. *IMA J. Math. Appl. Med. Biol.*, 15(2):165–85.

Pages, F., Galon, J., Dieu-Nosjean, M. C., Tartour, E., Sautes Fridman, C., Pages, F., and Sautes Fridman, C. (2010). Immune infiltration in human tumors: a prognostic factor that should not be ignored. *Oncogene*, 29(8):1093–1102.

Pappalardo, F., Lollini, P. L., Castiglione, F., and Motta, S. (2006). Analysis of vaccine's schedule using models. *Cell. Immunol.*, 244(2):137–140.

Pederson, P. L. (2007). Warburg, me and Hexokinase 2: multiple discoveries of key molecular events underlying one of cancers' most common phenotypes, the "Warburg Effect", i.e. elevated glycolysis in the presence of oxygen. *J. Bioenerg. Biomembr.*, 39(3):211–222.

Perez-Diez, A., Joncker, N. T., Choi, K., Chan, W. F. N., Anderson, C. C., Lantz, O., and Matzinger, P. (2007). CD4 cells can be more efficent at tumour rejection than CD8 cells. *Blood*, 109(12):5346–5354.

Poplawski, N. J., Agero, U., Gens, J. S., Swat, M., Glazier, J. A., and Anderson, A. (2009). Front instabilities and invasiveness of simulated avascular tumors. *Bull. Math. Biol.*, 71(5):1189–1227.

Poplawski, N. J., Shirinifard, A., Agero, U., Gens, J. S., Swat, M., and Glazier, J. A. (2010). Front instabilities and invasiveness of simulated 3D avascular tumors. *PLoS One*, 26(5):e10641. doi: 10.1371/journal.pone.0010641.

Powathil, G., Adamson, D. J. A., Chaplain, M. A. J., and Quaranta, V. (2013). Towards Predicting the Response of a Solid Tumour to Chemotherapy and Radiotherapy Treatments: Clinical Insights from a Computational Model. *PLoS Comput. Biol.*, 9(7):e1003120. doi: 10.1371/journal.pcbi.1003120.

Powathil, G., Swat, M., and Chaplain, M. A. J. (2014). Systems oncology: Towards patient-specific treatment regimes informed by multiscale mathematical modelling. *Sem. Cancer Biol.*, 30:13–20.

Quesnel, B. (2008). Dormant tumor cells as a therapeutic target? *Cancer Lett.*, 267(1):10–17.

Quezada, S. A., Simpson, T. R., Peggs, K. S., Merghoub, T., Vider, J., Fan, X., Blasberg, R., Yagita, H., Muranski, P., Antony, P., Restifo, N. P., and Allison, J. P. (2010). Tumour reactive CD4+ T cells develop cytotoxic activity and ericate large established melanoma after trasnfer into lumphopenic hosts. *J. Exp. Med.*, 207(3):637–650.

Racker, E. (1972). Bioenergics and the problem of tumour growth: an understanding of the mechanism of the generation and control of biological energy may shed light on the problem of tumor growth. *Am. Sci.*, 60(1):56–63.

Radunskaya, A. and de Pillis, L. G. (2003). The dynamics of an optimally controlled tumor model: A case study. *Math. Comp. Modelling*, 37(11):1221–1244.

Rejniak, K. A. and Anderson, A. R. A. (2011). Hybrid models of tumor growth. *Wiley Interdiscip. Rev. Syst. Biol. Med.*, 3(115):125.

Russell, J. H. and Ley, T. J. (2002). Lymphocyte-mediated cytotoxicity. *Annu. Rev. Immunol.*, 20:323–70.

Ryungsa, K., Manabu, E., and Kazuaki, T. (2007). Cancer immunoediting from immune surveillance to immune escape. *Immunology*, 121(1):1–14.

Sagalowsky, A. and Molberg, K. (1999). Solitary metastasis of renal cell carcinoma to the contralateral adrenal gland 22 years after nephrectomy. *Urology*, 54(1):162.

Sherratt, J. A., Eagan, B. T., and Lewis, M. A. (1997). Oscillations and chaos behind predator-prey invasion: Mathematical artifact or ecological reality? *Philos. Trans. R. Soc. Lond. B. Biol. Sci.*, 352(1349):21–38.

Shirinifard, A., Gens, J. S., Zaitlen, B. L., Poplawski, N. J., and Swat, M. (2009). 3D multi-cell simulation of tumor growth and angiogensis. *PLoS One*, 4(10):e7190. doi: 10.1371/journal.pone.0007190.

Smyth, M. J., Thia, K. Y., Street, S. E., Cretney, E., Trapani, J. A., et al. (2000a). Differential tumor surveillance by natural killer (NK) and NKT cells. *J. Exp. Med.*, 191(4):661–68.

Smyth, M. J., Thia, K. Y., Street, S. E., MacGregor, D., Godfrey, D. L., and Trapani, J. A. (2000b). Perforin-mediated cytotoxicity is critical for surveillance of spontaneous lymphoma. *J. Exp. Med.*, 192(5):755–60.

Sompayrac, L. (2012). *How the Immune System Works*. Wiley-Blackwell, 4th edition.

Stewart, T. H. M., Raman, S., and Hollinshead, A. C. (1991). Tumour dormancy: initiation, maintenance and termination in animals and humans. *Can. J. Surg.*, 34(4):321–5.

Street, S. E., Cretney, E., and Smyth, M. J. (2001a). Perforin and interferon activities independently control tumor initiation, growth, and metastasis. *Blood*, 97(1):192–97.

Street, S. E., Trapani, J. A., MacGregor, D., and Smyth, M. J. (2001b). Suppression of lymphoma and epithelial malignancies effected by interferon gamma. *J. Exp. Med.*, 196(1):129–34.

Swann, J. B. and Smyth, M. J. (2007). Immune surveillance of tumors. *J. Clin. Invest.*, 117(5):1137–1146.

Swat, M. H., Thomas, G. L., Belmonte, J. M., Shirinifard, A., Hmeijak, D., and Glazier, J. A. (2012). Multi-scale modeling of tissues using CompuCell3D. *Methods Cell. Biol.*, 110:325–366.

Swat, M. H., Thomas, G. L., Shirinifard, A., Clendenon, S. G., and Glazier, J. A. (2015). Emergent stratification in solid tumors selects for reduced cohesion of tumor cells: A multi-cell, virtual-tissue model of tumor evolution using compucell3d. *PLoS One*, 10(6):e0127972. doi: 10.1371/journal.pone.0127972.

Teng, M. W. L., Swann, J., Koebel, C., Schreiber, R., and Smyth, M. (2008).

Immune-mediated dormancy: an equilibrium with cancer. *J Luekoc. Biol.*, 84(4):988–993.

Upadhyay, M., Samal, J., Kandpal, M., Singh, O. V., and Vivekanandan, P. (2013). The Warburg effect: Insights from the past decade. *Pharmacol. Ther.*, 137(3):318 – 330.

Vaishnavi, S. N., Vlassenko, A. G., Rundle, M. M., Snyder, A. Z., Mintun, M. A., and Raichle, M. E. (2010). Regional aerobic glycolysis in the human brain. *Proc. Natl. Acad. Sci. USA*, 107(41):17757–17762.

Vajdic, C. M. and van Leeuwen, M. T. (2009). Cancer incidence and risk factors after solid organ transplantation. *Int. J. Cancer*, 125(8):1747–1754.

van den Broek, M. F., Kagi, D., Ossendorp, F., Toes, R., Vamvakas, S., et al. (1996). Decreased tumor surveillance in perforin deficient mice. *J. Exp. Med.*, 184(5):1781–90.

Van der Heiden, M. G., Cantley, L. C., and Thompson, C. B. (2009). Understanding the Warburg Effect: The Metabolic Requirements of Cell Proliferation. *Science*, 324(5930):1029–1033.

Wang, S., Hinow, P., Bryce, N., Weaver, A., Estrada, L., Arteaga, C., and Webb, G. (2009). A Mathematical Model Quantifies Proliferation and Motility Effects of TGF- on Cancer Cells. *Comput. Math. Meth. Med.*, 10(1):71–83.

Wang, Y., Bramson, J., Pilon, A., et al. (2000). Genetically Modified Dendritic Cells Prime Autoreactive T Cells through a Pathway Independent of

CD40L and Interleukin 12: Implication for Cancer Vaccines. *Cancer Res.*, 60(12):3247–3253.

Warburg, O. (1925). The metabolism of carcinoma cells. *J. Cancer Res.*, 9:148–163.

Warburg, O. et al. (1924). Ueber den stoffwechsel der tumeron. *Biochem.*, 152:319–344.

Warburg, O. et al. (1927). The metabolism of tumours in the body. *Gen. Physiol.*, 8:519–530.

Warburg, O. et al. (1956). On the origin of cancer cells. *Science*, 123:309–314.

Webb, S., Owen, M., Byrne, H., Murdoch, C., and Lewis, C. (2007). Macrophage-Based Anti-Cancer Therapy: Modelling Different Modes of Tumour Targeting. *Bull. Math. Biol.*, 69(5):1747–1776.

Wu, W. and Zhao, S. (2013). Metabolic changes in cancer: beyond the Warburg effect. *Acta. Biochim. Biopgys. Sin. (Shanghai)*, 45(1):18–26.

Zheng, J. (2012). Energy metabolsim of cancer: Glycolysis versus oxidative phosphorylation (Reveiw). *Oncol. Lett.*, 4(6):1151–1157.